

RCA REVIEW

a technical journal

→ ENGINEERING LIBRARY
SILVER SPRING LIBRARY, INC.

RADIO AND ELECTRONICS
RESEARCH • ENGINEERING

VOLUME VIII

MARCH 1947

NO. 1

RCA REVIEW

GEORGE M. K. BAKER
Manager

CHAS. C. FOSTER, JR.
Business Manager

SUBSCRIPTIONS:

United States, Canada and Postal Union: One Year \$2.00, Two Years \$3.50, Three Years \$4.50
Single Copies: 75¢ each

Other Countries: One Year \$2.40, Two Years \$4.30, Three Years \$5.70
Single Copies: 85¢ each

Copyright, 1947, by Radio Corporation of America, RCA Laboratories Division

Published quarterly in March, June, September, and December by Radio Corporation of America, RCA Laboratories Division, 30 Rockefeller Plaza, New York 20, N. Y.

Editorial and General Offices: RCA REVIEW, Radio Corporation of America, RCA Laboratories Division, Princeton, New Jersey.

Entered as second class matter April 3, 1946, at the Post Office at New York, New York, under the act of March 3, 1879

RADIO CORPORATION OF AMERICA

DAVID SARNOFF, *President*

LEWIS MACCONNACH, *Secretary*

ARTHUR B. TUTTLE, *Treasurer*

PRINTED IN U.S.A.

RCA REVIEW

a technical journal

RADIO AND ELECTRONICS
RESEARCH • ENGINEERING

Published quarterly by

RADIO CORPORATION OF AMERICA
RCA LABORATORIES DIVISION

in cooperation with

RCA VICTOR DIVISION
RADIOMARINE CORPORATION OF AMERICA
RCA INTERNATIONAL DIVISION

RCA COMMUNICATIONS, INC.
NATIONAL BROADCASTING COMPANY, INC.
RCA INSTITUTES, INC.

VOLUME VIII

MARCH 1947

NUMBER 1

CONTENTS

	PAGE
In Memoriam—Ralph R. Beal	3
Television Receivers	5
A. WRIGHT	
The Present Status and Future Possibilities of the Electron Microscope ..	29
J. HILLIER	
Television High Voltage R-F Supplies	43
R. S. MAUTNER AND O. H. SCHADE	
Determination of Current and Dissipation Values for High-Vacuum Rectifier Tubes	82
A. P. KAUZMANN	
Television Deflection Circuits	98
A. W. FRIEND	
The Pocket Ear	139
J. L. HATHAWAY AND W. HOTINE	
Power Measurements of Class B Audio Amplifier Tubes	147
D. P. HEACOCK	
Relative Amplitude of Side Frequencies in On-Off and Frequency-Shift Telegraph Keying	158
G. S. WICKIZER	
A Coaxial-Line Diode Noise Source for U-H-F	169
H. JOHNSON	
Technical Educational Requirements of the Modern Radio Industry	186
P. L. GERHART	
RCA Technical Papers	192
Contributors to This Issue	194

RCA REVIEW

BOARD OF EDITORS

Chairman

C. B. JOLLIFFE

*Executive Vice President
in Charge of
RCA Laboratories Division*

E. W. ENGSTROM

*Vice President in Charge of Research
RCA Laboratories Division*

D. F. SCHMIT

*Vice President in Charge of Engineering
RCA Victor Division*

I. F. BYRNES

*Vice President in Charge of Engineering
Radiomarine Corporation of America*

O. E. DUNLAP

*Director of Advertising and Publicity
Radio Corporation of America*

H. H. BEVERAGE

*Director of Radio Systems Research
Laboratory
RCA Laboratories Division*

G. L. BEERS

*Assistant Director of Engineering
in Charge of Advanced Development
RCA Victor Division*

A. F. VAN DYCK

*Assistant to the Executive Vice President
in Charge of
RCA Laboratories Division*

H. B. MARTIN

*Assistant Chief Engineer
Radiomarine Corporation of America*

H. F. OLSON

*Research Section Head (Acoustics)
RCA Laboratories Division*

O. B. HANSON

*Vice President and Chief Engineer
National Broadcasting Company, Inc.*

C. W. LATIMER

*Vice President and Chief Engineer
RCA Communications, Inc.*

E. A. LAPORT

*Chief Engineer
RCA International Division*

V. K. ZWORYKIN

*Vice President and Technical Consultant
RCA Laboratories Division*

A. N. GOLDSMITH

*Consulting Engineer
Radio Corporation of America*

S. M. THOMAS

*Assistant Chief Engineer
RCA Communications, Inc.*

I. WOLFF

*Director of Radio Tube Research Laboratory
RCA Laboratories Division*

R. E. SHELBY

*Director of Technical Development
National Broadcasting Company, Inc.*

S. W. SEELEY

*Manager of Industry Service Laboratory
RCA Laboratories Division*

W. F. AUFENANGER

*Superintendent
RCA Institutes, Inc.*

Secretary

GEORGE M. K. BAKER

*Staff Assistant to
Executive Vice President in Charge of
RCA Laboratories Division*

Previously unpublished papers appearing herein may be reprinted, abstracted or abridged, provided credit is given to *RCA REVIEW* and to the author, or authors, of the papers in question. Reference to the issue date or number is desirable.

Permission to quote other papers should be obtained from the publications to which credited.

IN MEMORIAM

RALPH R. BEAL

It is with deep regret that *RCA REVIEW* announces the death of a distinguished Member of its Board of Editors. Mr. Ralph R. Beal, Vice President in Charge of Engineering, RCA Communications, Inc., died suddenly in Doctor's Hospital, New York City, on January 24, 1947.



Mr. Beal was a pioneer in radio, television and electronics. As a field engineer in the early days of radio-telegraph communication, he participated in the first investigations into high-power point-to-point radio transmission and contributed toward the development of the art into a dependable means of worldwide international communication. Later, as Research Director of the Radio Corporation of America, he was given the responsibility

of coordinating research and advanced engineering development activities of RCA and its subsidiaries.

Serving as Research Director from 1934 to 1943, Mr. Beal originated and supervised programs of research which constantly broadened the field of radio products and services. Among major developments during this period were the application of radio-electronics to numerous non-communication purposes, the electron microscope, television, theater television, radar, radio relays, and the opening of the microwave section of the radio spectrum. In 1945, Mr. Beal assumed the position he held at the time of his death.

Mr. Beal served as a member of the Board of Editors of *RCA REVIEW* from the time of its first publication in 1936. Throughout the intervening years, his wholehearted interest and cooperation, friendly counsel and guidance, have contributed greatly to the success of this journal.

TELEVISION RECEIVERS*†

BY

ANTONY WRIGHT

Home Instrument Department, RCA Victor Division,
Camden, N. J.

Summary—The promise of a postwar public television service can be realized only by quantity production and merchandising of receiving instruments. The styling and performance of television receivers has been a subject for conjecture for many years. Artists conceptions of the possible appearance of the home television receiver have appeared in material ranging from the cartoon to the constructive magazine article. In parallel, engineering opinion has been expressed in technical journals and incorporated in the many experimental receivers which have been built and which have included new circuits and other arrangements in an attempt to evaluate commercial acceptance. The receivers discussed in this paper represent up-to-date developments in both electrical and appearance engineering. No doubt the current thinking as expressed in these designs will be modified by public acceptance, competition and by the engineering experience gained in their design and manufacture. These receivers are important because they will serve, along with others, as a basis for the future expansion of television service. Several models are described, followed by a statement of design policy and a detailed discussion of various components.

INTRODUCTION

THE television receivers described in this paper are completely new, incorporating wartime developments and representing substantial improvements over prewar designs both in performance and dependability. They were designed to provide brighter, clearer and steadier pictures.

Satisfactory brilliance has been achieved by the use of improved picture tube screen materials and high second-anode potentials. Clearer pictures are made possible by the use of improved video systems and the smaller spot obtained by high second-anode potentials. Steadier pictures are produced by improved synchronizing circuits which have good interference immunity. In addition, the application of new techniques for noise limiting and stabilization of the deflection generators provides very satisfactory synchronization.

All receivers incorporate a thirteen-channel tuner for maximum frequency coverage. The picture and sound intermediate-frequency

* Decimal Classification: R583.5.

† Presented at the Fall Meeting of the Institute of Radio Engineers at Stamford, Connecticut, on November 14, 1946.

channels operate at 21.25 megacycles for the sound and 25.75 megacycles for the picture. All receivers use electromagnetic deflection.

GENERAL DESCRIPTION

7-inch Table Model: This is a sight and sound table model receiver (Figure 1) equipped with twenty-one tubes including the 7-inch 7BP4 picture tube. A 4- x 6-inch speaker is mounted under the picture tube and is attached to the chassis (Figure 2). The picture tube is installed

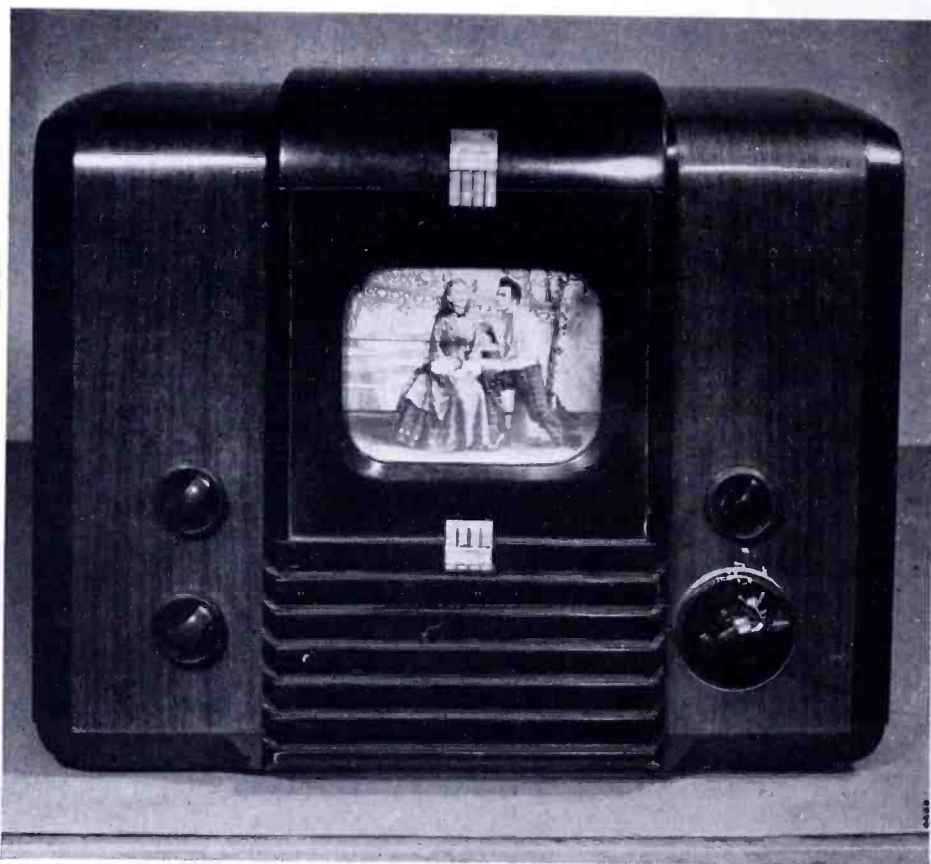


Fig. 1—7-inch table model television receiver.

by removing the safety glass front panel from the cabinet and the tube is then inserted from the front of the cabinet (Figure 3).

The receiver operates on 117 volts, 60 cycles, and is rated at 260 watts. The cabinet outside dimensions are $15\frac{3}{8}$ inches high by 19 inches wide by $16\frac{3}{16}$ inches deep, and it weighs 60 pounds.

There are seven operating controls on the front panel. Eight variable controls are accessible at the rear for setup adjustments.

The maximum brilliance in the picture highlights is 40-foot lam-

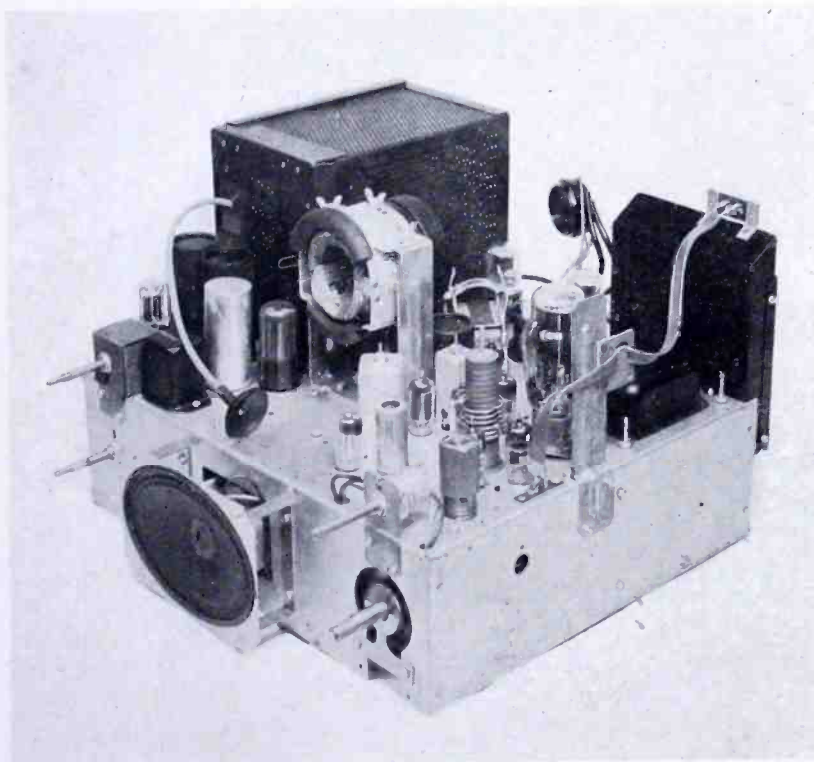


Fig. 2—7-inch table model chassis.

berts which is ample for well-illuminated rooms. The average sensitivity on all thirteen channels is such that a noise-free picture is obtainable from a 500-microvolt signal. The receiver will synchronize well on 150 microvolts and adequate sound is provided for the least usable picture. The schematic diagram for this receiver is shown in Figures 4 and 15 (pages 8 and 16).

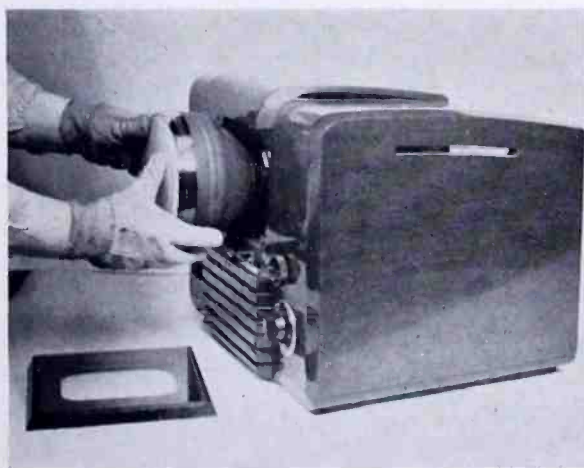


Fig. 3—Installing the picture tube in the 7-inch table model.

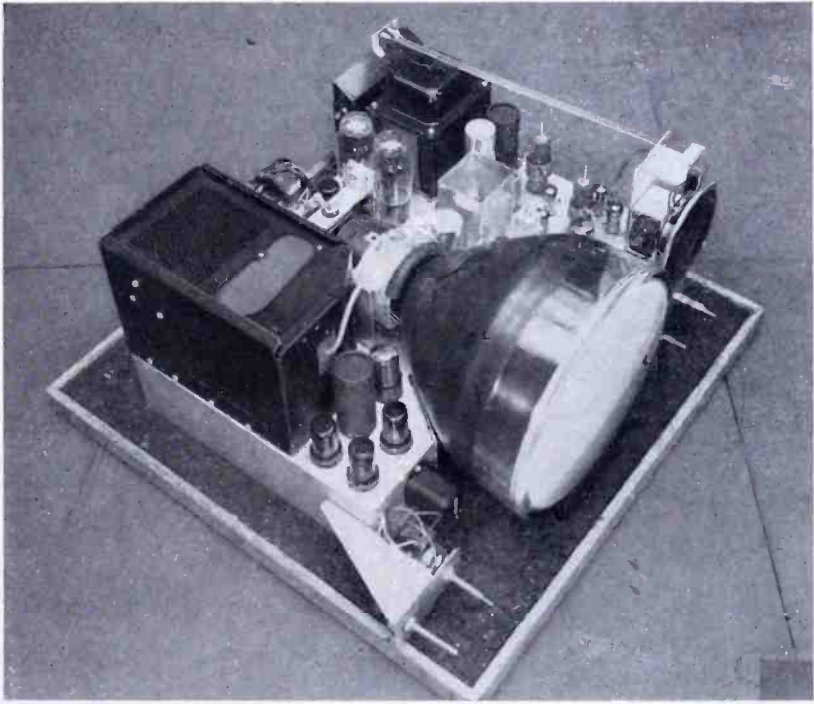


Fig. 6—10-inch table model chassis and tube.

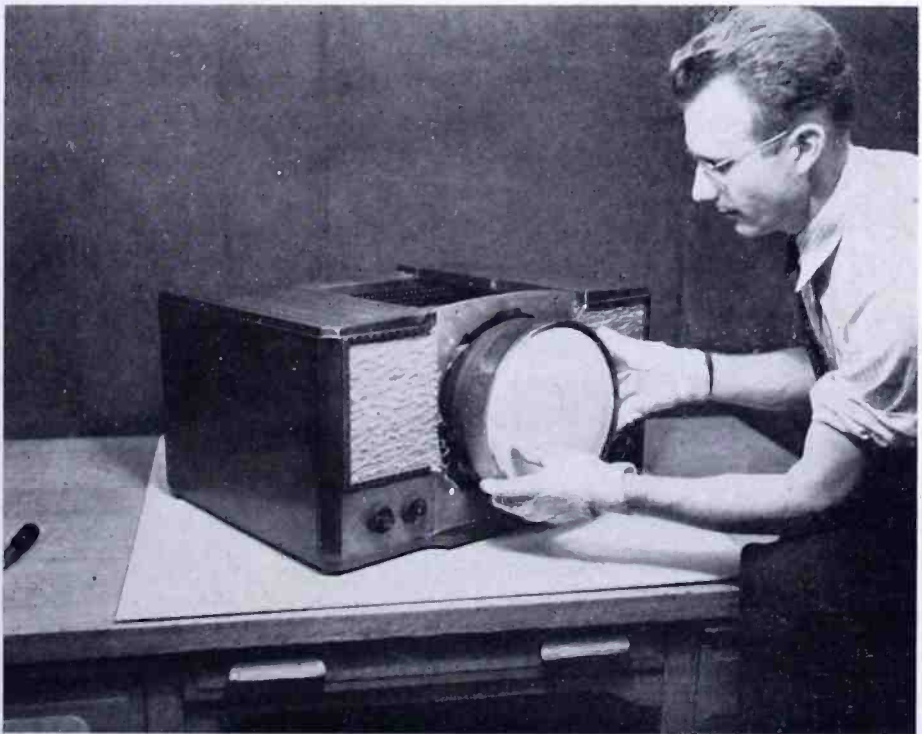


Fig. 7—Installing the picture tube in the 10-inch table model.

10-inch Table Model: This receiver is also a sight and sound table model (Figure 5), with a complement of thirty tubes including the 10-inch 10PB4 picture tube. The picture tube is nested into the chassis (Figure 6) in order to conserve space. The picture tube is installed from the front of the cabinet by removing the safety glass front panel (Figure 7).

This receiver operates on 117 volts, 60 cycles, and is rated at 380 watts. The cabinet dimensions are 14 $\frac{1}{4}$ inches high by 25 inches wide by 18 inches deep, and the weight of the receiver with tubes is 85 pounds.

Seven operating controls are provided, and nine adjustable controls are located at the rear of the chassis for setup adjustments.

The maximum brilliance in the picture highlights is 60-foot lamberts with an area contrast ratio of 90 to 1. The average sensitivity on all thirteen channels will provide for excellent entertainment with a 150-microvolt signal. Noise free pictures are obtained at 500 microvolts. The picture will synchronize well on a 50-microvolt signal. This receiver features an automatic horizontal hold control. The schematic diagram is shown in Figure 8.

Television-Radio-Phonograph Combination Console Model: This instrument is the complete home entertainment unit (Figure 9) having, in addition to television, an AM-FM* and short-wave radio, and a roll-out type phonograph record changer. A record storage compartment is also provided in the cabinet.

The television chassis is the same basic model used for the 10-inch table model to which the feature of automatic gain control has been added.

The radio receiver has eleven tubes, seven of which are on the operating chassis, the other four being used for the audio amplifier and radio power supply and mounted on a separate chassis. The three chassis are shown in Figure 10. The radio chassis is mounted on a tilt panel and the record changer is a roll-out device which can be loaded and set into operation within the complete enclosure of its compartment. When not in use, each or all of the units can be concealed behind doors which are provided for this purpose. Figure 11 (facing page 12) is the schematic diagram for the television receiver circuits.

Projection-type Television-Radio Combination Console Model: This is a large screen projection-type television receiver, and also includes AM-FM* and short-wave radio receiver, which is mounted on a tilt-out panel (Figure 12). The complete receiver employs forty-eight

* Amplitude modulation and frequency modulation.



Fig. 9—Television-radio-phonograph combination console model.

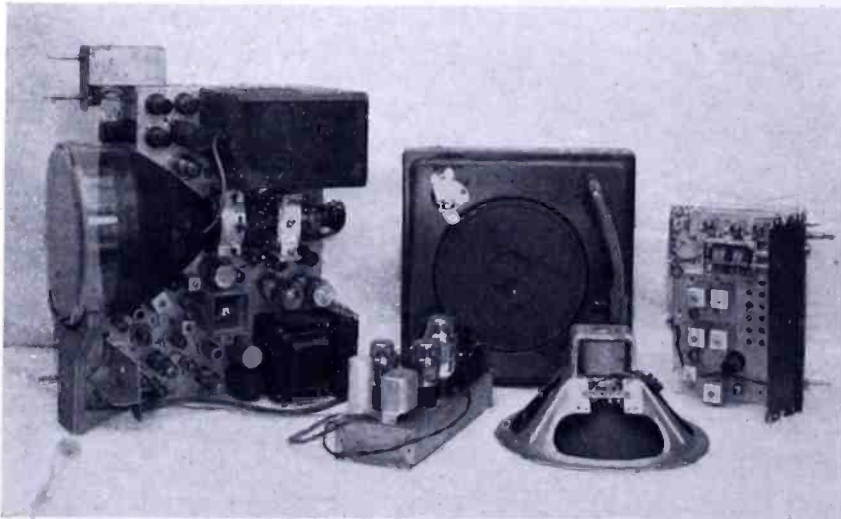


Fig. 10—Combination console model chassis equipment.

tubes including the picture tube. Of this number, eight are used for the radio, and four are used in the common audio amplifier. The receiver operates on 117 volts, 60 cycles, and is rated at 500 watts.

There are six operating controls for television and five for radio. The radio volume control is used for television sound.

The picture size is 15 inches x 20 inches obtained by the magnification of the image formed on the screen of a 5TP4, 5-inch picture tube. A magnification of approximately six times the original image is obtained by the projection optical system. Figure 13 is a photograph

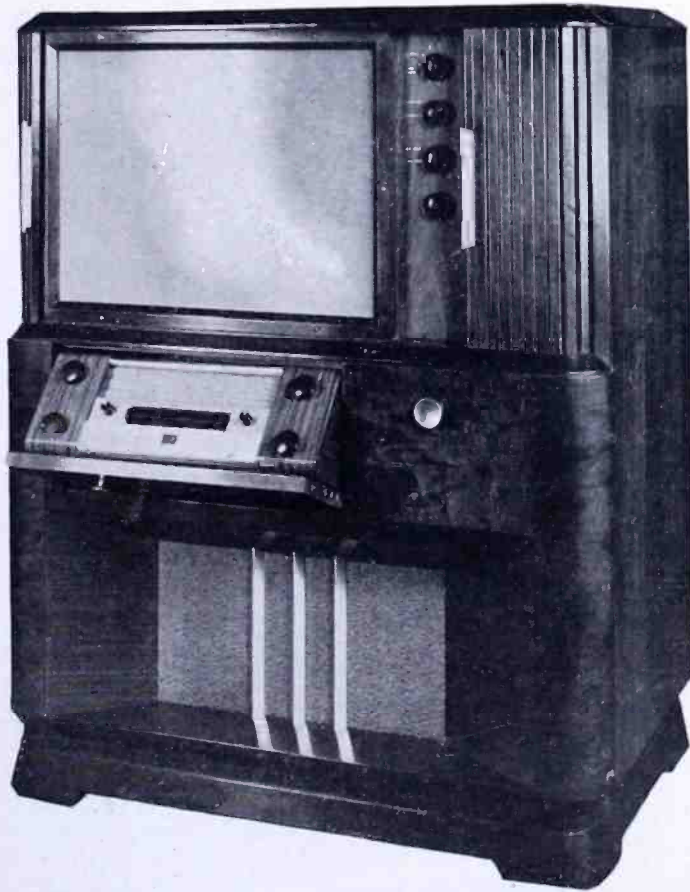


Fig. 12—Projection-type television-radio combination console model.

of the elements of this optical system. From left to right, these elements are:

- (1) the optical barrel,
- (2) the correcting lens,
- (3) the spherical mirror, and
- (4) the 45-degree mirror.

The viewing screen and the 5TP4 tube are in the background. A

complete analysis of this optical system is included in the literature.¹

It is necessary to apply 30 kilovolts to the second anode of the picture tube in order to obtain maximum picture brilliance. With this voltage, the picture brilliance in the highlights is 50-foot lamberts. This is adequate for viewing in a well illuminated room.

The instrument houses five separate chassis in addition to the optical system. A photograph (Figure 14) shows these chassis. From left

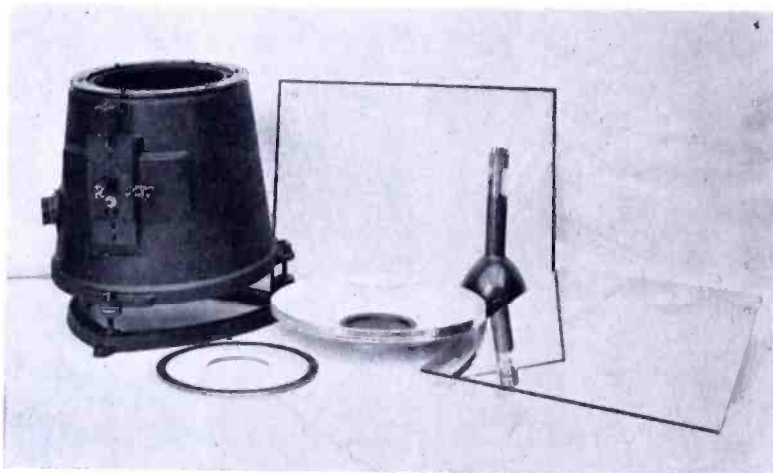


Fig. 13—Projection optical system elements.

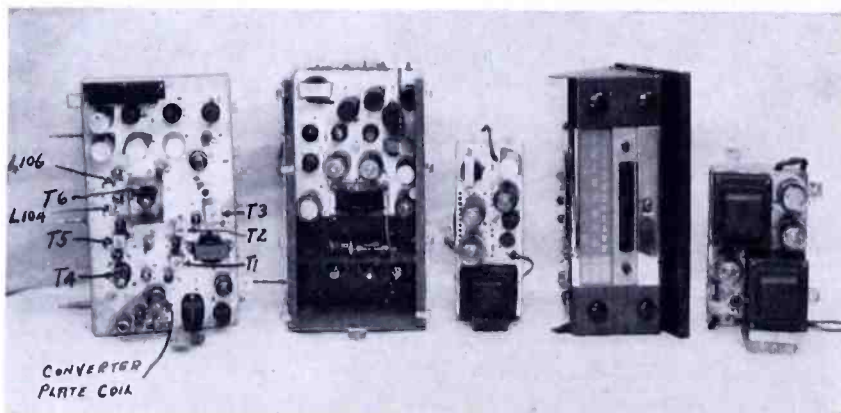


Fig. 14—Projection-type television-radio combination console model equipment.

to right, they are:

- (1) the television radio- and intermediate-frequency video chassis,
- (2) the high-voltage and deflection chassis,
- (3) the radio power and audio unit,

¹ I. G. Maloff and D. W. Epstein, "Reflective Optics in Projection Television", *Electronics*, December, 1944.

- (4) the radio chassis, and
- (5) the television power supply.

The electrical performance of this instrument is similar to that of the combination console model.

TELEVISION CIRCUIT DESIGN

A. Design Policy:

Postwar television product design began during the year 1945. Fortunately, the same group of engineers who, during the war years, had the assignment of designing television systems for the Armed Forces, were at that time available for home television receiver design. Thus, the television experience of the war years was applied to peace time applications. In addition, the considerable experience with prewar television was, of course, invaluable. With this background, it might be assumed that the task was not one of great magnitude. However, by using the performance and cost of the prewar sets as a yardstick and also considering the new Federal Communications Commissions' frequency allocations for television, many new problems were encountered.

It was found that completely new designs for the radio- and intermediate-frequency systems were necessary. In addition, the wide-angle deflection circuits for the new short picture tubes presented some difficult problems. It was also common knowledge that the synchronizing circuits used in previous designs were far from adequate and much work was being carried out on refined circuits for providing better synchronizing stability and ease of control to remove the jitter from television pictures. Another big problem was automatic volume control, now called automatic gain control (AGC) in television. The AGC circuits had been removed from some of the prewar receivers by a field operation because the AGC circuits set up when interference occurred and destroyed the picture information. For this reason, it was obvious that the development of an interference-immune AGC system was imperative for use in deluxe receivers.

Above all, in a period of rising prices, the retail cost of the television set had to be held to a minimum if television was to be a success. Finally, a vital concern was the dependability of postwar television products. Quality and dependability had to be such that the television receivers could be sold on a one year guarantee basis. This guarantee is now given under the terms of an installation contract for which a nominal charge is made and the guarantee covers the replacement of any defective part, including the picture tube, should a failure occur

within one year from the purchase date. This policy is designed to encourage the public's confidence and will no doubt help in fostering the rapid growth of the television art.

B. The Radio-frequency Tuner:

This unit functions to select the desired picture and sound carrier signals, amplifying and converting these signals to provide at the converter plate, a picture intermediate-frequency carrier at 25.75 megacycles and a sound carrier at 21.25 megacycles. A thirteen-channel selector switch is operated in continuous rotation and has no stop. Thus, the switch can be turned from channels one to thirteen in either direction.

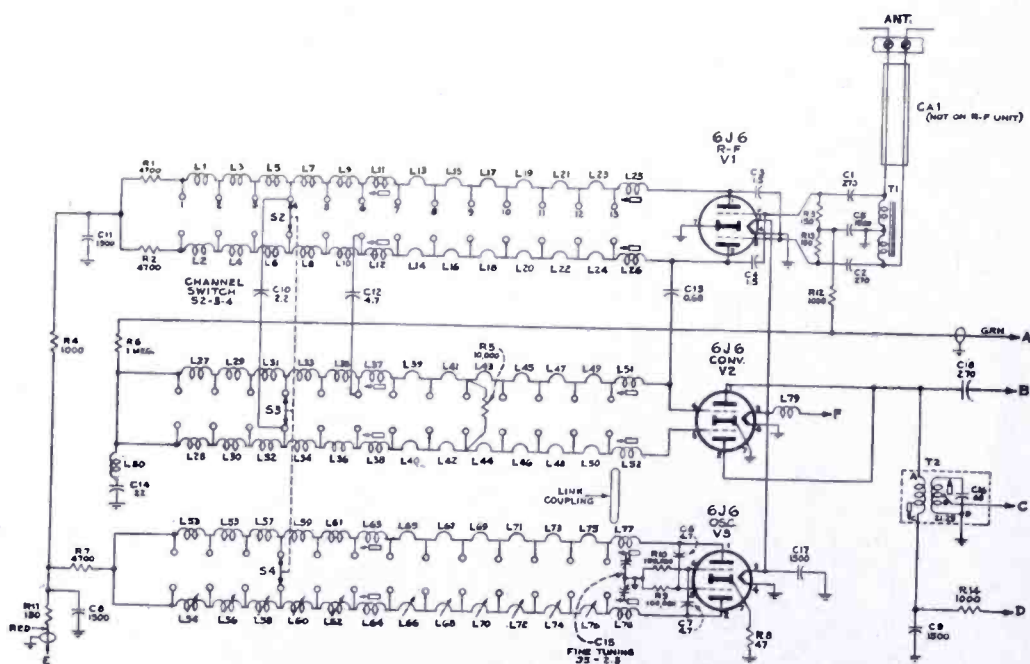


Fig. 15—Radio-frequency tuner circuit.

Referring to the circuit diagram (Figure 15), it will be seen that three 6J6 double triode tubes are used for the functions of radio-frequency amplifier, converter, and oscillator. The grids of the converter and the plates of the oscillator are connected to pairs of series inductances terminated at the far ends. These pairs of series inductances may be considered as a one-quarter wave section of a balanced transmission line. The resonance of the line is determined by the position of a shorting bar which connects to opposite switch points located at thirteen points along the line. The shorting bar is moved

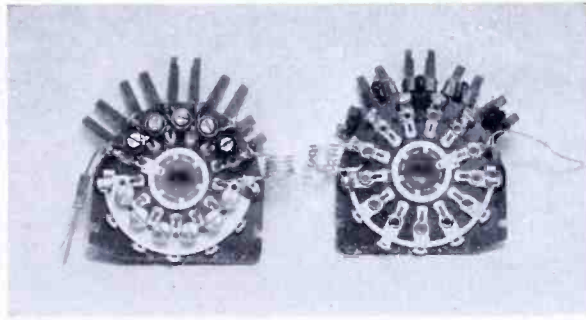


Fig. 16—Switch wafers.

along the line by the thirteen point switch and is properly located by the operator who selects the desired channel number. The lines are constructed of first, a variable inductance for channel thirteen, then a metal strap which is tapped by the switch contacts for channels 12 to 7, followed by an adjustable coil which provides the change from channels 7 to 6, and finally a series of figure-eight coils which are located between the contacts of channels 6 to 1. Thus, incremental inductances or length of line are added to the initial channel 13 inductance as the switch rotates from 13 to 1.

Figure 16 shows the switch wafers with the coils and straps. The wafers are for oscillator and radio-frequency sections viewing from left to right. The converter circuits are located between the heterodyne

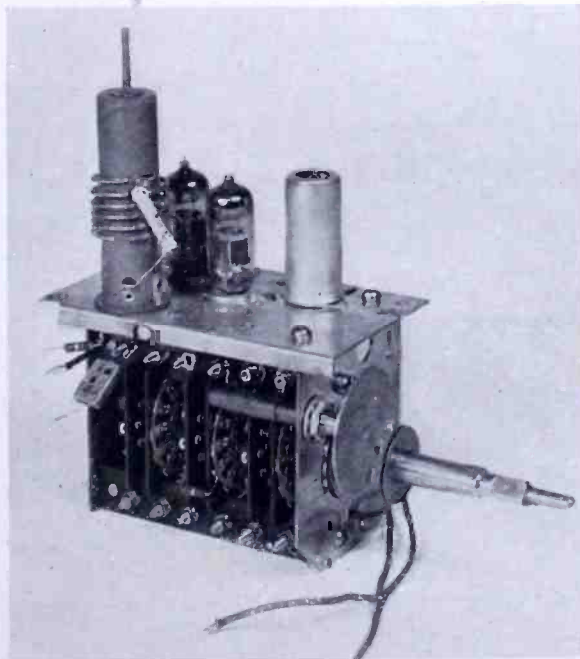


Fig. 17—Radio-frequency tuner assembly.

oscillator and the radio-frequency circuits. This location is chosen to provide signal and oscillator coupling to the converter. The coupling is augmented by the link shown in the schematic which is necessary to provide a reasonably uniform oscillator injection voltage to the converter over the complete tuning range.

Figure 17 presents the complete radio-frequency unit assembly which includes a converter plate coil and a sound carrier absorption trap. This unit is the tallest structure located on the rear of the chassis. The controls project from the front of the unit and are arranged on a dual knob for operation. The main shaft rotates the selector switch and the concentric shaft operates the oscillator vernier through a disc drive. The vernier adjustment varies a small capacitor which is electrically positioned across the oscillator lines to provide a plus or minus frequency variation of approximately one-half of one per cent. This, of course, requires that the oscillator frequency for each channel be accurately set.

The input circuit has an impedance of 300 ohms and the gain from the antenna to the converter grid is ten. Signal-to-noise measurements indicate a 12- to 14-decibel level above thermal noise. Considerable effort was spent on the reduction of oscillator radiation. This unit has at least 100 times less radiation than prewar receivers.

C. Picture and Sound Intermediate-Frequency Amplifiers:

The sound system is a conventional two stage amplifier followed by a balanced discriminator. It should be noted by reference to the schematic (Figure 8) that the signal input to this amplifier is taken from a tap on the first sound trap which is an absorption circuit coupled to the converter plate coil.

The picture intermediate-frequency amplifier departs considerably from the conventional coupled intermediate-frequency amplifiers. The function of this section of the receiver is to amplify a wide band of frequencies and to extract the video information from the intermediate-frequency carrier. To obtain sufficient gain and bandwidth, four stages of picture intermediate-frequency amplification follow the converter. The feature of this amplifier system is the use of staggered tuning. The converter plate and each successive stage utilize one tuned circuit only, but each stage is tuned to a different frequency. In addition, each coil is properly loaded by selecting the required plate or grid resistance so that its effective Q is properly adjusted to have the product of all the stages produce the desired response curve.

Figure 18 shows the relative gains and selectivities of the quintuple combination, the dotted curve indicating the approximate overall selec-

tivity of such a system. With this arrangement, it is possible to obtain approximately 80 per cent of the gain obtainable with conventional coupled circuits with single side loading.

The advantages of staggered tuning over coupled circuits are:

- (a) *ease of alignment*—Each stage may be aligned to its center frequency without regard to the others using ordinary peaking technique,

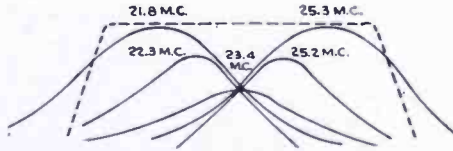


Fig. 18—Selectivity of stagger tuning.

- (b) *stability*—The system is less subject to regeneration since no two circuits are resonant at the same frequency,
- (c) *low cost*—No shielding or difficulties due to coupling; a single coil is more economical than a coupled transformer, and
- (d) *space saving*—A small single coil with no shielding between two tubes conserves space.

It is believed that these advantages compensate for the 20 per cent loss of optimum gain.

Figure 19 gives the schematic diagram of the circuit. It will be noted that four absorption-type traps are used. The converter plate trap is tuned to the accompanying sound. The first intermediate-frequency plate trap operates to attenuate the adjacent sound. The second intermediate-frequency plate trap is tuned to the adjacent picture and the cathode trap is placed in the fourth intermediate-frequency cathode and operates to reflect a high impedance in the cathode at the accom-

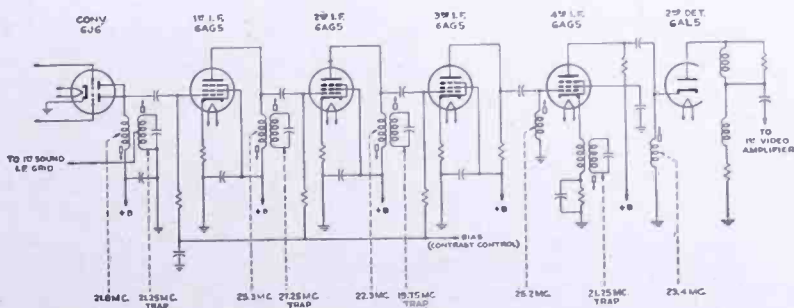


Fig. 19—Intermediate-frequency amplifier circuit.

panying sound intermediate frequency. This, of course, provides degeneration at this frequency, and it is of interest that the maximum attenuation is limited to the gain of the associated tube.

The schematic shows that the converter plate and the first intermediate-frequency plate are tuned to approximately the same frequency. This is because the addition of the traps to the circuit modifies the preceding theory so that, in practice, this arrangement of frequency becomes necessary in order to obtain the desired overall selectivity characteristic shown in Figure 20.

The overall schematic shows that the contrast control operates to vary the bias on the radio-frequency control grid as well as the first,

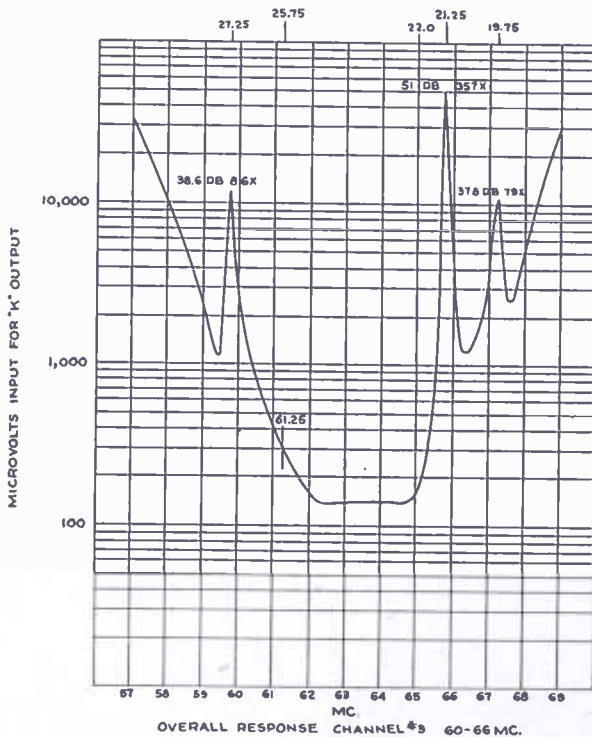


Fig. 20—Overall selectivity characteristic.

second, and third intermediate-frequency amplifier grids. This is in effect a manual gain control and is operated to provide the correct video output level from the second detector. The second detector is a conventional half-wave rectifier connected to provide the correct polarity of signal, i.e., synchronizing negative to the video amplifier.

D. The Video Amplifier:

Two stages of video amplification are used in the receivers. It is considered advantageous to use two tubes because the first amplifier tube can also be used as a grid cut-off limiter. With this arrangement,

the signal on the first video grid must be such that black information is negative in polarity with the synchronizing signal driving toward grid cutoff. The first amplifier tube has a sharp cut-off characteristic and its acceptance is limited to provide the correct voltage level required to produce adequate voltage at the output of the amplifier to drive properly the picture tube grid.

It is considered that 60 volts peak-to-peak video signal is ample for all picture tubes. The video amplifier used has an overall gain of thirty times so that the input voltage to the first grid is two volts peak to peak. Signals in excess of this voltage drive the first amplifier grid to cutoff and this excess signal will not appear at the first video amplifier tube output. Figure 21 shows the circuit of this amplifier and the video signal in its correct polarity at the input of the system. The sharp pulses extending beyond the synchronizing signal level represent noise pulses and if they are not limited, they will affect the synchroniz-

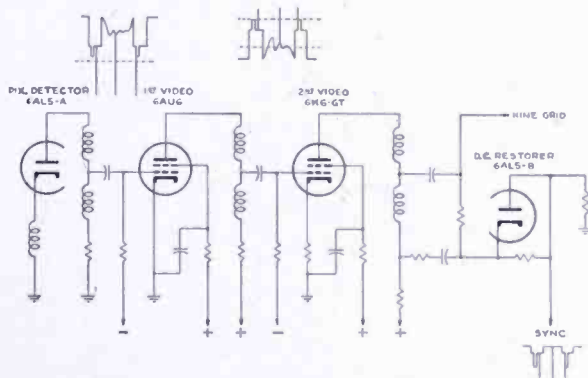


Fig. 21—Video amplifier circuit.

ing separators and the deflection generators, thus causing a visible disturbance in the picture. It will be noted that the level of the noise signal is reduced at the first video amplifier plate, the reduction being obtained by grid cutoff as described. It is obvious that a tolerance is required in the cut-off level so that the synchronizing signals are not cut off, and it is also true that limiting will not be as effective with black pictures as with white because the system is alternating-current coupled. However, the automatic synchronizing system used in these receivers can tolerate considerable interference in the signal so that tight limiting to the peaks of the synchronizing signal is unnecessary. The video output stage uses a 6K6GT tube which will deliver 120 volts peak-to-peak without distortion or saturation.

The signal output of the second detector swings out from a zero reference level and the blanking or black level is maintained regardless

of scene. Because the video amplifier is alternating-current coupled, an alternating-current axis is introduced and the signal swings around this axis. If no correction is applied, the background level adjustment for an all black scene will not be satisfactory for an all white scene. Therefore, a direct-current restorer circuit is introduced which corrects the picture tube grid bias with the changing scenes. The direct-current restorer circuit uses the second half of the 6AL5 double diode, the first half being used for the second detector. In addition, the direct-current restorer circuit provides partially separated synchronizing signals which are applied to the input to the synchronizing signal chain.

E. The Synchronizing Chain:

The partially-separated synchronizing signal appears negative at the input to this system. To remove completely the remaining blanking

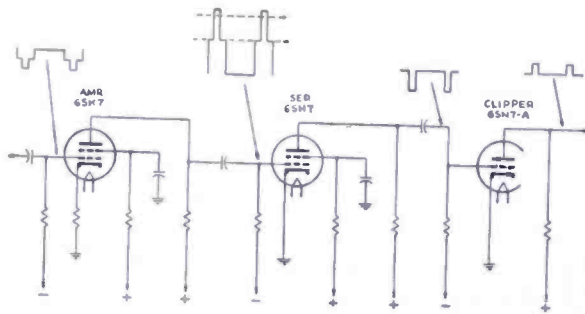


Fig. 22—Synchronizing amplifier circuit.

and video information, the signal is first amplified and inverted by the 6SK7 remote cut-off pentode (Figure 22). This tube is used because the level of the signal on the kinescope grid will vary with the carrier signal strength or the setting of the contrast control. Therefore, the tube must have a wide signal acceptance range which will preclude the possibility of the removal of the desired synchronizing information by grid cutoff. The amplified signal is applied to the grid of the 6SH7 synchronizing separator tube which is biased to cutoff so that only the desired information appears at the separator plate. This separated synchronizing signal is then clipped by the following 6SN7 triode tube to provide a constant synchronizing amplitude with a peak-to-peak video signal variation of from six to sixty volts on the picture tube grid. A properly functioning receiver will synchronize with any video signal within the above limits.

F. Horizontal Automatic Hold Control:

This circuit is unusual. Its functions to synchronize the picture in the horizontal direction. Its features are automatic operation and good interference immunity. The 6K6GT tube in Figure 23 is an extremely stable sine-wave oscillator operating at 15,750 cycles per second. In operation, the phase of the sine wave and the synchronizing pulse is compared. A phase change will produce direct-current information which is applied to the grid of the 6AC7 reactance tube which controls the frequency of the Hartley oscillator.

A double diode 6AL5 tube is used as a comparator, functioning in much the same way as a frequency-modulation detector. The plates of this tube are connected to a center-tapped coil which is inductively coupled to the coil of the Hartley oscillator. Referred to the center tap,

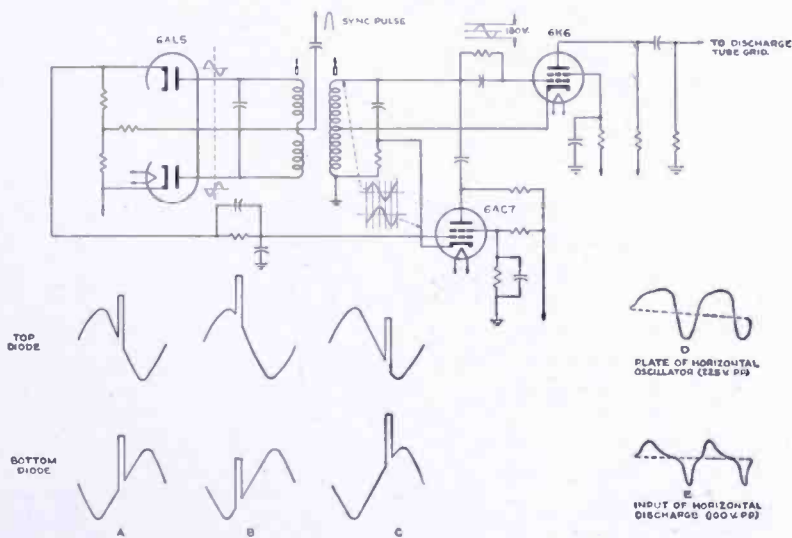


Fig. 23—Automatic frequency control synchronizing circuit.

sine-wave voltages of equal amplitude and opposite phase are applied to each of the diode plates. The synchronizing pulse is applied to the center tap and consequently this voltage appears at the same phase on each diode. When the synchronizing pulse and sine wave are in phase, as shown in Figure 23(A), there will be zero voltage at the output of the discriminator. If the phase of the pulse changes with respect to the sine wave, as shown in Figure 23(B), then the top diode will produce more voltage output than the bottom diode. In Figure 23(C) the reverse condition exists. Obviously, the direct-current output of the discriminator will run from positive through zero to negative depending on the phase relation of the pulse and the sine wave. In this way, the necessary control information is produced.

The 6AC7 control tube operates to produce a reactive plate current by virtue of the cathode input voltage obtained from a resistor in the tank circuit of the Hartley oscillator. This cathode connection produces a 90-degree phase shift of the sine wave as it is applied to the control grid. If the transconductance (G_m) of this tube is changed, its reactive plate current will change and because this reactive current is coupled into the oscillator tank circuit, the oscillator frequency will change accordingly. Thus, when the phase of the oscillator differs from the phase of the synchronizing pulse, direct-current information from the discriminator will bring the oscillator into correct phase. The output of the discriminator is fed to the control tube through a filter network which removes interference pulses and other misinformation which would otherwise affect the frequency of the oscillator. The circuit will maintain proper synchronism under severe interference conditions.

In order to obtain a pulse from the sine wave oscillator, which is necessary for the operation of the discharge tube, the oscillator functions as follows:

The oscillatory action takes place between the screen grid and the cathode of a 6K6GT tube. The peak-to-peak sine wave voltage on the oscillator grid is approximately 130 volts. This grid swing produces a wave shape on the plate which is differentiated by a resistance-capacitance network. The wave before and after differentiation is shown in Figures 23(D) and 23(E). The positive portion of the differentiated wave operates the discharge tube satisfactorily.

G. Horizontal-Deflection and High-Voltage Circuits:

Horizontal-deflection and high-voltage circuits are shown in Figure 24. This diagram shows the wave forms of the horizontal-deflection and high-voltage generators. To provide adequate deflection, a 6BG6G (807) type tube is used for a generator. The plate of this tube is connected to the primary winding of the deflection transformer and the sawtooth voltage output from the discharge tube is applied to its grid.

The negative pulse at the start of the sawtooth is produced by high peaking which prevents the discharge capacitor from being discharged completely by its associated tube. This negative pulse is needed to keep the 6BG6G tube cutoff during the retrace period when the voltage on the plate rises to a high positive value. The voltage on the grid produces a sawtooth of current in the plate. Since the plate load is inductive, a sudden change of current will result in a high inductive pulse. The sawtooth of current during the trace period stores energy in the yoke in the form of a magnetic field which is released rapidly during

retrace, producing the high-voltage pulse. The sudden ceasing of plate current caused by the cutoff of the tube during retrace causes the circuit to oscillate. One way of producing rapid retrace is to permit a deflection system to oscillate for a period of one-half cycle after which the oscillation is damped by the action of a damper tube.

A 5V4G tube is used for damping in this circuit. The wave forms at A, B, and C indicate various degrees of damping. In Figure 24(A) the damping is very poor and would produce irregularities in the rate of scan. At B the damping is fair and the rate of scan would be too rapid at the start producing a stretch on the left of the picture. At C the damping is perfect with the voltage remaining uniform during the trace period. This constant voltage across the yoke results in a linear sawtooth of current as shown at E.

The B^+ voltage is supplied through the 5V4G to the 6BG6G plate. In this connection, the rectified voltage obtained from the damper

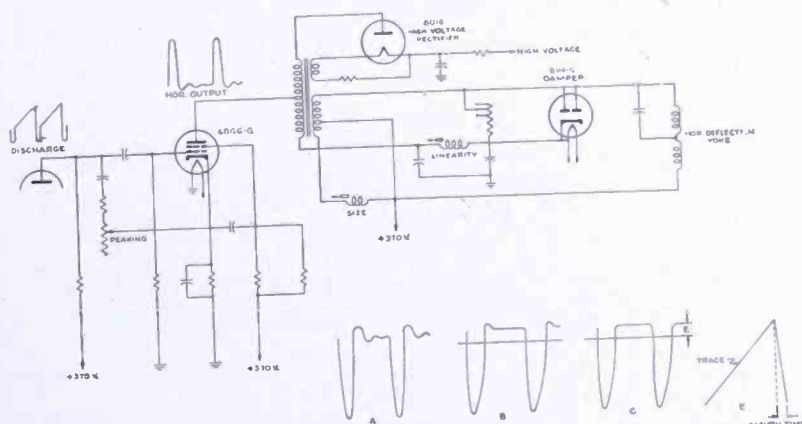


Fig. 24—Horizontal deflection circuits.

operation is added to the B^+ voltage. In this particular application, the plate of the 6BG6G is raised 50 volts by use of the B^+ boost providing more deflection and high voltage than can be obtained without the boost. The horizontal output transformer shown schematically in Figure 24 has four windings. The windings are arranged to provide safe operation at the high voltages involved. The secondary winding which has the lowest potential is wound next to the core. The primary winding is wound on top of this and then the high-voltage winding, which is a continuation of the primary, is wound on the outside. Thus, the potentials are safely distributed over the windings and proper spacing is obtained for these potentials.

The operating second anode potential is obtained by stepping up the pulse from the primary of the transformer by auto transformer

action. This high potential pulse is used to charge a 500-micromicrofarad capacitor through the 1B3-GT/8016 rectifier. This rectifier is heated by the fourth winding of the transformer. The heater winding consists of two turns of polyethylene covered wire which are placed adjacent to the other three windings. The beam is extinguished after each trace and the pulse occurs during retrace. The charge on the small capacitor is sufficient to supply 200 microamperes for the scanning period of one line which is 53 microseconds. The voltage under load is 9000 volts (direct current).

H. Picture Tube Accessories:

The 10BP4 is a magnetically deflected and focused kinescope requiring a deflection yoke and a focus coil for proper operation. In addition, an ion trap has been developed to prevent the discoloration of the screen caused by ion bombardment. Figure 25 shows the picture tube accessories—from left to right: the deflection coil, the focus coil, and the

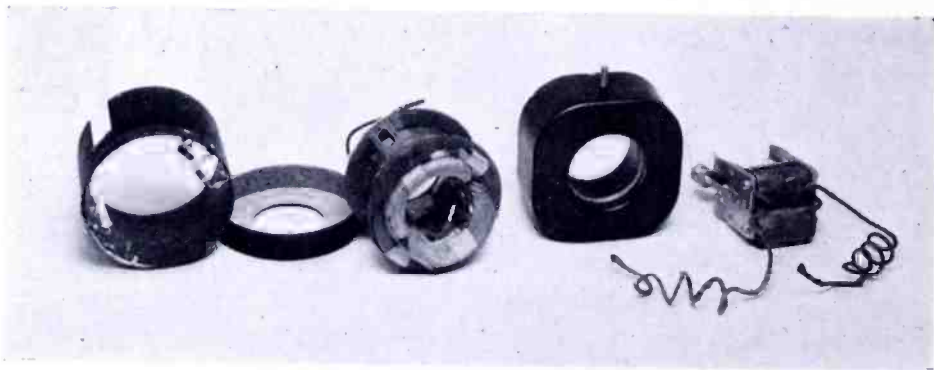


Fig. 25—Picture tube accessories.

ion trap magnet. The deflection coils at the center are designed for high efficiency deflection and low cost in manufacturing. The coils are self-supporting and lock into each other when assembled. No adjustment is required after they are assembled. The magnetic focus coil in the center is completely enclosed in a metal shell and the correct field is obtained through a small gap around the inside of the pole structure by an electrical adjustment of the current through the coil.

The ion trap magnet at the right is unusual and deserves some explanation of its operation because of its recent introduction. Both electrons and ions are emitted from an electron gun. While the electron beam can be deflected by an electrostatic or magnetic field, the ion stream will only be deflected by an electrostatic field. Thus, in an

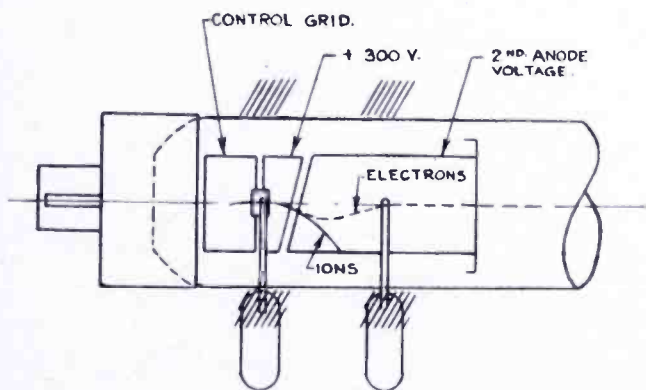


Fig. 26—Ion trap operation.

electromagnetic deflection type tube, the ion stream will impinge on the center portion of the screen and cause objectionable discoloration. Since a positively charged plate will attract both ions and electrons, it is possible to build the gun with such a plate and then correct the electron beam by a magnetic field. In this way, the ions and electrons are separated and the ions are trapped within the gun structure. Figure 26 shows the path of the ions and also the corrected path of the electrons. The correction is obtained by the proper strength and location of magnetic fields.

The ion trap magnets are designed so that they may be properly placed by adjusting the position of the structure on the neck of the

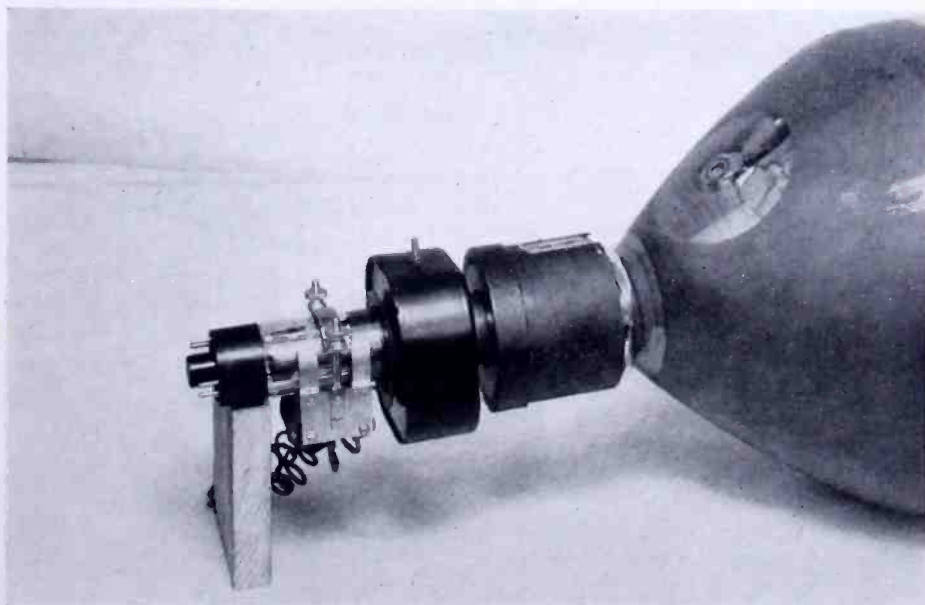


Fig. 27—Deflection components.

picture tube. This adjustment is non-critical and is first made by inspection where the rear magnet poles are placed over two small flags attached to the gun. This preliminary positioning of the magnet coils insures some illumination of the screen and the final adjustment is made by observation of the screen while the magnet is moved forward or backward with a slight rotational movement, the final position is that which gives maximum illumination of the screen. Two thumb-screws are then tightened to lock the assembly securely to the neck of the picture tube.

Figure 27 shows the deflection components mounted on the gun of the picture tube. The deflection coil is mounted next to the bulb, the focus coil in the center, and the ion trap is fastened at the rear.

PRESENT STATUS AND FUTURE POSSIBILITIES OF THE ELECTRON MICROSCOPE*

BY

JAMES HILLIER

Research Department, RCA Laboratories Division
Princeton, N. J.

Summary—A brief and general description of the applications and accomplishments of the electron microscope is given. It is shown that at present the electron microscope is accepted as a scientific tool, capable of providing visual images of solid material at magnifications as high as 100,000 (i.e. with a resolving power of 20 \AA^\dagger). It is further shown that in the laboratory the resolving power of the electron microscope has been increased by a factor of 2. The remainder of the paper discusses the problems involved in further increasing the resolving power of the electron microscope. The usual suggestions with regard to improving the objective lens by reducing aberrations are discussed and some of the limitations of the methods are described. It is concluded that the possibility of improving the performance of the electron microscope by work in this direction is not too promising. It is pointed out that a gain by a factor of 3-4 might be obtained by the use of protons instead of electrons, provided the formidable technical difficulties involved in that approach can be overcome.

I. INTRODUCTION

IN the past fifteen years the electron microscope has been developed from a theoretical possibility into a practical reality. Still more recently a new science—Electron Microscopy—has begun to grow around the use of this new instrument. Regardless of the standard of comparison, the development of the instrument and its associated science have been extremely rapid, so rapid in fact, that it has often been difficult to maintain a true perspective regarding the status of those developments. It now appears that research on the electron microscope as an instrument has reached a critical point where a true perspective is essential for the continuance of a rapid rate of development. An attempt will be made in this paper to aid in the formulation of such a perspective through the presentation of a coordinated picture of the present status of electron microscopy and an evaluation of its future possibilities.

The electron microscope is now recognized as being an instrument

* Decimal Classification: 621.375.604.

† \AA —Angstrom Units ($1 \text{ \AA} = 10^{-8}$ centimeters).

for delineating the *geometrical* structure of microscopic objects. In other words, it provides information regarding the shape, size and arrangement of the components of extremely small objects. It is now understood, though not always appreciated, that information beyond this must be obtained by the execution of properly planned experiments which usually involve the use of other equipment and techniques.

In the field of chemistry are some of the most direct applications of the electron microscope. While most of the properties of chemicals under investigation are determined by other techniques, some, such as particle size, size distribution, shape, structure and organization in the size range between 20,000 Å and 50 Å can be determined accurately only by means of the electron microscope. Thus, there are some aspects of an extremely wide range of chemical problems in which the electron microscope is of great value.

The applications in chemistry can be divided into three rather general categories. The first includes studies of specimens in which there is a degree of organization such as in diatoms, cellulose and other fibers, vulcanized rubber, etc.

In the second category are those investigations which involve the study of a process. This undoubtedly will eventually be the most important application of the electron microscope in chemistry, though at present the attack on this type of problem is only slightly more than initiated. Nevertheless, the beginnings that have been made are extremely promising. Preliminary studies made on the developing processes in photography have brought to light some new and unsuspected phenomena. Some work has been started on the growth of colloidal particles by means of which some fundamental theories on reaction rates are being verified.

The third category which has been and still is the most important application of the electron microscope in chemistry is the determination of particle size, particle shape and size distribution in powdered solid chemicals. In many industrial problems involving powdered chemicals the size, shape and size distribution are the only important properties of the material which could not be determined accurately by indirect methods. It is obvious, therefore, that the electron microscope should find an immediate and widespread application in this field. One of the first problems of this nature was in the correlation of particle size distribution in carbon blacks with their properties as reinforcing agents in rubbers or as pigments in printer's inks. Many other paints and pigments are especially adapted for investigation with the electron microscope—titanium dioxide, zinc oxide, iron oxide, and Azo blue—are only a few of these. Various types of clay have been

the subjects of many intensive investigations. Dusts and smokes have been studied in connection with industrial health problems. Many well-known colloids have been examined and deductions of the colloidal chemists have been verified. Metallic powders used in powder metallurgy have been examined before and after sintering. In brief, any chemical which is produced in the form of a powder may be examined with the electron microscope. The examination can be expected to be profitable whenever the size or shape of the particles influences the final use of the chemical.

In metallurgy the application of the transmission electron microscope has been made possible by the development of the replica technique. Having this technique the actual application is simply an extension in terms of resolution of the very familiar use of the metallographic microscope. Thus, in metallurgy it is to be expected that the electron microscope will find applications as widespread as those of the metallographic microscope at the present time. It is also to be expected that many of the established polishing and etching techniques will be found adequate for electron microscopy. On the other hand, the fact that the electron microscope has a much greater depth of field than the metallographic microscope, in addition to its greater resolving power, leads to the possibility of examining, at high magnifications, surfaces which no longer need to be almost ideal planes. While this is being done in a few laboratories, metallurgists as a group have not accepted the replica technique. Unfortunately, in the early stages of its development it earned the reputation of being an extremely tricky and unreliable technique, each method being really successful only in the hands of its originator. Now that replica techniques can be reliable, it will be necessary to overcome the handicap of this reputation before the electron microscope takes its proper place in metallurgy.

The layman and, for that matter, many scientific workers usually associate the microscope with biological research. Such has been the case with the electron microscope, though the most widespread use of the instrument up to the present time has not been in the field of biology. Nevertheless, the possible applications of this instrument in biology are almost without limit, so that as more instruments become available and as the difficulties of specimen preparation are overcome, more in the way of tangible results can be expected. The work already done has been exploratory in nature. Much valuable information has been obtained, though this is not as yet sufficient for an organized presentation.

Many structures in insects and animals are in such a form that they can be examined with the electron microscope without elaborate

preparation. Such objects have included in the past the scales of butterfly wings, the tracheæ of various insects and many membranes which can be easily removed. A long list of bacteria has been examined at high magnifications, and many new morphological details have been observed. Exploratory observations have been made of the effect of antisera, antibiotics and various chemicals on bacteria. All of the filterable viruses which have been isolated have been observed with the electron microscope, thus providing a direct check of the methods used by the biochemists in the studies of these organisms. In the case of the bacteriophages and some animal viruses the existence of rather complex structures has been demonstrated. There is no other known method by which this could have been done. A number of large protein molecules have been observed, though these are still at the limit of resolution of the electron microscope.

In this connection it should be pointed out that all the techniques which have been developed for the examination of biological material by means of the light microscope have been developed in the presence of the limitations of that instrument. For instance, an imbedding material which has a crystal structure somewhat beyond the resolving power of the light microscope may be ideal for that instrument but will be useless for electron microscope work. Distortions which occur on air-drying of bacteria or large viruses have never bothered the light microscopist for the simple reason that he normally could not see them. However, the electron microscopist can see them. In fact, most of the published electron micrographs of these subjects have shown the effects of such drying. These are just two examples to indicate that it is necessary to examine the problem of specimen preparation for the electron microscope from the point of view of that instrument and that the work that is done on biological material will not have great value until such methods of preparation are worked out. The foremost workers in this field are well aware of this and have taken the trouble to study their techniques of preparation.

Even from a survey of the uses of the electron microscope as brief as that given above it can be seen that the number of scientific problems to which that instrument can be applied is almost without limit. A more complete survey would show that in the short period of its existence the electron microscope has been accepted as a practical and useful tool by a large number of scientific workers.

The purpose of the present paper is not, however, to make an exhaustive study of the present value of the electron microscope to science. That value which exists today is the realization of the aims of the research work carried out by electron microscope laboratories

several years ago. Instead, the intention is to attempt an evaluation of the present status of the electron microscope, using the most recent results of research on the instrument. It is obvious that the discussion will have to center on the electron microscope itself since there is little basis on which to predict the effect of these recent developments on the science of its use—electron microscopy. On the other hand, there are now sufficient data available to permit a fairly accurate evaluation of the trend of development of the instrument.

Much of the discussion which follows concerns the difficulties which are now being encountered in the development of the electron microscope. *It must be emphasized that the discussion refers only to the use of the electron microscope at resolving powers better than 20 Å and in no case is it to be inferred that the difficulties described apply also to the present and normal use of the electron microscope as a scientific tool.*

II. THE PRESENT STATUS OF THE ELECTRON MICROSCOPE

Until the present the development of the electron microscope has followed a well defined program. In 1932, M. Knoll and E. Ruska set the pattern for the design of the magnetic electron microscope. Two years later Ruska carried out their design in the construction of an instrument which was the first serious attempt to attain high magnifications. That instrument used a series of simple electron lenses arranged in direct analogy to those in the light microscope. (Actually because a gaseous discharge tube was used as the source, Ruska did not consider a condenser lens necessary. However, when the discharge tube was discarded in favor of a thermionic emitter the condenser lens was introduced. It is interesting to note that at that time the condenser lens was considered essential to obtain sufficient intensity. It was not until some time later that it assumed the same significance as it has in the light microscope—namely, as a means of controlling the conditions of illumination in order to obtain the optimum electron-optical performance of the objective). This instrument also set the pattern for the design of the objective lens which used soft iron pole-pieces to concentrate the field of the exciting coil to a small volume, thus leading to short focal lengths.

The course of subsequent work on the electron microscope has been determined almost entirely by the fact that the theoretical limit of performance of this early microscope system was almost three orders of magnitude beyond that which was actually achieved in the initial work. Since fundamental improvements which would have circumvented the purely technical difficulties encountered in the first instru-

ments have not been forthcoming the development has involved a straightforward process of refinement. It is only now, twelve years later, that sufficient technical knowledge and skill has been achieved to consider the attainment of the theoretical limit of performance to be within reach in practice.

The electron source for electron microscopes has undergone many radical changes. It has already been noted that Ruska used a gaseous discharge tube in his initial design. However, he soon realized that it was inherently too unstable for use in an instrument using magnetic lenses. All subsequent instruments have used thermionic cathodes operating at high vacuum. An electrostatic instrument manufactured in Europe is the only design using a gaseous discharge tube at the present time.

Most of the high-vacuum thermionic sources in use are focused by mechanical adjustment of the electrodes or by the application of appropriate voltages to those electrodes. More recently a new mode of operation of the thermionic source for the electron microscope has been used by a few laboratories. In this system the cathode is operated under space-charge-limited and self-regulating conditions. In addition to many advantages connected with its operation, this gun has the fundamental advantage that, for identical conditions of intensity of irradiation of the specimen, the angular aperture of the irradiation is nearly an order of magnitude less than in the earlier systems.

These sources are satisfactory in that they give adequate intensities, are of high electron-optical quality and are not critical of adjustment. However, there is still considerable room for improvement. This will probably take the direction of further improvement in the symmetry of the source and of a better understanding of the relationships between the intensity of irradiation and disturbances in the specimen. If the present trend to higher instrument magnifications continues higher intensities will be desirable. It now appears that it will be necessary to accomplish this through the improvement of phosphors as the maximum intensity available in the present system is already too great for many specimens.

There have been few major changes in the general design of magnetic lenses since Ruska's work. This is probably so because the problems were inherently the same as those which had already been worked out in connection with the design of powerful electro-magnets.

A similar statement can be made specifically regarding the objective in spite of the fact that it has been the subject of intensive investigation for the past decade. There is a difference, however, in that the performance of the electron microscope as a whole can only be as

good as the performance of the objective and that earlier objectives did not behave according to the established theories. It is now known that while the theories were correct there were many aspects of those theories that were not appreciated by those working with practical lenses and also that the true performance of the objective was often masked by completely extraneous disturbances too numerous to mention here.

In the most advanced experimental electron microscopes this situation is now corrected, and it is well-established that the electron microscope objective behaves according to theory. It has been shown that a magnetic lens in which the field is accurately axially symmetrical will provide a resolving power close to that predicted by theory when operated *without* a physical aperture. It is assumed of course that all other instrumental requirements for the attainment of that resolving power are satisfied. It has similarly been shown that the introduction of a physical aperture of optimum size in such an objective invariably lowers the *limiting* resolving power in practice. While the specific reasons for this are not yet completely understood, it appears that there are numerous technical difficulties connected with the insertion of the aperture which have not yet been overcome.

Since the performance of the electron microscope is not critically dependent on the quality and performance of the projection lens, little fundamental work has been done on it other than studies on the distortion it produces and methods of correcting that distortion.

In Ruska's first microscope and other emission instruments in use at the time, the images were observed on a fluorescent screen as in present instruments. On the other hand permanent records were made by photography of the fluorescent image. It appears to have been Ruska's suggestion that the already well-known method of internal photography be used in electron microscopy. This has now been universally adopted. Other than a continuous increase in the efficiency of the phosphors used in the electron microscope there have been no further significant developments in the method of converting the electronic image into a visible one.

Although the subject of instrument structure is engineering in nature and outside the scope of this survey, it is of interest because it is in this regard that the electron microscope has undergone its most radical changes. There is little doubt, now, that the many difficulties with the early electron microscopes were the result of unstable power supplies and cumbersome vacuum systems. Fortunately, concurrent with the development of the electron microscope there has been a very rapid development in the vacuum mechanics of demountable systems

and in electronically-regulated power supplies. Electron microscope designers and engineers have taken advantage of these simultaneous developments to produce modern instruments in which difficulties of this type are no longer an important factor in determining the quality of the performance.

The accumulated results of these refinements has increased the attainable resolving power to 10 Å for the instrument in these laboratories. Of greater significance, however, is the fact that such resolving power can be achieved relatively frequently (one exposure in fifty) while the previous limiting resolving power of 20 Å can now be achieved in over fifty percent of the exposures on suitable specimens.

III. FUTURE DIRECTION OF ELECTRON MICROSCOPE RESEARCH

The preceding discussion has been devoted to the present status of some important phases of the development of the electron microscope and its applications. A discussion of trends in a science usually implies an attempt to deduce the future course of the work. It is obvious that there is no justification for making such an attempt in regard to the applications of the electron microscope. Therefore, the present discussion will restrict itself to an evaluation of the future capabilities of the electron microscope as an instrument for observing fine structure and to indicating the course which future research on this problem may take.

In the foregoing discussion it has been pointed out that the performance of the present form of electron microscope is ultimately dependent on the quality of a single uncorrected electron lens. It has also been pointed out that the refinement of this lens and the associated equipment are now at a stage where the behavior of the lens is approaching the theoretical limit for certain types of specimens.

Future fundamental research on the electron microscope will be directed toward two important goals in the observation of the fine structure of matter: (1) increasing the number of types of specimens in which the present limiting resolving power can be attained. (2) The attainment of still higher resolving powers for ideal specimens.

The first of these problems, which is of the greater practical importance, arises from the different conditions of contrast which are encountered with different types of specimens. It is now known, for example, that with the best lens used without an aperture it is not possible to resolve less than about 500 Å for the internal structure of bacteria, less than 50 Å for viruses on a collodion membrane or less than 30 Å for the collodion membrane itself, while for heavy metal particles in

an evaporated film or in Fresnel fringes, 10 \AA can be resolved. The reasons for these differences are two-fold. In the first place, the specimen itself may show differentiation with regard to chemical structure but none with regard to density, in which case there will be no differentiation in the electron image regardless of the lens performance. This is probably the case with bacteria and the large viruses. Secondly, the operation of the objective without an aperture, which is the only case in which the limiting resolving power attained in practice agrees with theory, is not the optimum one from the point of view of contrast. At the present time the technical difficulties which prevent the objective from being operated under optimum conditions are far from being overcome. Thus, in many specimens where slight differences in density do exist they are not observed in the electron image.

An immediately obvious method of attacking the first problem is through the treatment of the specimen to produce, selectively, differences in density, such as through selective staining or, in the case of some bacteria, through providing the organism with an appropriate diet. Some methods of staining for electron microscope work have been developed. It is too early to say, however, that staining which is selective on a chemical basis has been actually accomplished since in the cases tried there has been a corresponding morphology which can be shown almost as well by the shadow-casting technique and presumably could be shown with an objective operating under ideal conditions of contrast.

In theory, the introduction of a physical aperture into the objective lens should improve the resolving power for all types of specimens. If it is of optimum size for the particular lens it should provide the maximum improvement in the case of organic specimens. Experimental tests, however, have shown that *the introduction of an aperture gives results in agreement with theory only for relatively thick specimens in which the resolving power attainable does not approach the limit attainable with the lens*. Therefore, the aperture is useful in practical cases of thick specimens but may be discarded for cases of suitably-thin specimens. In those cases where the specimen is suitable for the demonstration of the limiting resolving power, except for the restrictions imposed by lack of contrast, results obtained through the use of a physical aperture have been consistent only insofar as they have reduced the limiting resolving power of the lens.

Now that accurate methods of testing the quality of the objective are available it has become apparent that the introduction of an aperture invariably partially destroys the symmetry of the lens, thus lowering the resolving power and making the measurements on contrast

meaningless. The reasons for this effect have not been obvious. The natural suggestions with regard to cleanliness, symmetry and centering have all been considered but no conclusions have been possible in view of the inconsistent nature of the observations.

In an effort to obtain some information concerning this difficulty an experimental objective having some interesting properties has been built in these laboratories. This objective consists of two components. The first is a weak lens with a focal length of about 11 millimeters adjusted to produce an image of the specimen at unity magnification on the object plane of the second component which is a short focal length lens of conventional design.

Electron optically the arrangement has many disadvantages. Its spherical and chromatic aberrations are both an order of magnitude larger than in a single lens. The regulation of the high voltage and lens-coil current supplies must similarly be an order of magnitude better than for a single lens. Because of its large opening and long working distance it is particularly sensitive to the disturbing effects of exterior magnetic fields and asymmetries due to contamination and material inhomogeneities. On the other hand, the system has several advantages which may give it practical significance. Its long working distance (22 millimeters) removes restrictions on the size of the specimen used, and considerably simplifies the design of special specimen stages or reaction chambers. It has *two* values of the exciting current for which a focused image of the specimen is obtained. The magnification ratio for the two images is approximately 30 to 1 so that low magnification work (300 X to 1000 X) and high magnification examination (10,000 X to 30,000 X) can be carried out without disturbing the specimen or lens systems.

For the present investigation its most important advantage lies in the fact that the physical aperture can be placed in the weak component and is an order of magnitude larger than is necessary in a single lens for the same angular aperture. Thus an aperture of 200 microns is optimum for the lens instead of 20 microns. An aperture of this larger size is easy to manufacture and center in the lens and suffers much less from the faults of the smaller aperture. Most of the expected disadvantages with this lens did not present any great difficulty with the result that images comparable with the best attainable with a conventional objective have been obtained (Figure 1). The introduction of the aperture, on the other hand, has not yet been accomplished without the introduction of some image astigmatism. Even so there are indications that the desired contrast can be obtained. This is particularly indicated in some images obtained with an aperture

which was much smaller than the optimum value (Figure 2). It is obvious that research should be continued in this direction.

Increasing the resolving power of the electron microscope beyond its present limiting value presents an entirely different problem. Here, as in the above, the performance of the objective is the determining factor. At present the possibility of improving the quality of the

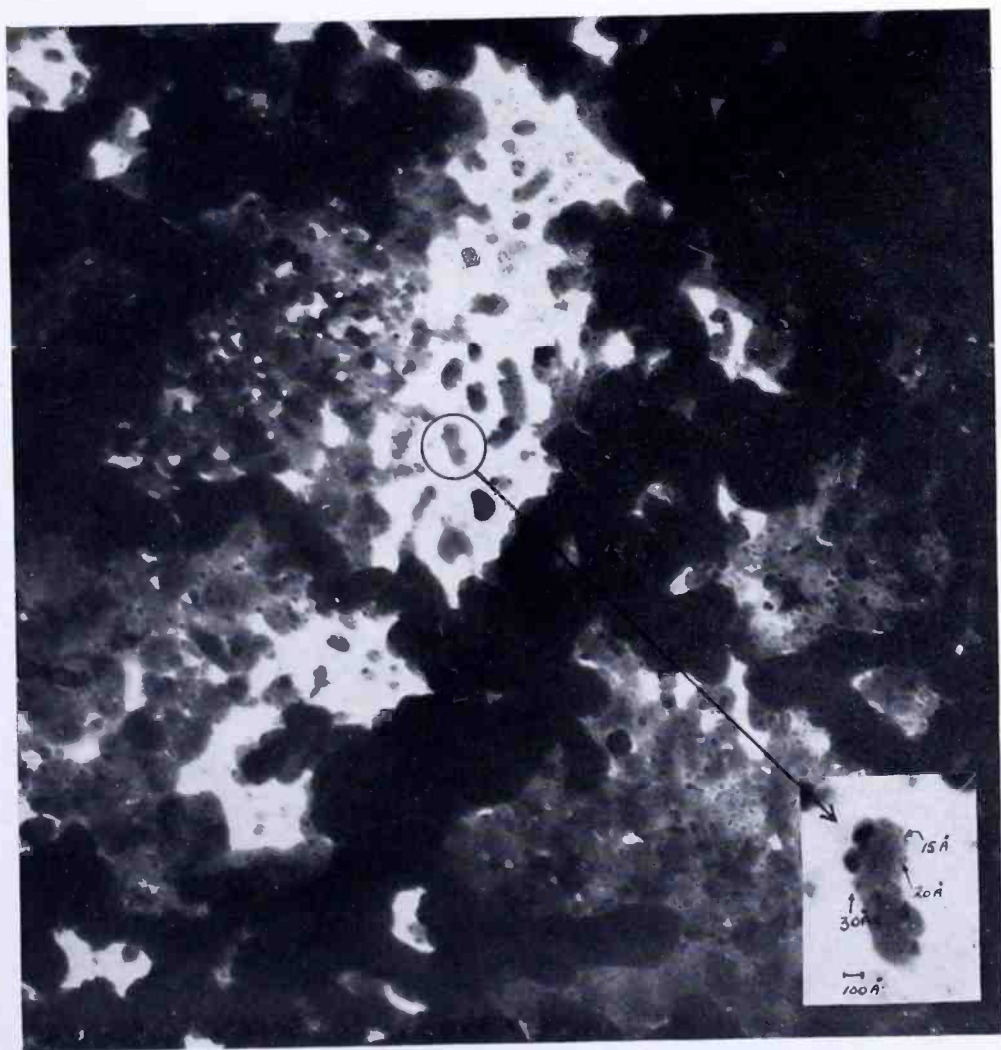


Fig. 1—An enlargement of an electron micrograph of an evaporated lead chloride film obtained with the double objective lens described in the text. This image demonstrates that a resolving power of better than 15 Å is obtainable with this lens.

objective has not been investigated experimentally. Theoretically, the possibilities do not look promising.

General theoretical investigations made to determine the shape of the lens field possessing minimum amounts of aberrations have led to field distributions which cannot be achieved in practice. On the other

hand studies on field distributions which are attainable have indicated that very little improvement in the magnitude of the aberrations can be expected. Since the aberrations affect the limiting resolving power only in the fourth root this direction of attack is not a promising one.

The use of high frequency variations in both the focal length of the objective and the incident electron velocity has been suggested as a possible method of correcting spherical aberration in the objective. Unfortunately the frequencies required are extremely high. This in itself would not present too great difficulties if it were not for the fact

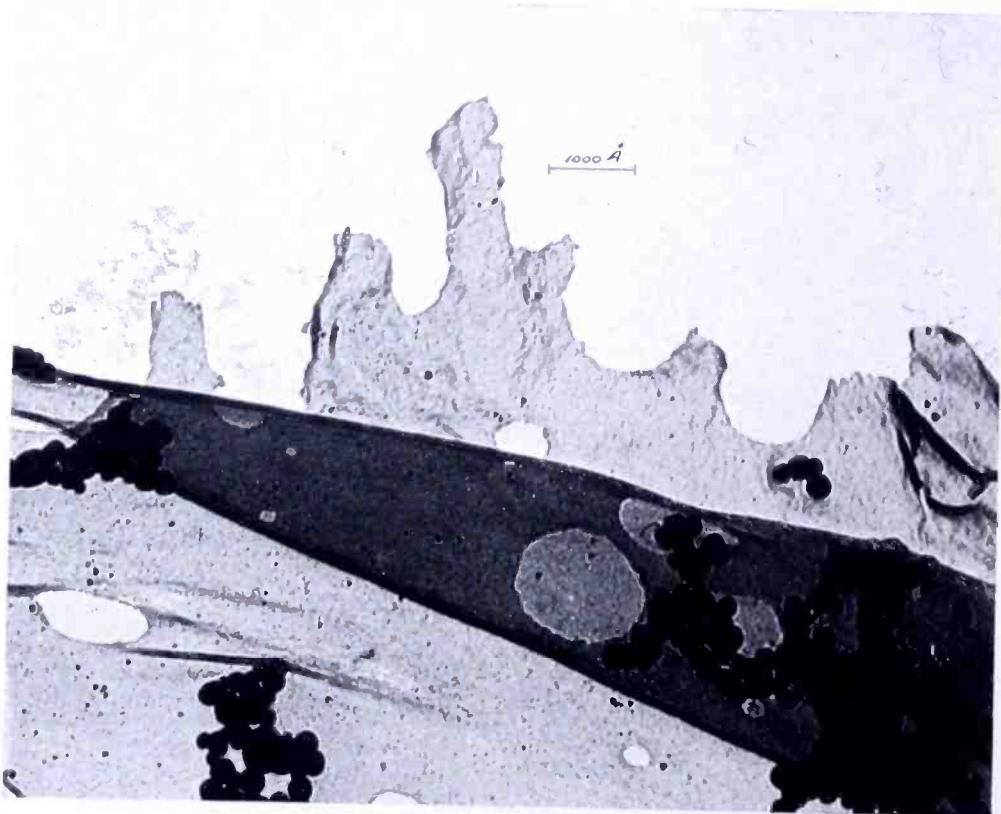


Fig. 2—An electron micrograph of a fragment of thin collodion membrane. The image was obtained with the double lens in which an aperture much smaller than the optimum value was used. The image demonstrates that the contrast is sufficient to make the collodion structure clearly visible. No other method of enhancing contrast was employed to obtain this picture.

that the method is not effective unless the wave shape of the applied potentials are accurately controlled. The techniques for doing this simply do not exist at the frequencies involved. Thus, while the method is of theoretical interest and may have possibilities eventually, it must be considered impractical in the immediate future.

Another method of correcting the aberrations of the objective is found in a suggestion by D. Gabor. His method involves introducing

an electron cloud with the proper charge distribution in the objective. The idea is theoretically sound, but at present there are no experimental data on which to judge its feasibility.

The final method, and probably the most obvious one, is the correction of aberrations by the combination of components of suitable properties. At the present time such components do not appear to exist. At one point the possibility of combining a negative electrostatic lens with the double-objective described above was considered as being practical if used with sufficiently high accelerating potential. Since such a negative lens would of necessity have a central conducting membrane the high potential would be necessary to overcome scattering. While the scheme is electron-optically operable, theoretical calculations indicate that the aberrations of the electrostatic negative lens are very slight and of the wrong sign. Thus, even in this case, there is no possibility of obtaining correction.

It would appear from the foregoing discussion that the likelihood of obtaining higher resolving power (i.e. better than 8 Å) through the correction of the aberrations of the objective is, for the present at least, a rather remote one.

This leads one to the consideration of systems other than electronic which may lead to higher resolving powers. One which was suggested almost simultaneously with the conception of the electron microscope is that of an ion microscope probably using protons. While no experimental work has been done in this direction the suggestion has been seriously considered for some time. The obvious advantage lies in the greater mass of the particles and hence, in the shorter wavelength for the same accelerating potential. Thus, with the present lenses which must be electrostatic, a smaller effective aperture can be used which leads to an immediate increase in resolving power by a factor of 3 to 4.

Practically, there are many difficulties involved in the design of a proton microscope. The most important of these is undoubtedly in the attainment of a proton source which gives sufficiently high intensity. The present sources give intensities which would require exposures 10^4 times as long as in present electron microscopes. Also of importance is the consideration of the effect of proton bombardment on the specimen. Because of the much higher momentum of protons, there is a possibility that specimens of the type used in the electron microscope will not stand up under proton bombardment. It is on the settling of this point that the future development of a proton microscope really depends.

In addition to the improved resolving power, theory indicates that considerably greater contrast is possible with protons.

IV, CONCLUSION

In the foregoing an attempt has been made to discuss the present status of research on the electron microscope particularly insofar as that research concerns the limiting resolving power attainable at present and in the near future. It has been shown that for certain types of specimens the technical performance of the electron microscope using a single uncorrected magnetic objective lens is approaching the theoretical limit. It now appears that future developments should include progress in engineering and education to make the resolving power now possible in experimental instruments available to all electron microscopists, research in the electron optical laboratories and electron microscope laboratories to make the ultimate resolving power available in a wider range of specimens and, ultimately, an attempt to obtain higher resolving power either through the improvement of the objective (an approach which does not appear too promising) or through the development of an instrument using a different type of irradiation.

TELEVISION HIGH VOLTAGE R-F SUPPLIES*

BY

ROBERT S. MAUTNER† AND O. H. SCHADE‡

Summary—The principles of operation and design of television high voltage r-f^s supplies have been previously described.¹ These are here reviewed and considered in greater detail. Constructional features of two typical units are shown and their performance is illustrated by curves indicating the magnitudes of current and voltage obtained under typical operating conditions. Sample calculations for the specific cases of a 75-watt, 90-kilovolt supply and a 10-watt, 30-kilovolt supply are included to illustrate the progressive steps in designing and calculating the circuit elements and operating conditions for a specified performance. A table of the symbols used is included at the end of the paper.

A TYPICAL r-f power supply circuit is shown in Figure 1. The oscillator voltage developed across the primary tank circuit, L_1C_1 , is stepped up by the square root of the ratio of secondary to primary impedances, and then rectified. Because of the high voltage developed across the secondary, the principal portion of the network loss occurs in this part of the circuit requiring a high unloaded impedance for good efficiency. Such values of impedances are realized in practical supplies by the use of special coil configurations, and a minimum secondary tuning capacitance C_2 . This capacitance is the sum of coil, wiring, and diode capacitances and is shown as a dotted capacitance in Figure 1.

In the following, the design of each portion of the circuit for satisfactory performance is considered in detail.

DESIGN

The design of r-f high voltage supplies may be divided into six consecutive steps:

1. Design the rectifier circuit and corona shielding

* Decimal Classification: R366 × R583.

† Industry Service Laboratory, RCA Laboratories Division, New York, N. Y.

‡ Tube Department, RCA Victor Division, Harrison, N. J.

§ Throughout this paper, the abbreviation "r-f" is used for "radio-frequency."

¹ Schade, O. H., "Radio-Frequency Operated High-Voltage Supplies for Cathode-Ray Tubes", *Proc. I. R. E.*, Vol. 31, No. 4, pp. 158-163, April, 1943.

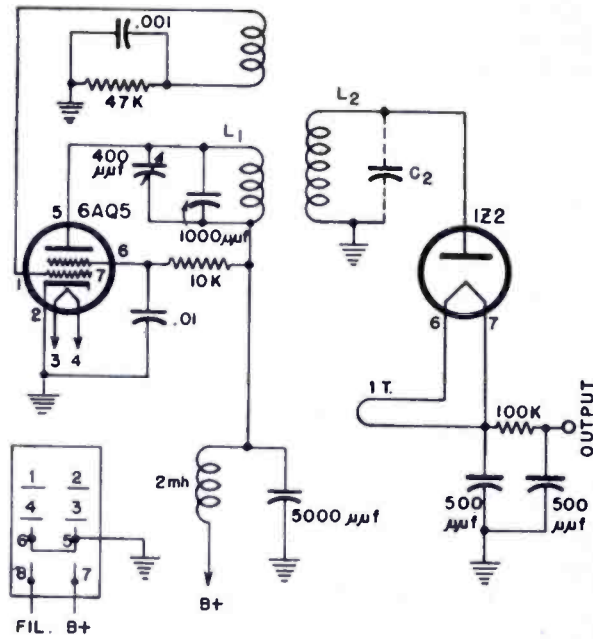


Fig. 1—Circuit of 4-kilovolt supply.

2. Determine the mechanical coil construction and compute the optimum winding and operating frequency for the high voltage coil
3. Estimate the required oscillator power; select the tube type and operating constants
4. Calculate the plate tank circuit and choke, if used
5. Calculate the diode filament transformers
6. Determine the regulation requirements of the supply.

RECTIFIER CIRCUIT, CORONA SHIELDING, AND CAPACITANCE

The basic circuit for voltage multiplication with diodes is shown in

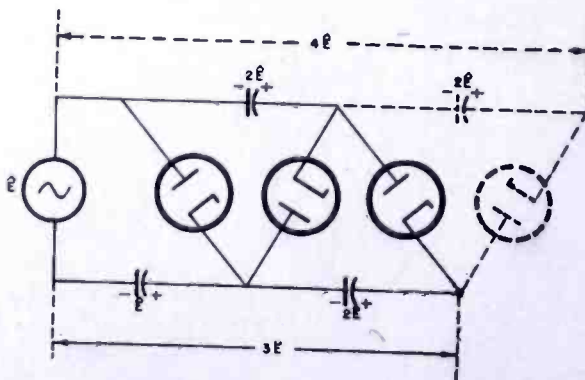


Fig. 2—Basic voltage multiplier circuit.

Figure 2. This circuit is particularly useful for 30 or 90 kilovolt operation. The focusing voltage for projection kinescopes, which generally runs about one-fifth of the second-anode voltage, can be conveniently obtained from the output of the first rectifier. The bleeder power loss is thus reduced to one-third of that otherwise dissipated in a bleeder connected to the full output voltage.

The choice of the number of rectifier stages depends on available rectifier types, the cost of circuit elements, and the impedance obtainable with practical high voltage coils.

The effective shunt load of the rectifier circuit on the tuned high voltage circuit is given by

$$R' = \bar{R}/2n^2 \quad (1)$$

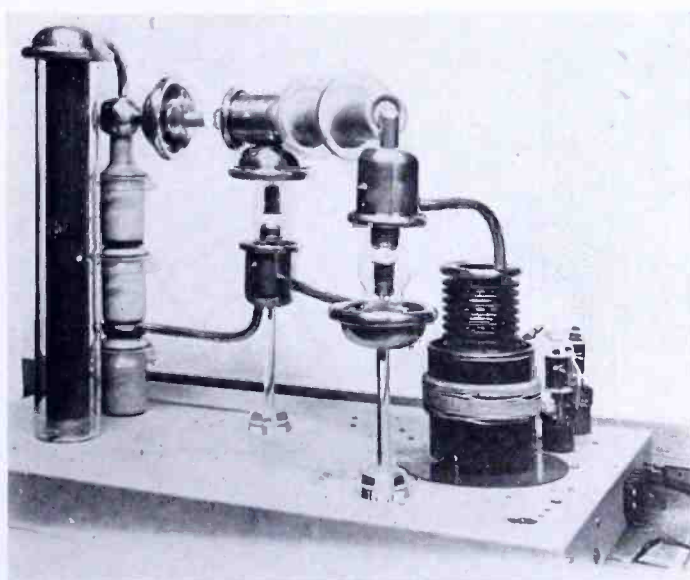


Fig. 3—Side view of 90-kilovolt tripler.

where \bar{R} is the direct-current load resistance on the rectifier output terminals and n the number of cascaded rectifier stages.

For an output voltage $\bar{E} = 90$ kilovolts and $\bar{I} = 0.8$ milliamperes, the direct current load is $\bar{R} = 110$ megohms. The inverse rating of 60 kilovolts for the R6194A experimental diode requires $n = 3$. Substitution in Equation (1) results in $R' = 6$ megohms. Similar computations for a 30-kilovolt supply with $n = 3$, $\bar{E} = 30$ kilovolts, and $\bar{I} = 0.2$ milliamperes result in $R' = 8$ megohms.

Arrangement of parts and corona shielding for the 90KV tripler is shown in Figure 3. The 90-kilovolt unit requires considerably more elaborate corona shielding than the 30-kilovolt unit and will be treated in greater detail.

The minimum conductor diameter D (in inches) for a peak voltage \hat{E} (kilovolts) is the diameter for which corona does not occur before spark-over occurs at a critical distance

$$D \approx \hat{E}/100 \text{ for } \hat{E} > 10\text{kv} \quad (60 \sim) \quad (2)$$

It decreases faster for potentials $\hat{E} < 10\text{kv}$. The required minimum spacing, i.e., the sparking distance between such conductors, is greater than the spheregap distance and is given by

$$S \approx 3D \quad (3)$$

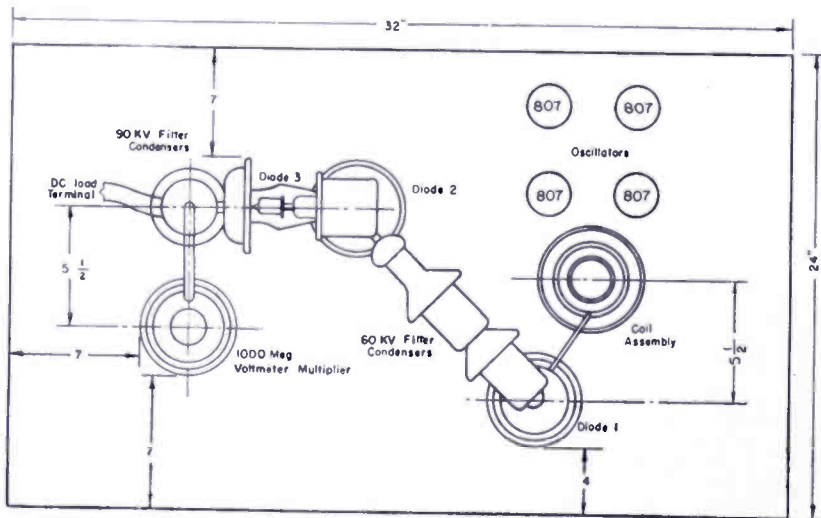


Fig. 4—Top view of chassis layout of 90-kilovolt supply.

For $\hat{E} = 90$ kilovolts, $D = 0.9''$ and $S = 2.7''$. It is good practice to use a somewhat larger diameter if feasible and provide spark-over clearances of double this value (triple at very high potentials; see Figure 4) to allow for the effects of scratches and dust particles on conductor surfaces. This is particularly advisable where conductors are exposed to, or at, r-f potentials as the power loss in air ionized by corona is much larger than that at low frequencies and serious loading of the power source results. All parts in the r-f fields as well as grounded objects must be given contours with a minimum radius $r \approx D/2$. Interconnecting leads at 60-kilovolt potential in the 90-kilovolt unit are thus made of one-half inch tubing while tightly wound phosphor bronze spring sections of one-quarter inch diameter are used in the 30-kilovolt unit. A clearance of 1.50 inches was used in this unit between output socket shell and shield wall. This spacing is the minimum recommended

and is a practical limit for safe operation, flashover occurring at slightly over 40 kilovolts.

Having determined the physical layout of the diode circuit, an estimate of its capacitance to ground is made to determine the secondary tuning capacitance C_2 of the high potential transformer winding.

The capacitance to ground of the circuit elements at r-f potential in the 30- or 90-kilovolts tripler circuits consists of three diode capacitances (3×2 micromicrofarad) and that of one condenser and two corona shield assemblies to ground. The latter may be estimated from its potential field contour which, for the 90-kilovolt unit, is similar to that of two spheres of roughly 12 centimeters diameter. As the space capacitance of a sphere is equal to its radius (in centimeters), the diode assembly at r-f potential has roughly $(12 + 6)$ micromicrofarad capacitance. Adding 2 micromicrofarads for the coil shield and 3.5 micromicrofarads for the winding capacitance (discussed later), the total shunt capacitance on the high voltage transformer winding of the 90-kilovolt unit will be in the order of $C_2 = 25$ micromicrofarads.

THE HIGH VOLTAGE SECONDARY CIRCUIT

The factors determining size, shape and type of winding used in the secondary of the transformer are:

1. Potential between layers and sections,
2. Distributed capacitance,
3. Corona,
4. Coil loss and temperature rise,
5. Coil impedance,
6. Coupling coefficient,
7. Coil form loss.

To minimize coil capacitance and voltage between layers it is practical to subdivide the winding into sections consisting of universal wound pies with five to ten turns per layer. Greater pie widths result in high distributed capacitance and increased voltage stress across layers. Narrower pies impose winding difficulties and result in weak coils. The voltage between layers should be less than indicated by the normal rating of the insulation inasmuch as the tendency of sections at the high potential end of the coil to produce corona as well as increased dielectric loss at r-f frequencies decreases the ability of the pie to resist breakdown. Values not exceeding 250 volts peak between layers have provided satisfactory operation. The space between pies should not be stressed with more than 12.5 kilovolts (peak) per inch (approximate double needle gap distance) to provide a safety factor for double

COIL DATA	4 KV COIL			10KV (and 30KV TRIP)			30KV UNBAL. DOUB.			90 KV TRIPLER		
	PRI.	SEC	TICK	PRI	SEC	TICK	PRI	SEC	TICK	PRI	SEC	TICK
FORM DIA	.750	.750	.750	1.25	1.25	1.25	3.75	2	3.75	4.375	2	4.375
FORM THICKNESS	.0625	.0625	.0625	.032	.032	.032	.125	.0625	.125	.125	.0625	.125
TURNS	100	1750	150	55	1400	75 - 100	2 parallel layers 35 t. ea.	2800	8	32	2800	9
PIE WIDTH	.1875	.0625	.0625	.1875	.0625	.0625		.125	close Solenoid		.125	close Solenoid
CROSS-OVERS PER TURN				6	10	10		6			6	
IND.	122 μ h	56 mh		178 μ h	43.5 mh	650 μ h	145 μ h	200 mh	18 μ h	175 μ h	220 mh	22 μ h
WIRE (LITZ)	15/38	3/41	3/41	50/38	3/41	5/41	50/38	10/41	5/41	250/38	14/41	7/41
NO. π 's	1	5	1	1	7	1	2 layer bank wound	10	single layer	3 layer bank	10	single layer
DISTANCE BETW π 's	.1875	.125	.3125	.25	.1875	.875		.1875			9/32	
SOLENOID LENGTH		.8125	TOT. SEC. LENGTH				1.375			1.5		

Fig. 5—Coil data for several practical coils.

voltage transients. A 30-kilovolt coil should thus have a total pie spacing of 2.4 inches. For a subdivision into 10 pies the clearance between pies should thus be a little over one-quarter inch. Lower voltage coils such as those used in the 30-kilovolt tripler can be designed with a somewhat greater safety factor, but are still subject to maintaining a form factor giving high Q and permitting sufficient coupling (see Figure 5).

The high voltage coil loss in r-f power supplies is a function of coil size and circuit capacitance. Larger power supplies require a high component-efficiency as high frequency power is relatively expensive. An over-all efficiency of 40 to 60 per cent requires the distribution of circuit losses as shown in Table I.

Table I—Circuit Efficiencies.

Circuit Element	30 kv-20w Eff. %	Power Loss Watts	90 kv-72w Eff. %	Power Loss Watts
Oscillator Tubes	70-75	6.5 - 8	75-80	30 - 37.5
Primary Tank Circuit	94-96	1 - 2	95-97	4.5 - 7.5
High Voltage Secondary Circuit	65-75	6 - 10	88-90	15 - 18
Rectifier Filament & Plate Loss	95-97	.75 - 1.5	90-95	7.5 - 15
	40-48%	14.25-21.5	48-62%	57 - 78

The overall efficiency of the 30-kilovolt tripler is less than 30 per cent at normal loads because of the small amount of power used compared with the power consumed in fixed losses such as that dissipated in the secondary coil and the minimum oscillator input. Higher efficiencies are obtained at higher load currents.

The figures in the second and fourth columns give design values. The required coupling is discussed later.

The necessary tuned impedance Z_{II} of the secondary is given by

$$Z_{II} = \frac{E_2^2}{2P_2} \quad (4)$$

where P_2 is power dissipated in that winding. To meet the requirements for the 90-kilovolt case (Table I) the r-f peak voltage $E_2 = 30$ kilovolts and the specified power loss required $Z_{II} = 25$ megohms.

The secondary coil used for the 30-kilovolt tripler was originally designed for a 10-kilovolt source, and resonated at approximately 280 kilocycles. When used in a tripler circuit the added shunt capacitance resulting from the additional diode and circuit capacitance lowered the resonant frequency to 180 kilocycles, reducing both coil Q and circuit impedance. However, both factors remain high enough to permit sufficient coupling for good regulation and satisfactory coil efficiency. The measured secondary impedance was over 9 megohms. From equation (4) the power loss for a 10-kilovolt peak voltage is $P_2 = 5.5$ watts which is within the rating of maximum dissipation (6.5 watts) for this particular coil.

Optimum wire size and number of turns are determined by a series of approximations. The coil inductance is given by

$$L = r^2 N^2 / [9r + 10(l + h)] 10^3 \text{ in millihenries} \quad (5)$$

where r = mean radius in inches

l = coil length in inches

h = pie height

N = number of turns

The frequency is computed with L and the estimated value C_2 ($C_2 = 20$ to 30 micromicrofarads) for the 90-kilovolt circuit and $C_2 = 17$ micromicrofarads for the 30-kilovolt circuit from the equation

$$\omega^2 = 1/L_2 C_2 \quad (6)$$

The r-f resistance is then computed from

$$r = r_0 (1 + k^2) \tag{7}$$

with

$$k = \frac{0.04 Nnd^3 f}{(l + h)}$$

where r_0 = direct-current resistance of winding

N = number of turns

n = number of strands

d = wire diameter in inches

l, h , from Equation (5)

Also

$$Q = \frac{\omega L}{r} \tag{8}$$

and

$$Z = Q\omega L \tag{9}$$

The current density in the wire is expressed in circular mils per ampere of coil current, and should be

$$\text{Circular mils/Ampere} = 350 (1 + k^2) \tag{10}$$

The secondary current is obtained with

$$I_2 (\text{rms}) = \hat{E}_2 / \omega L_2 \sqrt{2} \tag{11}$$

The approximate total copper cross-section is obtained in first approximation with equation (10) and (11) setting $k = 1$. The coil loss for several coil designs was calculated for the 90-kilovolt unit. This data is summarized in Table II.

Table II—Coil Loss Data

#	N	n	L (mh)	C ₀ (μuf)	f (kc)	k ²	r ₀	r	kilohms ωL	Q	Z (meg)	I ₂ (A)	c.m./a	P ₂ (w)
1	2800 (10 pies)	14	228	20	75	.31	194	254	107	422	45	.2	550	10
				30	61	.205		234	87	370	32	.245	450	14
2	2000 (10 pies)	20	116	20	104	.62	98	159	76	477	36	.28	560	12.5
				30	85	.41		138	62	450	28	.34	460	16
3	2500 (10 pies)	20	170	20	86	.65	122	201	92	456	42	.23	685	10.7
				30	70	.43		175	75	428	32	.283	555	14
4	3000 (12 pies)	20	250	20	71	.47	147	215	112	520	58	.19	880	7.8
				30	58	.31		192	91.5	475	43.5	.23	685	10.4

The first trial calculation with 2800 turns of 14×41 Litz wire happened to provide optimum design for its size as shown by a comparison with coils #2 and #3 using 20 strand Litz wire.

It is interesting to note that the power dissipated in a coil is a function of its size. This occurs as a result of being able to obtain both higher Q 's by the use of more strands and higher inductance by the use of more turns. Thus a larger coil results in a higher tuned impedance and lower loss. However, if cost, physical size and other reasons restrict coil dimensions, the alternative is to vary the strands and number of turns, maintaining a constant copper cross-section (and resultant coil size) until a compromise is reached between coil loss and Q . If a fixed tuning capacitance is assumed and the coil resistance is considered equal to r , regardless of frequency it can be shown that the power loss P_2 will be a constant. The effect of reducing the number of turns on a given coil to one half while maintaining a constant copper cross-section would then permit operation with the same coil loss at double the frequency, or $2f$, the coil having half the inductive reactance it had previously, and twice the Q . However, actually the coil resistance will not drop to 25 per cent of its former value of r because of added eddy current losses at $2f$, and the net result will be a coil of not quite $2Q$, and of half the original value of ωL . It is, of course, desirable to maintain the product of Q and ωL as high as possible for minimum coil loss, but a high Q is also necessary, in order to permit sufficient energy transfer with obtainable coupling coefficients and good regulation, and further permit adequate spacing between primary and secondary for insulation.

Referring again to Table II it can be seen that a minimum coil loss requires a larger coil (#4). Coils #1 and #2 have about the same copper cross-section. It will be seen that loss in inductive reactance by using 20 strand Litz is not compensated by a proportionate rise in Q , resulting in a lower tuned secondary impedance. Even where coil size is slightly increased as in coil #3 by adding 50 additional turns per pie, the loss will still exceed that of coil #1.

Coil #1 will operate at 60 to 75 kilocycles depending on the exact circuit capacitance C_2 , the degree of coupling, and the frequency to which the primary circuit is tuned.

The impedance of the secondary circuit will be somewhat lower than the computed value because of dielectric losses in the coil capacitance. The coil capacitance can be calculated from the capacitance between the two layers of one pie winding, which is approximately 1200 micromicrofarad (area $\frac{1}{8}'' \times 8''$, spacing 0.004", dielectric $\epsilon = 3$). As one pie has about 35 layers of 8 turns, its capacitance is 34 micro-

microfarads and ten pies in series will then have 3.4 micromicrofarads. The reactance of this capacitance at 60 kilocycles is $1/\omega C_c = 0.75$ megohm. The impregnating compound must be of excellent quality as a 0.5 per cent power factor results in a shunt resistance loss of $200 \times 0.75 = 150$ megohms, which is equivalent to a 3-watt power loss at 30 kilovolts. The power factor of the insulating material should be excellent and the field strength low (long supports) to avoid power loss.

During early development of secondary windings, various types of coil forms and materials were tried. Many of the materials used, normally considered good insulators, showed considerable dielectric loss and a resultant heat rise. Even in cases where the coil form loss was low, the relatively poor thermal conductivity of the material used did not permit the heat generated by the copper loss to be dissipated rapidly enough, and again overheating resulted. In some cases the process was regenerative, the coil form power factor becoming progressively worse as the temperature rose, producing still greater losses.

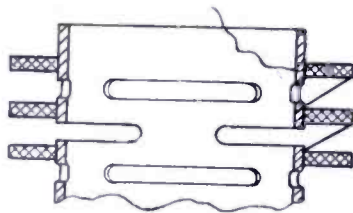


Fig. 6—Secondary coil form construction.

Consequently it is advisable to keep the coil form material in the field of the coil to a minimum and to provide as much air circulation around the pies as is practicable. Slotted thin wall impregnated paper bakelite tubing has been found to be one of the most satisfactory materials available, as well as one of the most economical. Figure 6 illustrates one satisfactory type of construction. For low voltage supplies horizontal coil mounting is preferable from the standpoint of air circulation (provided the coil is not placed too close to a metal surface). However, vertical mounting is generally used because of conveniences in wiring and greater adaptability to space requirements.

It will be noted that the calculated magnitudes of Q in Table II are quite high. For several reasons, it is not feasible to use the conventional Q -meter to measure these values. The frequency at which we are interested in the Q is close to the self resonant frequency of the coil so that in any series circuit such as used in a Q -meter the coil appears as a partially resonant circuit in series with the tuning capacitance rather than an inductance. Furthermore, the minimum value of capacity setting in the usual Q -meter is in the order of 30 micromicrofarads which is greater in most cases than the total second-

ary circuit capacity. Consequently the operating Q of the winding is most easily determined by adding sufficient high Q capacity to produce resonance at the desired frequency and then determining the frequency band required for the 70 per cent response points. Because of the very high impedances involved it is necessary to drive the secondary coil by means of a few very loosely coupled primary turns in order to prevent coupling an appreciable amount of generator impedance into the secondary. This will, of course, transfer a proportionately smaller amount of energy into the secondary and result in lower magnitude of detected voltage. A practical method of detecting the 70 per cent response points without the use of a vacuum tube voltmeter or other normally satisfactory "high impedance" device (which in this case would produce excessive loading and detuning) is through the use of a high gain oscilloscope and test probe. The input impedance of a typical

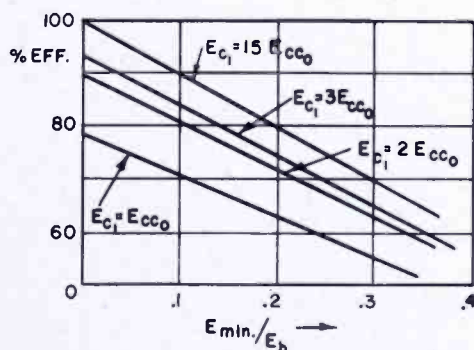


Fig. 7—Efficiency curves for class C operation.

probe may be equivalent to 5 or 10 micromicrofarads in shunt with 10 megohms. If this is placed about a half inch away from the secondary, negligible loading will result and a more accurate value of measured Q will be obtained. It is necessary that all other windings be removed from proximity to the secondary during this measurement or the loading effect of induced capacity currents in the coils coupled to it will result in incorrect readings of response points. When a tap at a small fraction of the total coil inductance is available it can be used with a high impedance oscilloscope probe to provide a further check of the Q value obtained from the first measurement. A signal generator with an incremental frequency dial graduated directly in small percentages of the output frequency has been found useful in permitting rapid and precise measurements to be obtained.

OSCILLATOR SPECIFICATIONS AND OPERATING CONDITIONS

In order to obtain high efficiency and high power output, the oscillator tubes are operated under class C conditions. In Figure 7

curves are given indicating efficiencies obtainable for bias values up to several times cutoff. Figure 8 shows the ratio of peak to average plate current plotted against the ratio of actual bias to cutoff bias. Operation at high bias and high excitation results in small angles of flow, high efficiency and low power output. High grid driving power is required which in an oscillator must be supplied from the plate circuit. The ratio of peak to average currents at high efficiencies rises rapidly imposing greater emission requirements and increased tube drop. Optimum performance is obtained with angles of flow between 90 and 120 degrees and peak to average plate currents in the order of 6 to 1.

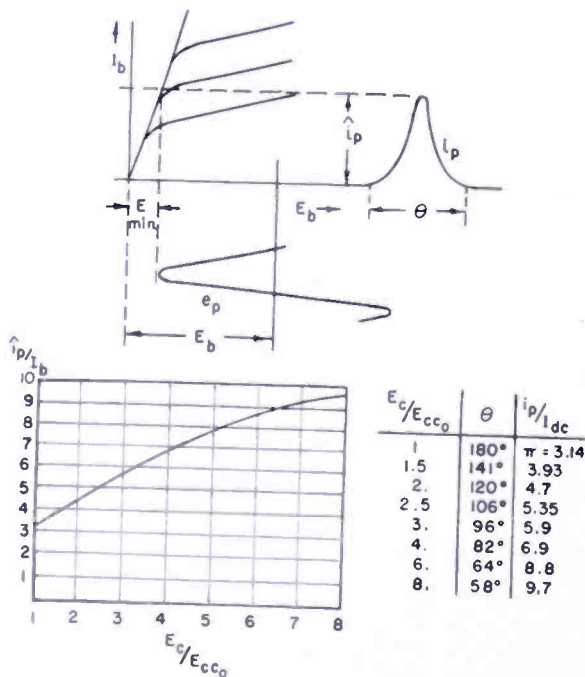


Fig. 8—Ratio of peak to average currents for various angles of flow.

The computations involved in designing an oscillator circuit of the 90-kilovolt unit are typical of those used for all r-f supplies and are considered in detail.

On the basis of a 50 per cent overall efficiency (see Table I) the oscillator power input is 150 watts. For 80 per cent tube efficiency the power output is $P_o = 120$ watts and the tube loss 30 watts.

A circuit (Figure 9) using four 807's in parallel was chosen because of the low cost and low power supply voltage required by these tubes.

From an inspection of Figures 11 and 12 (see pages 64-65) it will be noted that operation at 80 per cent efficiency requires in general

a) $E_{c1} = 2 E_{c0}$; (12)

or

$$b) I_p = 4 \times 0.362a \text{ at } E_{\min} = 84 \text{ volts}$$

Case (b) can just be realized as shown by the plate characteristics for 807's under the following operating conditions:

$$E_b = 600 \text{ volts}$$

$$E_{c_1} \approx -90 \text{ volts}$$

$$E_{c_2} = 250 \text{ volts}$$

$$+ E_{g_1} = +15 \text{ volts}$$

(positive grid swing)

$$I_p = 0.36 \text{ ampere}$$

$$I_{c_2} = 25 \text{ milliamperes}$$

$$I_{c_1} = 15 \text{ milliamperes}$$

The d-c plate current is

$$I_b = I_p / 5.7 = 63.2 \text{ milliamperes (factor for } E_c = 3E_{c_0})$$

The d-c screen current:

$$I_{c_2} \approx I_{c_2} / 5 = 5 \text{ milliamperes}$$

(see $I_{c_2} = f(E_b)$ from characteristic curves)

For four 807's the total B current I_B is therefore

$$I_{b(4)} \approx 250 \text{ milliamperes}$$

$$I_{c_2(4)} \approx 20 \text{ milliamperes}$$

$$I_B \approx 270 \text{ milliamperes}$$

The d-c grid current:

$$I_{c_1} \approx I_{c_1} / 8.8 = 1.7 \text{ milliamperes (factor for } E_g / +E_g = 6)$$

Each screen grid is fed by a series resistor $R_{sg} = \frac{600 - 250}{.005} = 70,000$

ohms. For the purpose of adjustment, it is practical to use 30,000 to 50,000 ohms per tube and a common 10,000-ohm adjustable resistor. The common grid resistor is

$$R_g = \frac{90}{4 \times 0.0017} \approx 13,200 \text{ ohms}$$

The power output of the tubes into the plate circuit is

$$P_o = (E_b \times I_b) \times \text{efficiency} = 120 \text{ watts} \quad (17)$$

and the plate load:

$$R_p = (E_b - E_{\min})^2 / 2 P_o \quad (18)$$

$$R_p = 516^2 / 240 = 1100 \text{ ohms}$$

These computations can be summarized for the 30-kilovolt tripler as follows:

From Table I average fixed losses are 16 watts. The power output is 10 watts and is the sum of the power dissipated in the bleeder load (2.5 watts) plus high voltage output (7.5 watts). If an oscillator efficiency of 73 per cent and an overall efficiency of 40 per cent is assumed, the power input will then be 25 watts.

$$\text{For } E_{c_1} = 3E_{c_{co}}; \text{ with } E_{\min}/E_b = 0.22$$

$$\text{then } \hat{I}_p/I_b = 5.7$$

and the peak power input is

$$\hat{P}_{in} = (\hat{I}_p/I_b) P_{in} = 143 \text{ watts}$$

and

$$I_p = \hat{P}_{in}/E_b = 0.44 \text{ ampere}$$

Two 6Y6G's operated at 325 volts must supply peak currents of

$$\hat{I}_p = 2 \times 0.22 a \text{ at } E_{\min} = 75 \text{ volts}$$

Summarizing and from inspection of 6Y6G characteristics:

$$\begin{array}{lll} \hat{I}_{o_2} = 25 \text{ milliamperes} & \hat{I}_{c_1} = 17 \text{ milliamperes} & E_{c_{co}} = -20 \text{ volts} \\ I_{c_2} = 7 \text{ milliamperes} & I_{c_1} = 1.38 \text{ milliamperes} & E_{c_1} = -60 \text{ volts} \\ & & + E_{g_1} = +12.5 \end{array}$$

The grid power dissipated is 83 milliwatts.

The d-c plate current is

$$I_b = \hat{I}_p / 5.7 = 38 \text{ milliamperes (for } E_c = 3E_{c_{co}})$$

For two 6Y6G's the total B current is therefore

$$I_b \approx 76 \text{ milliamperes}$$

$$I_{c2} \approx 14 \text{ milliamperes}$$

$$I_B = 90 \text{ milliamperes}$$

The series screen resistor is

$$R_{sg} = \frac{E_b - 100}{0.007} = 32,000 \text{ ohms}$$

The grid resistor is obtained from

$$R_g = E_{c1}/I_c = 44,000 \text{ ohms}$$

The power output to the plate circuit is

$$(E_b \times I_b) \times \text{efficiency} = 18.3 \text{ watts}$$

and the plate load

$$R_p = 254^2/36.6 = 1800 \text{ ohms}$$

COUPLING, PLATE LOAD, AND TUNING

The transfer of energy between two coupled circuits depends on the existence of a common electro-magnetic field. As a percentage of the total flux, it is expressed as the coupling factor K . For purely inductive coupling

$$K = M/\sqrt{L_1 L_2} \quad (19)$$

where M is the mutual inductance. The uncoupled or leakage-inductances can be cancelled by the series capacitances C_1 and C_2 , i.e., by tuning the circuits. The reaction of the secondary circuit on the primary circuit causes changes in its series impedance. Its series resistance changes to

$$r_1' = r_1 + T r_{II} \quad (20a)$$

and its inductive reactance to

$$\omega L_1 = \omega L_1 - \mathcal{T} x_{II} \quad (20b)$$

where r_{II} is the total series equivalent resistance, and x_{II} the series reactance of the secondary circuit. \mathcal{T} is a transfer factor depending on coupling, frequency and series impedance z_{II} of the loaded secondary circuit. It is given by

$$\mathcal{T} = \omega^2 M^2 / z_{II}^2 = \omega^2 M^2 / [r_{II}^2 + (\omega L_2 - 1/\omega C_2)^2] \quad (21)$$

RESISTANCE TRANSFER AND COUPLING

\mathcal{T} has its largest value $\mathcal{T}_{(o)}$ when the secondary circuit is in resonance, as the denominator is then reduced to r_{II}^2 .

$$\mathcal{T}_{(o)} = \omega^2 M_o^2 / r_{II}^2 \quad (22)$$

Resonant or near resonant conditions in the secondary circuit are obtainable by changing the frequency ω , that is by varying C_1 of the primary tank circuit.

With Equation (19) and Equations (22) and (20a) one obtains an expression for the minimum coupling coefficient $K_{(o)}$ required to obtain a specified series resistance r_1' in the primary tank circuit tuned for resonance of the secondary circuit:

$$K_o = \sqrt{\frac{1}{Q_{II}'} \left(\frac{1}{Q_1'} - \frac{1}{Q_I} \right)} \quad (23)$$

where $Q_I = \frac{\omega L_I}{r_I}$ (Q value of primary tank circuit without load)

$Q_1' = \frac{\omega L_I}{r_1'}$ (Q value of loaded tank circuit; see Equation 20(a))

$Q_{II}' = \frac{(Z_{II} \text{ in parallel with } R')}{\omega L_2}$

(Q_{II}' is the Q value of secondary circuit with rectifier load R' ; see Equation (1))

K_o is then the critical coupling necessary to reflect the proper shunt load to the oscillators under full power output conditions.

For the 90-kilovolt supply and selecting $F_o = 65$ kilocycles (see Table II): $Q_I \approx 400$ (A small loss in C_1 is to be expected.) The design will

be for: $Q_1' = 10$ and

$$Q_{II}' = \frac{\overbrace{(35 \text{ in parallel with } 150 \text{ in parallel with } 6)}^{\substack{\text{megacycles} \quad \text{megacycles} \quad \text{megacycles}}} \underbrace{\hspace{10em}}_{Z_2} \underbrace{\hspace{10em}}_{R'}}{.093 \text{ megacycles}} = 53$$

(This is the Q value for max. load)

where: 35 megohms is shunt coil loss at $F = 65$ kilocycles

150 megohms is shunt impregnant loss

6 megohms is effective load

The minimum coupling is with (23), therefore

$$K_{(o)} = 0.043$$

This coupling will transfer the power to the secondary circuit but will give very poor regulation. It is the condition where the desired energy transfer occurs, and the primary is tuned so that maximum voltage at full load is produced across the secondary. Under these conditions the reactance x_{II} is tuned out and Equation (20a) reduces to

$$r_1' = r_1 + \omega^2 M^2 / r_{II} \quad (24)$$

Any reduction of the load (decrease of r_{II}) results in an increase in r_1' , a lower shunt primary impedance, and higher oscillator power output. This results from the tendency of the oscillator to maintain a constant voltage amplitude across the primary tank circuit for moderate variations in load. The increased power supplied results in a rapid rise in secondary voltage.

Good regulation requires that

$$K \geq 5K_o \quad (25)$$

By adjustment of ω , i.e., by tuning the primary, the transfer factor \mathcal{T} in Equation (21) can be made to equal $\mathcal{T}_{(o)}$ in Equation (22) so that proper energy transfer results.

For $K/K_o = 5$ we may write the requirement:

$$r_1' = r_1 + [(5\omega Mo)^2 / (r_{II}^2 + x_{II}^2)] r_{II} \quad (26)$$

In order to maintain the same magnitude of coupled resistance to the primary under full load conditions, the term $(r_{II}^2 + x_{II}^2)$ must increase so that $r_{II}^2 + x_{II}^2 = 25r_{II}^2 \text{ max}$. This necessitates an operating condition where the magnitude of the coupling factor is determined by the residual reactance left in the secondary circuit at oscillator frequency, rather than by its resistance $r_{II} \text{ max}$. Operation under such conditions, i.e., off resonance as far as the secondary self-resonant frequency is concerned, introduces a coupled reactance to the primary which is given by

$$x_{II} \approx 5r_{II} \text{ max} \quad (27)$$

which follows from the fact that r_{II} is in quadrature and has little effect on amplitude of the transfer factor when Equation (27) is true. The denominator in Equation (21) varies less than 4 per cent for all values of secondary resistance between no load and full load.

Equation (26) can then be replaced by:

$$r_I' = r_I + \left[\frac{(5\omega M_o)^2}{x_{II}^2} \right] r_{II} \approx r_I + \left[\frac{\omega M_o}{r_{II} \text{ max}} \right]^2 r_{II} \quad (28)$$

where the bracketed term is constant. A reduction of the load r_{II} now causes a reduction of r_I' . The oscillator power is thus transferred to the secondary in a manner similar to that occurring when a 100 per cent coupled transformer is used.

The required coupling $K \approx 5K_o$ may be computed with the aid of Equation (23). Should this coupling be unobtainable, the value Q_I' may be increased by reducing L_I . This will result in better regulation but at the expense of additional primary power loss.

The coupling can be increased by connecting L_2 in series with L_1 as shown in Figure 9, which gave $K = 0.235$. A slight decrease in spacing increases K considerably ($K = .25$ for S decreased by 12 per cent), and serves as a practical coupling adjustment. The coupling of a finished transformer is checked by measuring the frequency difference ΔF between the peaks of the two resonant responses, as $K \approx \Delta F/F_o$. This check must be made with the primary tuned to the frequency ω_o . This is the frequency of the secondary circuit measured with $C_1 = 0$. The primary circuit is then tuned to ω_o as indicated by equal frequency deviations $\Delta F/2$ of both peaks. Figure 10 shows this case (curve 4) as well as the operating condition (curve 7). The test circuit is indicated. The response curves of Figures 10 and 11 do not give

direct information on the voltage output under oscillating conditions, for which the primary voltage (not the current) is maintained nearly constant.

REACTANCE TRANSFER AND PRIMARY CONSTANTS

The reactance of the primary circuit is increased by the transferred series reactance x_{11} when the reactance of the secondary is capacitive.

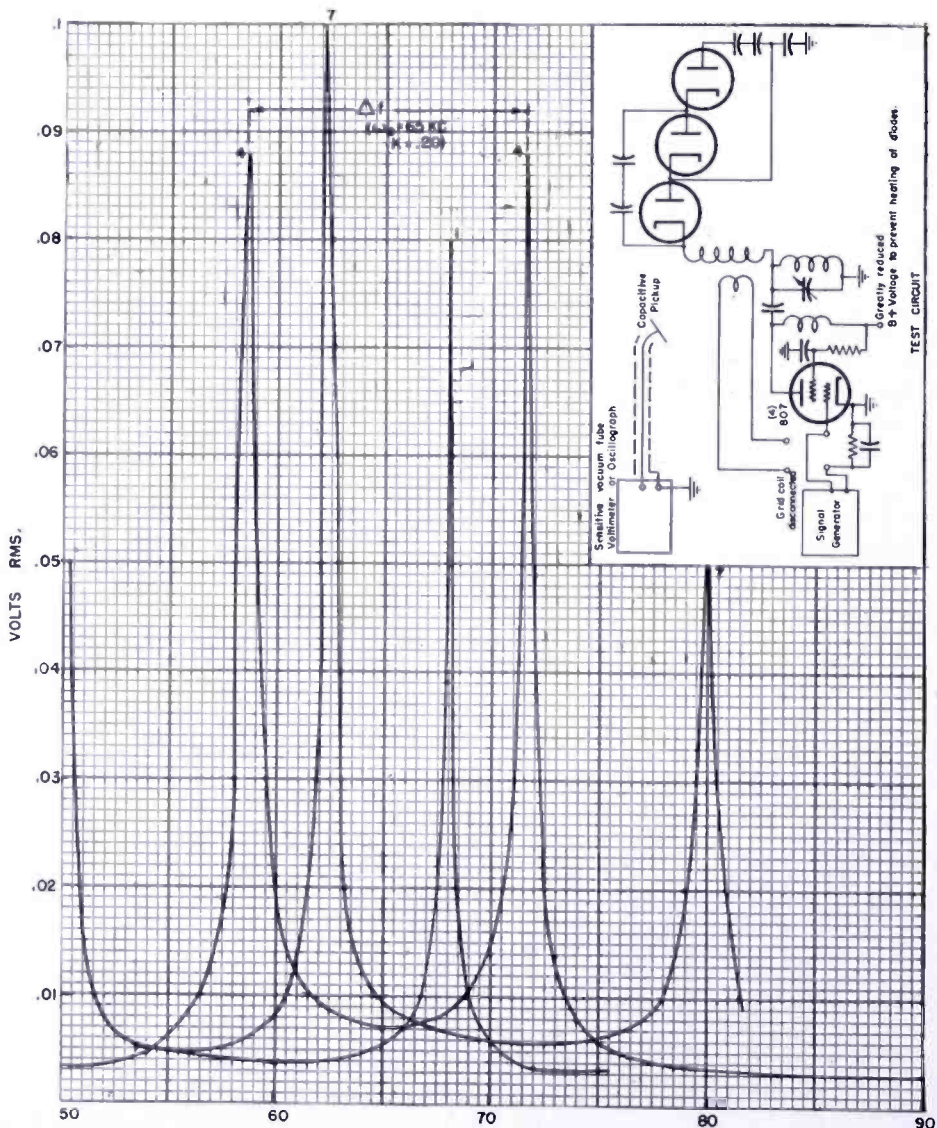


Fig. 10—Frequency characteristics of 90-kilovolt circuit (rectifiers not heated) for primary tuning conditions 1, 4, and 7 shown in Figure 11.

This is the desired operating condition, the circuit oscillating at the lower coupling frequency ω_1 , with the secondary operating at a somewhat higher frequency than that obtained when equal primary and secondary tuning is used, but still below its self-resonant frequency ω_0 .

For this operation, and $K \geq 5K_o$ the inductive primary circuit reactance is given by

$$\omega L_1 = \omega_1 L_1 + KK_o \omega_1^2 L_1 L_2 / r_{11} \max \quad (29)$$

which can be derived from (20b) with

$$T = [\omega_1 M_o / r_{11 \max}]^2 x_{11}$$

by substituting

$$x_{11} = 5r_{11 \max} \omega_1^2 M_o^2 = K_o^2 \omega_1^2 L_1 L_2, \text{ and } K = 5K_o.$$

$$\text{Factoring } L_1 \text{ results in } L_1 = L_1 / (1 + KK_o Q_{11}') \quad (30)$$

It is now necessary, to determine ω_1 in terms of ω_o , K , K_o and Q_{11}' so that a value of L_1 can be computed from L_1 (effective primary inductance including effect of coupled secondary reactance).

The oscillator frequency ω_1 is given by

$$\omega_1 / \omega_o = 1 - (K / 2K_o Q_{11}') \quad (31)$$

which can be computed with the aid of Equations (25) and (27) by substituting

$$r_{11}' = \frac{\omega_o L_2}{Q_{11}' o}$$

and setting

$$\Delta x = x_{11} / 2.$$

For the specific example $F_o = 65$ kilocycles, $K = 0.21$, $2K_o = 0.086$ and $Q_{11}' o = 53$

$$\omega_1 / \omega_o = 1 - (0.21 / .086 \times 53) = 0.954$$

$$F_1 = 62 \text{ kilocycles}$$

and

$$L_1 = 0.675 L_1$$

The tank circuit is to be designed for a full load value $Q_1' = 10$. Then

$$\omega L_1 = R_p / Q_1' \quad (32)$$

Substituting $R_p = 1100$ from (18), and $F = 62$ kilocycles, a value of $\omega_1 L_1 = 110$ is obtained and $\omega_1 L_1 = 74.5$ ohms. L_1 is then 190 microhenries. The necessary tuning capacitance is

$$C_1 = 1/\omega_1^2 L_1 = 0.0233 \text{ microfarads.} \tag{33}$$

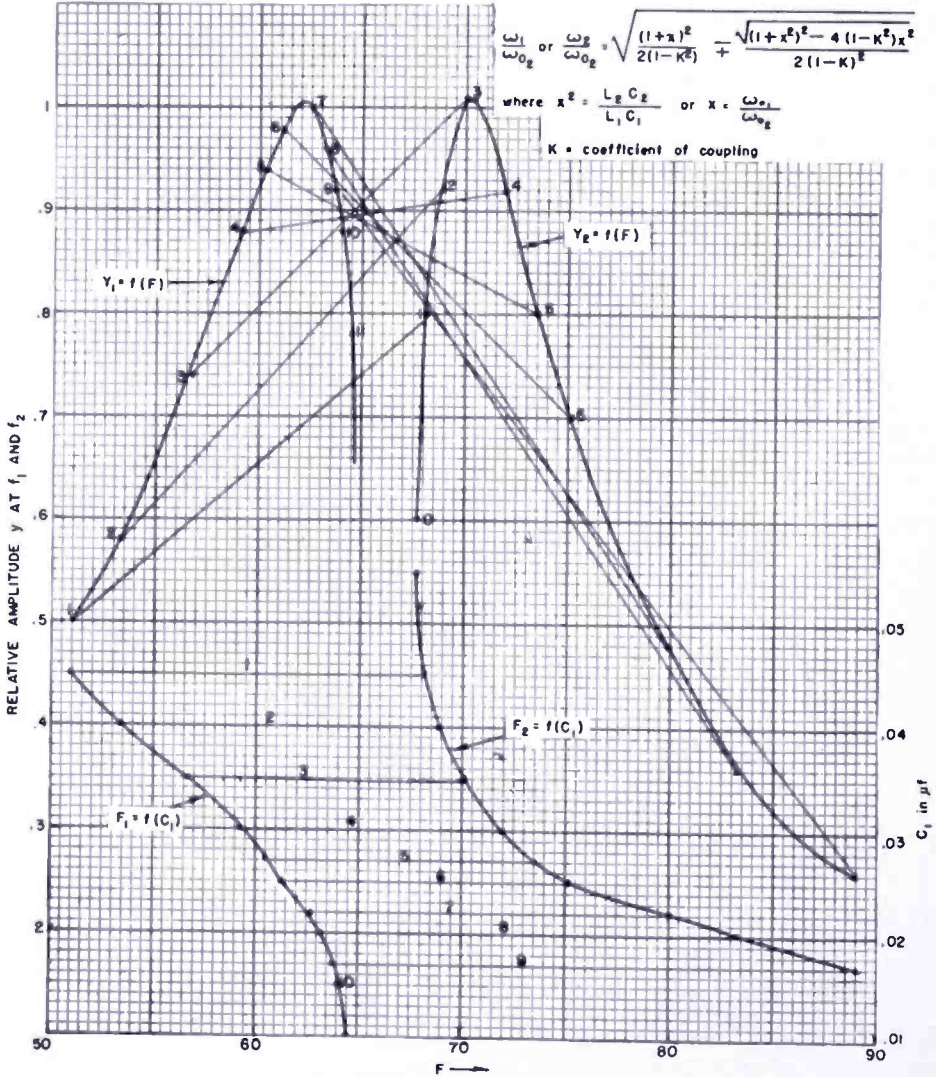


Fig. 11—Secondary output curves for various operating frequencies.

Figure 11 shows the envelope curves and relative amplitudes of corresponding coupling frequencies F_1 and F_2 obtained with constant grid excitation of the oscillator tubes (from a separate source) as a function of the primary tank tuning capacitance C_1 . For the case where $C_1 = 0.04$ microfarad (points 2) the lower peak F_1 (53.5 kilocycles) produces a relative output of $Y_1 = 0.58$ and the upper peak F_2 (69 kilocycles) produces an amplitude $Y_2 = 0.92$. Operation at the lower frequency, near the peak of the curve (points 7 or 8) requires a smaller

tuning capacitance C_1 than operation at the higher frequency peak (points 2 to 3). Self-excitation by feedback from the secondary winding causes stable oscillations at the preferred frequency F_1 with normal feedback coil polarity (as if the secondary circuit did not exist). Operation at F_2 obtains upon reversal of the feedback coil polarity but causes lower tank circuit efficiency and somewhat poorer regulation. These relations are shown in vector form in Figure 12. The voltage induced in the secondary lags i_1 by 90 degrees, and that induced in

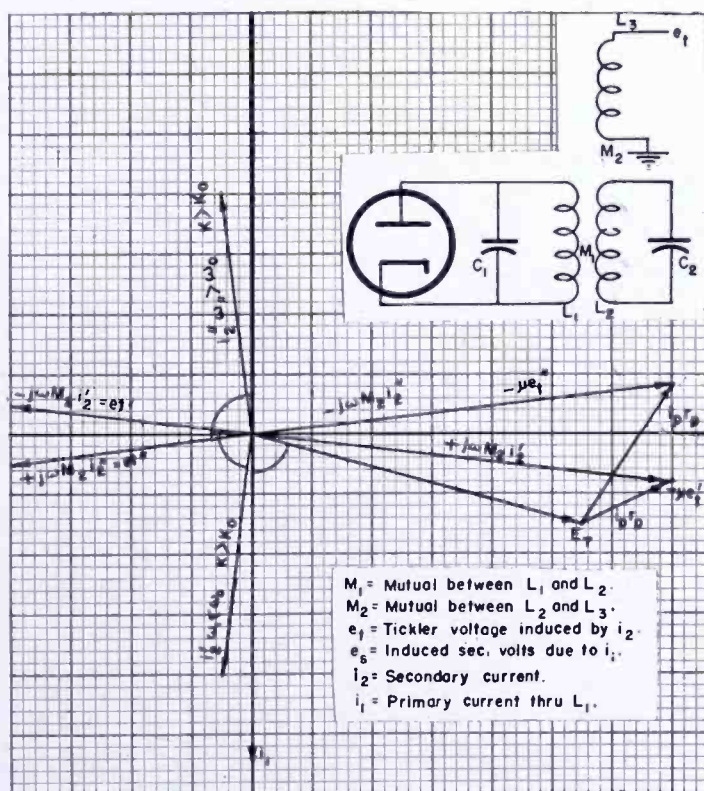


Fig. 12—Vector diagram of oscillator phase relations.

the tickler will either lead or lag i_2 , the secondary current, by an additional 90 degrees. When $K > K_0$ and the tickler is inductively coupled to the secondary, oscillation can occur at either of the two peaks depending on the sign of the mutual inductance between tickler and primary. When $\omega_1 < \omega_0$ (the preferred condition), i_2' will lead the induced secondary voltage e_s . Inasmuch as the voltage vector e_t must lie in the third or fourth quadrant for oscillations to occur, the tickler voltage $e_t' = -j\omega M_2 i_2'$ is the effective vector for producing oscillations. Reversing the tickler with $\omega_1 < \omega_0$ results in the vector $+j\omega M_2 i_2'$ which has no component in the direction necessary for oscillation. Operation

at $\omega_2 > \omega_0$ will occur when the tickler is reversed. Reversing the direction of winding of the secondary has no effect as the signs of the mutual inductances between primary and secondary and between secondary and tickler are changed simultaneously.

Another phenomenon, not normally encountered under the usual conditions of oscillator operation, has resulted in a particular method of obtaining feedback. In the conventional oscillator circuit, the tickler winding is coupled to the primary and is so connected that the mutual inductance of the proper sign for oscillation is obtained. If a loaded tuned circuit of approximately the same frequency as that of the primary circuit is now tightly coupled to the primary there will be two new frequencies at which the primary tank circuit is substantially resistive. It is now assumed that the oscillator is operating at a frequency ω_1 which is below the self-resonant frequency ω_0 of the secondary, and the primary self-resonant frequency is above ω_0 . As the primary is tuned still higher in frequency the frequency of oscillation will approach ω_0 , the output voltage will rise, and the loading on the primary will increase. A point will finally be reached at which the reflected load resistance is so high that insufficient primary tank impedance for continued oscillation will remain. At this point the oscillator frequency will "jump" to a higher frequency at which the primary tank is again sufficiently high to again permit oscillation. However the coupled secondary resistance will now be smaller and the resultant oscillator loading considerably less. If the primary is now tuned lower in frequency, the coupled resistance will again increase until a point is reached where the same condition of instability results. The oscillator will then readjust its frequency as described.

Thus, it can be seen that if the oscillator is tuned past a stable operating point and then turned off, it may start in its second mode of oscillation, where it possesses greater stability but does not provide the desired output voltage. This is obviously an undesirable operating condition. Ollendorf² has shown that this instability results from an abrupt increase in oscillator loading and has quantitatively analyzed the effect for various magnitudes of coupling and tuning directions.

Coupling the tickler to the secondary avoids such instability as the grid excitation increases with higher secondary voltages. While a jump in frequency will not be experienced with this arrangement, oscillator loading will increase with detuning in the normal manner. The smaller power supplies described including the 30-kilovolt tripler use this method of obtaining excitation. The 90-kilovolt unit obtains most of

² Ollendorf, S., *DIE GRUNDLAGEN DER HOCHFREQUENZ-TECHNIK*, J. Springer, Berlin, Germany, 1926 (pp. 393-411).

its excitation in this manner, a smaller part being supplied by the primary to tickler coupling.

Proper tuning with operation at ω_1 results in a decreasing high voltage with increasing values of C_1 and vice versa. Variation of C_1 causes a variation of the transfer constant and provides thereby an adjustment of the reflected oscillator plate load, and the high voltage output.

CALCULATION OF THE 90-KV PRIMARY COIL

A power loss of n per cent requires the ratio of the tuned impedance of the fully loaded primary to the unloaded primary to equal n . Thus:

$$n = R_L / Q_1 \omega L_1 \quad \text{and} \quad Q_1 = Q_1' / n \quad (34)$$

For $n = 3$ per cent (see Table I), Q for the primary circuit with Equation (34) is:

$$Q_1 \cong 10 / 0.33 = 333 \quad (35)$$

The magnitude of ωL_1 can be obtained from (29) and (30), and the desired value of Q_1 from (35), giving a value of r . The direct-current resistance r_o (see Equation 7) can then be estimated, substituting a value of 1 for k^2 . The safe value of 1000 circular mils/ampere (Equation 10) is assumed to be satisfactory for a first trial to estimate the wire size from the circulating tank current. The peak voltage $\hat{E}_1 = (E_b - E_{min}) = 516$ volts causes the root-mean-square tank current $I_2 = 516 / \omega L_1 \sqrt{2} = 3.3$ amps, and results in a wire size of $1000 \times 3.3 = 3300$ circular mils.

If #38 litz (15.7 circular mils) is chosen, the wire should have $3300 / 15.7 = 200$ strands for a first approximation. The litz wire diameter is roughly 50 per cent larger than that of the equivalent bare solid wire (#15), i.e., $D_{200} \approx 0.085$ inches. This wire will wind with 12 turns per inch.

For good coupling to the secondary, the tank circuit coil should not be too long and its diameter only as large as required by spark over distances to the high voltage winding.

A table can now be constructed with values for these coils with different strand numbers (see Table III), computed for $F_1 = 63$ kilo-

Table III—Primary Coil Data

#	N	Layers	l	a	n	Lu _h	k ²	r _o	r _i	ωL_1	$\frac{\omega L_1}{r_i}$	$\frac{\omega L_1}{r_l}$	I _I	I _I ² r _i	KVA (1)
1	32	3	0.9"	0.2 "	200	180	1.1	0.13	0.27	71	260	410	3.3a	3.00w	1.2
2	32	3	1.1"	0.24"	250	175	1.16	0.11	0.24	69	290	460	3.3a	2.65w	1.2
3	33	3	1.3"	0.3 "	330	180	1.5	0.09	0.22	71	320	500	3.3a	2.42w	1.2

layout would result in long filament leads with added insulation problems and capacitance. In this case the latter system is preferable.

When a one- or two-turn loop is used, the size of the loop and its position in the energizing field can be adjusted until inspection of the rectifier filament indicates proper operation. Accurate adjustment is facilitated by comparison with a similar rectifier tube fed from a 60-cycle source.

A typical filament transformer assembly is shown in Figure 14 (90 kilovolts). The computations involved in calculating filament trans-

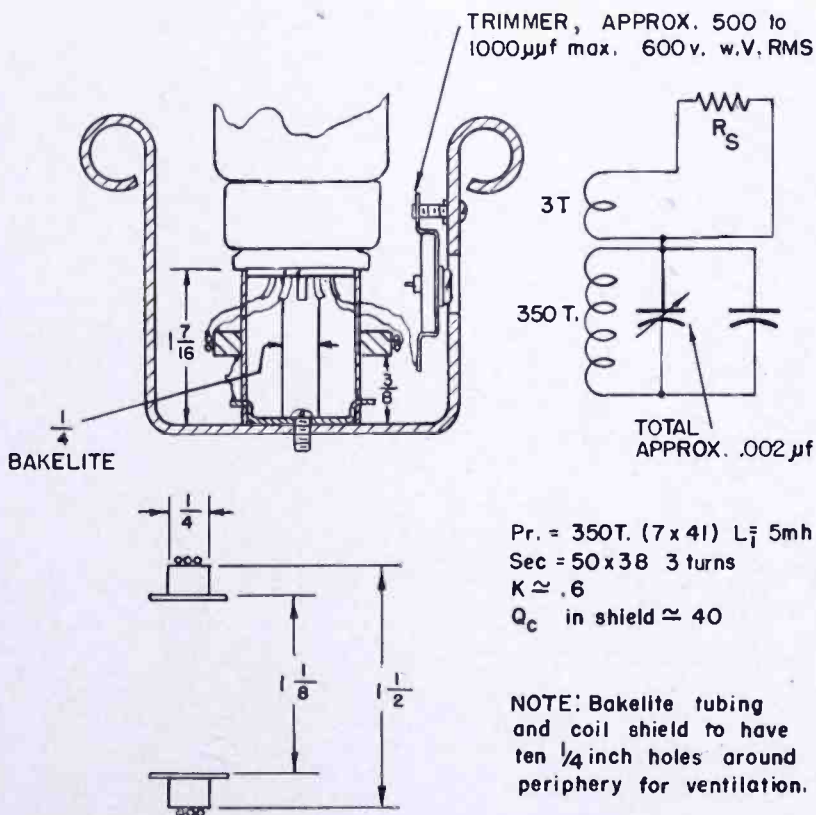


Fig. 14—Typical filament transformer assembly.

former performance are best illustrated by the following examples. For all cases the equivalent circuit is that represented by Figure 15. The line current (i_1) is given by

$$i_1 = \frac{E_{rms}}{X_c} \tag{37}$$

Where X_c is the diode capacitance (plate-to-cathode) and E_{rms} the r-f voltage across the diode. The transformer efficiency of η specifies the

power and resistance ratio for parallel circuits

$$\frac{R_1}{R_L} = \frac{\eta}{(1 - \eta)} \tag{38a}$$

where R_1 is the equivalent coil loss resistance and R_L the equivalent or reflected useful load resistance in shunt with the parallel-tuned circuit resistance. The ratio of the circuit Q with a load to that without load is given by:

$$Q_o'/Q_o = 1 - \eta \tag{38b}$$

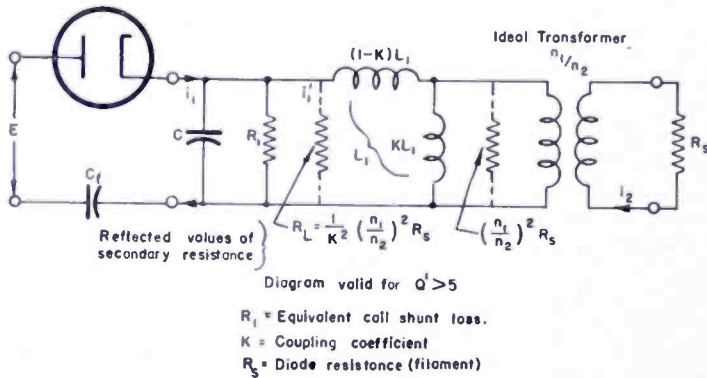


Fig. 15—Equivalent circuit of filament transformer.

It should be stated that the following expressions for the transformer design are based on the requirement that the loaded Q value (Q_o') of the primary circuit must be

$$Q_o' > 5. \tag{38c}$$

Inasmuch as the reactive currents cancel out there is a division of the constant current i , between R_L and R_o . The fraction of current producing useful power output is therefore given by $i_1' = i_1\eta$. Hence

$$R_L = P_o/i_1'^2\eta^2 \tag{39}$$

and with Equation (38)

$$R_1 = \frac{P_o}{\eta(1 - \eta)i_1'^2} \tag{40}$$

provided the LC circuit is in resonance with the driving frequency ω , i.e.

$$C = 1/\omega^2L \tag{41}$$

In the equivalent transformer circuit Figure 15 the reflected load resistance $(n_1/n_2)^2 R_s$ is shown in shunt with the coupled inductance $(K L_1)$. For Q values > 5 it is reflected across the tank circuit as the equivalent load resistance

$$R_L = \left(\frac{1}{K} \times \frac{n_1}{n_2} \right)^2 R_s \quad (42a)$$

the bracketed term being the effective transformer ratio. Substituting Equation (39) and $P_o = i_2^2 R_s$, it follows from (42a) that

$$\left(\frac{1}{K} \times \frac{n_1}{n_2} \right)^2 R_s = \frac{P_o}{i_1^2 \eta^2} = \frac{i_2^2 R_s}{i_1^2 \eta^2} \quad (42b)$$

The turns ratio for a given coupling is thus

$$\frac{n_1}{n_2} = \frac{K i_2}{\eta i_1} \quad (43a)$$

This equation shows that higher values of coupling indicate a greater required turns ratio. In general it will be found that there are two values of K which will give the same secondary current. In one case the reflected shunt load will be considerably less than the tuned tank impedance, the efficiency will be high, and the voltage drop across the tuned primary slightly higher than that obtained for a condition of perfect match with a loss-free transformer. In the second case the reflected shunt load will be higher than the unloaded tuned tank impedance and more power will be wasted in the transformer than is developed in the load. This, of course, will result in poor efficiency and an excessive voltage drop across the tuned circuit. The rectifier peak charging current will be unnecessarily limited and poorer regulation will result.

The inductance value can be obtained from the following expression

$$L = \frac{P_o}{\eta(1-\eta) Q_c \omega i_2^2} \quad (43b)$$

which can be derived from the previous equations.

A typical transformer calculation will be illustrated for the 90-kilovolt case where the following data are given or assumed:

$$K = 0.6 \qquad P_o = 2 \text{ watts} \qquad Q_o = 40 \text{ (assumed)}$$

$$\omega = 390,000 \qquad i_2 = 1.25 \text{ amperes} \qquad i_1 = 10\text{-}12 \text{ milliamperes}$$

Calculations should be made for the lower i_1 to provide a safety factor.

The turns ratio, inductance, and loaded Q can be computed from Equations 43a, 43b, and 38b respectively. These results are shown in Table IV.

Table IV—Filament Transformer Data

10 ma			12 ma	
$\eta\%$	Lmh	$\frac{N_1}{N_2}$	Lmh	$\frac{N_1}{N_2}$
85	10.1	88	7.	73
75	6.9	100	4.8	84
65	5.65	115	3.94	96
55	5.1	136	3.56	114

$n = 0.75$				$n = 0.65$		
Q	Q'	Lmh	$\frac{N_1}{N_2}$	Q'	Lmh	$\frac{N_1}{N_2}$
40	10	6.9	100	14	5.65	115
50	12.5	5.5	100	17.5	4.54	115
60	15	4.6	100	21	3.77	115
70	17.5	3.9	100	24.5	3.23	115

The inductance value used is arbitrarily chosen to be about 5 millihenries as this will result in a coil which is not so large that its Q is adversely affected when it is placed in the corona shield. Powdered iron cores permit higher values of Q and inductance to be obtained. Higher efficiencies, smaller coils, and better couplings result.

The turns ratio, inductance, and other data for the 30-kilovolt tripler filament transformer follows:

$$Q_o = 50$$

$$L_1 = 5.6 \text{ millihenries}$$

$$\text{Coupling} = 0.4$$

$$\text{Diameter of form} = \frac{3}{8}''$$

$$\text{Tuning capacitance} = 22 \text{ micromicrofarads (for partial resonance)}$$

$$\text{Primary turns} = 500 \text{ \#10/41 Litz}$$

$$\text{Secondary turns} = 20 \text{ \#15/38 Litz}$$

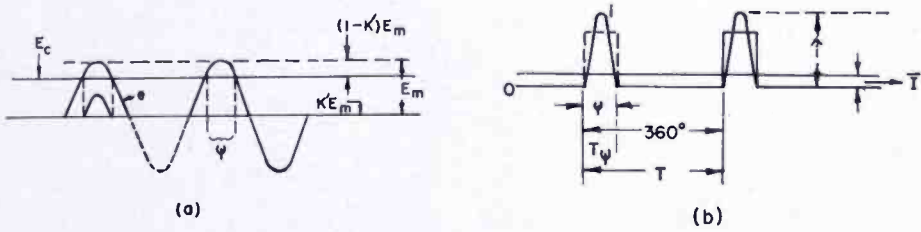


Fig. 16—Diode conduction.

DIODE CURRENTS AND REGULATION OF THE RECTIFIER CIRCUIT

The relatively high frequency used in an r-f supply permits the use of a simple economical filter circuit. This circuit generally consists of a pi section resistance-capacitance (R-C) combination with the output capacity being formed from the shield to center conductor capacitance of the second anode supply lead. Inasmuch as the time constant of the filter condenser-load resistance combination is long compared with the discharge period between successive r-f pulses, the output voltage can be considered constant, and will have the value $K'E_m$, (where K' is a percentage of the peak voltage E_m) for a given load. This is shown graphically in Figure 16. The diode conduction angle can be derived from the equation $\psi^\circ = 2 \cos^{-1} K'$ (44)

The magnitude of ψ for various values of K' has been computed and listed in Table V.

Figures 16(a) and 16(b) show the relation between the conduction time and the diode peak to average currents. The equivalent average diode current is determined by the ratio of the total time to conduction

Table V—Rectifier Data

K'	$\psi/2$	ψ	$\frac{360}{\psi}$	$\frac{2k'}{(1-k')}$	$\frac{R_t}{Z_s} = \frac{2k'}{(1-k')} \frac{360}{\psi}$	$\frac{\hat{I}}{\bar{I}} = \frac{360\pi}{2\psi}$
.995	5.75	11.50	31.3	398.	12420.	49.
.99	8.1	16.2	22.2	207.	4400.	35.
.98	11.5	23.0	15.65	100.	1560.	24.6
.97	14.1	28.2	12.75	65.9	827.	20.
.96	16.25	32.5	11.1	48.3	522.	17.5
.95	18.2	36.4	9.9	37.9	378.	15.6
.94	20.	40.	9.	30.4	283.	14.2
.92	23.1	46.2	7.8	22.9	178.	12.3
.90	25.9	51.8	6.95	18.	124.	10.9
.88	28.4	56.8	6.35	14.5	92.7	10.
.86	30.7	61.4	5.87	12.3	84.5	9.25
.84	32.9	65.8	5.5	10.5	57.6	8.65
.82	34.9	69.8	5.16	9.1	47.0	8.1
.80	36.9	73.8	4.88	8.0	39.2	7.65
.78	38.79	77.5	4.65	7.05	32.8	7.3
.76	40.9	81.	4.45	6.32	27.8	7.

time for a cycle, $(T/T\psi)$. If this factor is multiplied by $\pi/2$, a ratio of peak to average current is obtained which, for sinusoidal diode currents, is a sufficiently close approximation for all practical purposes.

Hence:

$$i/I = \pi T/2T\psi \quad (45)$$

where $T/T\psi = 360 \text{ degrees}/\psi \text{ degrees}$ (for sine waves) or $T/T\psi = T_H/T\psi = T_H \times 180 \text{ degrees}/T_R \times \psi \text{ degrees}$ (for surge pulse voltages) T_H/T_R is the ratio of the total time of one cycle to the time duration of the surge pulse.

The energy delivered by the source during $T\psi$ must equal that dissipated during T . Thus equating the direct-current to alternating-current power

$$TE^2/R_L = T\psi (K' E_m)^2/2R' \quad (46)$$

The equivalent alternating-current load R' during $T\psi$ is therefore

$$R' = T\psi R_L/2T \quad (47)$$

Replacing the diode load in Figure 17 by R' it is obvious that the voltage ratio $(1 - K') E_m/K' E_m = Z_s/R'$, and $R' = K'/(1 - K') Z_s$. With Equation (47) this furnishes $R_L/Z_s = 2K' T/(1 - K') T\psi$ (48)

which is the ratio of the direct-current load resistance R_L to the effective series impedance Z_s . Computed values for this equation are given in Table V. Rectification efficiency $E/K' E_m$ and the peak-to-average diode current ratio \hat{i}_d/\bar{I} can thus be plotted as a function of the resistance ratio R_L/Z_s , as shown in Figure 17.

The impedance Z_s of the tuned circuit source is its surge impedance

$$Z_s = \sqrt{L/C} = \omega L = \frac{1}{\omega C}$$

The energy delivered by the tuned circuit occurs at a time when no energy is being supplied to the tank circuit by the oscillator, as shown in Figure 18. During the diode conduction time a series combination of the diode resistance and the input filter capacitance is shunted across the tank circuit. The relatively large power supplied during this short interval has the effect of "braking" the normal flywheel characteristic of the tank circuit, slowing the frequency of oscillation, and producing phase delay of the tank current. During the next half cycle the oscillator will deliver sufficient energy to compensate the tank for the power delivered to the rectifier circuit, plus the normal tank circuit losses, resulting in a gain in phase.

The curves in Figure 17 are based on the relation $\omega CR \cong 500$, which should still hold when the last stage of a voltage multiplier circuit is

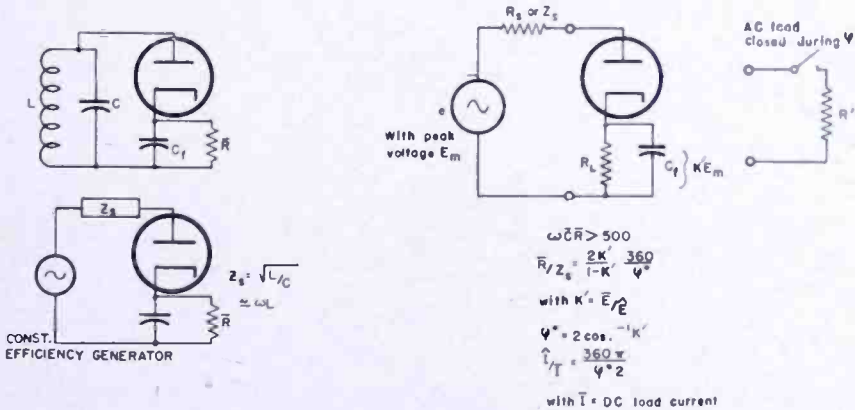
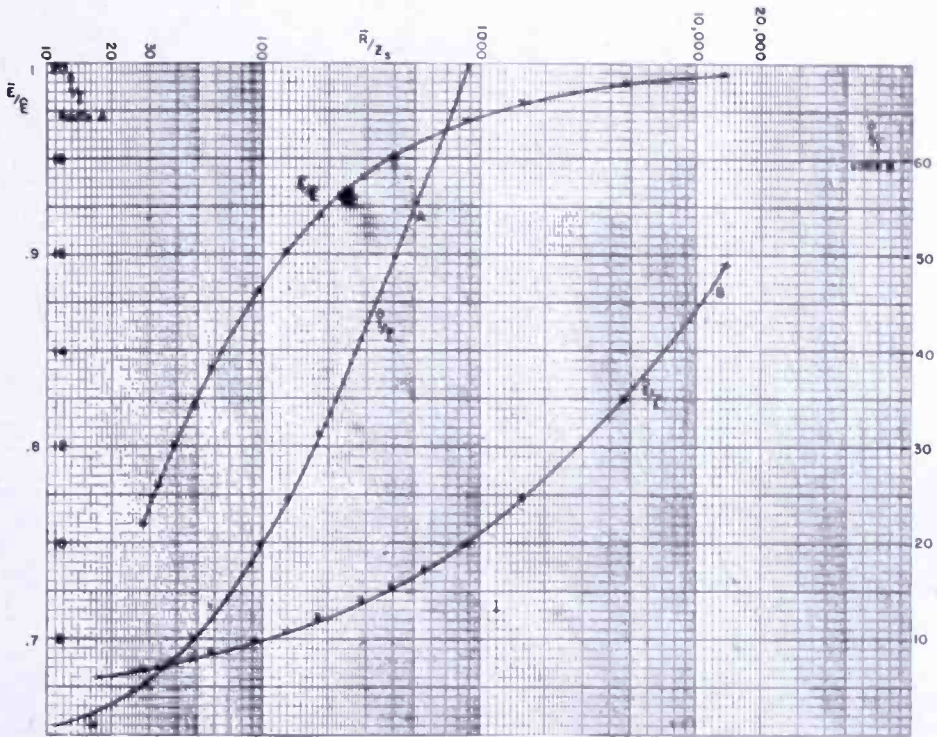


Fig. 17—Rectifier conduction curves.

connected over a number of series filter condensers.

In r-f supplies the effective filter capacitance C_f forms a voltage divider with the diode capacity, the ripple voltage being largely determined by the ratio of these capacitances. To prevent this voltage from causing excessive power loss in the output filter condenser, its capacitance should be large compared to the diode capacitance.

The effective series impedance Z_s of the 90-kilovolt circuit is given by $\sqrt{L/C} = 95,000$ ohms. The 110-megohm direct-current load of the tripler circuit can be reduced to parallel diode circuits with equivalent direct-current loads carrying the normal direct current for the same

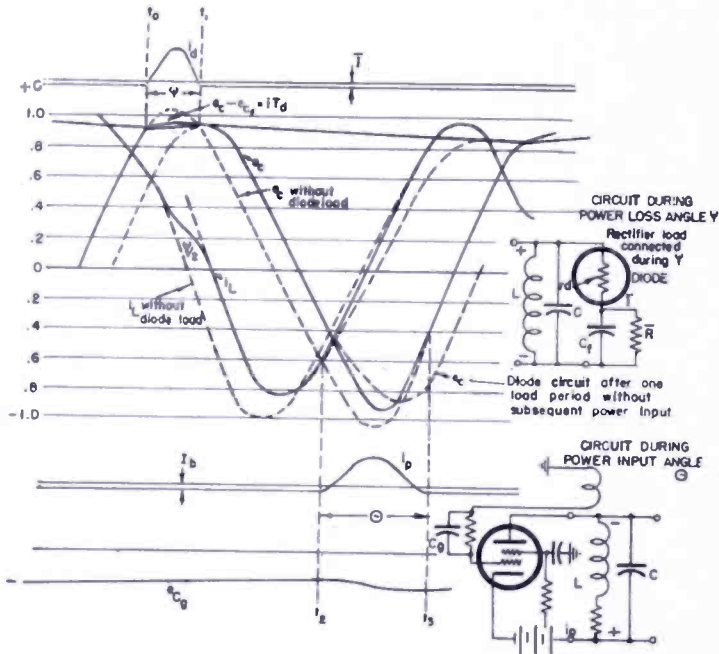


Fig. 18—Oscillator-rectifier circuit power relations.

total power dissipation, as shown in Figure 19. For the diode D_1 operating singly on one half cycle $R_L/Z_s = 378$ and from Figure 17 $i/I = 15.6$. The rectifier efficiency for D_1 is $E/E = 0.95$. Thus a regulation of about 5 per cent of 30 kilovolts or 1.5 kilovolts may be expected from the diode D_1 which conducts during one portion of the positive half cycle. During a portion of the negative half cycle diodes D_2 and D_3 conduct reducing the effective direct-current load to 18.3 megohms., R_L/Z_s will be 193 indicating a regulation of approximately 7.5 per cent from these diodes. This is equivalent to a 2.25-kilovolt drop for the 30 kilovolts from each diode. Adding these three output voltages, a loss of 6.0 kilovolts (or 6.7 per cent of 90 kilovolts) is obtained. In the previous derivations the diode resistance has been neglected. However,

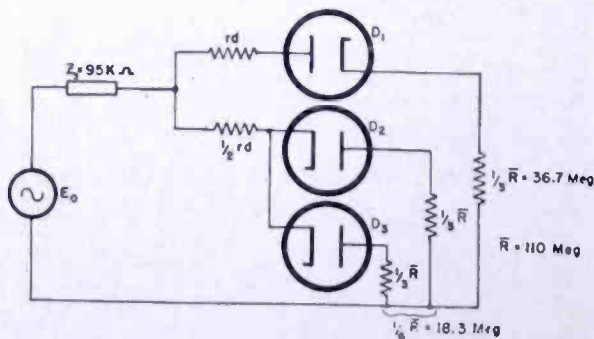


Fig. 19—Equivalent rectifier load circuit.

if this is large it should be added to the series generator impedance.

The oscillator tank circuit voltage is reduced during the time that it delivers power to the rectifier circuit, and is restored to its original value during the time that energy is supplied to the tank from the oscillator. The data in Figure 17 are based on constant oscillator efficiency. Actually the oscillator efficiency changes as a function of the load. The difference in oscillator efficiency between no load and full load is easily calculated. It is approximately 8 per cent for the 90-kilovolt circuit and this difference represents the power diverted from the tank circuit to tube loss. The corresponding primary voltage change is equal to the square root of the efficiency change. Therefore the oscillator regulation for this particular case is approximately 4 per cent.

The overall total regulation will then be in the order of 10 per cent at 800 microamperes.

MISCELLANEOUS OPERATING DATA

After constructing a supply in which the oscillator tubes are operated close to their maximum ratings, it may be desirable to check plate dissipation more accurately than is possible by estimating many circuit losses. In this case the operating data should be taken and the oscillator then disconnected and operated as a driven class C amplifier under the identical voltage and driving conditions. A plate load consisting of a single tuned circuit of known Q plus an added shunt resistance adjusted for the same plate current should replace the step-up transformer and associated circuit. A determination of actual power normally delivered to load plus all other dissipative elements is thus readily made, and actual tube dissipation easily calculated.

Excessive power input for the desired output can result from losses which are not readily apparent. The point at which these losses occur is most readily determined in the higher voltage supplies as heating progresses more rapidly due to greater energy dissipation. It is advisable to keep as much material as possible out of the field of the high voltage secondary even though such material is normally considered a good low loss insulator. A number of the plastics show rapidly increasing power factors with rising temperatures, resulting in a cumulative tendency toward breakdown. The importance of the impregnant used for the high voltage winding has been previously considered.

Several of the supplies have been built on plastic bases in order to simplify insulation problems, and reduce capacity and eddy current losses. The spacing used for the outer shield is determined by spark over, and secondary capacity loading. Close shielding of the secondary

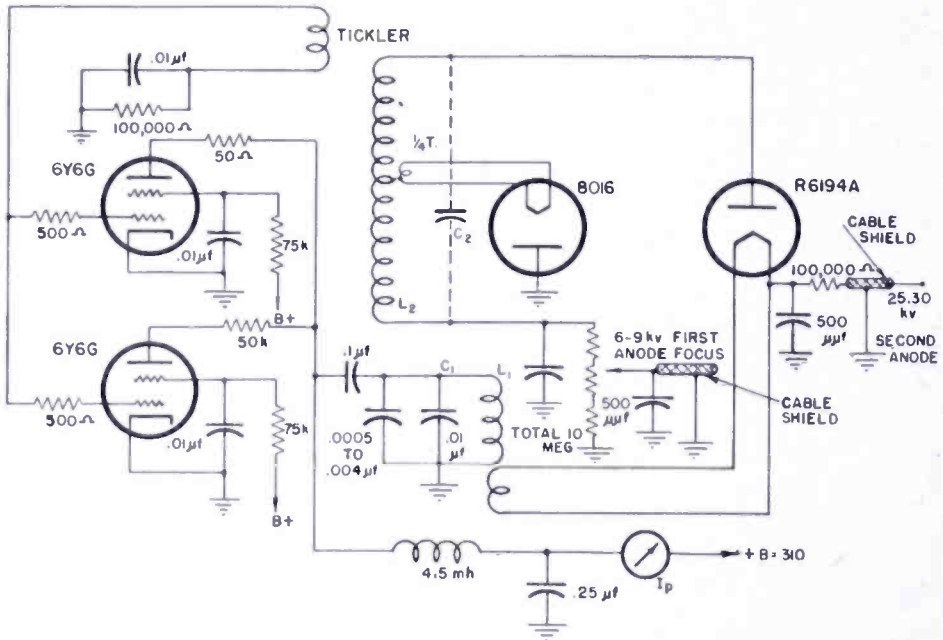


Fig. 20—Circuit of 30-kilovolt unbalanced doubler supply.

lowers its impedance, requiring greater oscillator current, and may cause increased corona difficulties.

The lead to the first diode from the top pie of the secondary should be large in diameter to avoid corona. It is advisable to start this lead at the center of a plane drawn through this pie. Any considerable mass in the field of the coil will become excessively hot after short

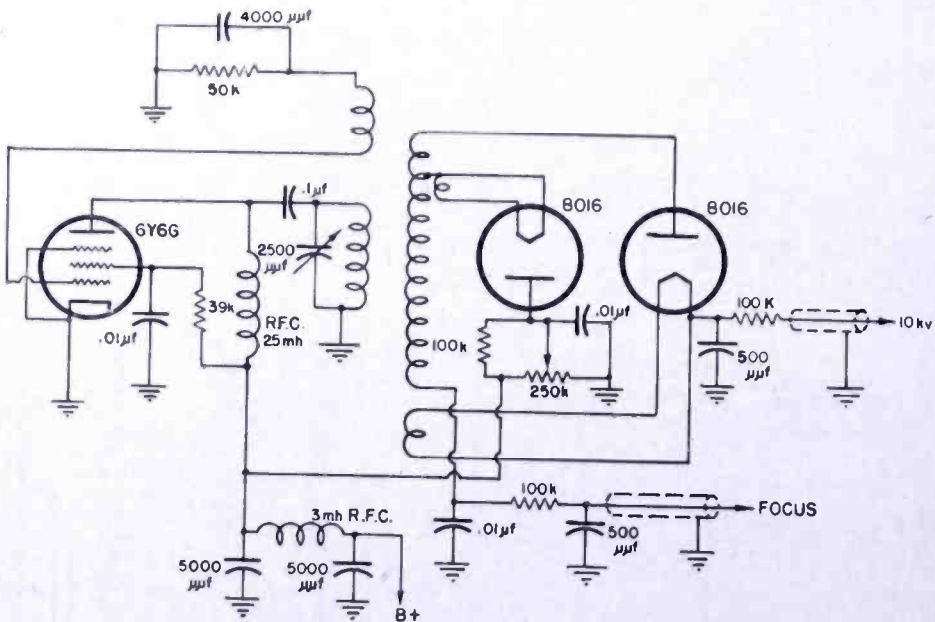


Fig. 21—Circuit of 10-kilovolt supply.

periods of operation, indicating the desirability of *very thin walled* tubing or preferably a closely wound spring. The latter arrangement is convenient for making connections and has worked satisfactorily.

Another cause of excessive oscillator current is the rectifier shunt loss occurring as a result of glass bombardment by cold emission on the inverse cycle. The 1B3GT tube will provide proper operation in the 30-kilovolt tripler, and the R-6194 in the 90-kilovolt supply.

Radiation from a supply can be largely reduced by proper filtering of the power leads, and by the use of full shielding. Ventilation must be supplied for the oscillator tubes and has been provided in most of the models illustrated by the use of holes punched in the shield near

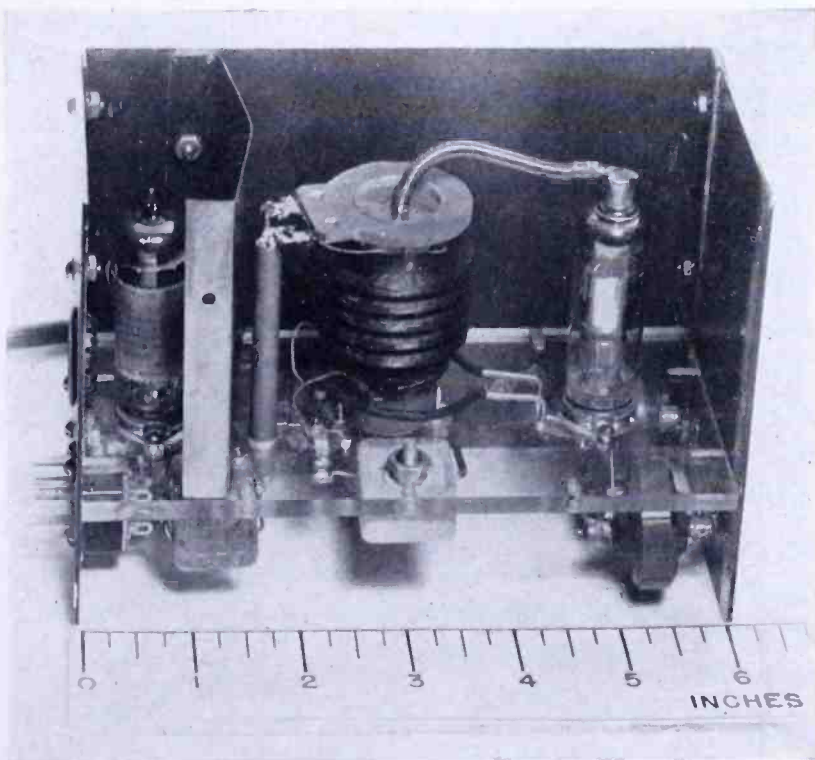


Fig. 22—Side view of 4-kilovolt supply.

bases and tops of the oscillator tubes. A close mesh screen is used over these holes, and an internal baffle placed between the tubes and the r-f transformer to minimize stray fields.

It has been found that the temperature rise can be considerably reduced by painting the inside and outside of the coil housing black, permitting better heat radiation.

Filament and high voltage output leads use polyethylene insulated wire. In order to minimize excessive voltage stress at the junction of the wire insulation and its shield, rounded corona-free fittings are

sweated to the shield at these points. These fittings also serve to anchor the wire shield tightly to the housing.

The type of resistor used for a bleeder must be carefully selected and particular attention given to its voltage rating per unit. In general more resistors will be required than indicated by their normal dissipation rating. This is caused by a change in resistance under high voltage stress and is another cause of excessive oscillator current under "no load" conditions. This may occur under actual operating conditions even though measurement of the bleeder with the usual low-voltage ohmmeter shows a normal value of resistance.

The circuits of the various supplies are given in Figures 1, 9, 13, 20, and 21. Photographs indicating the general layout and construction are

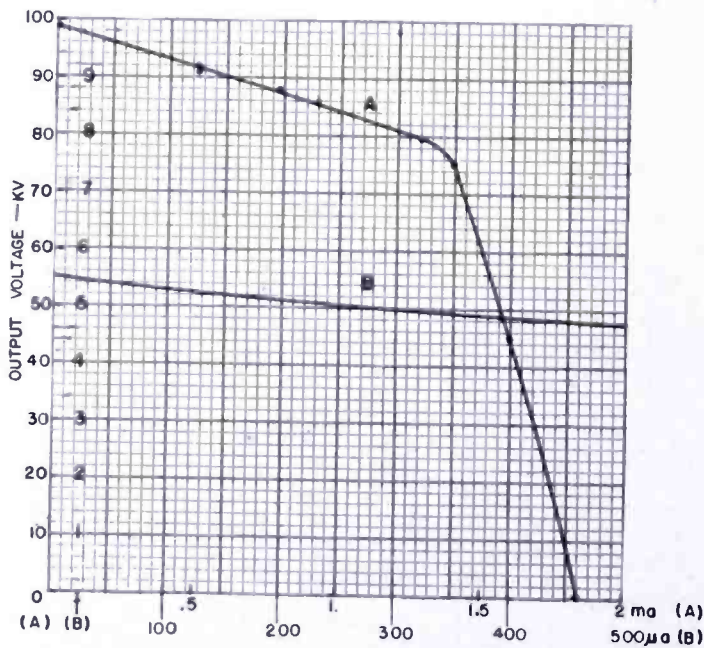


Fig. 23—Regulation curve for 90-kilovolt supply.

shown in Figures 3, 4 and 22. Regulation curves are shown in Figure 23.

A summary of coil data for several practical coils is given in Figure 5.

TABLE OF SYMBOLS

R'	effective shunt alternating current load on the secondary
R	direct current load resistance
R_p	total effective plate load resistance
r_I'	total effective series resistance of loaded primary circuit
r_I	series loss resistance of primary circuit
r_{II}	total effective resistance of secondary circuit with any load

$r_{II \text{ max}}$	total effective resistance of secondary circuit with maximum load
R_i	equivalent shunt loss of primary circuit
R_L	equivalent shunt load resistance on primary circuit
R_g	filament load on secondary of filament transformer
P_1	power dissipated in primary coil
P_2	power dissipated in secondary coil
\hat{P}_{in}	peak power input
P_{in}	average power input
P_{II}	power dissipated in secondary circuit
$\omega = 2\pi F$	operating frequency
$\omega_0 = 2\pi F_0$	self resonant frequency of secondary circuit
$\omega_1 = 2\pi F_1$	lower coupling frequency
$\omega_2 = 2\pi F_2$	upper coupling frequency
Q_I	value of primary tank circuit Q without load
Q_{II}	value of secondary tank circuit Q without load
Q_I', Q_{II}'	are respective Q values of loaded circuits
\mathcal{T}	transformer transfer factor
$\mathcal{T}_{(0)}$	transformer transfer factor at resonance
K'	rectification efficiency
K	coupling factor
K_c	minimum or critical coupling of coupled circuits
k	eddy current factor
ωL_1	reactance of primary coil
ωL_1	<i>effective</i> inductive reactance (series) of primary circuit
L_1	primary coil inductance
L_2	secondary coil inductance
\hat{E}_2	peak secondary voltage
E_{min}	minimum plate voltage
Z_{II}	parallel resonant impedance of secondary circuit
z_{II}	series impedance of secondary circuit
C_1	primary tuning capacitance
C_2	secondary tuning capacitance
n	number of cascaded rectifier stages
ϵ	dielectric constant
x_{II}	total effective series secondary reactance at the operating frequency
i_2	rectifier filament current
η	transformer efficiency

NOTE—In general, capital letters indicate shunt values, as R , R_p and lower case letters, series values, as r_f .

Peak values are indicated by a circumflex: \hat{P}_{in} , \hat{E}_2 .

Average values are indicated by a horizontal bar: \bar{E} , \bar{R} .

DETERMINATION OF CURRENT AND DISSIPATION VALUES FOR HIGH-VACUUM RECTIFIER TUBES*

BY

A. P. KAUZMANN

Tube Department, RCA Victor Division,
Harrison, N. J.

Summary—Rectifier data are shown graphically with generalized parameters from which it is possible to determine the peak steady-state current, the maximum possible hot-switching current, and the dissipations in the diode and in any added series resistors. The paper covers capacitive-input filters with large capacitors and includes half-wave, full-wave, and voltage-doubler circuits. A table of operating conditions and efficiency for a group of typical rectifiers is included.

INTRODUCTION

IN RECTIFIER CIRCUITS using high-vacuum diodes, very large currents may flow when the tubes are "hot-switched." A maximum current will flow when the supply voltage, at the instant of maximum amplitude, is applied to the plate of the rectifier while the cathode is still hot but after the circuit has been off for a sufficient length of time for the filter capacitor to discharge through the load resistor. A quantitative determination of this "hot-switching" current is presented in this paper. In order to prevent these currents from damaging the diode rectifier, many of the receiving-tube rectifiers, as given in their published characteristics, require a minimum protective series resistor in the plate circuit. For this reason it is believed useful to include in this paper the average power dissipated in any added series resistors and in the diodes. Previous papers^{1, 2, 3, 4} on rectifier operation have either neglected the dissipation of the added series resistors or have lumped them together with the dissipation of the diode. In addition,

* Decimal Classification: R366.32 × R258.1.

¹ O. H. Schade, "Analysis of Rectifier Operation." *Proc. I. R. E.*, Vol. 31, No. 7, pp. 341-361, July, 1943.

² N. H. Roberts, "The Diode as Half-Wave, Full-Wave, and Voltage-Doubling Rectifier." *Wireless Eng.* (Brit.), Vol. 13, pp. 351-362, July, 1936; also Vol. 13, pp. 423-470.

³ J. C. Frommer, "Operating Data and Allowable Ratings of Vacuum-Tube Rectifiers." *Proc. I. R. E.*, Vol. 29, No. 9, pp. 481-485, September, 1941.

⁴ W. H. Aldous, "The Characteristics of Thermionic Rectifiers." *Wireless Eng.* (Brit.), Vol. 13, pp. 576-580, November, 1936.

an expression for peak steady-state currents which greatly simplifies the analyses is presented.

SYMBOLS AND DEFINITIONS

The symbols used in this paper are similar to those used by O. H. Schade.¹

\bar{I} is the direct-current component of current per plate. This is the equal to half of the d-c† output current for full-wave rectifiers, to the full d-c output current for half-wave rectifiers, and to the full d-c output current for voltage-doubler rectifiers of the full-wave type.

I is the peak steady-state current through the diode.

I_{max} is the peak hot-switching current.

\bar{E} is the d-c output voltage across the input-filter capacitance.

\tilde{E} is the peak a-c† voltage per plate where the instantaneous voltage $e = \tilde{E} \sin(2\pi f_0 t)$.

f_0 is the frequency of the power source.

f_1 is the frequency of the peak steady-state current, I , resulting from the assumption that the instantaneous diode current, i , is a half-sinusoid during its conduction period, $i = I \sin(2\pi f_1 t)$ where $1/2f_1 \geq t \geq 0$.

ϕ is one-half the diode conducting angle measured in terms of the power supply frequency, i.e. $1/f_0$ represents 360 degrees.

η is the voltage rectification efficiency,

$$\eta = \rho \frac{\bar{E}}{\tilde{E}}$$

where $\rho = 1$ for full-wave rectifier
 $\rho = 1$ for half-wave rectifier
 $\rho = 1/2$ for voltage-doubler.

n is the ratio of peak steady-state diode current to the direct current per plate, $n = I/\bar{I}$.

R_s is the resistance added in series with the diode and positioned so that all peak currents must flow through it. In a full-wave circuit, for example, this requirement is met by placing the series resistor in the common transformer center-tap lead or in the lead common to both cathodes.

\hat{r}_d is the peak diode resistance in the steady-state condition and is equal to the quotient of the peak tube drop, \hat{e}_d , divided by the peak steady-state current, I . $\hat{r}_d = \hat{e}_d/I$

\hat{r}_{ds} is the diode resistance when the hot-switching current is at its maximum, I_{max} .

† "d-c"—direct current; "a-c" alternating current.

R_L is the d-c load resistance shunting the input-filter capacitance.

m is a constant depending on the rectifier type, where

$$\begin{aligned} m &= 1 \text{ for half-wave rectifier} \\ &= 2 \text{ for full-wave rectifier} \\ &= \frac{1}{2} \text{ for voltage-doubler.} \end{aligned}$$

$e_d, \hat{e}_d, \hat{e}_{ds}$ are the instantaneous, peak steady-state, and peak hot-switching voltage-drops respectively across the diode.

$e_r, \hat{e}_r, \hat{e}_{rs}$ are the instantaneous, peak steady-state, and peak hot-switching voltage-drops respectively across the added series resistance.

C is the filter capacitance immediately following the diode rectifier. In the case of the voltage-doubler circuit it is the value of one of the two series capacitors across the input to the load.

W_p is the plate dissipation of the diode.

W_R is the dissipation of all added series resistance.

W_{do} is the d-c power output.

ASSUMPTIONS

In order to simplify the analysis of the circuits discussed, several assumptions are made. The first of these is the assumption that the current flowing during the conduction period of the diode is a half-sinusoid having a peak value equal to the peak steady-state diode current and an average value equal to the d-c output per plate. The peak currents and total dissipations predicted on the basis of this assumption agree remarkably well with the experimental data obtained by previous studies on this subject. Further justification is obtained by plotting a half-sinusoid on several oscillographs of the conduction current of the 5V4-G in full-wave operation. The correspondence is found to be very good except for the low current regions which are of small consequence since low currents contribute but slightly to the dissipations and direct-current outputs.

A second assumption, greatly simplifying the analysis, is that the filter capacitor is infinitely large. This assumption, of course, is not practical in itself but inspection of the results obtained by Schade¹ or Roberts² shows that the output voltage and peak currents reach their maximum values with finite values of filter capacitance. For the purpose of this analysis, the assumption of infinite input-filter capacitance is justified therefore when,

$$q(2\pi f_0)CR_L \cong 24 \quad \begin{array}{l} \text{where } q = 4 \text{ for full-wave rectifier} \\ \quad = 2 \text{ for half-wave rectifier} \\ \quad = 1 \text{ for voltage-doubler.} \end{array}$$

The remaining assumptions are self-evident. These are that the relationship of the voltage drop to the conducting current of the diode obeys the three-halves power law; that the diode does not reach temperature-saturation currents; that the input supply voltage is a sinusoid; that there is negligible leakage reactance in the supply lines and transformer; and, that all added series resistances are lumped into a single equivalent resistance through which all conduction currents must pass. This last assumption does not neglect the resistances of the primary and secondary of the supply transformer since in present-day receiving sets, for example, these are designed on the basis of cost and space considerations which result in equivalent series resistances on the order of several hundred ohms. This equivalent series resistance of the transformer referred to the diode side or secondary of the supply transformer may be found from:

$$R_{equiv\ sec} = R_{sec} + a^2 R_{prim} \quad (2)$$

$$\text{where, } a = \frac{E_{sec\ (rms\ volts)}}{E_{prim\ (rms\ volts)}}$$

It should be remembered that E_{sec} and R_{sec} are the induced voltage and resistance respectively of one-half the secondary for the usual center-tapped full-wave circuit.

PEAK STEADY-STATE CURRENT

Since the steady-state current pulses through the diode are assumed to be half-sinusoids against time, it is possible to obtain a generalized expression showing the relationships between the peak steady-state current, i , the d-c load current per plate, \bar{I} , and the voltage rectification efficiency, η . In Figures 1(a) and 1(b) are shown a typical half-wave circuit and the voltage-current relationships resulting from its use.

The average value of the current may be found by integrating the instantaneous current and equating it to the average current flowing during a cycle,

$$\int_0^{t_1=1/2f_1} i \sin(2\pi f_1 t) dt = \frac{\bar{I}}{f_0}$$

From this the ratio, n , of peak steady-state current to the direct current value is obtained:

$$n = \frac{\hat{i}}{\bar{I}} = \pi \frac{f_1}{f_0} \tag{3}$$

However, the relationship between the assumed pulse current frequency, f_1 , and the power-supply frequency, f_0 , and the half-conduction angle, ϕ , expressed in terms of the power-source angular frequency is

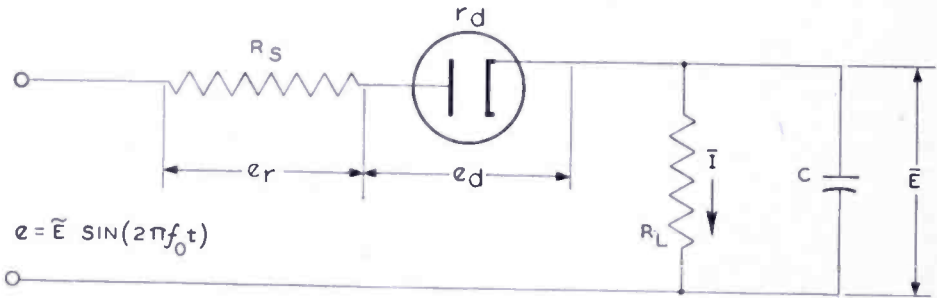


Fig. 1 (a)—Rectifier circuit in steady-state operation.

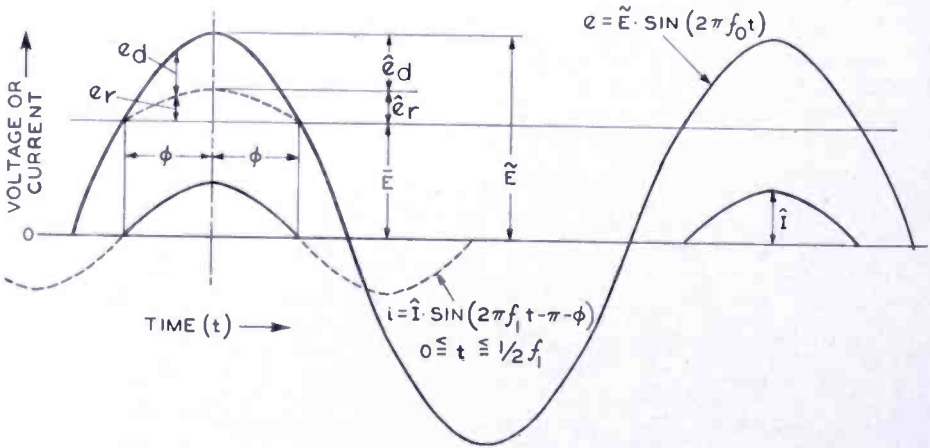


Fig. 1 (b)—Voltage and current waveforms.

simply $f_1 / f_0 = 180^\circ / 2\phi$ (3a)

The voltage rectification efficiency, η , is expressible as

$$\cos^{-1} \eta = \phi \tag{3b}$$

The inconvenient quantities ϕ and f_1 , are eliminated by substituting (3a) and (3b) into (3) giving for the ratio of peak steady-state cur-

rent to direct-current value
$$n = \frac{\hat{I}}{\bar{I}} = \frac{\pi}{2} \cdot \frac{180^\circ}{\cos^{-1}\eta} \tag{4}$$

This equation is shown graphically as the lower curve in Figure 2.

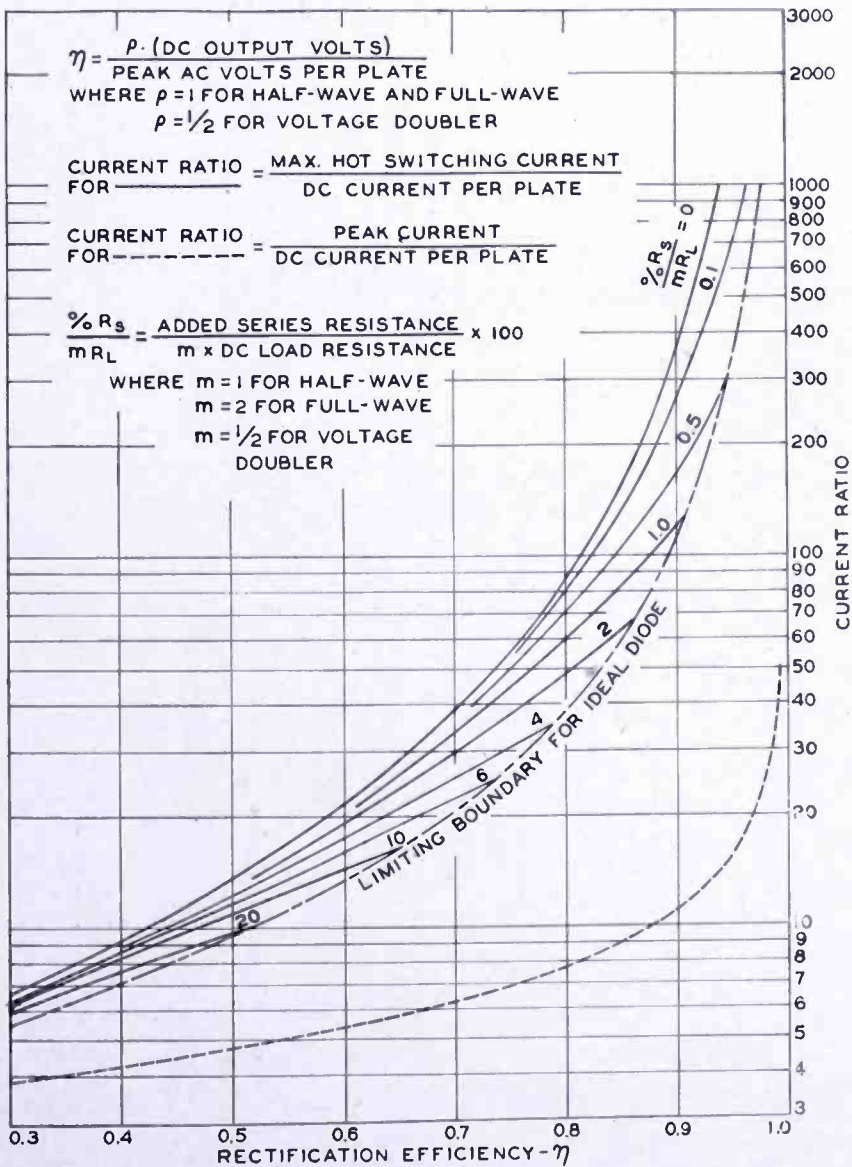


Fig. 2—Peak steady-state current and maximum hot-switching current characteristics of high-vacuum rectifier with capacitive-input filter. (Current values normalized to direct-current value per plate.)

As pointed out previously, this characteristic is in excellent agreement with the peak-current data given in Schade's analysis.¹ In order to include full-wave circuits, it is desirable to express the average current

on a "per plate" basis. In such circuits, the d-c load current receives half of its current from each plate, and, therefore, I will be equal to half the output current.

Similarly, in the voltage-doubler circuit, which is essentially two half-wave rectifier circuits in series, the \bar{I} is equal to the load current. The rectification efficiency, η , however, due to the series addition of voltages can reach a maximum of twice unity. To preserve a single curve for all three cases, the rectification efficiency for the voltage-doubler circuit should be divided by two. Thus, the ordinates showing the rectification efficiency, η , on all the curve data following can be expressed as

$$\eta = \rho \bar{E}/\tilde{E} \quad \text{where } \rho = 1 \text{ for full-wave rectifier} \quad (5)$$

$$\rho = 1 \text{ for half-wave rectifier}$$

$$\rho = 1/2 \text{ for voltage-doubler.}$$

This curve is single-valued. When the direct-current output voltage is numerically equal to the root-mean-square voltage per plate, the ratio of peak steady-state to average current is 6.3 to 1. A ten per cent increase in output voltage above this value increases this ratio to 7.2 to 1. Also, the addition of any more series resistance will lower the voltage rectification efficiency with a resulting lowering of the peak current.

MAXIMUM HOT-SWITCHING CURRENT

The peak hot-switching current, i_{max} , is of interest because it is this current that the diode must supply if the load resistance, R_L , were short-circuited. This condition occurs in the practical case when a diode is "hot-switched." The peak secondary voltage per plate then appears across the diode and any added series resistance. If the polarity is positive with respect to the cathode, currents on the order of amperes may flow through the diode; and, since the emitter materials, such as the oxide coatings used almost exclusively in present-day receiving tubes, have considerable volume resistivity, it is possible to melt and even vaporize the coating by the excessive heating. This condition produces visible sputtering and possibly arc-back in the diode. In addition to making the diode inoperative, the electrolytic filter capacitor is usually blown out by having it placed across the wrong polarity during arc-back. The common method for limiting this hot-switching current is to specify the addition of a minimum value of series resistance.

As shown in Figure 3, the total input voltage across the diode and

its added series resistance at the instant of peak supply voltage, is

$$\tilde{E} = \hat{e}_{rs} + \hat{e}_{ds} \tag{6}$$

The voltages on the right-hand side of this equation may be expressed in terms of the corresponding values of maximum hot-switching current and resistances:

$$\tilde{E} = \hat{I}_{max} \cdot R_S (1 + \hat{r}_{ds}/R_S) \tag{6a}$$

Similarly, the voltage distribution can be set up from Figure 1 for the

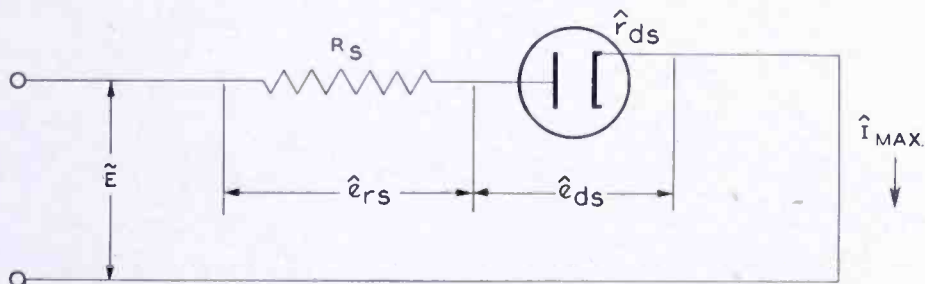


Fig. 3(a)—Rectifier circuit in maximum hot-switching-current condition.

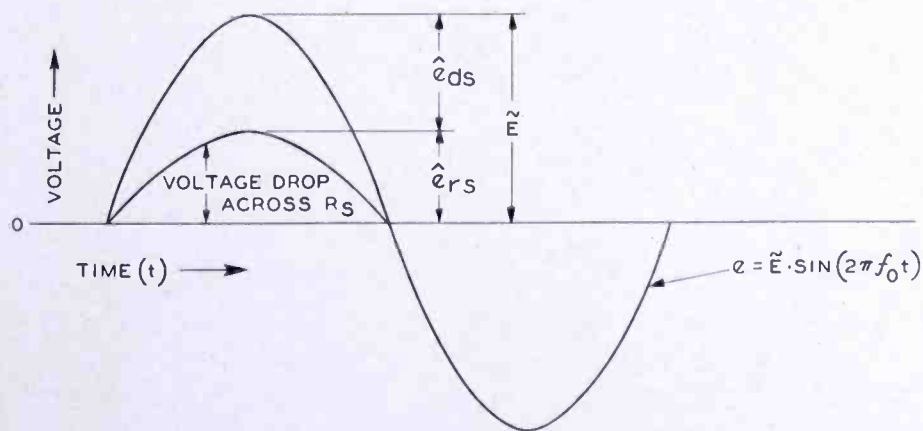


Fig. 3(b)—Voltage and current waveforms.

steady-state case at the instant peak current is flowing.

$$\tilde{E} (1 - \eta) = \hat{e}_r + \hat{e}_d \tag{7}$$

$$\tilde{E} (1 - \eta) = \hat{I} R_S (1 + \hat{r}_d/R_S) \tag{7a}$$

If Equation (7a) is divided by Equation (6a),

$$\eta = 1 - \frac{\hat{I}}{\hat{I}_{max}} \left[\frac{1 + \hat{r}_d/R_S}{1 + \hat{r}_{ds}/R_S} \right] \tag{8}$$

The diode maximum hot-switching resistance, \hat{r}_{ds} , is eliminated from the above equation by application of the three-halves power relation of voltage and current in a diode:

$$\hat{r}_{ds} = \hat{r}_d \left(\frac{\hat{I}}{\hat{I}_{max}} \right)^{3/2}$$

which by substitution into Equation (8) produces

$$\eta = 1 - \frac{\hat{I}}{\hat{I}_{max}} \left[\frac{1 + \hat{r}_d/R_S}{1 + (\hat{r}_d/R_S) (\hat{I}/\hat{I}_{max})^{3/2}} \right] \quad (8a)$$

As it has already been shown in Equation (4) that the ratio of peak steady-state current to direct current value per plate, \hat{I}/\bar{I} , is a single-valued function of the voltage rectification efficiency, η , the peak steady-state current in the above expression may be replaced by $\hat{I} = n\bar{I}$ where $n = f(\eta)$ and is numerically equal to the ratio of peak steady-state current to average current per plate:

$$\eta = 1 - \left(\frac{\hat{I}_{max}}{\bar{I}} \right)^{-1} n \left[\frac{1 + \hat{r}_d/R_S}{1 + (\hat{r}_d/R_S) \left(\frac{\hat{I}_{max}}{n\bar{I}} \right)^{-3/2}} \right] \quad (9)$$

In the upper family of curves of Figure 2, the boundary curves have been plotted from Equation (9) by first placing $\hat{r}_d = 0$ and then $R_S = 0$. The ratio, \hat{r}_d/R_S , could have been plotted between these curves as a parameter but since the peak diode resistance, \hat{r}_d , is inconvenient to determine, it has been replaced by the more convenient term, R_S/mR_L , involving easily measurable resistances and a constant, m , whose value is determined by the type of rectification, half-wave, full-wave, or voltage-doubler. This substitution will not be discussed in detail but arises from the observation that for large capacitor sizes, the voltage rectification efficiency, η , is expressible¹ as

$$\eta = f \left(\frac{R_S + \hat{r}_d}{mR_L} \right) \quad (10)$$

Since this is a single-valued curve the ratio \hat{r}_d/R_S in Equation (9) can be replaced, after some mathematical transpositions with

$$R_s/mR_L = F \left(\eta, \frac{\hat{i}_d}{R_s} + 1 \right) \tag{10a}$$

The results of this substitution are shown graphically in the top family of curves in Figure 2. The order of magnitude of the peak hot-switching current for a typical rectification efficiency of 0.75 is twenty-five to fifty times the average current per plate.

DISSIPATIONS IN DIODE PLATES AND ADDED SERIES RESISTANCES

The average power dissipated in the plate of the diode may be found by integrating the instantaneous wattage over the conduction time and dividing the resulting integration by the repetition time between conduction periods. Referring to the half-wave case of Figure 1, the average plate dissipation is

$$W_p = \int_0^{t_1} \frac{e_d i dt}{1/f_0} = \int_0^{1/2f_1} f_0 e_d i \sin(2\pi f_1 t) dt \tag{11}$$

The diode voltage drop, e_d , since it follows Child's space-charge-limited law may be written as

$$e_d = \left(\frac{i}{K} \right)^{2/3} = \left[\frac{\hat{i}}{K} \sin(2\pi f_1 t) \right]^{2/3} \tag{11a}$$

where K is a constant depending on diode geometry. This expression substituted into equation (11) will after integration‡ produce

$$W_p = 2 \frac{\hat{i}^{5/3}}{K^{2/3}} \frac{f_0}{2\pi f_1} \left[\frac{\sqrt{\pi}}{2} \frac{\Gamma(8/6)}{\Gamma(11/6)} \right] \tag{11b}$$

‡ The solution of the definite integral applicable in this case is given in terms of the Gamma function:

$$\int_0^{\pi/2} \sin^n x dx = \frac{\sqrt{\pi}}{2} \frac{\Gamma\left(\frac{n+1}{2}\right)}{\Gamma\left(\frac{n}{2}+1\right)}$$

where n may have any value > -1

Solving the gamma functions and substituting the previously determined value of the ratio f_1/f_0 of equation (3) gives

$$W_p = 0.84 (\bar{I}/K)^{2/3} \bar{I}. \quad (11c)$$

$$\text{But, } (\bar{I}/K)^{2/3} = \hat{e}_d \quad (11d)$$

$$\text{so that } W_p = 0.84 \bar{I} \hat{e}_d. \quad (12)$$

This Equation (12) is an expression giving the plate dissipation in terms of the diode peak-voltage drop, \hat{e}_d , and the direct-current value, \bar{I} . Since a universal curve including the effect of adding series resistance R_s is desired, the diode voltage drop, \hat{e}_d , is next replaced by its equivalent. This equivalence, indicated by Equation (5) and Figure 1, is

$$\hat{e}_d = (1 - \eta) \tilde{E} - \bar{I}R_s. \quad (12a)$$

Substituting this into equation (12) produces

$$W_p = 0.84 \bar{I} [(1 - \eta) \tilde{E} - \bar{I}R_s]. \quad (12b)$$

To obtain a dimensionless expression, compare the above plate dissipation to the d-c power output, W_{dc} which may be written in the following several convenient forms:

$$W_{dc} = \bar{I} \eta \tilde{E} \equiv \bar{I}^2 R_L. \quad (12c)$$

Forming a ratio between equations (12c and 12b) gives

$$\frac{W_p}{W_{dc}} = 0.84 \bar{I} \left[\frac{(1 - \eta) \tilde{E}}{\bar{I} \eta \tilde{E}} - \frac{\bar{I}R_s}{\bar{I}^2 R_L} \right] \equiv 0.84 \left[\left(\frac{1 - \eta}{\eta} \right) - \frac{\bar{I}R_s}{\bar{I}R_L} \right] \quad (12d)$$

The ratio \bar{I}/\tilde{I} , between the peak steady-state current and the direct current value per plate, has already been designated as n and is a function only of the voltage rectification efficiency, η . Furthermore, to include half-wave and voltage-doubler circuits and make the expression generally applicable, the constant, m , is again introduced so that the plate dissipation is the total plate dissipation. Equation (12d) takes its final form

$$\frac{W_p}{W_{dc}} = 0.84 \left[\left(\frac{1 - \eta}{\eta} \right) - \frac{n}{m} \frac{R_s}{R_L} \right] \quad (13)$$

where again, $m = 1$ for half-wave rectifier
 $= 2$ for full-wave rectifier
 $= \frac{1}{2}$ for voltage-doubler,

This Equation (13) is shown graphically in Figure 4. For example, it is of interest to note that with no series resistance the plate dissipation at a voltage rectification efficiency of 0.75, is 28 per cent of the useful output power. Adding series resistance lowers the plate dissipation which means that for the same rectification efficiency a diode

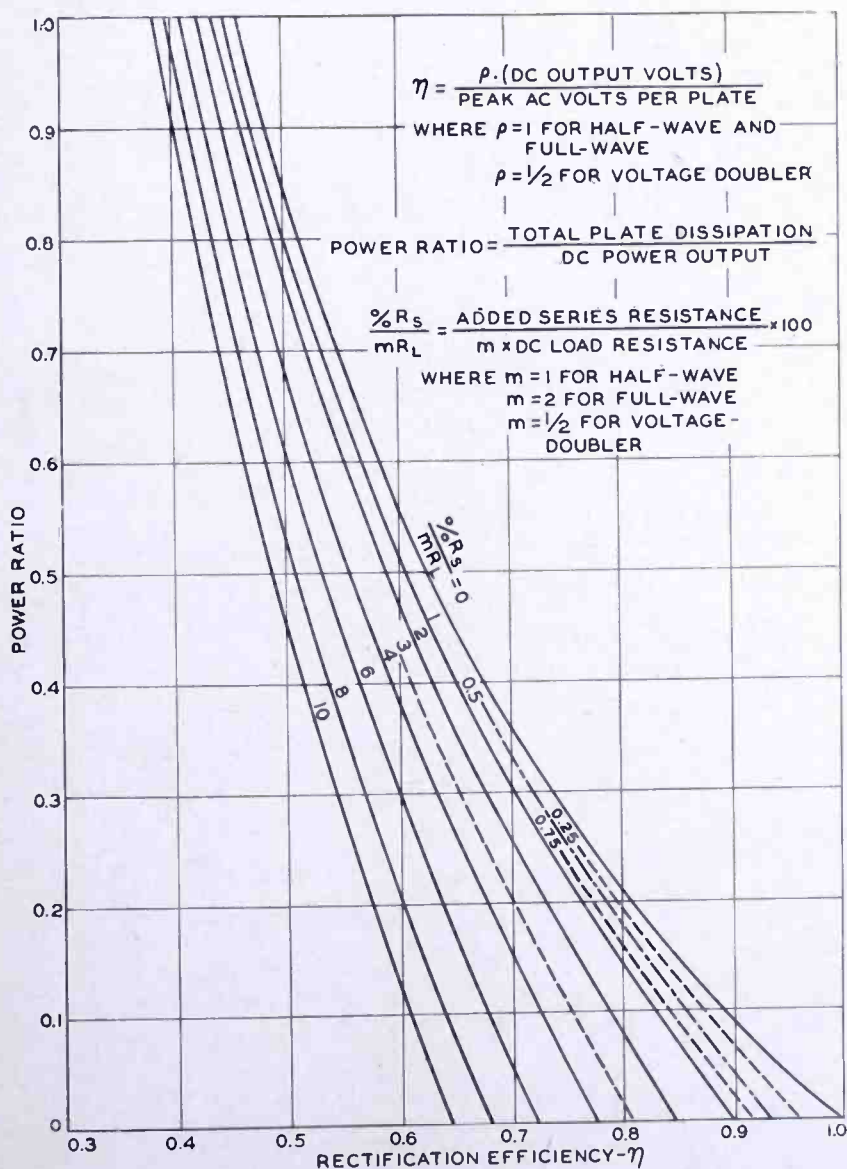


Fig. 4—Plate dissipation contours of high-vacuum rectifier with capacitive-input filter. (Plate dissipation values normalized to d-c power output.)

with less loss must be used, or in other words, one having a larger cathode or closer spacing.

The power, W_R , dissipated in the added series resistance is determined in a similar manner as the plate dissipation:

$$W_R = \int_0^{t_1} \frac{i^2 R_s}{1/f_0} dt = f_0 R_s \int_0^{1/2f_1} i^2 \sin^2(2\pi f_1 t) dt \quad (14)$$

$$W_R = \frac{\pi}{4} R_s I I \equiv 0.785 n I^2 R_s \quad (14a)$$

Normalizing this Equation (14a) by dividing it by the direct current output power, W_{dc} , and applying, as before, the parameter, m , to include full-wave and voltage-doubler operation gives

$$\frac{W_R}{W_{dc}} = \frac{0.785 I^2 R_s n}{I^2 R_L m} \equiv 0.785 \frac{n R_s}{m R_L} \quad (15)$$

where $m = 1$ for half-wave rectifier
 $= 2$ for full-wave rectifier
 $= 1/2$ for voltage-doubler.

This relationship is presented graphically in Figure 5.

The total dissipation of the diode plate and series resistances, $W_R + W_p$, referred to the d-c output power, W_{dc} , is the sum of Equations (15) and (13):

$$\frac{W_R + W_p}{W_{dc}} = 0.84 \frac{1 - \eta}{\eta} - 0.055 \frac{n R_s}{m R_L} \quad (16)$$

For a first approximation the second term may be omitted. Under the most unfavorable conditions this will amount to an error of approximately 10 per cent for voltage-doubler operation, 2.5 per cent for full-wave operation, and 1.25 per cent for half-wave operation. This condition assumes a perfect diode having no voltage drop. For most practical cases, however, the actual error will be about half the above percentages. With the omission of this second term Equation (16) becomes

$$\frac{W_R + W_p}{W_{dc}} \approx 0.84 \left(\frac{1}{\eta} - 1 \right) \quad (17)$$

This expression is the same as the top curve of Figure 4, labelled, " $\% \frac{R_s}{mR_L} = 0.$ "

Finally from Equation (17) an expression for the total power, W_T , which the alternating-current supply must furnish in terms of the d-c power output and voltage-rectification efficiency is

$$W_T \approx W_{dc} \left[0.16 + \frac{0.84}{\eta} \right] \tag{18}$$

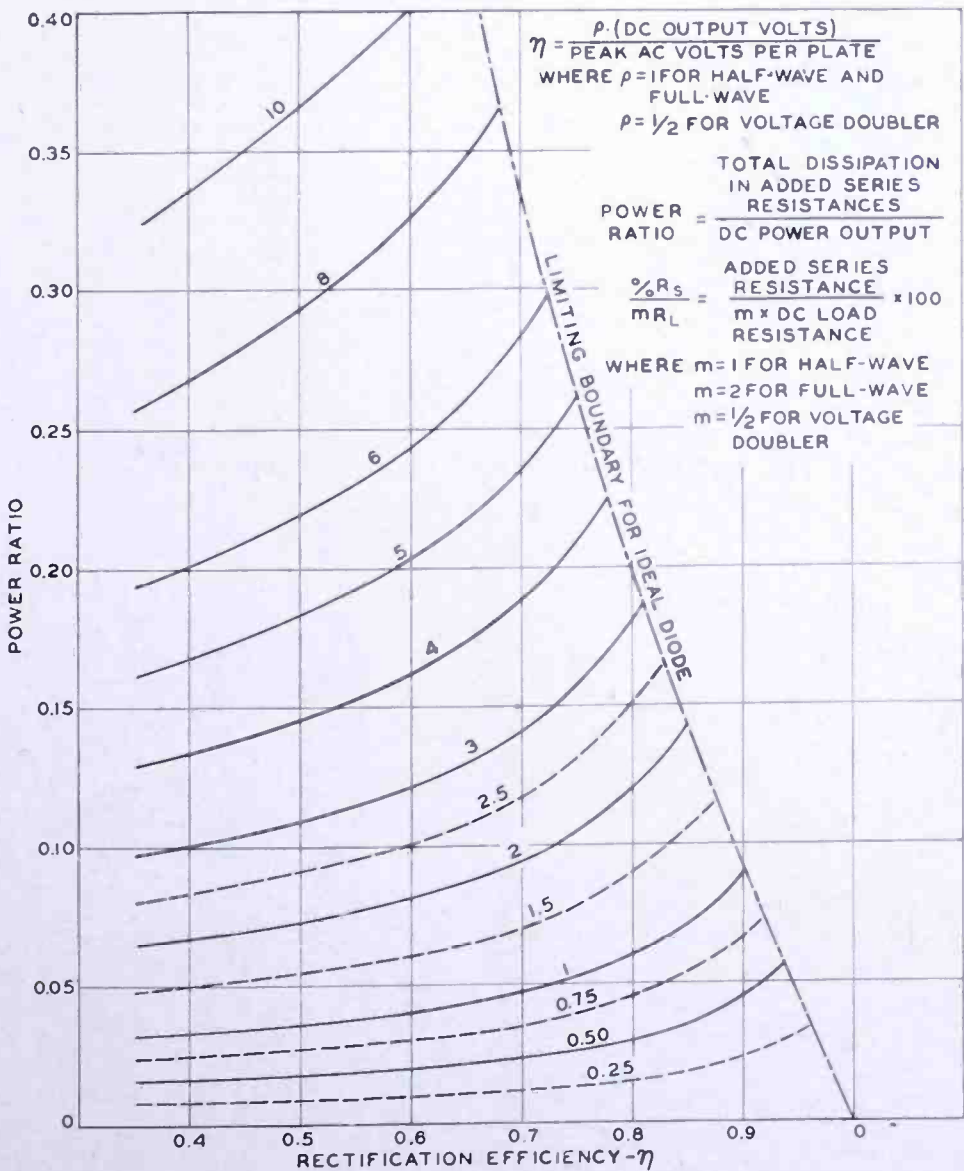


Fig. 5—Dissipation in series plate resistance of high-vacuum rectifier with capacitive-input filter. (Dissipation values normalized to d-c power output.)

In the case of a transformer supply source, this will include all the copper losses of the transformer as part of the added series resistance, R_g .

CONCLUSION

Table 1 lists a group of typical receiving-tube rectifiers arranged in order of ascending rectification efficiencies. In most cases the operating conditions are taken directly from the RCA Receiving Tube Handbook and are for maximum published values of d-c output current and applied a-c voltage. If the value of the added series resistance is not published, it is computed from data supplied with the transformer used for producing the handbook curves. The values of the several currents and dissipations shown in this table are calculated by applying the given data to the curves of Figures 2 and 4. The ratios of peak steady-state current to direct current per plate fall in the range of 5.5 to about 9. Similarly, the ratios of maximum hot-switching current to direct current per plate fall in the range of 25 to 100.

Table 1. Operating Conditions and Efficiency of Typical High-Vacuum Rectifiers with Capacitive-Input Filters.

(See opposite page)

Tube Type	\bar{E}_{rms} input per plate ac volts		R_s added series I_o Total resist. dc per plate output plate Ohms		Rectification Efficiency %	Peak Current		Max. Hot-Switching Current		Total Plate Dissipation		Added Series-Resistance Dissipation		dc output W_{dc} watts	
	Class	dc output volts	ma	ma		I/I per plate	ma	I_{max}/I per plate amp.	I_{max}	W_p/W_{dc} output	W_p watts	W_r/W_{dc} output	W_r watts		
25Z5, 25Z6	VD	117	208	75	35	62.8	5.6	420	21	1.57	0.380	5.9	0.110	1.7	15.6
5Y3	FW	350	335	125	95	67.5	6.0	375	27	1.66	0.320	13.4	0.079	3.3	41.8
81	HW	700	690	85	200	69.5	6.2	525	22	1.87	0.243	14.4	0.127	7.6	59.5
5U4	FW	450	445	225	85	70.0	6.25	705	28	3.15	0.245	24.5	0.102	10.2	100.0
35Z5, 35Z4	HW	235	235	100	100	70.7	6.33	633	26	2.60	0.128	3.0	0.204	4.8	23.5
5W4	FW	350	362	100	125	73.0	6.6	330	34	1.70	0.220	8.0	0.085	3.1	36.2
5V4	FW	375	415	175	95	78.4	7.4	647	48	4.20	0.110	8.0	0.116	8.4	72.6
12Z3	HW	235	261	55	75	78.5	7.4	407	47	2.64	0.130	1.9	0.094	1.4	14.3
6X5	FW	325	370	70	150	80.5	7.8	273	55	1.92	0.123	3.2	0.086	2.2	25.9
5Z4	FW	350	420	125	30	84.9	8.9	556	102	6.27	0.115	6.0	0.031	1.6	52.5

TELEVISION DEFLECTION CIRCUITS*†

Part I MOLDED IRON DUST CORES FOR USE IN HORIZONTAL DEFLECTION CIRCUITS

BY
A. W. FRIEND

Home Instrument Department, RCA Victor Division,
Camden, N. J.

Summary—The horizontal deflection of electron beams in television systems has required excessive dissipation of energy and expensive circuit components. For deflection by magnetic means, the deflection transformer and yoke have presented serious problems in the economical design of television receivers.

Transformer and yoke cores have been molded from powdered iron materials especially prepared for these applications. Very low cost materials have been developed to produce useful effective alternating-current permeabilities between 40 and 230. The precise value depends upon the peak amplitude of the alternating-current flux density.

Small particle thicknesses available, at low cost, in powdered iron materials make high-Q systems possible. Increased efficiency eliminates the necessity for dissipating large amounts of energy from the transformer and deflecting yoke structures. Molded core structures, in comparison with laminated core structures, produce negligible acoustic radiation.

Low-loss systems have been constructed with energy recovery arrangements. Such systems, requiring no additional electrical energy, provide large increases in deflection capability. Simultaneously, there are reductions in costs of transformer cores to less than one fourth those of equivalent laminated sheet or strip metal types.

A low-cost system has been constructed to provide full deflection and 27 kilovolts second anode potential for a fifty-degree kinescope driven by two type 807 or 6BG6G beam-tetrodes. The present pulse voltage ratings of available tubes limit the second anode voltage to approximately 17 kilovolts for a kinescope which is to be scanned from a circuit driven by a single 6BG6G tube. This second anode voltage may be derived from windings on the same deflection transformer via a voltage doubling rectifier.

INTRODUCTION

THE horizontal deflection of electron beams and the high-voltage power supply for the electron beam acceleration in the kinescope in television receivers has accounted for a large portion of the

* Decimal Classification: R583.13.

† Much of the material contained in the two parts of this paper was presented as a combined paper at the National Electronics Conference, Chicago, Illinois, on October 4, 1946.

required total energy dissipation, physical volume and cost. The advent of modern short-length, sharp-focus kinescopes of wide deflection angle increased the energy consumption and the cost of the required component parts. Means have been found for decreasing the cost appreciably, and at the same time providing an equally efficient system.

The major component parts are the horizontal deflection transformer and its associated deflection yoke. These devices have been responsible for at least half the energy loss in many systems. The introduction of very thinly laminated cores in both units resulted in a considerable reduction in energy loss and a marked increase in the deflecting capability of any standard driver tube.

The cost of cores with very thin laminations is quite high. To reduce this expense, a special type, low-cost, high-permeability molded iron-dust core has been developed. Although its characteristics are different from those of the laminated cores, the operating results are similar and the cost of the cores is a small fraction of that of other adequate cores. In addition, the acoustic radiation from iron-dust cores is negligible.

As stated, low-cost sponge iron and electrolytic iron powders have been used. In each case the mean particle thickness was about 0.0005 inches. The cost of sponge iron is about half that of the electrolytic iron, and it requires no additional interparticle insulation.

MOLDED CORES

In the manufacture of molded iron-dust cores, the iron powders, after being mixed with very small amounts of binders, are pressed into core shapes under very high molding pressures. These materials do not flow appreciably under compression, so the molds must be of the straight thrust type. The minimum satisfactory molding pressure is about 15 tons per square inch. Higher values up to 60 tons or more are desirable magnetically. The cost of higher pressures requires careful balancing against the technical advantages.

In Figure 1 the apparent permeability of the powdered sponge iron core material is plotted relative to molding pressure at a number of values of flux density, in low frequency operation. The increase in apparent permeability with increased molding pressure is to be noted.

The Figure 2 shows a plot of the total energy loss per cycle per unit volume as a function of the maximum flux density B_{max} at the peak of the sine-wave-excited flux density, in molded sponge iron powder cores. The hysteresis power-loss appears to entirely predominate within the frequency range between 60 and 16,000 cycles per second.

MOLDED CORES OF SPONGE IRON POWDER

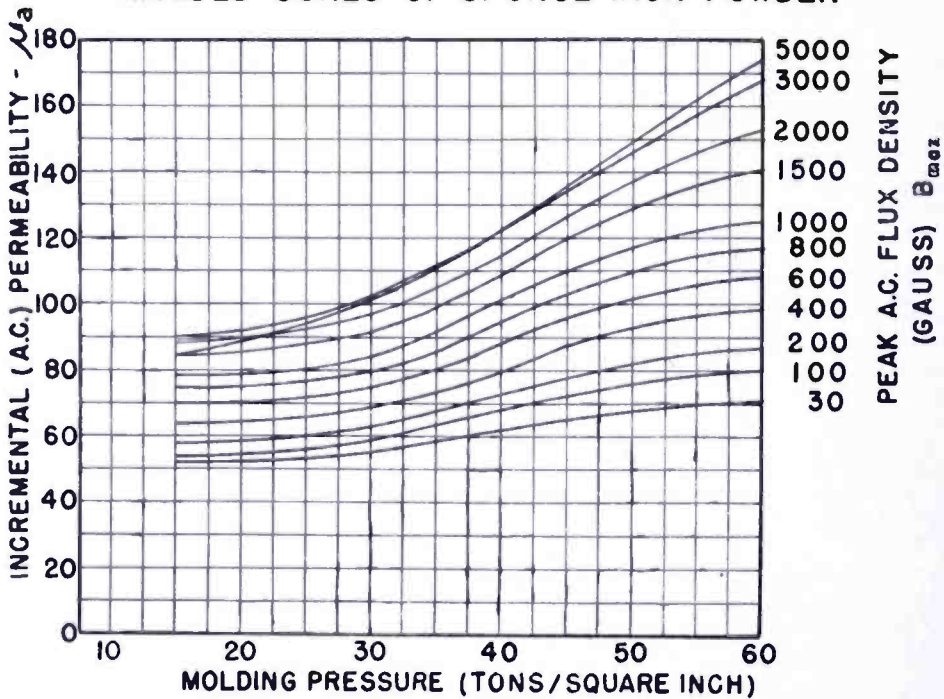


Fig. 1—Apparent incremental (alternating-current) permeability (μ_a) of molded sponge iron powder core materials as a function of molding pressure, plotted for various values of peak alternating-current flux density (B_{max}) in gauss, at 60 cycles/second.

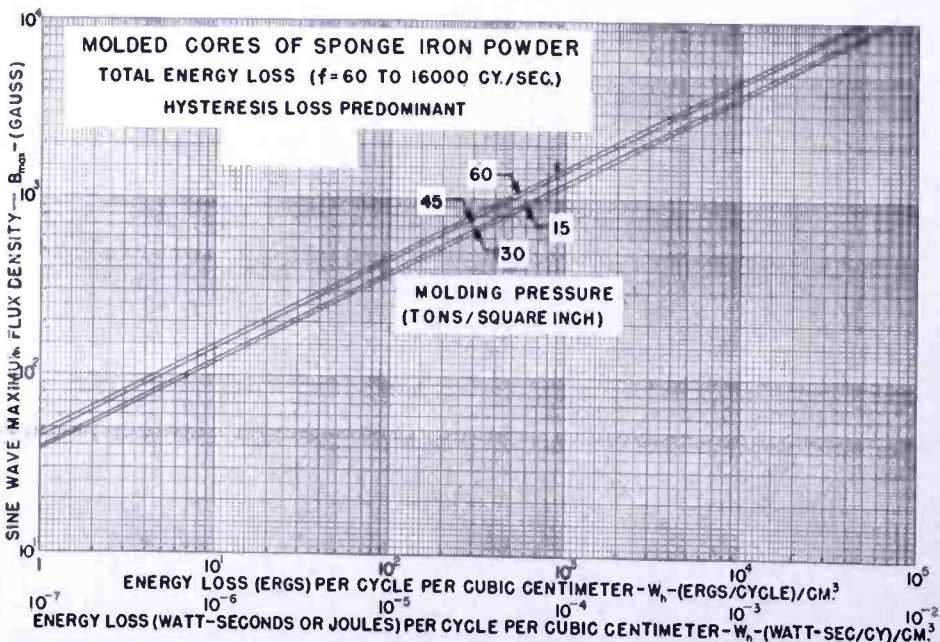


Fig. 2—Energy loss per cycle per unit volume in molded sponge iron cores as a function of sine wave produced maximum flux density (B_{max}). Only hysteresis loss is of importance within the frequency range considered. For the 15 tons per square inch material these data are valid to at least 40 kilocycles/second. For the 60 tons per square inch material they may be used up to 16 kilocycles/second.)

The standard empirical hysteresis power-loss equation, $P_h = kfB_{\max}^x$, where k and S are constants, may be used to represent the curves of Figure 2, when divided by the frequency f to yield the energy loss per cycle per unit volume in the iron, $W_h = kB_{\max}^x$. It is noted that instead of the value, $x = 1.6$, generally assumed for most magnetic materials, the sponge iron cores yield a value, $x = 2.0$. The sponge iron powder molded at a pressure of 15 tons per square inch requires a value of $k_{15} = 7.4 \times 10^{-4}$ to represent the energy loss in ergs per cycle per cubic centimeter. Similarly, for the 30, 45, and 60 tons per square inch molded sponge iron powder, the values of k are, $k_{30} = 6.6 \times 10^{-4}$, $k_{45} = 5.1 \times 10^{-4}$ and $k_{60} = 4.5 \times 10^{-4}$, respectively.

The curves of Figure 2 apply throughout the audio-frequency range and up to the frequency at which eddy current considerations become important. For the case of the sponge iron powder molded at 15 tons per square inch, the upper limit which might be considered for the application of these data is approximately 40 kilocycles/second. For the same material molded at a pressure of 60 tons per square inch the upper frequency limit is near 16 kilocycles/second, since the apparent particle size is increased on account of short circuiting effects.

At higher frequencies corrections must be made in accordance with a dual function of flux density and frequency, in order to take into account the eddy current effect and the resultant magnetic skin effect. The latter of these corrections may be approximated according to a solution in terms of combined hyperbolic and trigonometric functions. A solution is required for each combination of frequency and flux density.

This difficulty may be most easily by-passed for the moment by measuring either the dissipation factor or the Q of test samples at higher frequencies with various flux density values. The relative Q values of identical coils on toroidal sponge iron cores made at various molding pressures are plotted in Figure 3. These were measured with a maximum flux density B_{\max} of 40 gauss.

At frequencies in the vicinity of 70 kilocycles/second a large portion of the losses is contributed by eddy currents in the particles of the core material. While increasing the molding pressure produced a reduction in Q at these higher frequencies, the reduction is not sufficiently great to be particularly disturbing for television horizontal deflection uses.

The values of Q for electrolytic iron cores are similar to those of 30 tons/square inch sponge iron cores. These values do not vary with pressure changes between 15 and 60 tons per square inch. This powder is especially treated to produce a superior insulating surface on each particle.

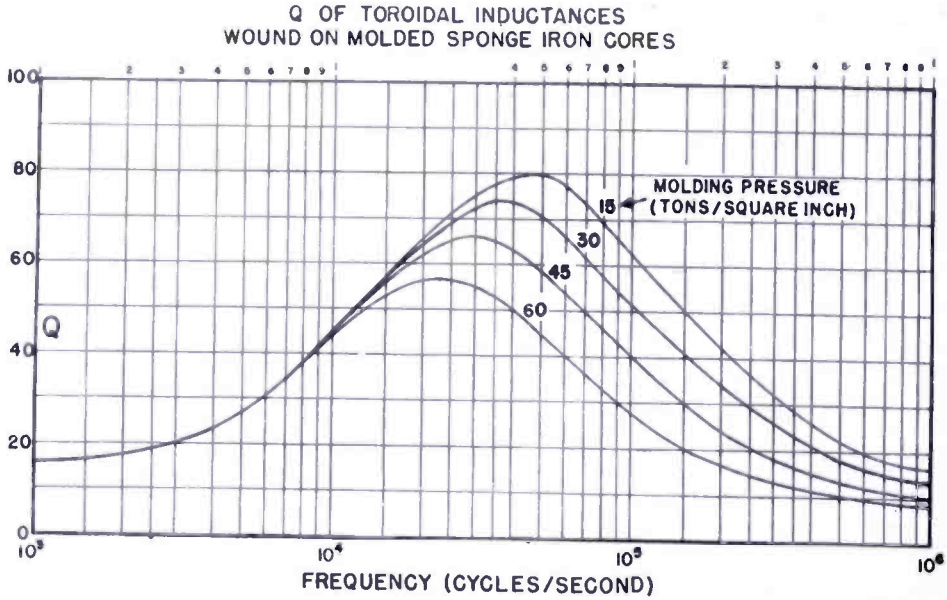


Fig. 3—Plot of Q as a function of frequency and molding pressure for samples of molded sponge iron powder cores with identical toroidal windings of litz wire.

It is interesting to observe the effect of changing frequency upon the apparent permeability of the various samples of materials at the different molding pressures. Figures 4 and 5 illustrate these results

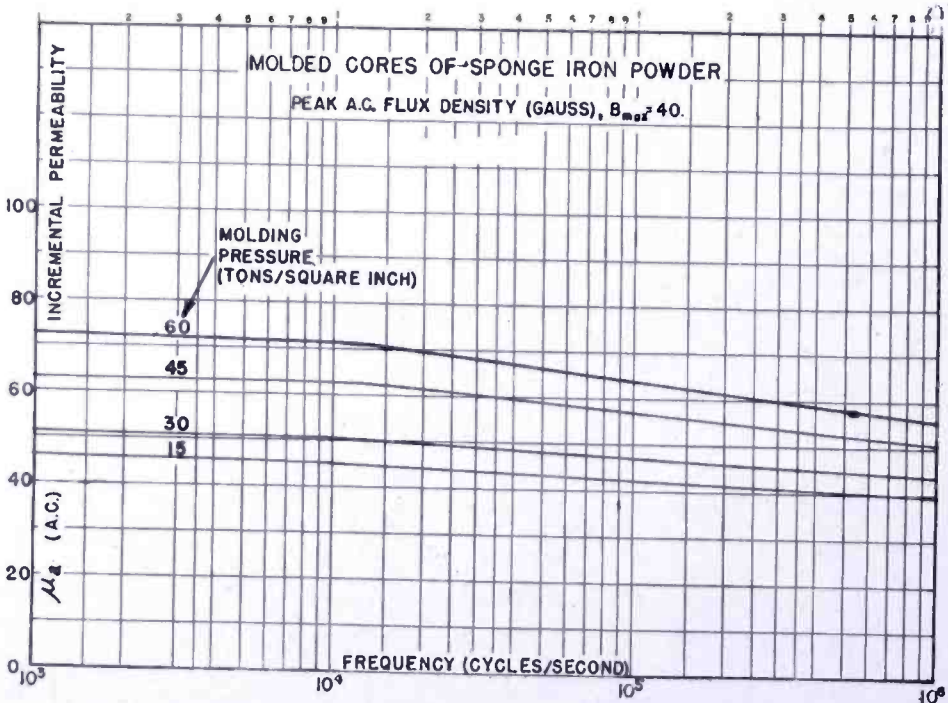


Fig. 4—Incremental (alternating-current) permeability (μ_a) of sponge iron powder cores, molded at various pressures, as a function of frequency, at a peak alternating-current flux density (B_{max}) of 40 gauss.

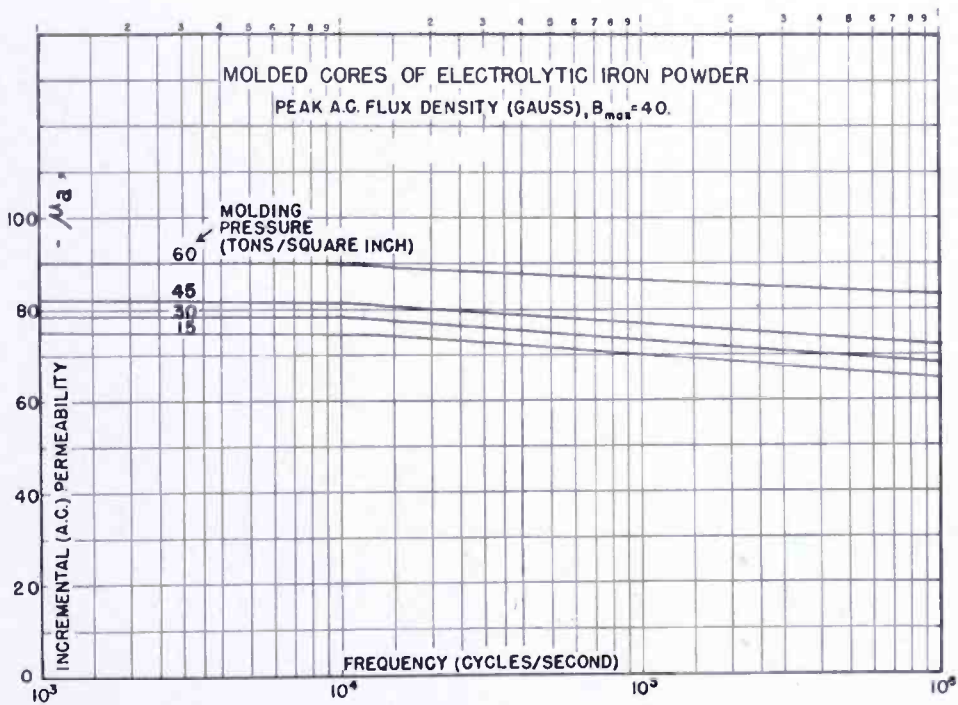


Fig. 5—Incremental (alternating-current) permeability (μ_a) of electrolytic iron powder cores, molded at various pressures, as a function of frequency, at a peak alternating-current flux density (B_{max}) of 40 gauss.

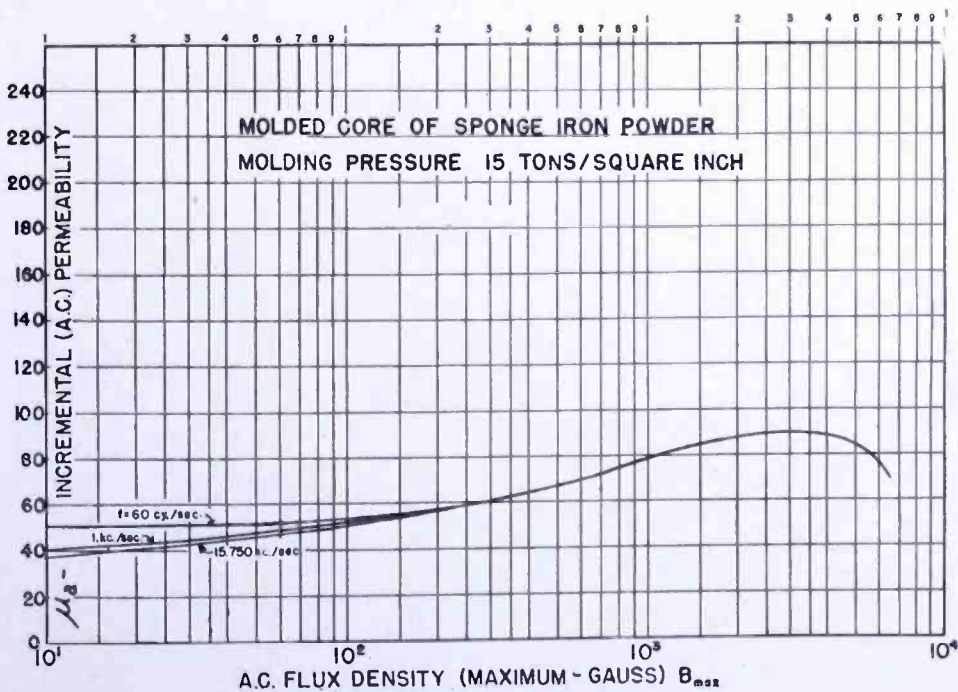


Fig. 6—Incremental (alternating-current) permeability (μ_a) of a sponge iron powder core, molded at a pressure of 15 tons/square inch, as a function of peak alternating-current flux density (B_{max}), in gauss, at frequencies of 60, 1000 and 15,750 cycles/second.

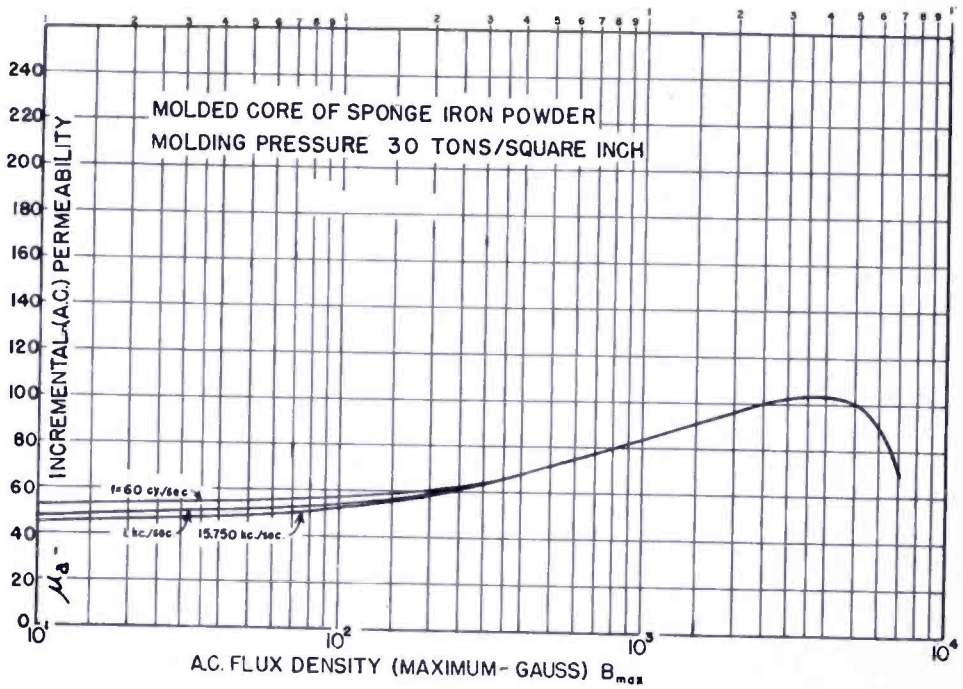


Fig. 7—Incremental (alternating-current) permeability (μ_a) of sponge iron powder core, molded at a pressure of 30 tons/square inch, as a function of peak alternating-current flux density (B_{max}), in gauss, at frequencies of 60, 1000 and 15,750 cycles/second.

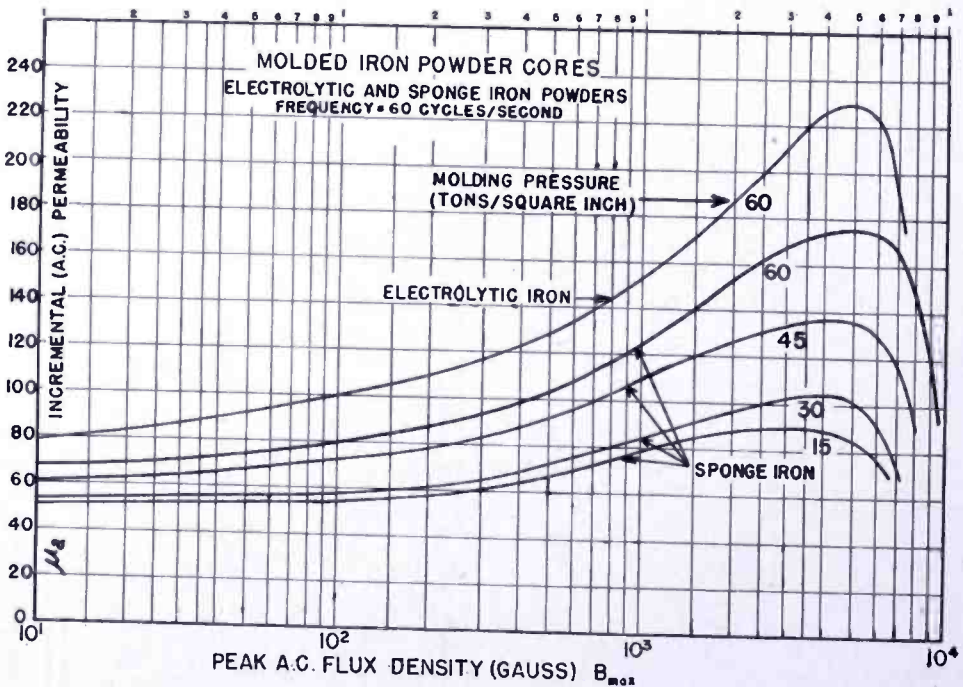


Fig. 8—Incremental (alternating-current) permeability (μ_a) of sponge and electrolytic iron powder cores, molded at various pressures, as a function of peak alternating-current flux density (B_{max}), in gauss, at 60 cycles/second.

for low flux density operation with sponge and electrolytic iron respectively. The particle sizes were chosen so that the apparent permeability remained very nearly constant over the range of frequencies up to 150 kilocycles per second. The spectrum between 15 and 150 kilocycles per second contains all the useful horizontal scanning frequencies, insofar as the present monochrome television is concerned.

The effects of variation of the maximum alternating-current flux density B_{\max} (at several frequencies) upon the apparent incremental permeabilities of the various cores are illustrated by Figures 6, 7, and 8. It is interesting to note that as the material is more closely compacted, the variation in apparent permeability with changing magnetic flux density becomes progressively greater. The maximum value indicated for any of the tested materials is 230, for electrolytic iron molded at 60 tons per square inch. At the same pressure, sponge iron yields a permeability of 175.

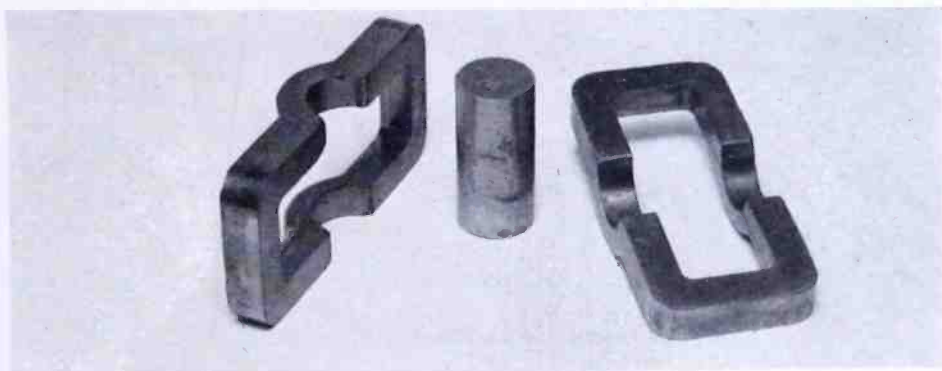


Fig. 9—A view of the three parts of a sponge iron powder transformer core, molded with a two-piece frame and a cylindrical central leg.

Various sample moldings are shown in the photographs of Figures 9 and 10. Figure 9 shows a view of the three parts of a transformer core molded with a two piece frame and a cylindrical central leg. Figure 10 shows samples of molded yoke core sections used in early tests.

Figure 11 shows a view of an unassembled production type horizontal deflection transformer. The iron-dust molded core is to be clamped together by the two sheet metal clips which are then held together by the long tiestrap. The coil and terminal board assembly are held in place by the core members. The two-turn coil of polyethylene insulated wire is supported between the two textolite disks. It is used as a filament winding for a type 1B3-GT/8016 pulse rectifier tube which supplies the first and second anode voltages to the kinescope. Two views of the assembled transformer are shown in Figures 12 and 13.

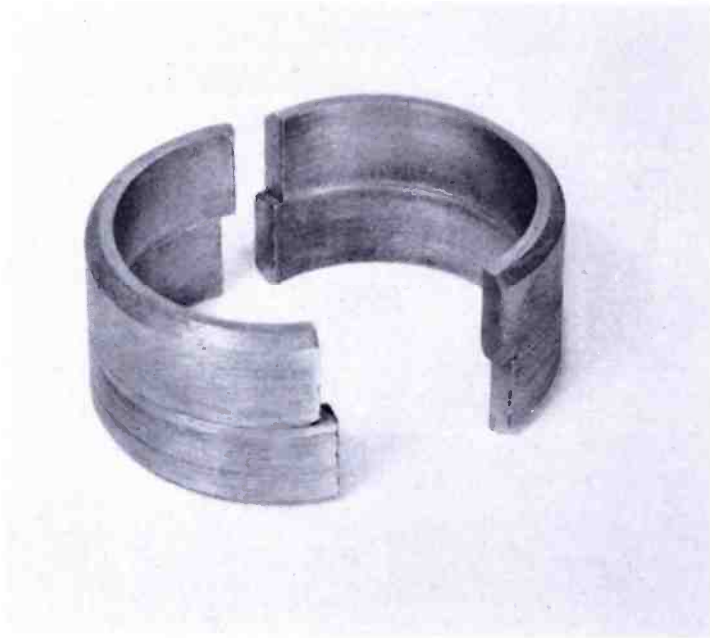


Fig. 10—Samples of developmental moldings of deflection yoke core sections of sponge iron powder.

Figures 14, 15 and 16 are three views of a production type deflection-yoke. It will be noticed, in Figure 14, that this particular yoke has an iron wire-wound magnetic core. The iron-dust-sector core may be substituted directly in this identical yoke arrangement in place of the iron-wire core. Figure 17 shows a developmental sample yoke with an iron dust core in place.

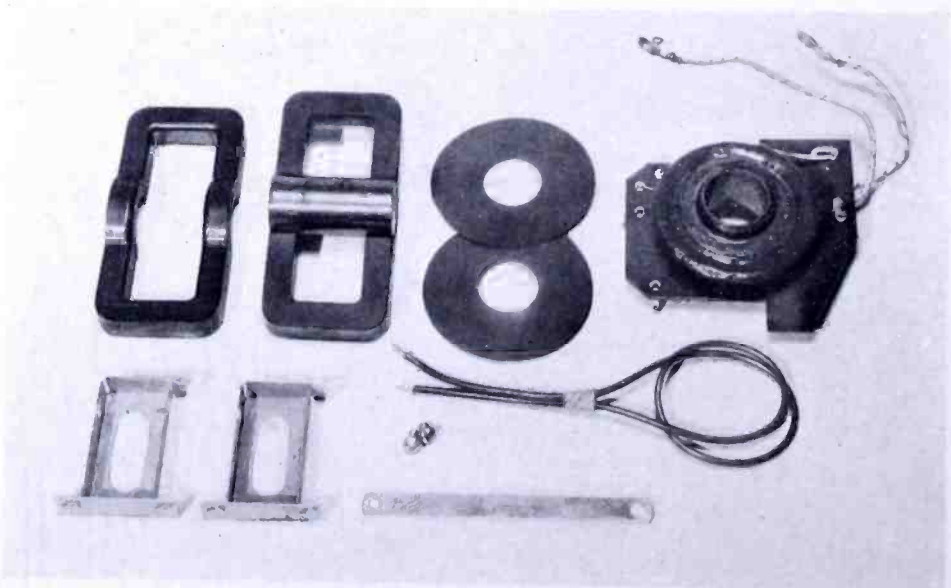


Fig. 11—A view of an unassembled production type horizontal deflection transformer with a high voltage winding.

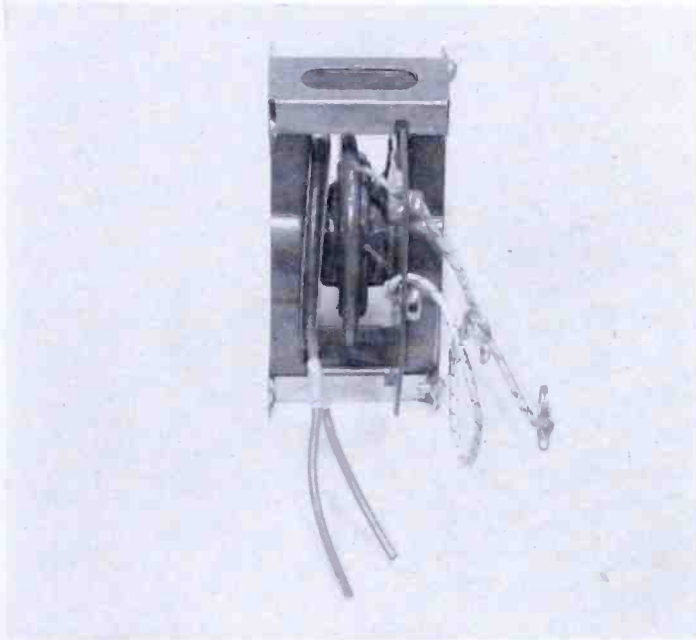


Fig. 12—Side view of a horizontal deflection transformer with molded sponge iron powder core.

It is interesting to note some of the effects of substitution of various core materials with the same deflection yoke windings. Figure 18 shows a plot of Q values as a function of frequency for two different windings each of which has been measured in combination with differ-

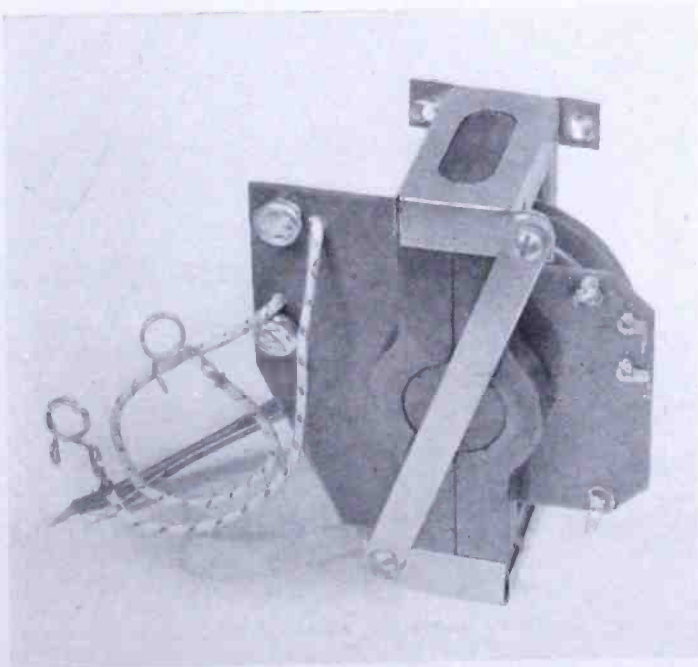


Fig. 13—Top view of horizontal deflection transformer with molded sponge iron powder core.

ent core materials. The amazing increase in Q when the iron dust core is used is notable. This is a true index of relative energy loss conditions. It reflects the relative adaptability for use in systems, to be discussed later, in which an attempt is made to recover a maximum

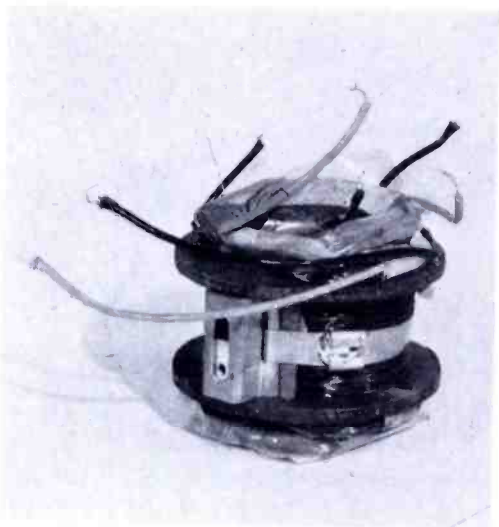


Fig. 14—Unmounted deflection yoke with iron wire-wound core. (A molded iron dust core may be used on this same yoke without other alterations.)



Fig. 15—Deflection yoke of Fig. 14 with terminals and side cover in place.

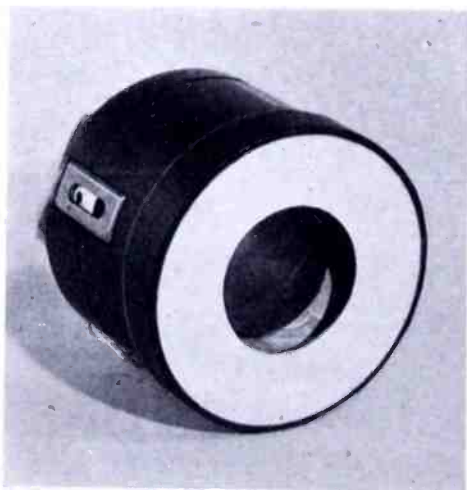


Fig. 16—Complete deflection yoke with all covers in place.



Fig. 17—First developmental sample deflection yoke with molded iron dust core in place.

amount of the stored energy of the magnetic circuits of the deflection system. The iron dust core provides a significant approach toward quite low energy requirements for low-cost horizontal deflection systems.

CONDITIONS OF OPERATION OF THE MATERIALS

In present production the various cores are being molded in the 15 to 30 tons per square inch pressure range. Depending upon economic factors, higher pressures may later be used in the molding of transformer cores.

The curves of Figures 6, 7, and 8 indicate the apparent incremental or alternating current permeability μ_a as a function of the maximum magnetic flux density B_{max} for samples of sponge-iron core materials molded under pressures of 15, 30, 45, and 60 tons per square inch, respectively. The maximum values of permeability occurred in each

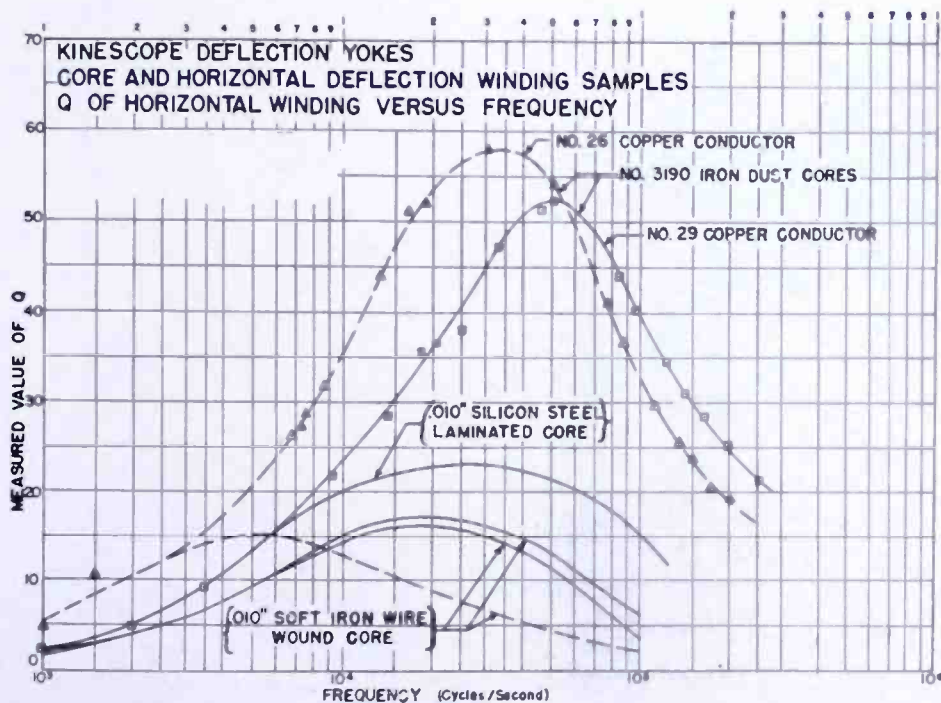


Fig. 18— Q of kinescope deflection yoke samples, with various cores and wire sizes, as a function of frequency.

case at values of B_{max} about ten times that of the normal working range. At 15 tons per square inch, the maximum permeability is approximately one and one half times that of the normal working range. The 60-ton-per-square-inch sample had a peak permeability almost twice that attained at lower values of B_{max} .

At the horizontal scanning frequency (15,750 cycles per second) the apparent permeability μ_a of the 15 tons per square inch sponge-iron material increases from 57 to 70 as B_{max} increases from 200 to 600 gauss (peak). The 30 tons per square inch sample exhibits an apparent permeability μ_a varying from 58 to 76 in the same range of maximum flux density. Pressures in this range are employed in

making the present production type iron-dust cores for television horizontal deflection transformers, the operating levels of which are within the above stated range of maximum flux density B_{\max} . The operating incremental permeability is approximately 63. Molding pressures of 45 and 60 tons per square inch yield operating incremental permeabilities of approximately 90 and 110, respectively.

When these materials, molded at pressures up to about 30 tons per square inch, are used, it is noted that, within the normal working range of flux density (Figures 6 and 7), the large equivalent series air gap masks a considerable part of the effect of the variation of the true permeability of the iron particles with changes in the magnetomotive force. Therefore, the apparent incremental (or alternating-current) permeability measured at quite low flux densities is of the same order of magnitude as the working value at somewhat higher levels. In fact, the direct-current magnetizing flux may cancel a portion of this increase. Within the limits of the required engineering accuracy, the operating value of apparent alternating-current permeability may be corrected by reference to the curves from the value determined by low level measurements to the operating value. Values determined by means of a standard laboratory-type bridge or Q -meter may be thus utilized in calculations that involve normal operating flux densities. Such corrections *may* introduce considerable error if applied to powdered materials molded at higher pressures, or to laminated iron cores of either the stacked or wound type.

The higher apparent permeabilities attained at higher values of peak magnetic flux density B_{\max} are not available for use in horizontal deflection transformers on account of inductance value and winding requirements. The greater losses incurred at the higher frequencies involved in this application also make it impossible to utilize more than a small fraction of the maximum indicated permeability of practical laminated core materials. For instance, in the case of one type of material of 0.003 inch lamination thickness, the apparent operating permeability range, for horizontal deflection transformer uses, is between 200 and 300, depending upon the precise operating conditions.

THE DEFLECTING CYCLE

In the horizontal deflection of the electron beam in television picture tubes, there are two major periods, those of the trace and of the retrace.

During the trace period, the electron beam should trace a single horizontal line of the picture at a constant rate of movement. To pro-

retrace period and to return as much as possible of the stored energy, in the resonant system, to active use in the next trace period. V_3 is usually a high perveance triode, or perhaps, for economic reasons, a diode.

In this circuit the high-voltage winding N_{hv} is added to provide a maximum total peak return-sweep pulse voltage across the sum of all the transformer windings. The rectifier tube V_4 is employed in the conversion of this high peak pulse voltage to a steady high voltage, of perhaps ten kilovolts, for connection to the kinescope second anode, for acceleration of the electron beam.

In Figure 19 the energy abstracted from the deflecting system during the period of damper operation is dissipated in the damper tube V_3 and its load resistor R_D . Otto H. Schade* has devised a method for recovering a portion of that energy by substituting in place of all or a part of the load resistor R_D a portion of the driver tube load upon the power supply system.

An example of a system of this type is shown in Figure 20. This is a booster-damper circuit. The voltage developed across the damper load resistor R_D is added in series with the power supply $B +$ voltage to increase its value.

When certain circuit proportions may be realized, the damper load resistor R_D may be entirely dispensed with in favor of the useful loading of the driver tube energy supply circuit. It is in this case that the low energy losses of the iron dust cores, used in the deflection transformer and yoke, yield their maximum advantage. Except for energy losses in the tubes and in the second anode power supply the low loss circuit components allow a large portion of the stored energy to be reused in the following and succeeding deflection cycles.

It will be observed that Figure 20 shows a voltage doubler high voltage power supply for the kinescope second anode. With a single 6BG6G driver tube V_2 this may provide up to 17 kilovolts accelerating voltage within the present pulse ratings of the vacuum tubes. At the same time full deflection of the beam is provided for a 50-degree kinescope.

Another possible connection is illustrated in Figure 21, where a diode damper tube is used to provide the boost-voltage while a triode damper tube controls the linearity of sweep.

In systems such as these the power input may be perhaps thirty watts. Of this perhaps five watts may be dissipated in the 6BG6G driver tube, six watts in the deflection transformer and yoke combina-

* It is anticipated that this method will be described in a forthcoming issue of *RCA REVIEW*.

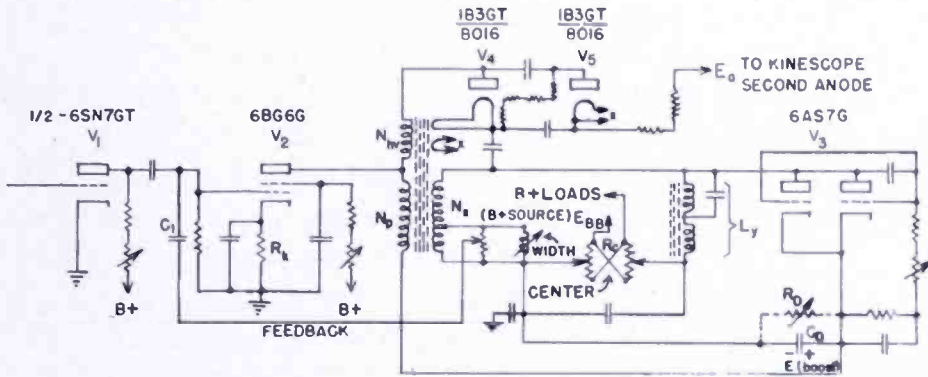


Fig. 20—The basic booster-damper circuit for recovering energy from low-loss horizontal deflection system. (A voltage doubler second anode power supply circuit is shown.)

tion, three watts in the kinescope second anode power supply system and load, seven watts in the auxiliary damper load resistor, eight watts in the damper tubes, and the balance of about one watt in the damper linearity control resistors.

The best available laminated core transformers with laminated or wire-wound yoke cores have a combined loss about fifty per cent greater than that of the powdered iron core system. The use of laminations of more than 0.005 inches thickness produces a very inefficient system. One previously-used system, with 0.014-inch transformer lamination thickness, was responsible for a 20-watt power loss in the transformer and yoke while deflecting a 7-kilovolt beam only sufficiently for a 40-degree kinescope. The same system with iron-dust cores adequately deflects a 12-kilovolt beam for a 50-degree kinescope.

With certain inductance and tube combinations, with a power supply furnishing less than 400 volts, the direct-current boost voltage approaches 200 volts. In this case no auxiliary damper load resistor is required, so its energy dissipation is eliminated.

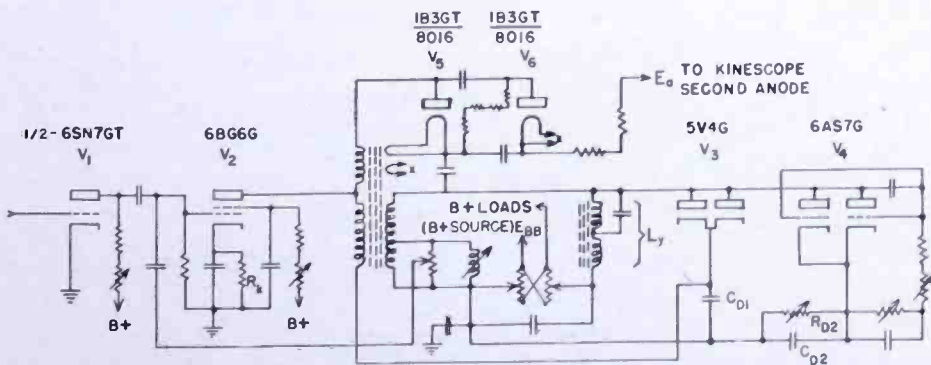


Fig. 21—The booster-damper circuit with a double damper arrangement for use with low inductance horizontal deflection windings and a single 6BG6G or 807 driver tube.

A high boost voltage may be attained without exceeding vacuum tube peak pulse ratings, and with the present production value of 8.2 millihenries yoke inductance, if *two* 6BG6G driver tubes are used in a highly efficient system with no auxiliary damper load resistor.

High energy recovery systems are possible only when low-loss transformer and yoke cores are used. At present the iron-dust core is the only low-loss, inexpensive core available for this application. Present estimates of powdered-iron cores indicate cost figures approximating one-fifth to one-tenth that of the nearest equivalent laminated-iron transformer core types.

As previously stated, tube ratings at this time allow the development of up to 17 kilovolts with full deflection of a 50-degree kinescope by means of a single 6BG6G driver tube with an 8.2-millihenry horizontal deflection yoke winding. With two 6BG6G beam tetrode driver tubes in parallel it is not difficult to produce at least 27 kilovolts second anode potential when employing a pulse-voltage-tripler rectifier system. Under these circumstances more than adequate horizontal deflection of the electron beam is available for a standard 50-degree kinescope. It has been found necessary to use a type 6AS7G duo-triode damper tube to produce the desired deflection linearity under these operating conditions.

CONCLUSIONS

Molded powdered-iron cores for television horizontal deflection transformers and yokes offer a simple solution to the problem of providing a high performance system at a *very* low cost. The great reduction in acoustic output from this core is fortunate. Higher permeabilities are desirable to increase the coupling coefficient of the deflection transformer. Higher molding pressures may provide higher permeabilities if costs can be maintained at a low level.

A single driver tube, with a single damper tube and two small rectifier tubes, can provide full deflection and second anode high-voltage for a 50-degree kinescope, at accelerating voltages up to 17 kilovolts under present tube ratings. Two 6BG6G driver tubes can easily provide full deflection for a standard 50-degree kinescope operated at 27 kilovolts second-anode potential which may be produced by a voltage-tripler rectifier arrangement from the deflection system retrace pulse.

ACKNOWLEDGMENTS

In developing these cores and transformers, the author has had the encouragement and assistance of a large and diverse group. G. L.

Grundmann, L. Pessel, A. T. Harding, and H. R. Shaw have been especially helpful. The previous work of Otto H. Schade has been particularly useful as a background for the entire program. Data for some of the experimental curves were measured with the assistance of Harold B. Stott. The coil arrangement of Figures 11 and 12 was originated by H. R. Shaw.

PART II

THEORY AND DESIGN OF COMBINED LOW-LOSS HORIZONTAL DEFLECTING AND HIGH VOLTAGE POWER SUPPLY SYSTEMS

Summary—When the special, low-cost, low-loss, molded iron powder cores described in Part I of this paper are used in the construction of television horizontal deflecting transformers and yokes, the energy losses are reduced sufficiently to permit the employment of certain simplified equivalent circuits and equations in the design procedure. The theory of low-loss horizontal scanning systems has progressed so that now the resultant transformer designs may be relied upon to produce the expected results, within approximately the tolerance limits which apply in the design of most of the other component parts. Design equations and charts are provided for application in the development of horizontal deflecting and high-voltage second-anode power supply systems.

INTRODUCTION

NEW low-cost molded iron powder core materials, for use in television horizontal deflection and high-voltage second-anode power supply systems, were described in detail in Part I of this paper. Photographs showed developmental and production type molded core parts and a number of families of curves outlined the magnetic properties of certain of the materials most useful in these applications.

Three system circuit diagrams were suggested as possible methods of use of the component parts employing these core materials. Certain of the performance data were outlined to indicate possible operating conditions and characteristics.

The purpose of this second part is to indicate methods which may be employed in the predetermination of those results which may be anticipated *before* a deflecting system is constructed. An additional purpose is to provide the necessary equations and charts to facilitate the design of the transformer windings and deflection and high-voltage systems in general.

There are certain phases of the design which are not fully covered in this paper, but which it is hoped may be included in an additional paper, at some later date. It is believed that the data presented here

provide the basic details which should enable a skillful engineer to produce equipment yielding the desired results.

BASIC SYSTEM OPERATION

A circuit diagram illustrating a basic arrangement of a horizontal deflecting and high-voltage power supply system is given in Figure 1. Here the discharge tube V_1 is actuated by the positive pulse applied to its grid and discharges capacitor C_1 . This produces a sawtooth voltage-wave across the terminals of C_1 , as it is repeatedly charged through the resistor R_1 and discharged by the operation of the triode V_1 . A negative voltage pulse, fed-back, at the correct time from the deflection circuit, is added at the negative peak of the voltage sawtooth wave.

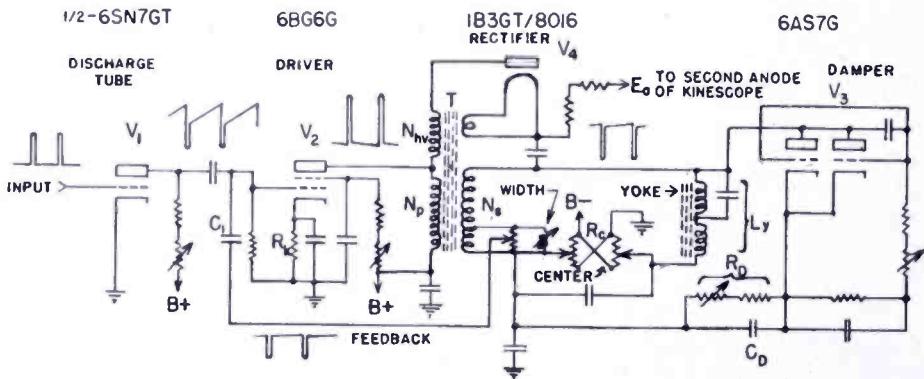


Fig. 1—Basic circuit diagram of a horizontal deflection system with provision for supplying the required high voltage to the second anode of the kinescope.

The output or driver tube V_2 , a beam tetrode, is controlled by application of the sawtooth voltage-wave in its grid circuit. At a voltage representing the approximate midpoint of the sawtooth wave the plate current of V_2 begins to flow, with its value increasing at a nearly linear rate. The linear rate of current increase continues until the occurrence of the sudden negative excursion of the grid voltage. This drives the grid of the tube V_2 to a negative value, considerably beyond the cut-off voltage.

The plate-load circuit, into which the beam tetrode works, consists chiefly of the almost pure inductance L_y of the deflecting yoke. The practical inductance value of this yoke winding is transformed, by the deflection transformer, to a value which is satisfactory in combination with the particular conditions of operation of the given driver tube.

These conditions, in addition to those governing the design of the yoke winding, may be influenced to a considerable extent, by the characteristics of the damper tube V_3 . This tube is connected across

the deflection yoke windings for the purpose of arresting the free oscillation which ensues from the instant of plate current cut-off of the driver tube V_2 . The first half-cycle of free oscillation is required to produce the retrace, or return, function of the deflection system.

As the second alternation commences the plate of the damper tube is driven positive; this causes conduction of current from the deflecting yoke by the damper tube. Appropriate damping, of more than critical value, may be effected when a high-perveance vacuum tube is utilized. A high-perveance triode, such as the new type 6AS7G, is an excellent choice for many of the probable applications.

When cost is a ruling consideration, it is possible to use certain high-vacuum diodes, of which the 5V4G is an excellent example, in place of the suggested triode. On account of the control over the flow of current through the triode afforded by connection of its grid to an appropriate network, it provides a superior damping performance which allows for the adjustment of the deflecting current to an almost perfect uniformity of variation. When a diode is used, the required time-linearity of deflection may be obtained only by sacrificing an appreciable fraction of the deflecting capability or by additional circuit complications. The addition of other circuit elements is required in order to provide an acceptable linearity of sweep; otherwise an extremely high-loss deflecting system may be used. When high-loss systems are employed, it is quite difficult to obtain the necessary deflecting field for the modern kinescopes, which utilize large deflection angles.

When a diode is substituted directly in place of one of the better triode damper tubes, it is generally found to provide excellent linearity of sweep throughout all of the trace period except approximately the first ten per cent.

The diode may be constructed to have a very low internal voltage drop. This fact makes it quite useful in reducing the energy-loss in the damper tube. When energy recovery systems are employed this advantage becomes of importance if the cost of the linearity correction system is not prohibitive.

At the moment, it appears that the added advantage of the ease of linearity control provided by using a very high perveance triode damper is sufficient to more than compensate for its higher energy loss. The type 6AS7G dual-triode, with the two triode sections connected in parallel, is the most satisfactory tube available for this purpose. In the parallel connection its plate resistance is only 140 ohms. At zero grid-bias, one-quarter ampere of plate current may be passed with only about 35 volts drop across the tube. The rated average operating plate

current is one quarter ampere. The transconductance for the parallel sections is 15,000 micromhos.

The stored energy in the magnetic fields at the end of the retrace period is dissipated chiefly in the equivalent resistances of the deflecting yoke and transformer, the damper tube and the damper load circuit. If the damper load by-pass capacitor is of adequate capacitance, the last of these three may be considered to be a load of constant voltage drop. Its voltage is polarized in a sense opposed to the induced voltage of the system. The time constant of the discharge system is therefore determined from the constants of the system composed of the deflecting transformer and yoke and the damper tube.

In a low-loss deflecting system, when the damper load conditions are correct, the essentially linear portion of the exponential decay of current, with the progress of time, is active for approximately the first forty per cent of the trace period. As the rate of decay begins to decrease beyond the allowable limit, the driver tube begins to conduct. The driver current increases at a very slow rate at first. The rate of increase becomes greater as conduction progresses through the low-current non-linear region of the mutual characteristic. As the discharge of energy stored in the magnetic fields of the deflecting system approaches completion, the driver tube steps into its role of supplying current of almost constantly increasing value for the balance of the trace period. After this time, the process repeats again with each succeeding cycle.

An approximate diagram of current relations is shown in Figure 2. Actually it may be desirable to allow a *very slight* damper current to flow throughout the entire trace time in order to smooth any possible fluctuations in yoke current. The damper-tube clipper action may be thus used for controlling the maximum value of the voltage across the deflecting yoke windings.

During the trace period, there is a constant positive voltage across the yoke windings which is proportional to the time rate of change of deflecting current multiplied by the yoke inductance. In addition there is a small amplitude sawtooth voltage which must be added to compensate for the voltage drop across the resistance component, if the sweep is to be truly linear. This voltage may have an amplitude of ten to thirty per cent of the square wave constant amplitude value. During the retrace periods there are high-amplitude negative pulses of approximately half-sinusoidal form. Much higher frequency leakage reactance resonance waves are generally to be found superimposed on the retrace voltage wave. They are usually of a small amplitude, of perhaps two to ten per cent of that of the retrace pulse. This voltage wave is also illustrated in Figure 2.

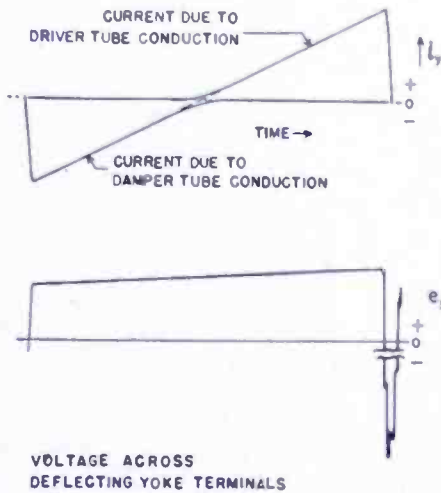


Fig. 2—Plot of approximate current and voltage variations associated with the deflection yoke windings.

DESIGN ANALYSIS

The Simplified Equivalent Circuit

Reference to Figure 1 leads to the simplified equivalent circuit of Figure 3, for that portion embracing the deflecting transformer T and the deflecting yoke L_y , when the performance is to be considered during only that portion of the trace period in which the driver tube V_2 is essentially the sole source of deflecting current. The voltage variation during this period is relatively small, and the equivalent air-gap of the molded iron-dust core transformer rather effectively masks the variation of core permeability with flux density; therefore, the transformer inductance values may be considered essentially constant during the period in question. The low core-loss and the resultant high-Q of the component inductances make initial calculations with reference to an assumed non-dissipative network reasonably accurate. This assumption is valid especially because the dissipation corrections involve second order corrections in the preliminary considerations.

In Figure 3 the deflecting transformer is converted to its unity ratio equivalent "T" network involving two leakage inductances of

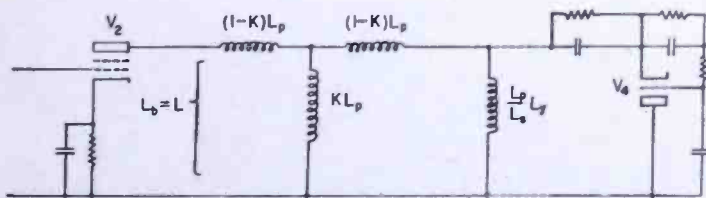


Fig. 3—Simplified equivalent schematic diagram of a horizontal deflecting system employing inductive components having low energy dissipation.

value $(1-K) L_p$ in the series arms and a shunt magnetizing inductance of value KL_p , where K is the coupling coefficient between the primary and the secondary, and L_p is the inductance of the primary winding. The inductance L_y of the deflecting yoke is represented in its trans-

formed state at the transformer primary equivalent value $\left(\frac{L_p}{L_s} L_y \right)$

All dissipative elements of the transformer and yoke are intentionally omitted for the sake of simplicity. As stated above, this procedure is valid for the present purposes if iron dust or equivalent low-loss cores are used. If the value of Q at the scanning frequency is greater than ten, there should be little doubt concerning the validity of the assumption.

For successful performance with the present television standards, the natural resonant frequency of the system must be greater than 69 kilocycles/second. It may be designed to be about 77 kilocycles/second in order to insure a sufficiently short retrace period (one half-cycle of this resonant frequency). The standard sweep-recurrence rate (15,750 cycles/second) is roughly one-fifth of the desired resonant frequency. It is possible to neglect the distributed and lumped capacitances in considerations of the equivalent circuit during the sweep period, since, at the scanning frequency, the ratio of capacitive to inductive reactance is approximately twenty-five.

Upon admitting the above assumptions, it follows that the equivalent plate-load inductance of the driver tube V_2 is given by

$$L_b = L = L_p \left[1 - \frac{K^2}{1 + (L_y/L_s)} \right] \quad (1)$$

- where: L_b = plate load inductance of driver tube V_2
 L = inductance between the input terminals of the deflection system network
 L_p = transformer primary winding inductance
 L_s = transformer secondary winding inductance
 $K = M / \sqrt{L_p L_s}$ = coupling coefficient of transformer
 M = mutual inductance between primary and secondary of transformer
 L_y = inductance of the horizontal deflection windings of the yoke.

It is to be expected that the full input deflecting ability which might be obtained from a directly connected deflecting yoke of the correct inductance L will not be available in a circuit that utilizes a coupling

transformer. The series leakage inductances $(1-K)L_p$ and the shunt magnetizing inductance KL_p unite to form an attenuating network between the driver tube V_2 and the deflecting yoke windings.

Suppose that a practical deflecting yoke is available and that a low-loss inductance-changing or "deflection" transformer is constructed to provide the desired inductance $L_b = L$ to match with the characteristics of the driver tube V_2 . This combination of transformer and yoke windings with the driver tube V_2 possesses a certain electron-beam-deflecting ability measured in terms of the beam-deflecting angle $2\theta_h$ for a beam-accelerating voltage (E_a). Consideration of only the deflecting yoke operation yields the equation

$$\theta_H = \sin^{-1} (\alpha s N_y \hat{i}_y / 2\sqrt{E_a}) \quad (2)$$

where: θ_H = half the total deflection angle (degrees)

α = a constant depending upon the geometry of the yoke magnetic path

s = the equivalent yoke length (centimeters)

N_y = the total number of turns on the yoke horizontal windings

\hat{i}_y = the peak-to-peak value of the yoke winding current (amperes)

E_a = the electron beam accelerating potential (volts).

Suppose that a special type of yoke might be designed to provide the correct load inductance L_b without the use of a matching transformer, but with the same values of α , s , and E_a , so that $L_y = L_b = L$. If the same driver tube is employed, the deflection angle is increased, due to removal of the transformer attenuating factors. From Equation (2), it is apparent that this is equivalent to increasing the number of yoke peak to peak ampere turns ($N_y \hat{i}_y$).

It can be shown, from the simplified equivalent circuit, of Figure 3, that the ratio of the yoke peak to peak ampere-turns, with a practical transformer, to that value with no transformer (or with an *ideal* transformer) is equal to the deflection factor

$$F_D \equiv \frac{(N_y \hat{i}_y) \text{ (practical transformer)}}{(N_y \hat{i}_y) \text{ (ideal transformer)}}$$

$$= 1 / \sqrt{\frac{L_s}{L_y} \left[\frac{1}{K^2} - 1 \right] + \left[\frac{2}{K^2} - 1 \right] + \frac{1}{K^2 L_s / L_y}} \quad (3)$$

The maximum deflection factor (F_D) is generally desirable and may be determined as a function of K and the ratio (L_s/L_y) from the equation

$$(L_s/L_y) = 1/\sqrt{1 - K^2} \tag{4a}$$

which yields

$$F_{D(max)} = F_{Dm} = \sqrt{\frac{(L_s/L_y) - 1}{(L_s/L_y) + 1}} = \frac{K}{1 + L_y/L_s} \tag{4b}$$

when 4(a) is satisfied.

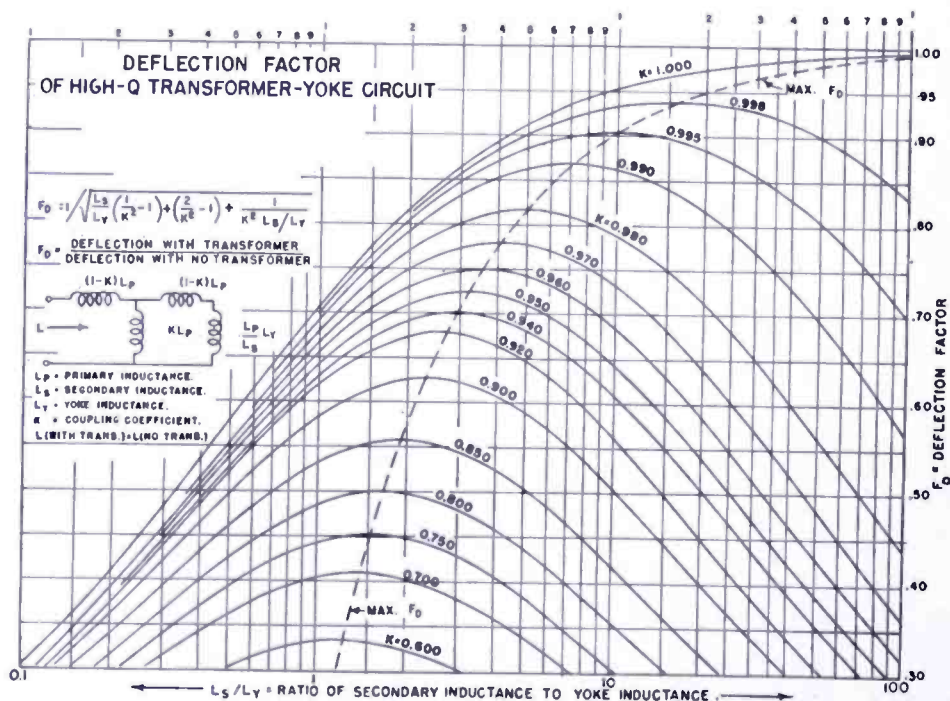


Fig. 4—Curve family depicting deflection factor (F_D) versus transformer secondary winding inductance to deflecting yoke inductance ratio (L_s/L_y) as a function of the transformer coupling coefficient (K).

A family of curves representing (3) together with a dashed plot of (4) is shown in Figure 4. If the approximate value of the coupling coefficient for a particular type of transformer winding and core is known, the optimum value of (L_s/L_y) and the corresponding value of F_D may be determined from the curves of Figure 4.

As an example, for a certain winding and core structure arrangement, $K = 0.94$. Hence, from the dashed curve for maximum F_D values, $(L_s/L_y) = 2.92$. From the deflection factor scale, $F_D = 0.702$. In other words, the best transformer which can be constructed with a coupling coefficient of 0.94 will yield 70.2 per cent of the deflection ampere turns which could be obtained with a perfect transformer.

It is difficult to build a satisfactory horizontal deflection transformer with a deflection factor greater than about 0.85. When a kinescope second-anode voltage supply is to be operated from the same transformer, it is even more difficult.

Designing the Horizontal Deflection Transformer

There are a number of viewpoints from which one may begin in the design of a horizontal deflection transformer, depending upon the known factors. Generally, an intended driver tube (or tubes) and a damper tube are assumed.

The maximum inductance of the yoke may be limited by the damper tube peak-inverse voltage rating. From experience, or from calculations, it may be determined that a certain yoke inductance is approximately the maximum which may be used within the peak voltage rating of a given damper tube while deflecting an electron beam of known characteristics.

Suppose that a type 6AS7G damper triode is to be used. This tube, according to its present design characteristics, has a peak inverse pulse rating of 1750 volts. The maximum yoke inductance across which it may be utilized in the present average application is approximately 10.0 millihenrys. A production-type yoke is available with an inductance of 8.2 millihenrys.

The deflection characteristics of a developmental sample yoke of this inductance have been determined by experiment and plotted. It is convenient to determine the product αs of equation (2) for a particular type yoke structure. With a given number of turns and a certain required value of maximum horizontal deflection angle $2\theta_H$ it is possible to plot the peak-to-peak yoke current \hat{i}_y versus the electron beam accelerating voltage E_a . These values for the particular developmental sample yoke are plotted in Figure 5. This curve represents the results obtained with a yoke employing a molded-iron-dust yoke-core. A plot of Q values of several deflection yokes as a function of frequency was presented as Figure 18 of Part I. A very large increase in Q was noted when the iron-dust core was used.

In the transformer design sequence, the peak yoke current \hat{i}_y is selected from the curve of Figure 5 for the full deflection of a normal 4/3 aspect ratio picture of a kinescope utilizing 50 degrees total deflection angle 2θ for the picture diagonal, or a horizontal deflection angle of $2\theta_H = 40.92$ degrees.

The time of one horizontal sweep cycle T_H is the reciprocal of the horizontal sweep frequency f_H .

$$T_H = 1/f_H \quad (5)$$

According to the present television standards, $T_H = 1/15750 = 63.49 \times 10^{-6}$ seconds or 63.49 microseconds. Horizontal blanking is allowed for 16 to 18 per cent of this time. After allowing for tolerances, there is a remainder of not more than about 11.5 per cent or 7.33 microseconds, maximum time for the retrace period. Conservatively, it is wise, in making design calculations, to allot about 6.5 to 7.0 microseconds for the return time. The retrace time T_r is

$$T_r = 1/2f_r \quad (6)$$

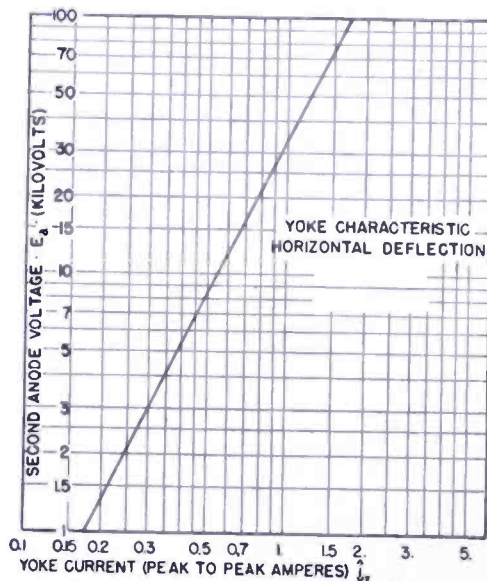


Fig. 5—Required peak-to-peak deflecting yoke current versus kinescope second-anode (accelerating) potential for a developmental sample yoke with a molded iron dust core. (No loss of deflection due to connection of a width control was considered in plotting these data.)

where f_r is the free resonant frequency of the system. The trace time is

$$T_t = T_H - T_r = \frac{1}{f_H} - \frac{1}{2f_r} \quad (7)$$

Hence, the trace time T_t should be about 56.5 to 57.0 microseconds.

To reproduce an acceptable picture, the rate of change of current through the deflection yoke windings during the trace period must be constant to within about five per cent, when any two portion of the trace are compared. Within this limit, it is admissible to regard the rate of change of yoke current during trace as a constant. The required

peak-to-peak yoke current \hat{i}_y is taken from the deflection current curve, or data, and the trace time T_t is determined by (7). The rate of change of current during trace is

$$(di_y/dt)_t = \hat{i}_y/T_t \quad (8)$$

To allow for picture width-control operation and for variations in component parts and tubes, there should be an increase of about 10 per cent in \hat{i}_y above the value indicated by the curve of Figure 5.

The required direct-current voltage E_{Lyt} applied across the inductive component of the yoke during trace may be determined from the equation

$$E_{Lyt} = L_y (di_y/dt)_t \quad (9)$$

When the sawtooth current through the deflection yoke windings reaches its peak value it is being supplied by transformer action from the driver tube V_2 . At this moment V_2 is suddenly and completely cut off, allowing the deflecting system to begin a period of free oscillation, at its resonant frequency of about 75 kilocycles/second. The rapid change of magnetic flux may induce perhaps 1500 peak volts or more across the yoke windings.

The free oscillation begins with maximum current. At the end of the first half-cycle, the yoke current reaches a new maximum value in the reverse direction. At this instant the induced yoke voltage reverses polarity and initiates damper tube V_3 conduction, to begin the next sweep cycle. At this time the current is less than that at the start of oscillation on account of the circuit damping. It may be shown that the effects of damping produce a ratio of current defined by the current factor:

$$F_I = i/i(Q_r=\infty) = \epsilon^{-\pi n/Q_r} = \epsilon^{-\pi/2Q_r} \quad (10)$$

where: F_I = current factor

i = the current in a circuit possessing the measured value of Q_r

$i(Q_r=\infty)$ = the current in a circuit possessing infinite Q_r

$\epsilon = 2.71828$

$\pi = 3.1416$

n = the number of cycles after the start of the damped wave = $\frac{1}{2}$ cycle

$Q_r = 2\pi$ (energy stored)/(energy lost per cycle at the resonant frequency)

This function is plotted in Figure 6 for values of Q from 0 to 100. A value of $Q_r = 15$ may be common in low-loss deflection systems. From Figure 6, this yields $F_I = 0.902$.

During the first part of the trace period the yoke current is passed through the damper tube V_3 (Figure 1) to an energy storage capacitor C_D . This damper load capacitor may be made large enough to stabilize effectively the voltage level into which the damper tube operates. Its stable voltage, plus the direct-current component of the plate voltage drop of the damper tube, provides the potential across which the inductive component of the yoke windings operates. The loss factors in the yoke require a sawtooth voltage component which is supplied

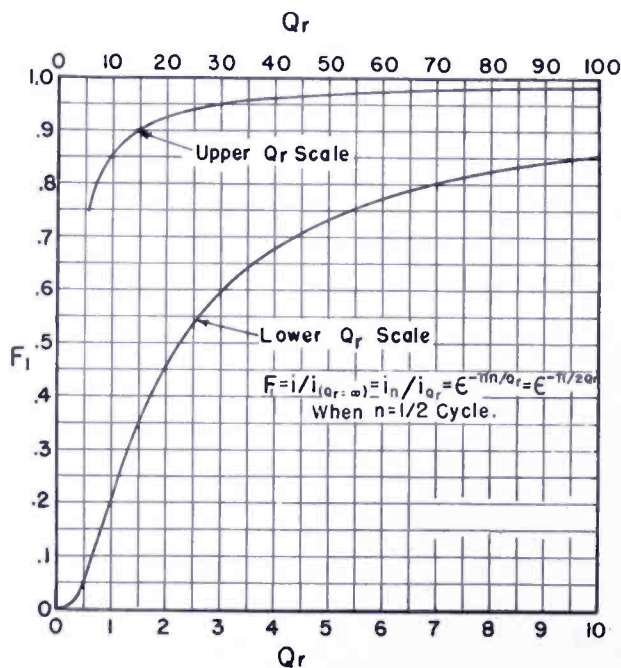


Fig. 6—Current factor (F_I) plotted as a function of the Q of the deflecting system at its free resonant frequency (f_r).

by the action of an RC (resistance-capacitance) network connected to the grid of the damper triode.

As the energy stored in the magnetic circuit diminishes to the point at which it provides an inadequate rate of current change in the deflection yoke windings, the driver tube V_2 begins to conduct. This tube carries its portion of the deflection burden to the end of the trace period. The damper tube should conduct only slightly during this period, mostly during the initial or transitional phase.

It is important for the designer to know at what point in the trace period the burden of producing the change of yoke current is handed over from the damper system to the driver system. It is evident that

the period of damper action dominance must be less than half the trace time, since the only energy involved is that stored in the magnetic fields at the end of trace, minus the amount deducted to satisfy the system losses during the retrace period. The transition time is defined as that time at which the projected linear rate of yoke current change passes through the zero current axis.

In view of (4a) and (4b) the final yoke current, at the end of the trace period, may be designated as

$$i_{yf} = \hat{i}_p \Phi_D a_{ps} \quad (11)$$

where: \hat{i}_p = peak driver plate current

$\Phi_D \equiv$ deflection function $\equiv K/[1 + L_y/L_s]$ which is equal to the *maximum* deflection factor F_{Dm} from (4b) when (4a) is satisfied

a_{ps} = the primary-to-secondary transformer turns ratio $= N_p/N_s$

From (10) and (11), the initial yoke current is found to be

$$i_{yi} = \hat{i}_p \Phi_D F_I a_{ps} \quad (12)$$

By simple proportion, and in view of (11) and (12), it may be shown that the fraction of the trace time allotted to damper dominance is

$$n_D = i_{yf} / (i_{yi} + i_{yf}) = F_I / (1 + F_I) \quad (13)$$

Alternately, the fraction allotted to the driver period is found to be

$$n_d = i_{yf} / (i_{yi} + i_{yf}) = 1 / (1 + F_I) \quad (14)$$

so that

$$n_D + n_d = 1 \quad (15)$$

From (14), if $F_I = 0.902$, the active driver portion of trace is $n_d = 1/1.902 = 0.526$, or 52.6 per cent.

The time of each conducting cycle of the driver tube V_2 is

$$T_d = T_t n_d \quad (16)$$

These data, with the value of peak plate current, allow the calculation of the rate of change of the primary current of the transformer. That current is also the driver tube V_2 peak plate current \hat{i}_p .

$$(di_p/dt)_t = \hat{i}_p / T_d \quad (17)$$

The probable maximum peak plate current for one type 807 or for one 6BG6G is 0.220 amperes.

From (3), (8), and (17), the required transformer turns ratio is

$$a_{ps} = N_p/N_s = (di_y/dt)_t / (di_p/dt)_t \Phi_D = \hat{i}_y T_d / \hat{i}_p T_t \Phi_D \quad (18)$$

To determine the number of turns required for the primary and secondary windings the geometry of the core structure must be decided upon and the permeability of the core material must be known under the operating conditions. From these data the operating value of reluctance \mathcal{R} or its reciprocal the permeance \mathcal{P} of the magnetic core may be determined by well-known methods of calculation. Alternately the operating permeance \mathcal{P} of a proposed core structure may be determined by measurement. It is convenient to utilize the permeance in combination with the constants of the equation for the inductance

$$L = 4\pi N^2 \mathcal{P} \times 10^{-9} = N^2 \beta \quad (19)$$

where: L = the inductance of the winding, in henries

$$\beta = 4\pi \mathcal{P} \times 10^{-9}$$

\mathcal{P} = the permeance of the core structure

In the case of the production type transformer, shown in Part I of this paper, the value of β for the assembled core structure should be equal to approximately 2.70×10^{-7} .

From (4), or from Figure 4, the value of L_s/L_y may be found in terms of the coupling coefficient K . Since the yoke inductance L_y was assumed to be known, it follows that the secondary inductance is

$$L_s = (L_s/L_y) L_y \quad (20)$$

From (19), the number of transformer secondary turns is

$$N_s = \sqrt{L_s/\beta} \quad (21)$$

and from (18), the number of transformer primary turns is

$$N_p = a_{ps} N_s \quad (22)$$

The primary inductance (L_p), from (19) and (21), is

$$L_p = N_p^2 \beta = a_{ps}^2 N_s^2 \beta = a_{ps}^2 L_s \quad (23)$$

The voltage across the inductive component of the driver-tube load during the trace period may be determined if the value of the primary inductance is known. Equation (1) may be solved in terms of the results of Equations (4) and (23).

From the plate load inductance and the rate of change of plate current $(di_p/dt)_t$ during the trace period, the voltage drop across the inductive component of the plate load is

$$E_{Lb} = L_b (di_p/dt)_t \quad (24)$$

This is a constant voltage during the trace period. During retrace there is a pulse of opposite polarity. During the trace period there is, in addition, a sawtooth voltage wave caused by the sawtooth current wave passing through the small equivalent resistance component. The energy loss is proportional to the square of the amplitude of this voltage wave. It should therefore be minimized. A rigorous solution for the value of the equivalent resistance may involve the solution for an equivalent value for each harmonic frequency of the sawtooth wave.

A short-cut method, generally, of sufficient accuracy, involves the assumption of a sine-wave sweep of the fundamental scanning frequency and of the sawtooth amplitude, together with a system with an energy storage factor Q_1 evaluated at the same frequency. From the known plate load inductance, frequency and Q_1 values, the *approximate* equivalent resistance is

$$R_1 = 2\pi f_H L_b / Q_1 \quad (25)$$

From the above short-cut method, the dissipative peak voltage drop across the load is

$$\hat{e}_{Rb} = \hat{i}_p R_1 = 2\pi f_H L_b \hat{i}_p / Q_1 \quad (26)$$

The minimum driver-tube plate voltage occurs when the voltage across the load is at its maximum value. In view of allowable screen power dissipation, the minimum plate voltage e_p for either the 807 or 6BG6G should be *not less than* 60 volts. The total required plate power supply voltage \bar{E}_B is the sum of these values plus the voltage drop \bar{E}_k across the driver tube cathode resistor R_k and that E_c across the picture horizontal centering control R_c . Hence

$$\bar{E}_B = \bar{E}_{Lb} + \hat{e}_{Rb} + \bar{E}_k + \bar{E}_c + e_p \quad (27)$$

\bar{E}_B may be used as a value of power supply voltage.

This total power supply voltage is not directly applied to the plate

of the driver tube as a continuous voltage. The plate voltage wave should be a sawtooth superimposed upon a small steady voltage, to provide a minimum of more than 60 volts and a maximum of perhaps 125 volts when a 6BG6G driver tube is used in a low-loss system. At the retrace time there is a positive half-sine-wave retrace pulse of several kilovolts peak amplitude applied to the plate of the driver tube.

The Amplitudes of the Retrace Voltage Pulses

The amplitude of the retrace voltage pulse across the horizontal deflection windings of the yoke may be calculated from the theory of damped free oscillations. It may be shown that with a starting current i_o , the damped voltage across the inductance-resistance of inductance-capacitance-resistance circuit is represented by

$$e = i_o \left(L\omega_r + \frac{R}{4Q_r} \right) (\sin \omega_r t) e^{-\omega_r t/2Q_r} \quad (28)$$

where Q_r is the resonant Q of the system and

$$\omega_r = \pm \sqrt{\frac{1}{LC} - \frac{R^2}{4L^2}} = 2\pi f_r \quad (29)$$

where f_r is the resonant frequency.

The maximum value of the first half cycle of this wave is the peak value of the major retrace wave across the yoke, when $i_o = \hat{i}_y n_d$ and $L = L_y$. From (28) this maximum is

$$\hat{e}_{yr} = \hat{i}_y n_d \left(L_y \omega_r + \frac{R}{4Q_r} \right) [\sin (\tan^{-1} 2Q_r)] e^{-(\tan^{-1} 2Q_r)/2Q_r} \quad (30)$$

A pulse factor F_p may be defined as the ratio of the peak voltage with any value of Q_r to that voltage when Q_r is infinite. When Q_r becomes infinite (30) becomes

$$\hat{e}_{yr} |_{(Q_r=\infty)} = \hat{i}_y n_d L_y \omega_r \quad (31)$$

So

$$F_p = \hat{e}_{yr} / \hat{e}_{yr(Q_r=\infty)} = \left(1 + \frac{1}{4Q_r^2} \right) [\sin (\tan^{-1} 2Q_r)] e^{-(\tan^{-1} 2Q_r)/2Q_r} \quad (32)$$

The curve of F_p versus Q_r is plotted in Figure 7 for values of Q_r from 0.1 to 100. For values of Q_r less than unity, the value of F_p is chiefly of academic interest, since the resonant frequency f_r is depressed by the increased R/L ratio (29), requiring other changes to maintain the correct value of resonant frequency f_r and retrace time t_r . Hence, the increasing value of F_p , as Q_r decreases below 0.8, does not imply any increase of retrace pulse voltage when the Q is reduced.

In view of (31) and (32), the yoke retrace pulse voltage (30) becomes

$$\hat{e}_{yr} = \hat{i}_y n_d L_y \omega_r F_p = 2\pi f_r \hat{i}_y n_d L_y F_p \tag{33}$$

The peak damper tube retrace voltage \hat{e}_{Dr} may be determined by adding the peak yoke retrace voltage \hat{e}_{yr} and the damper load voltage

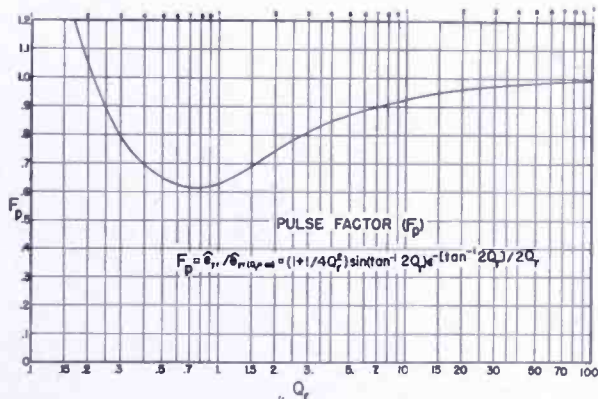


Fig. 7—Pulse factor (F_p) as a function of the Q of the deflecting system its free resonant frequency (f_r).

\bar{E}_{RD} . \bar{E}_{RD} is equal to the voltage induced in the yoke during trace E_{Lyt} minus the damper-tube voltage drop e_{Dt} and the dissipative component voltage e_{R2t} drop of the inductive network. The initial voltage drop across the damper tube e_{Dti} , at the beginning of the trace period may be determined from the plate characteristic chart of the damper tube. At this instant the grid of the triode is driven *very slightly* positive, so that the true value of the damper tube plate voltage drop may be quite closely approximated by the value read from the zero-bias line at the value of initial damper trace current i_{Dti} .

The initial peak damper current during the trace period is the sum of the initial yoke current during trace i_{yi} and the similar current i_{mi} from the transformer magnetizing inductance. It may be shown that

$$i_{mi} = i_{yi} (1 - K + L_y/L_s) / K \tag{34}$$

From this it follows that

$$i_{Dti} = i_{yi} + i_{mi} = i_{yi}(1 + L_y/L_s)/K = \hat{i}_p F_I a_{ps} \quad (35)$$

This value i_{Dti} represents a close approximation to the maximum value of current flowing through the damper tube at the beginning of each trace period. It is the value of current which should be used in connection with the vacuum tube plate characteristic family chart for the determination of the damper tube voltage drop e_{Dti} . The value of e_{Dti} for a single 6AS7G triode damper, with the two triode sections connected in parallel, is generally between 40 and 80 volts in most receiver applications. At the same instant, of maximum trace initiating current, a maximum of dissipative voltage drop e_{R2ti} occurs in the inductive network.

The general voltage relation is

$$\bar{E}_{RD} = E_{Lyt} - e_{R2t} - e_{Dt} \quad (36)$$

wherein the sum $e_{R2t} + e_{Dt}$ is a constant during the period of damper tube conduction. At the initiation of trace the relation becomes

$$\bar{E}_{RD} = E_{Lyt} - e_{R2ti} - e_{Dti} \quad (37)$$

wherein it may be shown that the initial maximum voltage drop across the resistive component of the deflecting network, during the trace period, is approximated by the value

$$e_{R2ti} = 2\pi f_H \hat{i}_{yi} L_y / Q_1 = 2\pi f_H \hat{i}_p \Phi_D F_I a_{ps} L_y / Q_1 \quad (38)$$

By adding (33) and (37) the peak inverse damper tube voltage is found to be

$$\hat{e}_{Dr} = \hat{e}_{yr} + \bar{E}_{RD} = \hat{e}_{yr} + E_{Lyt} - e_{R2ti} - e_{Dti} \quad (39)$$

The peak of the major pulse of the driver tube plate voltage during retrace \hat{e}_{dr} is closely approximated by the equation

$$\hat{e}_{dr} = \hat{e}_{yr} a_{ps} K + \bar{E}_B - \bar{E} - \bar{E}_c \quad (40)$$

The leakage reactance resonance wave may add perhaps 5 to 10 per cent to this value.

Second Anode High Voltage Power Supply

The accelerating or second anode voltage \bar{E}_a for the kinescope may be derived from the retrace voltage pulse of the deflection system. A known value of second anode voltage \bar{E}_a was assumed as a starting point in the transformer design data. With the available vacuum tubes and components, it appears impractical to attempt to obtain more than about 12 kilovolts peak pulse from a deflection system transformer while a linear rate of picture spot deflection is provided, and while operation is kept within the vacuum tube ratings. A voltage-multiplier-rectifier system (See Figure 20 of Part I) is required to produce higher voltages. Experience with the distributed capacitances encountered in such devices indicates that 18 kilovolts is near the limit which may be obtained with a voltage doubler system under these conditions. This limit is imposed by driver and damper tube peak voltage ratings and by retrace time requirements.

An extra transformer winding is necessary to produce the additional required voltage. This winding of N_{hv} turns is connected as an addition to the primary winding to produce an autotransformer arrangement.

Connection of the rectifier system across the primary winding N_p , the deflection secondary winding N_s , and the high voltage, winding N_{hv} , all in series-aiding connection, yields a winding of total turns N_t , and maximum output voltage \hat{e}_{tr} , during retrace. The coupling coefficient K_{ts} indicates the fractional coupling between the secondary N_s and the total N_t winding. The number of voltage multiplier stages may be designated as m and the total to secondary turns ratio as

$$a_{ts} \equiv N_t/N_s = (N_p + N_s + N_{hv})/N_s \quad (41)$$

Supposing the free resonant frequency of the system to remain the same as previously assumed, the maximum value \hat{e}_{tr} of the major retrace pulse across the entire winding may be found in a manner similar to that of (40). The total surge voltage is multiplied by a leakage-reactance-resonance voltage wave correction $(1 + g)$ and the number of multiplying stages m . When the proper d-c voltages are added the result is the value of the *no-load*, second-anode, voltage

$$\bar{E}_{a0} = (1 + g) \hat{e}_{tr} a_{ts} K_{ts} m + \bar{E}_B - \bar{E}_c \quad (42)$$

The value of g is generally between 0.05 and 0.1. Combining (40) and (41) and solving for the number of turns on the high-voltage winding

produces

$$N_{hv} = N_s \{ [(\bar{E}_{ao} - \bar{E}_B + \bar{E}_c) / (1 + g) K_{ts} m \hat{e}_{yr}] - 1 \} - N_p \quad (43)$$

The ability to produce the required voltage is contingent upon the maintenance of a sufficiently low distributed capacitance value to produce the assumed values of free resonant frequency and retrace time. The prevention of silent discharge, or corona, and other current leakage paths is likewise very important, if the full voltage is to be realized. Corona shields and insulation that allows leakage of no more than a few microamperes are required for best operation.

The Average Current and Power

The average d-c plate current of the driver tube may be determined with reasonable accuracy, without the use of an elaborate integration method, by computation from the geometry of an assumed current-time plot. A triangular conduction current-time area may be assumed, with a 20 per cent current addition to account for the additional current caused by the lack of the ideal sharp current cut-off, required by the triangular wave theory. From these data it may be shown that the average plate current \bar{I}_p is

$$\bar{I}_p = 1.20 \hat{i}_p T_d / 2 T_H = 0.60 \hat{i}_p T_d / T_H = 0.60 \hat{i}_p f_H / \left(\frac{1}{f_H} - \frac{1}{2f_r} \right) n_d \quad (44)$$

The energy dissipation on the plate of the driver tube is quite low on account of the low plate voltage during the conduction period. The value of the plate power dissipation in watts P_p may be closely approximated by considering the peak sawtooth voltage \hat{e}_{Rb} , the minimum plate voltage e_p , the maximum plate current \hat{i}_p , the driver conduction time interval T_d , and the time of one sweep cycle T_H . Power dissipation is derived from the basic form

$$P_{p1} = \frac{1}{T_H} \int_0^{T_d} i_p e_p dt \quad (45)$$

from which it may be shown that, in the idealized case,

$$P_{p1} = \frac{1}{T_H} \int_0^{T_d} \left\{ (e_p + \hat{e}_{Rb}) \int_0^t \left(\frac{di_p}{dt} \right) dt - R_o \left[\int_0^t \left(\frac{di_p}{dt} \right) dt \right]^2 \right\} dt$$

$$= i_p [(\hat{e}_p + \hat{e}_{Rb})/6 + e_p/3] T_d/T_H \quad (46)$$

The addition of the 20 per cent remote cut-off current approximation allowance, of equation (44), at plate voltage $(e_p + \hat{e}_{Rb})$ adds a term

$$P_{p2} = 0.20 i_p (e_p + \hat{e}_{Rb}) T_d/2T_H \quad (47)$$

to yield the completed equation

$$P_p = P_{p1} + P_{p2} = \frac{i_p T_d}{T_H} [0.60 e_p + 0.267 \hat{e}_{Rb}] \quad (48)$$

In a typical example P_p may show six watts driver tube *plate* power dissipation. The rated value for the 6BG6G driver tube is 20 watts.

In this class of service, efficiently operated driver tubes are *not* limited by plate-power dissipation, but rather by the energy dissipation on the screen grid. Limitation of the minimum plate voltage to values greater than 60 volts, with no more than 300 volts applied to the screen grid, usually assures operation of the 6BG6G tetrode below its maximum screen dissipation rating of 3.2 watts. Operation with a minimum plate voltage of 80 may be desirable in certain applications for greater conservatism.

Damper Load Conditions

The time duration of the conducting period of the damper T_D is given by the equation

$$T_D = n_D T_t \quad (49)$$

The average (or d-c) damper current I_D may be approximated by the equation

$$\bar{I}_D = 1.20 i_{Dt} T_D/2 T_H = 0.60 i_{Dt} T_D/T_H \quad (50)$$

Combination of (37) and (50) allows the approximate value of the damper load resistance R_D to be calculated by Ohm's law, to yield

$$R_D = \bar{E}_{RD}/\bar{I}_D \quad (51)$$

This is the value of resistor required, if the booster-damper circuit is *not* used. In booster-damper circuits the current may divide between the plate circuit of the driver tube and a parallel resistor. The

parallel combination of these two loads should then have the calculated value of resistance R_D .

The Booster-Damper Circuit

The booster damper circuit (shown in Figure 20 of Part I and originally developed by Otto H. Schade) makes possible the utilization of the stored energy retrieved from the magnetic circuit during the first part of each trace or sweep period while the damper tube is functioning. This energy is fed back into the power supply circuit of the driver tube. If the damper tube *average* current is made equal to the average of the driver tube plate current, plus any other load current, then the voltage of the damper load circuit may be added directly to the voltage \bar{E}_B of the power system. If the rate of change of yoke current differs greatly from that of the driver plate current, the equalizing of the average plate currents requires some alterations of the circuit. The required voltage from the main power supply is

$$\bar{E}_{BB} = \bar{E}_B - \bar{E}_{RD} \quad (52)$$

The required load resistor R_D across the boost voltage is determined from the equation

$$R_D = \bar{E}_{RD} / \bar{I}_{RD} = \bar{E}_{RD} / (\bar{I}_D - \bar{I}_P) \quad (53)$$

It is desirable to make this resistance as large as possible, by adjustment of the system proportions, in order to minimize the losses. In some arrangements it may be made of infinite value, and omitted. This is the optimum condition. The total input power to the plate circuit of the driver tube from the power supply source is

$$P_{BB} = \bar{E}_{BB} \bar{I}_P \quad (54)$$

As stated in Part I, with perhaps 31 watts input to a single driver tube plate circuit, there may be about six watts dissipated at the plate of the 6BG6G driver tube, approximately six watts in the combined deflection transformer and yoke system, three watts in the kinescope second-anode power supply system and load, seven watts in the auxiliary damper load resistor, about eight watts in the damper tubes, and the balance of about one watt in the damper linearity control resistors.

A pair of type 6BG6G beam tetrodes may be operated in parallel, in a low-loss deflection system, with a voltage tripling high-voltage rectifier system. This combination is capable of supplying more than

27 kilovolts to the second anode of a projection type (5TP4) kinescope, and of deflecting the resultant electron beam considerably beyond the required amplitude. The rate of deflection of the electron beam may be caused to remain sufficiently constant so that it differs by less than five per cent, in its rate of sweep across the kinescope screen, between any two points along the path of trace.

Under these operating conditions, with about 380 volts derived from the power supply, the plate input power is usually between 40 and 50 watts. Perhaps six watts of this input power is delivered to the second-anode power supply. The remainder is distributed among the various system components to yield a dissipation of about six watts per driver tube, about twelve watts in the transformer and yoke combination, and the balance in the auxiliary parts. These include the picture width control, the linearity controls, and the bias resistors.

CONCLUSIONS

The procedure and equations outlined for use in designing horizontal deflection and high-voltage power-supply systems have been found useful in making preliminary designs and in interpreting the minor shortcomings of the experimental models. On account of the variations which are likely to be found in distributed capacitances, with different arrangements, no attempt has been made here to analyze the capacitance parameters. Full use should be made of all knowledge leading to the reduction of various distributed capacitances which might cause the free resonant frequency of the system to fall below about 75 kilocycles/second. It is further suggested that careful attention be given to corona discharge possibilities and to insulation leakage, both in the insulation and on its surface, in case the output voltage of the second-anode power supply system is lower than is expected, and if the resonant frequency is correct.

The equations herein yield excellent design results when the above mentioned precautions have been taken. It has been assumed that, when required, these data will be supplemented by additional methods in common use in the design of previously standardized equipment. This is particularly true when designs concerning the shape and dimensions of the transformer core structure are undertaken.

ACKNOWLEDGMENTS

These developments have been carried forward with complete interchange of data, ideas and materials with members of other groups

working in this field in various divisions and departments. In the RCA Victor Division, D. D. Cole, K. A. Chittick, C. M. Sinnett, and G. L. Grundmann have been particularly helpful in providing constructive criticism of results. Data and materials have been exchanged with O. H. Schade, A. Wright, H. R. Shaw, E. L. Clark, A. T. Harding, S. I. Tourshow, C. E. Torsch, and others of the RCA Victor Division, and with Karl Wendt of the RCA Laboratories Division. The author wishes to express his appreciation of the many instances in which those of this group have been of assistance in helping and encouraging the procedure incident to these developments.

THE POCKET EAR*

BY

J. L. HATHAWAY AND WILLIAM HOTINE

Engineering Department, National Broadcasting Company, Inc.,
New York, N. Y.

Summary—The “Pocket Ear” is a pocket type radio with a flexible tube for conducting sound into the ear. It was developed in the National Broadcasting Company Laboratory to replace the telephone headset equipment formerly used by the television stage directors in studio operation. The work of the stage director to be effective demands complete freedom of movement when directing actors and stage crew on the various sets in the studio and when cueing sound effects. At the same time, audio contact must be maintained with the program producer located in the control booth. The ordinary headset limited movement and, after hours of continued use, the wearer’s ears developed the numbed feeling so familiar to wireless operators.

The need for a system of communication in television studio work is first discussed, followed by an example of the television studio production problem which activated the present investigation¹ and resulted in the communication system now being used. A description of the electrical and mechanical construction of four different receivers is included with illustrations and circuit schematics.

Since the receiver has reached its present stage, other applications have become apparent. While it was originally developed to meet a specific problem in television studio production it is obviously useful as a “cue” receiver in both field pickup and studio broadcasting. Its service to the legitimate stage and motion picture production has yet to be realized.

THE “Pocket Ear” was developed to satisfy the need for improved communication in television studio production. Communication between the program producer and the studio director is a necessity to coordinate studio action with the transmitted picture. The program producer from his vantage point in the studio control booth can observe the picture with the aid of a monitor (receiver) while it is being transmitted and when the occasion arises he must contact the studio director on the production set to effect a required change.

An example can best illustrate the problem. An actor in the scene being televised is needed on the next set for the scene which immediately follows to create the desired illusion and give continuity to the story. The timing is very important. The camera “pans” in on the heroine for a close-up. As soon as the actor is out of the vision of the camera he is cued by the studio director to the other set where that

* Decimal Classification: R361 × R583.3.

¹ Originally investigated in 1939 by R. W. Clark and R. R. Davis of the Television Operations Section of the National Broadcasting Company, Inc.

scene is televised 20 seconds later. The exact time of the cue was given to the director by the producer. This is but one case when instantaneous direct communication between director and producer is required.

The easiest and most obvious method of maintaining communication is by means of a telephone headset but the studio director must be able to move freely through a maze of equipment and personnel to direct effectively and cue the actors and technicians. Crowded into the studio are two sets of scenery, three cameras (one of which is mounted on a dolly), a large microphone boom, several floor lights, sound equipment, a large double turntable, plus the operating personnel, the studio technicians and the actors. With the telephone headset and attendant cable, complete freedom of movement was impossible since the telephone cord continually was tangling with equipment and personnel.

The problem was to replace the telephone headset with a radio receiver which would remove the restrictions of the telephone system, fulfill the requirements of compactness and ease of operation, and be sensitive enough to receive from any location in the studio. In addition, comfort was a prime requirement.

To supply the necessary radio signal, a transmitter with less than one quarter watt radiated power was centrally located and suspended from the ceiling of the studio. Operation of the transmitter is subject to FCC regulations and tests indicate that no outside signal is sufficiently strong in the studio to be a source of interference. At the same time, radiation from this transmitter is restricted almost entirely to within the studio.

First efforts to develop a receiver resulted in the "Man from Mars" unit pictured in Figure 1. While not entirely satisfactory it did demonstrate the feasibility of the plan of employing radio. As can be seen, this unit used an ordinary headset supporting a vertical rod antenna, a tuning circuit and a crystal detector. Besides being uncomfortable and clumsy to wear the reception was very poor.

In the next unit, the "Happy Hooligan" model (Figure 2), a tuned coil was used as the receiving antenna. Within this coil were the tuning circuit, a crystal detector and an audio amplifier. Batteries, connected to the amplifier by a long flexible cable, were carried in the wearer's pocket. This was a workable unit and was immediately placed in service. Even though clumsy, lacking in sensitivity and with no provision for volume control, it was such a decided improvement over the telephone system that it was used until a more refined unit was developed.

The receiver (Model 3) which is now being used is shown in Figure



Fig. 1—"Man from Mars" model.

3 and is called the "Pocket Ear". As a result of experience gained on the first two models, many improvements were incorporated in this third model of which the outstanding one was the replacement of the



Fig. 2—"Happy Hooligan" model.

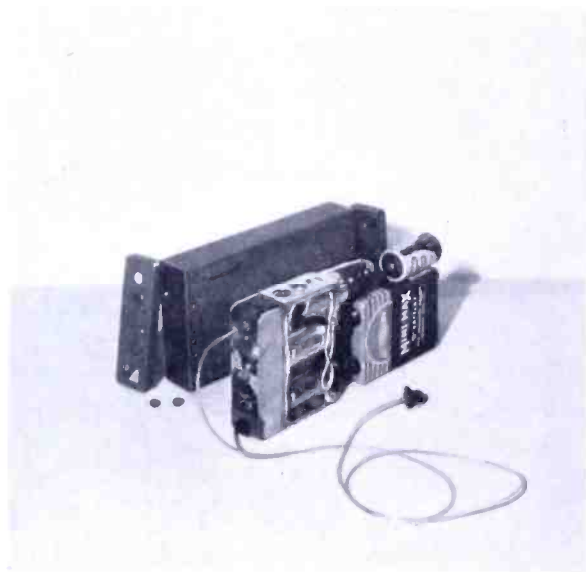


Fig. 3—"Pocket Ear" (model 3).

headset by a tiny rubber ear plug.

These plugs (removeable for washing or replacing) are molded of soft rubber $\frac{1}{4}$ inch in diameter, $\frac{1}{2}$ inch long with a holding flange on the receiver end $\frac{1}{2}$ inch in diameter. Sound is transmitted to the ear



Fig. 4—"Pocket Ear" in use.

from an electro-acoustic transducer in the receiver by a thin-walled transparent vinylite tube 30 inches long. This provides better fidelity than any of the commercially available ear phones and at the same time creates no audible sound except to the ear of the wearer. As this sound tube is used to carry conveniently the antenna (since it is No. 38 wire, it creates no measurable sound attenuation) there exists the paradoxical arrangement of the output of the unit being in physical contact with the input.

The radio receiver, battery supply and the electro-acoustic transducer along with a tuned radio-frequency amplifier are located in the metal housing. This housing is free from protuberances except on top and thus can be easily carried in a pocket. The "off-on" switch, two small tuning holes covered by thin sliding protective plates, and the

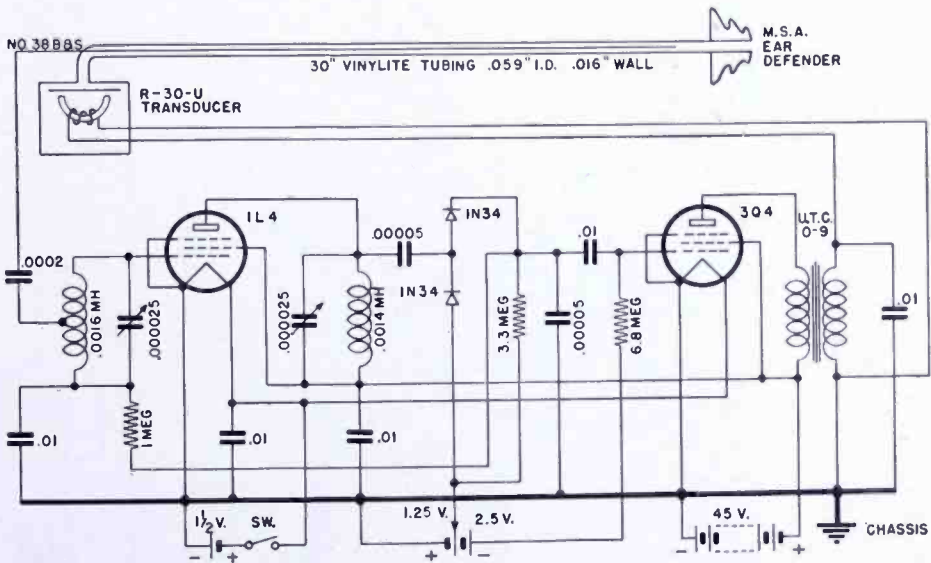


Fig. 5—Schematic of "Pocket Ear" (model 3).

sound antenna tube are on the top. Strap clips are also attached to the case which enable the user to carry it conveniently slung over the shoulder or strapped to the waist (Figure 4).

To obtain sufficient sensitivity and automatic volume control, a tuned radio-frequency amplifier operating into a voltage-doubling detector is employed as indicated in the circuit schematic (Figure 5). Additional pickup sensitivity is obtained by substituting the short wire antenna for the coil antenna used in Model 2. The receiver requires only enough sensitivity for its automatic-volume-control to maintain signals at all locations in the studio. The bias voltage for the audio amplifier is supplied by the "C" battery source consisting of 2 Mallory cells.

The filament power supply (A supply) is provided by a "C"-size flashlight cell with a life expectancy of 10 hours under normal operating conditions. The plate power supply is provided by a 45-volt type-455 Eveready battery with an approximate life of 150 hours. The unbalanced "A" and "B" supplies were designed to cover the contingency of inadvertently leaving the receiver with the switch in the "on" position. In this event, the "A" battery, inexpensive and readily available, becomes exhausted without doing much damage to the relatively expensive "B" battery. The batteries use spring terminal connectors similar to those used in a flashlight. By pressing the side of the case and then slipping off the bottom cover, they can be changed and the receiver placed back in operation in less than a minute.

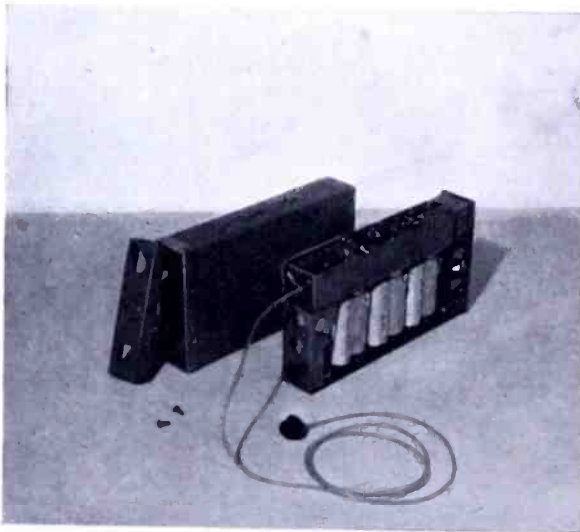


Fig. 6—"Pocket Ear" (model 4).

Measured sensitivity for this unit is 15 millivolts at 90 per cent modulation when the audio output is 3 milliwatts. This was measured by capacitively coupling a signal generator to the antenna of the receiver. In the field test, using a two-watt transmitter, the reliable range of the receiver was 100 yards on one of the NBC relay broadcast frequencies close to 30 megacycles. Out to 200 yards the reception was spotty and beyond that range very little was heard.

The "Pocket Ear" was completely successful as a "cue" receiver in the television studio and numerous other applications have been proposed. Most of these could be satisfactorily handled by Model 3. But to cope with the proposed applications where the sensitivity of Model 3 would be too low for the required results, another receiver was developed (Figure 6) which resulted in a 15 per cent reduction in size



Fig. 8—The four models.

The "Pocket Ear" as a "cue" receiver or a studio instruction link has replaced the telephone headset with its motion restricting cord. The "Pocket Ear" can supply the needed communication as demanded by any studio or field set-up whether it be for television or radio. Since it is used many hours each week both in production and rehearsals the qualities of wearing comfort, reliability and ease of operation are very important. It is felt that both Model 3 and Model 4 will more than answer the present requirements in both television and broadcasting as well as certain proposed applications in the theatre and motion picture industry.

POWER MEASUREMENT OF CLASS B AUDIO AMPLIFIER TUBES*

BY

DAVID P. HEACOCK

Tube Department, RCA Victor Division
Harrison, N. J.

Summary—An accurate method of determining the performance of two triodes, or two triode units of the same tube, operating as a class B push-pull amplifier by a simple measurement of the plate current of a single triode unit is described. This method is particularly adaptable as a production test on electron tubes designed primarily for operation as class B amplifiers. The errors attendant upon the use of conventional measuring technique for class A power output when applied to the non-sinusoidal output of a single triode unit operated class B are discussed.

IT IS advantageous to measure the output power available from a single triode unit operated in a typical class B push-pull amplifier circuit by means of a simplified circuit that simulates push-pull operation. Two tubes could, of course, be measured in some typical push-pull circuit with the signal supplied from a suitable driver and the power delivered to the load measured directly. This method of test, however, is complicated from a production standpoint and, since it tests two triode units at a time, it gives no direct measure of the performance of each individual tube.

A more practical approach is to simplify the push-pull circuit. A first simplification results when the driver stage is replaced by a fixed alternating-current signal in series with a resistor equal to the effective supply resistance of the driver. Further simplification to simulated push-pull operation in a single triode unit can best be developed by a consideration of true push-pull operation.

Push-Pull Operation

Two triode units connected in push-pull and operated class B will give a nearly sinusoidal output when a sine wave is applied to the grids. The total power output of such a system is

$$P_0 = I_{p1}^2 R_L = \frac{I_{p1m}^2}{2} R_L$$

where I_{p1} is the effective value of the fundamental output current,

* Decimal Classification: R245 X R363.222.2.

I_{p1m} is the peak value of the fundamental output current, and R_L is the load resistance (equal to $\frac{1}{4}$ the total plate-to-plate load). The power output delivered by each triode unit is one half of this or

$$P_o \text{ (each unit)} = \frac{I_{p1m}^2 R_L}{4}$$

The objectives, then, are twofold. The first is to provide a suitable load for a single triode unit which simulates the load condition existing in an actual push-pull circuit. The second is to provide a simple method for measuring I_{p1m} in the simulated circuit so that the power output which would be delivered by each triode in an actual push-pull amplifier can be calculated. This is not the same as the fundamental power output of the single unit due to the non-sinusoidal output current form.

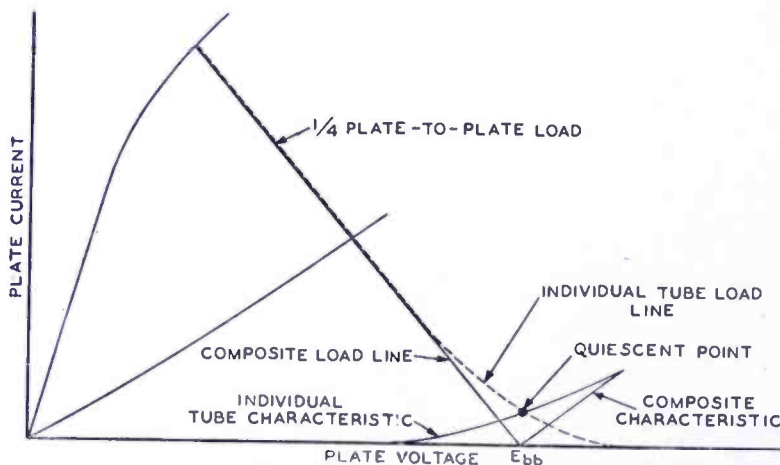


Fig. 1—Characteristic curves of class B push-pull amplifier.

Having defined what is to be measured in terms of push-pull operation, it is desirable to consider the composite characteristics of two triode units operating as a class B push-pull amplifier (Figure 1). The following statements may be made:^{1, 2}

1. Since the test will commonly be made with full signal, the conduction angle is close to 180 degrees.
2. Under these conditions, the composite tube characteristics are the same as the individual tube characteristics except near the quiescent point.

¹ B. J. Thompson, "Graphical Determination of Performance of Push-Pull Audio Amplifiers", *Proc. I.R.E.*, Vol. 21, No. 4, p. 591, April, 1933.

² *RADIOTRON DESIGNERS HANDBOOK*, F. Langford Smith (Chapter 34), Amalgamated Wireless Valve Company, Sydney, Australia (RCA Victor Division, Harrison, N. J.).

3. Similarly, the individual tube load line is the same as the composite or dynamic load line except near the quiescent point.
4. The composite load line is identical to a resistive load line of value equal to $\frac{1}{4}$ the recommended plate-to-plate load with its origin at $E_b = E_{bb}$, $I_b = 0$.

Simulated Push-Pull Operation

From the preceding facts, it is evident that push-pull load conditions may be simulated in a single triode unit by use of a simple series plate resistor of a value equal to $\frac{1}{4}$ of the rated "plate-to-plate" load. This is suitable even with appreciable values of quiescent current and

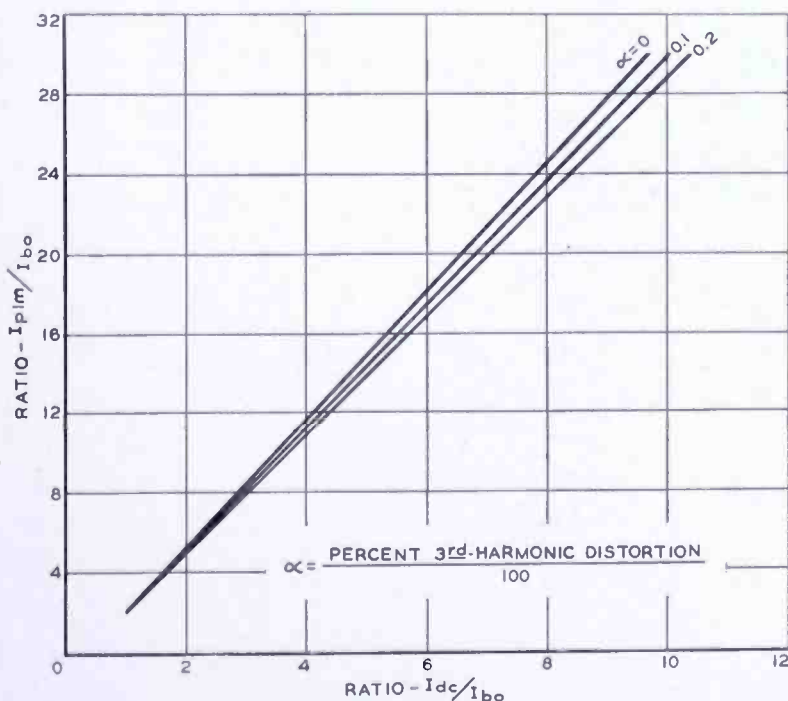


Fig. 2—Generalized current relationship for class B push-pull amplifier.

provides a simple load whose load line remains fixed regardless of changes in average current as the signal is varied. The problem then resolves itself into the measurement of I_{p1m} by some simple means. In an unpublished report, E. W. Herold[†] has developed by Fourier analysis the relation between I_{p1m} and the single-tube full-signal average current, I_{dc} , considering the presence of quiescent current, I_{b0} , and the third-harmonic distortion, α times 100 per cent. Details of the analysis are in the appendix. The results of this analysis are plotted in Figure 2 as I_{p1m}/I_{b0} against I_{dc}/I_{b0} with α as a parameter.

[†] RCA Laboratories Division, Princeton, N. J.

Since these curves are very close to straight lines and since α has relatively little effect upon the results and is usually unknown anyway, a straight line was fitted to the curves with an error not exceeding 3 per cent for all cases between $\alpha = 0$ and $\alpha = 0.1$ and over the range $I_{dc}/I_{bo} = 1.1$ to $I_{dc}/I_{bo} = \infty$. Under usual test conditions the error is probably much less. The equation of this line is

$$\frac{I_{p1m}}{I_{bo}} = \pi \left(\frac{I_{dc}}{I_{bo}} - 0.25 \right)$$

$$I_{p1m} = \pi (I_{dc} - 0.25 I_{bo})$$

This equation then gives the relation between I_{p1m} and the easily measured quantities I_{dc} and I_{bo} . It is necessary to measure with a direct-current meter only the quiescent current, I_{bo} , and the full-signal average current, I_{dc} . The power output then becomes

$$P_0 = \frac{I_{p1m}^2 R_L}{4} = \frac{\pi^2}{4} (I_{dc} - 0.25 I_{bo})^2 R_L$$

Since I_{bo} is small compared to I_{dc} and its coefficient is also small, an average value for I_{bo} may be inserted in the formula and assumed constant. Therefore, for each tube type and a given set of test conditions the power output is a function of I_{dc} only. Production testing is thus possible using a calculated low limit value of I_{dc} . The actual test circuit is shown in Figure 3.

A similar method of analysis deriving I_{p1m} in terms of I_{bo} and the total root-mean-square plate current would permit a similar method of test using a root-mean-square meter in the plate circuit. The second method, however, offers no advantages and has the disadvantage of requiring the use of the root-mean-square meter.

Use of Conventional Class A Measurement Technique

Since the measurement of class A power output usually involves the use of shunt feed for the d-c plate voltage, and since the use of shunt feed is usually implied in a discussion of power output under given conditions, it is worth-while to point out the consequences of calculating the power output of a conventional circuit as shown in Figure 4 under high-signal, Class B conditions by measuring the effective value of either all the alternating-current components or just the fundamental component.

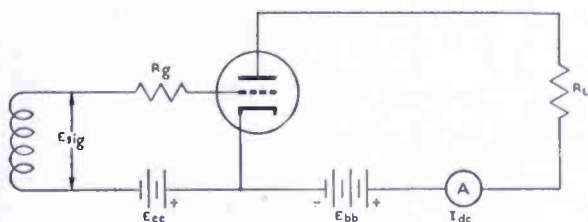


Fig. 3—Circuit diagram of simulated class B push-pull amplifier.

Rectification effects will be considered first.^{2,3} Due to non-linearity of tube characteristics, there is an increase in the value of the average plate current with increasing signal. This increase is, of course, quite appreciable for a tube operating as a Class B amplifier and, where shunt feed is employed, it causes an undesirable shifting of the alter-

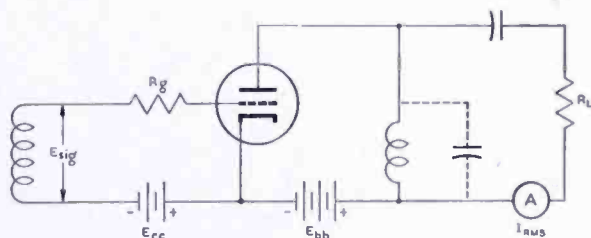


Fig. 4—Circuit diagram of class A power amplifier used for power measurement.

nating-current load line. Although the quiescent point and the load line which might be drawn through it lie close to the load line for push-pull operation, the alternating-current load line moves up as the signal is increased and the average current remains at the intersection of the alternating-current and direct-current load lines (Figure 5). This condition causes an increase in the average and fundamental

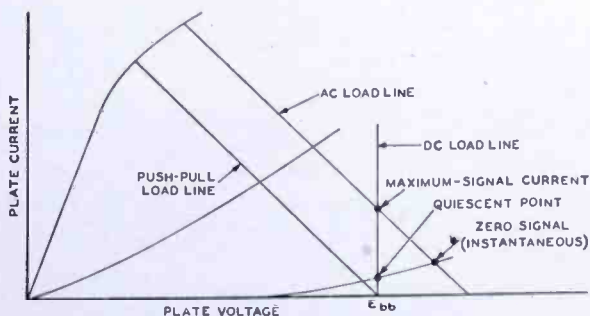


Fig. 5—Triode plate characteristic showing rectification effects.

³ "Graphical Analysis of Output Tube Performance", C. E. Kilgour, *Proc. I.R.E.*, Vol. 19, No. 1, p. 42, January, 1931.

currents over the currents existing in a single triode unit operating in a push-pull circuit. Push-pull operation is no longer being simulated under these conditions and it is difficult to justify the use of shunt feed.

Since the shunt-feed type of test set usually measures the effective alternating-current components from which the power delivered to the load resistor is calculated, it is illuminating to consider how power calculated in this way compares with the power which the tube would deliver in a push-pull circuit under similar operating conditions. For purposes of illustration, the shifting of the load line is not considered and the quiescent current is assumed as zero. The plate current is a half sine wave,

$$I_{av} = \frac{1}{\pi} I_m \quad \text{and} \quad I_{rms} = \frac{1}{2} I_m$$

These are familiar values and may be found in any handbook. I_{rms} is the effective value of a half sine wave including the effective value of I_{av} . A meter in series with the load measures the effective value of the alternating components of the half sine wave which is equal to

$$\sqrt{I_{rms}^2 - I_{av}^2} = I_m \sqrt{\frac{1}{4} - \frac{1}{\pi^2}} = I_m \sqrt{0.1487} = 0.385 I_m$$

In the light of the assumptions which have been made, $I_m = I_{p1m}$ and the power which the triode unit would deliver in push-pull operation is

$$P_0 = 0.25 I_{p1m}^2 R_L$$

The power delivered to the load with shunt feed is

$$P_0 = 0.385^2 I_m^2 R_L = 0.1487 I_{p1m}^2 R_L$$

The power output with shunt feed, therefore, is only about 60 per cent of the push-pull value.

To carry the illustration further, it may be assumed that the choke is tuned to the fundamental frequency and offers no impedance to the second harmonic. Under these conditions, the fundamental current

only flowing in the load is equal to $\frac{I_m}{2\sqrt{2}}$ and the power delivered to

the load is only 50 per cent of the push-pull value.

The actual readings obtained in a test circuit using shunt feed are

somewhat higher because of the increase in fundamental output current due to the shift of the alternating-current load line. A typical example may be found in the appendix, where, by graphical methods, the operation of a 6N7 is analyzed for a push-pull circuit, for the series plate-resistor method, and for the shunt-feed method. Some actual measured data are also presented.

APPENDIX

I. Derivation of relation between I_{p1m} and I_{av}

Consider the output current of a practical tube with a dynamic characteristic as shown in Figure 6. The output consists of a sine wave of current slightly distorted by third harmonic and with part of the lower peak cut off. The output may be expressed as a sine wave $A \sin \omega t$ superimposed on the quiescent current and containing third

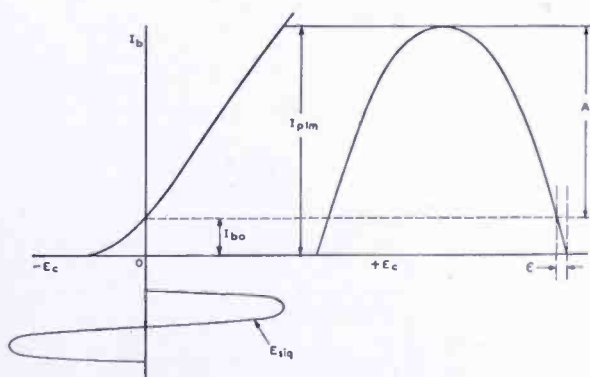


Fig. 6—Dynamic characteristic of a single-tube class B amplifier.

harmonic of α times 100 per cent. Because the lower portion is cut off it is clear that the output current is zero between the angles $\omega t = \pi + \epsilon$ and $\omega t = 2\pi - \epsilon$ where ϵ is given by

$$\sin \epsilon + \alpha \sin 3\epsilon = \frac{I_{bo}}{A} \tag{1}$$

The peak fundamental current for push-pull operation is

$$I_{p1m} = I_{bo} + A \tag{2}$$

so that

$$\sin \epsilon + \alpha \sin 3\epsilon = \frac{I_{bo}}{I_{p1m} - I_{bo}} \tag{3}$$

The solution of (3) is easily obtained graphically. The average current is given by

$$\begin{aligned}
 I_{dc} &= \frac{1}{2\pi} \int_0^{2\pi} i d(\omega t) \\
 &= \frac{1}{\pi} \int_{\pi/2}^{\pi+\epsilon} (I_{bo} + A \sin \omega t + \alpha A \sin 3\omega t) d(\omega t) \\
 &= \frac{1}{\pi} \left[I_{bo} \left(\frac{\pi}{2} + \epsilon \right) + A \cos \epsilon + \frac{A\alpha}{3} \cos 3\epsilon \right] \quad (4)
 \end{aligned}$$

Usually, I_{dc} and I_{bo} are given and I_{p1m} is calculated. The equations (3) and (4) are not suitable for direct calculation and an attempt to solve them for I_{p1m} by elimination of ϵ is very involved. A graphical solution is readily made, however, and Figure 2 gives such a solution for I_{p1m}/I_{bo} using values of third-harmonic distortion up to 20 per cent. Fortunately, the effect of third harmonic is very small in the result. It is, therefore, unnecessary to know the amount of third-harmonic distortion in order to obtain reasonably accurate values for I_{p1m}/I_{bo} .

Inasmuch as the curves appear to be very close to straight lines, it should be possible to arrive at a simple approximate formula for I_{p1m} in terms of I_{dc} . Assuming $\alpha = 0$ and ϵ small in Equation (4) leads directly to

$$I_{dc} = \frac{1}{\pi} \left[I_{bo} \left(\frac{\pi}{2} - 1 \right) + I_{p1m} \right]$$

or

$$I_{p1m} = \pi (I_{dc} - 0.18 I_{bo})$$

Assuming that, on the average, $0 < \alpha < 0.05$ in practical cases, better agreement with Figure 3 is reached by the following equation

$$I_{p1m} = \pi (I_{dc} - 0.25 I_{bo})$$

II. Typical calculations based on graphical analysis of type 6N7 in circuits discussed.

(The following calculations were made using published curves on type 6N7 and making a Fourier analysis of the plate current using 10-degree intervals.)

(a) Two triode units in push-pull, Figure 8 (page 157), under the conditions:

$$E_b = E_{bb} = 300 \text{ volts} \quad R_g = 500 \text{ ohms}$$

$$E_c = -5 \text{ volts} \quad \text{Plate-to-Plate load} = 10,000 \text{ ohms}$$

$$E_{sig} = 35 \text{ volts root-mean-square}$$

The dynamic characteristic of the tube, Figure 7, was plotted from the published plate family. Standard methods of harmonic analysis gave the following results:

$I_{p1m} = 96.5$ milliamperes and the total push-pull power output is $P_0 = \frac{I_{p1m}^2}{2} R_L = 11.6$ watts. The power output of one triode unit = 5.80 watts and the average current per unit is

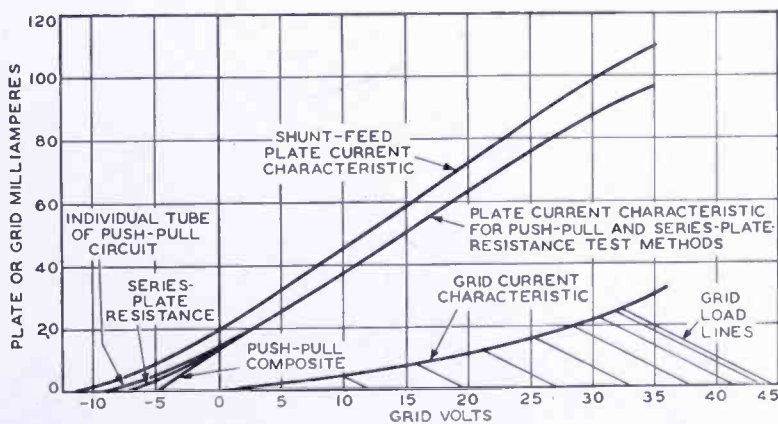


Fig. 7—Dynamic characteristics of 6N7 showing current relationship under three test methods.

$$I_{dc} = 31.4 \text{ milliamperes}$$

From the characteristic curves $I_{b0} = 5.5$ milliamperes

(b) Single triode unit in series plate-resistance circuit, (Figure 3), under the conditions:

$$E_{bb} = 300 \text{ volts} \quad R_g = 500 \text{ ohms}$$

$$E_c = -5 \text{ volts} \quad R_b = 2500 \text{ ohms}$$

$$E_{sig} = 35 \text{ volts root-mean-square}$$

The dynamic characteristics are the same for this case as the individual tube current line in the preceding case except for a barely detectable change in the characteristic near the quiescent point (Figure 7). This slight change does not affect I_{dc} in the preceding example but I_{bo} is now 4.5 milliamperes. Thus

$$I_{dc} = 31.4 \text{ milliamperes}$$

$$I_{bo} = 4.5 \text{ milliamperes}$$

Substituting these values in the formula $P_0 = \frac{\pi^2}{4} (I_{dc} - 0.25 I_{bo})^2 R_L$ gives 5.65 watts.

This value is within 3 per cent of the push-pull calculation.

(c) Single triode unit with shunt feed under the conditions (Figure 4):

$$E_{bb} = 300 \text{ volts}$$

$$R_g = 500 \text{ ohms}$$

$$E_c = -5 \text{ volts}$$

$$R_b = 2500 \text{ ohms}$$

$$E_{sig} = 35 \text{ volts r-m-s}$$

$$\text{Choke Resistance} = 50 \text{ ohms}$$

The dynamic characteristic is in the position shown in Figure 7 when the load line has been corrected. This was assumed to have negligible effect on the grid current. Again, standard methods of harmonic analysis gave the following results:

$$I_{dc} = 35.8 \text{ milliamperes}$$

and the alternating components are:

$$\text{Fundamental} = 38.9 \text{ milliamperes r-m-s}$$

$$\text{2nd harmonic} = 14.2 \text{ milliamperes r-m-s}$$

$$\text{3rd harmonic} = 2.4 \text{ milliamperes r-m-s}$$

$$\text{4th harmonic} = 3.8 \text{ milliamperes r-m-s}$$

The effective value of these alternating-current components is

$$\sqrt{38.9^2 + 14.2^2 + 2.4^2 + 3.8^2} = 41.6 \text{ milliamperes r-m-s}$$

If the measurement is made of this current, the calculated power output becomes

$$P_0 = \overline{41.6^2} \times 2500 \times 10^{-6} = 4.3 \text{ watts}$$

or about 75 per cent of the push-pull value. If the choke is tuned to the fundamental, the current will be somewhat less and, assuming only fundamental present,

$$P_0 = \overline{38.9^2} \times 2500 \times 10^{-6} = 3.8 \text{ watts}$$

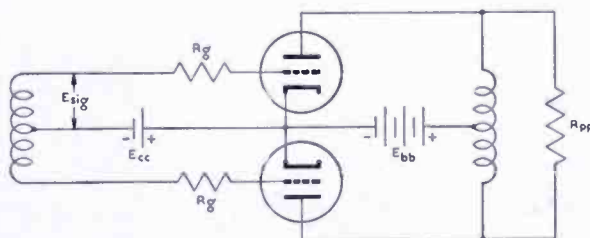


Fig. 8—Circuit diagram of class B push-pull amplifier.

III. Actual measurement taken for 10 tubes

The following measurements were made in support of the preceding calculations under the test conditions used for the calculations on type 6N7-GT.

(a) Measurements using series plate-resistance method of test, Figure 3, gave an average value of $I_{bo} = 4.50$ milliamperes and $I_{dc} = 31.8$ milliamperes. Calculating average P_0 from formula,

$$P_0 = \frac{\pi^2}{4} (I_{dc} - 0.25 I_{bo})^2 R_L = 5.82 \text{ watts.}$$

(b) Measurements using shunt-feed method of test, Figure 4, gave an average value $I_{bo} = 4.89$ milliamperes, $I_{dc} = 34.7$ milliamperes and $I_{rms} = 39.4$ milliamperes. Calculating power output, we obtain

$$P_0 = I_{rms}^2 R_L = 3.9 \text{ watts.}$$

RELATIVE AMPLITUDE OF SIDE FREQUENCIES IN ON-OFF AND FREQUENCY-SHIFT TELEGRAPH KEYING*

BY

GILBERT S. WICKIZER

Research Department, RCA Laboratories Division
Riverhead, L. I., N. Y.

Summary—Measurements and calculations of the side-frequency amplitude in on-off and frequency-shift keying indicate that frequency-shift keying requires less bandwidth than on-off keying, as now generally practiced, for the same keying rate. The advantage of frequency-shift keying lies in the ability to shape the characters by means of low-pass filters. At frequencies more than 1 kilocycle away from the carrier frequency, the reduction in side-frequency amplitude depends upon the degree of shaping and the keying rate. The measured reduction in side-frequency amplitude at 1 kilocycle from the carrier, (mid frequency) when using frequency-shift keying at 40 and 80 dots per second, was found to be roughly 18 decibels. Changing from a single-section to a two-section filter on the frequency-shift keyer input increased this ratio to approximately 30 decibels.

INTRODUCTION

A RADIO telegraph transmitter being keyed at high speed, radiates, in addition to the carrier, side frequencies on both sides of the carrier. The amplitude of the side frequencies, and the frequency spectrum they occupy, depend on the signalling method, the keying rate, the shape of the keyed characters, and the per cent mark. This paper presents a brief comparison of the bandwidth requirements of two widely used signalling methods, namely "on-off" and "frequency-shift" keying. Quantitative measurements of the amplitude of the individual side frequencies are plotted for both keying methods, at various keying rates between 40 and 180 dots per second. Plots of the calculated side-frequency spectrums are also shown, for both keying methods.

EQUIPMENT AND METHOD OF MEASUREMENT

The inspection of side frequencies requires (a) a high degree of selectivity to observe the individual frequencies, (b) a means of measuring the relative frequency of the side frequencies, for purposes of identification, and (c) a means of measuring the relative amplitude of the individual frequencies. The above requirements were met by using

* Decimal Classification: R531.

a direct-reading frequency-measuring receiver of the superheterodyne type, in conjunction with a General Radio wave analyzer.

The "on-off" measurements were made on WQJ, 21,240 kilocycles, located at Rocky Point, a distance of 13.5 miles from the receiver. The received signal was predominantly ground wave, and fading was seldom troublesome. The "frequency-shift" transmissions were obtained from a low-power frequency-shift keying unit set up in the laboratory especially for the side-frequency measurements.

A block diagram of the essential parts of the receiver is shown in Figure 1. The selectivity and mid-band frequency at various points in the receiver are indicated. The interpolation oscillator, labelled " Δf OSC", was directly calibrated to indicate the frequency difference from the mid-band frequency. The smallest division on this oscillator dial was 2 cycles, thus providing a measurement of relative frequency

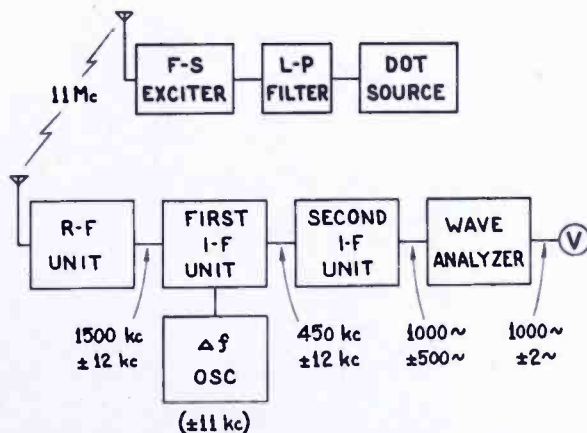


Fig. 1—Block diagram of equipment.

in keeping with the selectivity of the wave analyzer.

In making side-frequency measurements, the receiver was tuned to the transmitter carrier frequency and the radio-frequency stages checked for alignment to insure a uniform response over the spectrum to be measured. The final heterodyne oscillator was operated off the edge of the intermediate-frequency selectivity curve to provide single audio-sideband reception. Under these conditions, with an intermediate-frequency bandwidth of 1 kilocycle, the frequency of the audio output of the receiver was between 500 and 1500 cycles. The wave analyzer was connected to the receiver audio output and adjusted to operate at approximately 1000 cycles. In this way, the receiver bandwidth was restricted to only a few cycles and portions of the radio-frequency spectrum could be closely examined by varying the interpolation oscillator " Δf OSC".

RESULTS AND DISCUSSION

The two methods of radio telegraph signalling to be discussed are special examples of the two fundamental modulation methods, amplitude modulation and frequency modulation. On-off keying is equivalent to 100 per cent amplitude modulation of a carrier with square waves and, in a similar manner, frequency-shift keying* represents frequency modulation of a carrier with square waves. To simplify the calculations and measurements, the keyed characters were in the form of square dots, transmitted at rates normally used on radio circuits.

In on-off keying, the relatively wide frequency band occupied by a high-speed transmitter is due, not so much to the transmission speed in words per minute, but to the high rate at which the individual characters are formed. The steep sides on the characters are an indication that strong harmonics of the keying rate are present in the transmitter output. These harmonics appear as modulation on the transmitter carrier, with the result that a band of frequencies rather than a single frequency is transmitted. For example, in the transmission of square dots, measurable side frequencies may be found out to the vicinity of the 50th harmonic of the dot rate. If these high-order harmonics could be eliminated, bandwidth requirements would be greatly reduced.

Shaping the characters in on-off keying is not easily accomplished in the average transmitter, as the keying is done at low level, and the clipping and limiting in successive Class C amplifier stages effectively squares up any shaping which may have been present on the original characters. Rounded characters might possibly be obtained by modulation methods. For instance, sine-wave dots could be produced by amplitude modulating a telephone transmitter 100 per cent with a pure audio tone.

In frequency-shift keying, rounded characters at the keying stage may be obtained by passing the square characters through a low-pass filter. Since the keying stage converts amplitude changes into frequency changes, the frequency-shifted characters retain their original shape at the transmitter output. In the example of the sine-wave dots, frequency-shift keying becomes a case of frequency modulation with a single tone. The equivalent carrier is midway between the mark and space frequencies, and the deviation is thus one half the frequency shift. The side-frequency spectrum for this ideal condition may be readily calculated by means of Bessel functions, to provide a standard

* The term "frequency-shift keying" as used herein denotes the shifting in frequency of one carrier and not the alternate keying of two independent carriers separated in frequency by the amount of the shift.

of comparison for measured values. Calculation of the side-frequency spectrum for dots other than sine-wave becomes involved due to the many cross products present, and is beyond the scope of this paper.¹ At this point it may be seen that on-off keying produces side frequencies due to the high harmonic content of the individual characters, while frequency-shift keying generates side frequencies in the process of frequency modulation, even with perfect (sine-wave) characters.

Calculated and measured side frequencies for on-off keying at 40 dots per second are found in Figure 2. The calculated spectrum was

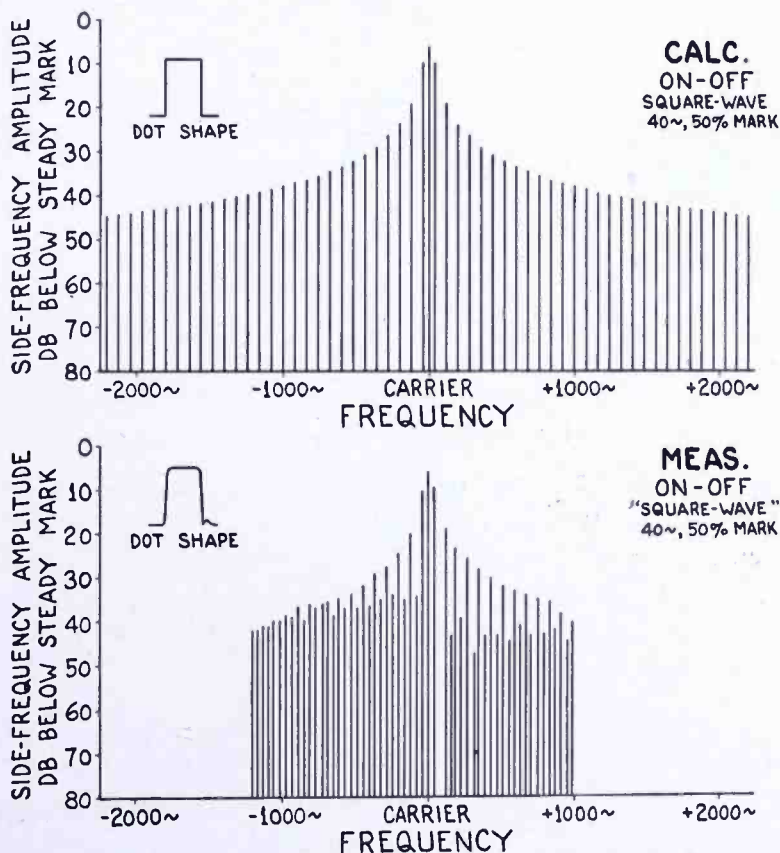


Fig. 2—Comparison of calculated and measured side-frequency spectrums for on-off keying. 40-cycle keying, 50 per cent mark.

obtained from the Fourier analysis of a square wave. At exactly 50 per cent mark, the even harmonics of the dot rate are missing, leaving only the carrier and side frequencies produced by the odd harmonics of the dot rate. The envelope of the measured spectrum is in good agreement with the calculated envelope out to about the twentieth harmonic of the dot rate, but beyond this point, the measured values

¹ Murray G. Crosby, "Carrier and Side-Frequency Relations with Multi-Tone Frequency or Phase Modulation", *RCA REVIEW*, Vol. III, No. 1, pp. 103-106, July, 1938.

decrease more rapidly than calculated, which would be expected when the dot shape is not exactly square. The relatively strong even harmonics of the dot rate indicate that the per cent mark was not exactly 50 per cent. From the amplitude of the even harmonics, it is estimated that the per cent mark was either 49 or 51 per cent. The absence of measurements beyond 1 kilocycle is not significant, as individual side frequencies have been measured out to 3 kilocycles from the carrier, and spot measurements have been made out as far as 8 kilocycles from the carrier, at this dot rate.

Figure 3 permits a comparison of the ideal with the practical, for frequency-shift keying. The frequency shift between mark and space frequencies was 850 cycles, corresponding to a frequency deviation of plus and minus 425 cycles from an unmodulated carrier frequency. Measurements made when using a single-section low-pass filter are plotted in Figure 3, center. The dot rate was well below the filter cut-off, with the result that the low-order harmonics were not attenuated and the dots remained reasonably square. For this reason, the side-frequency spectrum was noticeably wider than that calculated for sine-wave dots. A second section was added to the filter on the keyer input to improve the dot shape. After several adjustments were made, a symmetrically shaped dot was obtained, with a flat top and rounded corners. The results of improving the dot shape are apparent in the bottom graph of Figure 3, where side frequencies more than 600 cycles from the carrier are attenuated rapidly.

A comparison of the frequency spectrum required for the two keying systems is definitely in favor of frequency-shift keying at this point. Although there is an appreciable reduction in bandwidth at 40 decibels below the steady mark level, the reduction in side-frequency amplitude at 1 kilocycle from the carrier is of greater practical interest. Comparison on this basis reveals an improvement of 18 decibels with a single-section filter, and somewhat more with a two-section filter.

Figure 4 contains calculations and measurements of side frequencies present in the transmission of dots by on-off keying, at a rate of 84 dots per second. The top graph was included for comparison with the graph in the center, to show that in on-off keying, the amplitude of the individual side frequencies varies over a wide range as the per cent mark is changed. However, the overall envelope, with the exception of the immediate vicinity of the carrier, remains the same. Measured values, shown in the bottom graph, are in good agreement with calculated values on the low-frequency side of the carrier. From the arrangement of the side frequencies on the high-frequency side of the carrier, it appears that the per cent mark was about 25.5 per cent

when these measurements were made. Thus, the wide variation in individual side-frequency amplitude mentioned above may be used to determine the per cent mark to rather close limits.

The spectrums for frequency-shift dots at 80 per second are shown

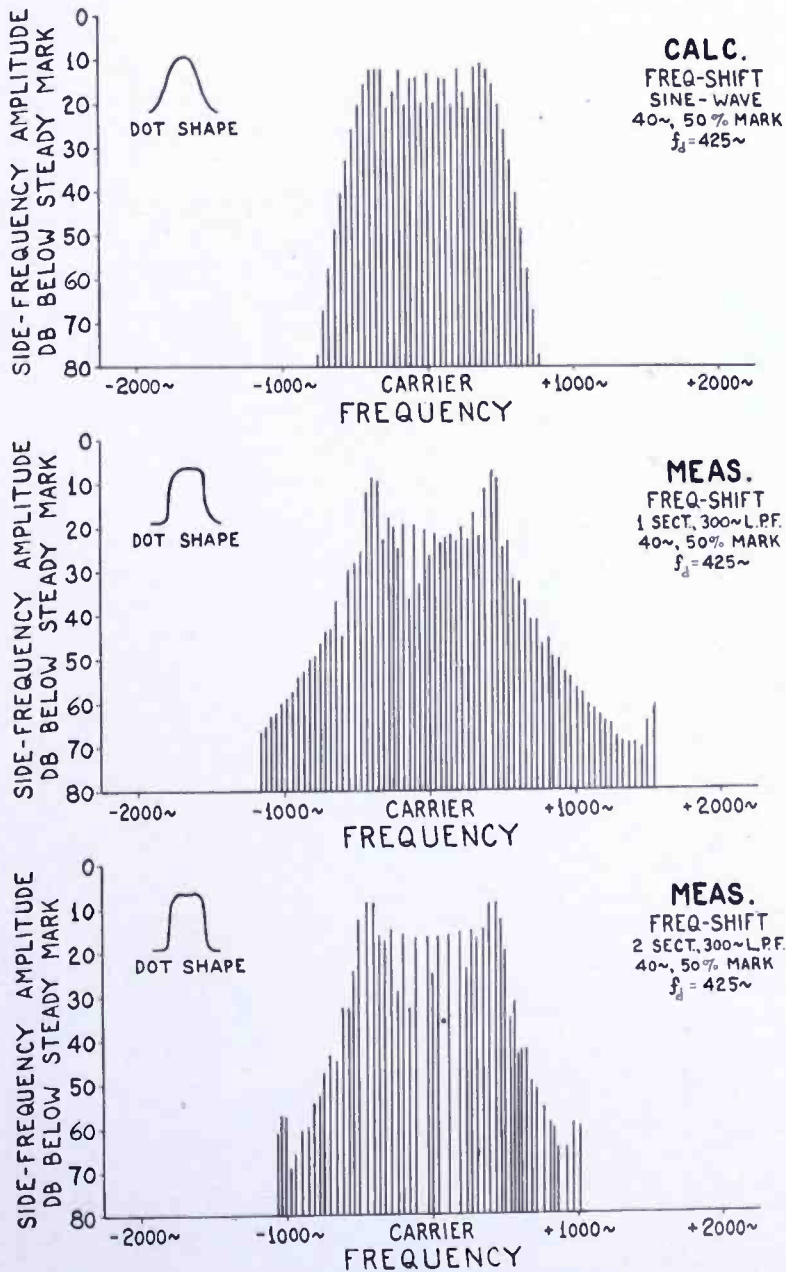


Fig. 3—Comparison of calculated and measured side-frequency spectrums for frequency-shift keying. 40-cycle keying, 50 per cent mark.

in Figure 5. The modulation index is one half its value at 40 dots per second, but the frequency difference between adjacent harmonics of the dot rate is doubled, with the result that the calculated spectrum

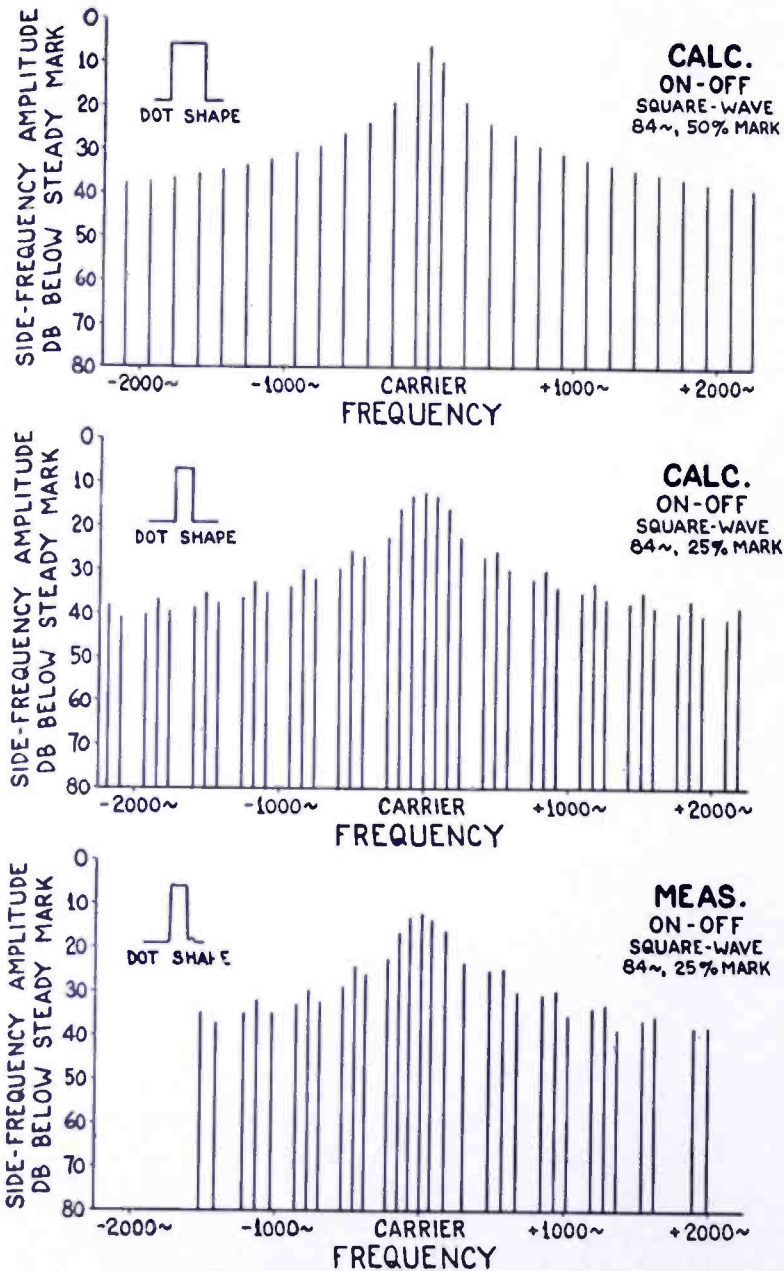


Fig. 4—Comparison of calculated and measured side-frequency spectrums for on-off keying. 84-cycle keying, 25 and 50 per cent mark.

is only slightly wider than with 40-cycle dots. The two lower graphs of Figure 5 indicate the greater effectiveness of the low-pass filter in suppressing harmonics at the 80-cycle dot rate. When using a two-section filter, the measured spectrum agreed very well with the spectrum calculated for sinusoidal modulation. A comparison of on-off and frequency-shift keying at this keying rate is very much in favor of frequency-shift keying. At 40 decibels below the steady mark level, the spectrum occupied by on-off keying is about 5,000 cycles wide,

while frequency-shift keying, with a single-section filter, is only 1600 cycles wide. This latter figure may be reduced somewhat by using a two-section filter, as demonstrated by the measured spectrum at the bottom of Figure 5.

Figure 6 contains one calculated and two measured spectrums for frequency-shift keying at a dot rate of 150 per second. A single section of the 300-cycle low-pass filter was sufficient to suppress harmonics of the dot rate, as indicated by the middle graph of Figure 6. The

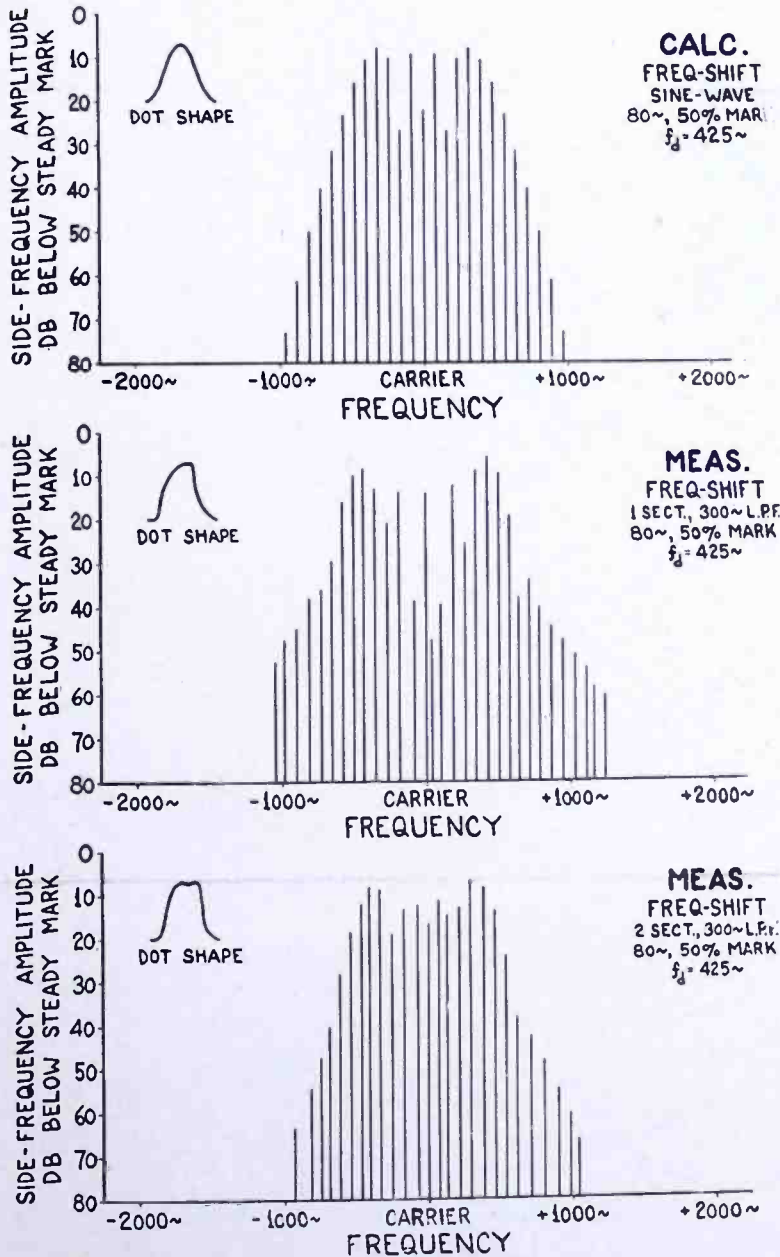


Fig. 5—Comparison of calculated and measured side-frequency spectrums for frequency-shift keying. 80-cycle keying, 50 per cent mark.

result of doubling the filter cut-off frequency is apparent in the bottom graph, where the side-frequency spectrum at 60 decibels below steady mark was found to be nearly 4,000 cycles wide, and a number of cross-product side frequencies were measured.

A comparison of the two methods of keying at 180 dots per second is found in Figure 7. This keying rate is approximately the same as would be required for the transmission of eight-channel multiplex. Although no side-frequency measurements are available for on-off

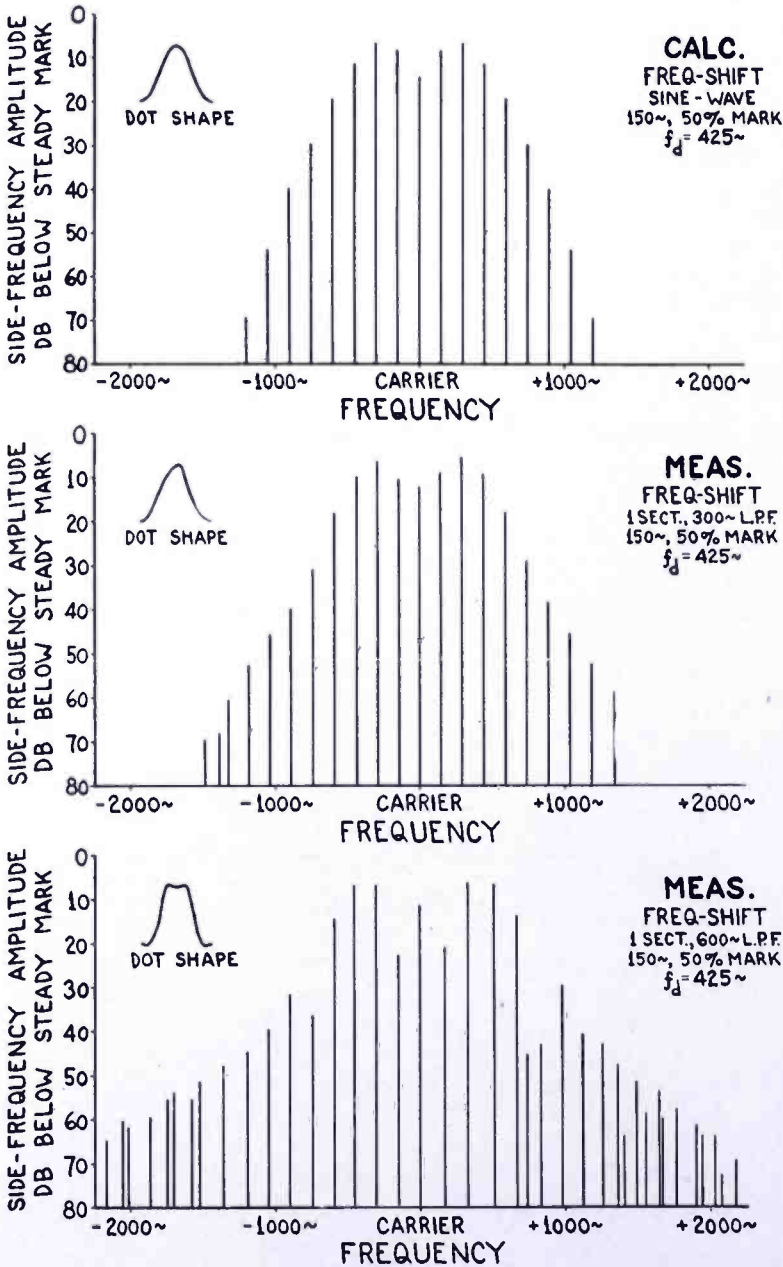


Fig. 6—Comparison of calculated and measured side-frequency spectrums for frequency-shift keying. 150-cycle keying, 50 per cent mark.

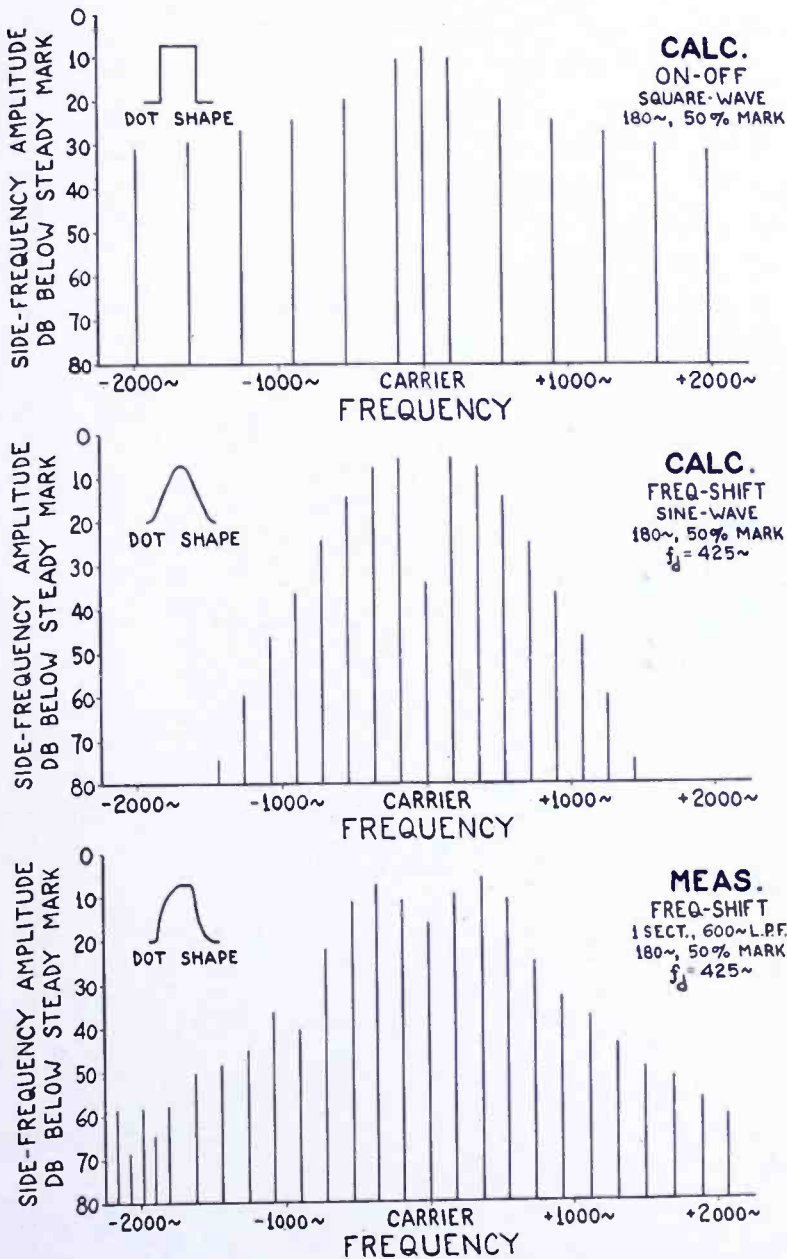


Fig. 7—Comparison of calculated spectrum for on-off keying with calculated and measured spectrums for frequency-shift keying. 180-cycle keying, 50 per cent mark.

keying at this dot rate, the close agreement observed at slower dot rates would lead one to believe that the calculated spectrum is at least a good approximation of actual conditions at this keying rate. It is apparent from the top graph that the eleventh harmonic of the dot rate is roughly 2,000 cycles from the carrier, with an amplitude only 31 decibels below the steady mark level. The calculated spectrum for frequency-shift keying, assuming a sinusoidal dot shape, is shown in

the middle graph of Figure 7. At this higher keying rate, there is a much larger reduction in bandwidth at 40 decibels below steady mark than was observed with 40-cycle keying in Figure 3, and there is not as much improvement in side-frequency amplitude at 1 kilocycle from the carrier. The side-frequency spectrum is now so wide that comparisons at 2,000 cycles from the carrier are of more practical interest. The bottom graph is a plot of measured side frequencies at 180 dots per second, using a single-section, 600-cycle low-pass filter on the keyer input. With this amount of filtering, the improvement over on-off keying in the vicinity of 2,000 cycles from the carrier was 27 to 30 decibels. This figure could quite likely be improved by more careful filtering, as was found to be the case in Figure 5.

CONCLUSIONS

On-off keying, although apparently operating on a single frequency, requires a relatively wide band of frequencies for high-speed telegraph transmission with the types of radio-telegraph transmitters now generally used. The sidebands on both sides of the transmitter carrier are the result of the abrupt manner in which the individual characters are formed. The amplitude of the individual side frequencies may be calculated by evaluating the separate terms of a Fourier Series for a square wave.

Frequency-shift keying, in spite of the fact that it employs two separate frequencies, may be confined to a comparatively narrow bandwidth by shaping the individual characters of the keying. The higher-order harmonics of the keying rate can be suppressed conveniently by means of low-pass filters at the transmitter input.

Comparison of the side-frequency spectrums required for the two keying methods as herein defined, is clearly in favor of frequency-shift keying. The amount of improvement is dependent on the keying rate and the characteristics of the low-pass filter used on the frequency-shift keyer input.

A COAXIAL-LINE DIODE NOISE SOURCE FOR U-H-F*†

BY

HARWICK JOHNSON

Research Department, RCA Laboratories Division
Princeton, N. J.

Summary—The 50-ohm coaxial line construction of the present diode extends the usefulness of temperature-limited diode noise sources in untuned circuits through the ultra-high frequency region. A direct measurement of receiver sensitivity is obtained by doubling the noise power output of the receiver. The noise factor is given by the diode current in milliamperes except for a transit time correction and a minor correction for spurious responses of the receiver. A maximum temperature-limited emission of 100 milliamperes enables the measurement of receiver noise factors up to about 20 decibels. The transit time reduction of noise is 3 decibels at 3000 megacycles which is probably the upper limit of usefulness of the diode. The effect of standing waves introduced by the diode and its termination on the accuracy of measurement is discussed.

INTRODUCTION

THE temperature-limited diode has proved to be a convenient known noise source in receiver measurement work. However, its use at ultra-high frequencies has been limited by the lack of tubes of suitable construction and, even at very-high-frequencies where present tubes must be used in conjunction with tuned circuits, the temperature-limited diode has lost much of its convenience. The purpose of this work has been the development of a diode that may be used as a noise source at ultra-high frequencies and, moreover, that will be adaptable for use with untuned circuits.

This is accomplished in the present tubes following the suggestion of E. W. Herold‡ in 1942 to construct the diode as a section of coaxial line with the electron stream flowing between the inner and outer conductors. By the use of suitable electrode spacing a structure is obtained in which the electron transit time is small and which is readily adapted to wide-range coaxial-line circuits. Developmental tubes known as the R-6212 were designed and constructed by H. A. Finke# during 1944.

* Decimal Classification: R261.2 x R361.114.

† Presented at the 1947 I.R.E. National Convention in New York, N. Y., on March 3, 1947.

‡ RCA Laboratories Division, Princeton, N. J.

Formerly RCA Laboratories Division, Princeton, N. J.

The internal structure of this early type was subsequently revised to produce the type R-6212A described in this paper. This tube is a laboratory development only.

The noise diode as a means of determining the noise factor of a receiver is first considered with some generality. The construction of the R-6212A is then described and the operating characteristics of the tube given. This is followed by consideration of various factors which affect the accuracy of measurement when using the noise diode as a noise source. These factors include the transit time reduction of noise, for which an approximate calculation is given, and sources of reflection due to the diode such as the diode filament capacitance. The diode termination is briefly discussed and the results of experimental measurements are given.

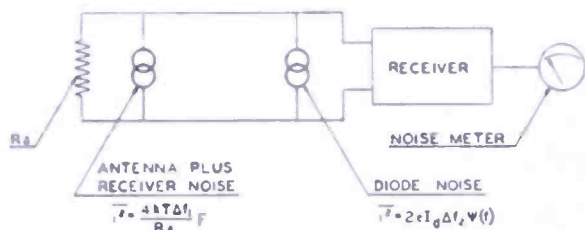


Fig. 1—Equivalent circuit for receiver sensitivity measurements.

THE NOISE DIODE IN RECEIVER NOISE FACTOR MEASUREMENTS

As a noise source, one of the most important applications for the noise diode is the measurement of the noise factor of a receiver. The use of a noise source in such a measurement will be shown to be much simpler than the conventional method using a signal generator.

Since, at present, no standard definition for the noise factor of a receiver has been established, it is well to point out that the noise factor referred to herein is that based on the use of the noise bandwidth of the *useful signal channel alone* as the noise bandwidth of the receiver.¹ This definition, as far as is known, is that most often used in laboratory measurements using signal generators. Thus agreement should be secured in the quotation of noise factors measured by the conventional signal generator procedure and those measured by a diode noise generator as described below.

¹ D. O. North, "Noise Figures of Radio Receivers" (Contributed discussion), *Proc. I.R.E.*, Vol. 33, No. 2, p. 125-126, February, 1945.

For the original definition of noise factor see D. O. North, "The Absolute Sensitivity of Radio Receivers," *RCA REVIEW*, Vol. VI, No. 3, pp. 332-343, January, 1942.

If F is the noise factor of a receiver, the total noise output of a receiver may be considered to result from a noise current generator of value (Figure 1)

$$\overline{i_n^2} = \frac{4kT \Delta f_1}{R_a} F \quad (1)$$

at the receiver input, where k is Boltzmann's constant (1.38×10^{-23} joules per degree Kelvin), T is the temperature in degrees Kelvin, Δf_1 is the noise bandwidth of the useful signal channel alone and R_a is the antenna resistance.

If a temperature-limited diode carrying an average current, I , is placed across the receiver terminals, this diode may also be represented by a current generator of value²

$$\overline{i^2} = 2eI \Delta f_2$$

where e is the electronic charge (1.60×10^{-19} coulombs) and Δf_2 is the overall receiver noise bandwidth including possible responses at image frequency or in the vicinity of frequencies harmonically related to that of the local oscillator.

For use at ultra-high frequencies, with tubes in which the electron transit time is an appreciable part of a period, the diode noise must be modified to account for the transit time reduction of noise.³ In this case

$$\overline{i^2} = 2eI \Delta f_2 \Psi(f) \quad (2)$$

where $\Psi(f)$ is the frequency-dependent correction for the transit time reduction of noise. This correction will be discussed later.

With the system shown in Figure 1, the noise factor of the receiver may be most readily obtained in the following manner. With the diode turned off, the noise output of the receiver is observed on the receiver output meter. This meter may be of any type capable of being calibrated in terms of noise power. The diode is turned on and its filament emission increased until the noise output power of the receiver is double its original reading. The diode current I_d is recorded. This procedure of doubling noise output of the receiver means that the current generator representing the diode is equivalent to that representing the

² W. Schottky, "Spontaneous Current Fluctuations in Various Conductors," *Ann. Physik*, Vol. 57, p. 541, 1918.

³ S. Ballantine, "Schrot-Effect in High Frequency Circuits," *Jour. Frank. Inst.*, Vol. 206, p. 159, August, 1928.

receiver noise, and (1) and (2) may be equated using I_d for the diode current

$$\frac{4kT \Delta f_1}{R_a} F = 2eI_d \Delta f_2 \Psi(f)$$

whence

$$F = \frac{e}{2kT} R_a I_d \frac{\Delta f_2}{\Delta f_1} \Psi(f) \quad (3)$$

Many ultra-high frequency receivers are designed to work from an antenna impedance of 50 ohms as seen through a standard connect-

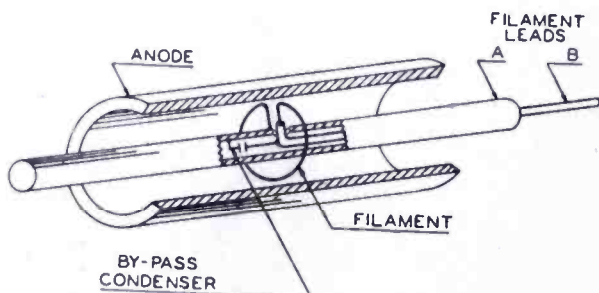


Fig. 2—Outline drawing of coaxial-line noise diode.

ing cable of 50-ohm characteristic impedance; thus, if R_a is 50 ohms and T is taken as 290° Kelvin,

$$F = I_d' \frac{\Delta f_2}{\Delta f_1} \Psi(f) \quad (4)$$

where I_d' is the diode current in milliamperes.

Further, in the many cases where the spurious responses of the receiver are negligible, the bandwidth correction, $\Delta f_2/\Delta f_1$, becomes unity so that

$$F = I_d' \Psi(f) \quad (5)$$

Expressing the noise factor in decibels the expression is simply

$$F_{(db)} = 10 \log_{10} \{ I_d' \Psi(f) \}$$

It is thus seen that the noise factor is readily measured using a temperature-limited diode by the simple procedure described above, requiring only a single observation made without tuning adjustments

or knowledge of the receiver bandwidth. If the bandwidth correction, $\Delta f_2/\Delta f_1$, must be evaluated to obtain an accurate measurement of noise factor, the noise diode loses some of its convenience.

DESCRIPTION OF THE NOISE DIODE

The R-6212A coaxial-line noise diode is shown in outline in Figure 2 and consists of an outer cylinder (anode) and a central conductor whose diametric ratio is that of a coaxial line of 50-ohm characteristic impedance. The tungsten wire filament is supported from the central conductor into which is constructed a mica condenser to by-pass the filament lead brought in coaxially through one end of the center con-

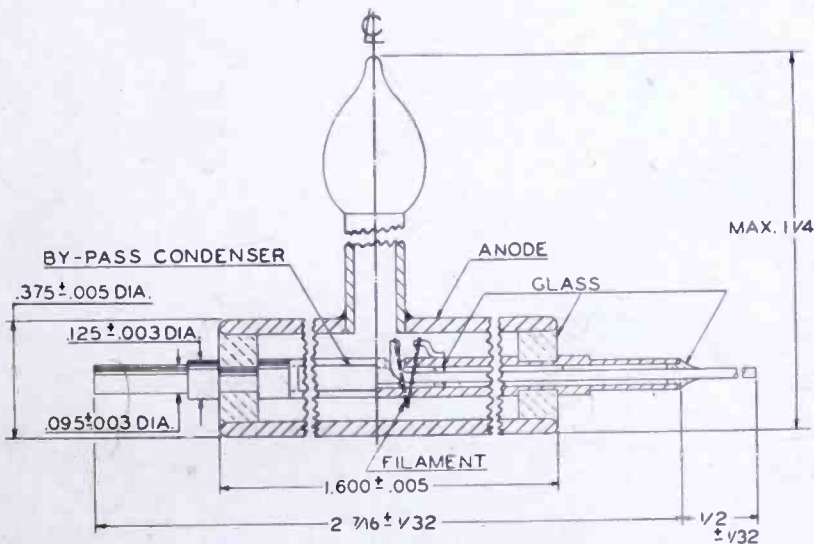


Fig. 3—Details and dimensions of coaxial-line noise diode.

ductor. This construction makes both filament terminals available at one end of the tube. The constructional details of the tube are shown in Figure 3, while the photograph of Figure 4 shows the central conductor subassembly, the anode outer conductor, and the completed tube. The central conductor is undercut at the position of the glass seals to compensate partially for the change in characteristic impedance at this point due to the presence of the glass.

The operating data for the tube are given in Table I. With an anode voltage of 300 volts the filament emission is temperature-limited up to about 100 milliamperes. From Equation (4) it is seen that this emission enables noise factors up to about 20 decibels to be measured at low frequencies by the method described above. Transit time effects reduce this to about 17 decibels near the upper end of the ultra-high frequency band.

Table I

Anode Voltage	300 Volts
Anode Current	100 milliamperes (maximum)
Filament Voltage	3.0-3.5 volts (approximately)
Filament Current	2.5 amperes (approximately)

Static characteristics of three sample tubes are shown in Figure 5. Differences result from a variation of the geometry of the .005-inch

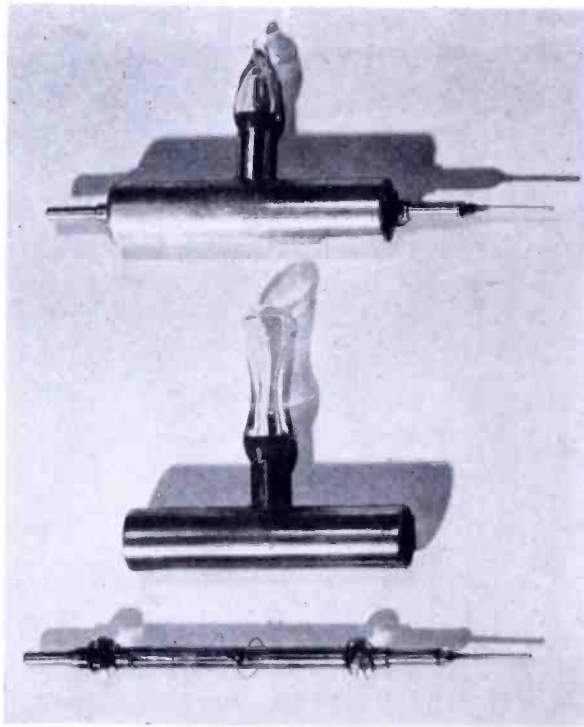


Fig. 4—Central conductor subassembly, anode outer conductor and the completed tube.

tungsten filament with respect to the anode; however, all tubes are temperature-limited at the operating voltage of 300 volts. It is necessary to provide means of cooling the anode when the anode dissipation exceeds 18 watts. This is most readily accomplished by thermal conduction to the adjoining radio-frequency plumbing.

Figure 6 shows the calculated⁴ minimum life expectancy of the tungsten filament, by computation of the time for 10 per cent evaporation (by weight) of the filament.

⁴ Calculations by H. A. Finke based on data published by Howard A. Jones and Irving Langmuir "The Characteristics of Tungsten Filaments as Functions of Temperature—Part II" *G.E. Review*, Vol. 30, No. 7, pp. 354-361, July, 1927.

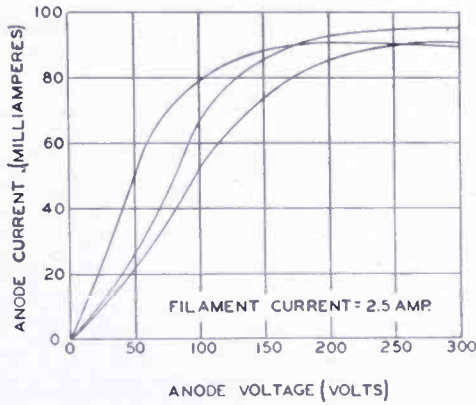


Fig. 5—Typical static characteristics of coaxial-line noise diode.

TRANSIT TIME CORRECTION

The Schottky equation for the shot noise in a temperature-limited diode

$$\overline{di^2} = 2eIdf$$

is based on the assumption that the current induced by the passage of one electron through the diode is (in the limit of negligible transit time) an impulse function whose Fourier transform shows the energy distribution to be uniform throughout the frequency spectrum. However, as the transit time of an electron approaches an appreciable part of the period of the frequency components of interest, the current pulse due to the passage of one electron can no longer be idealized as an impulse function and the induced current pulse must be analyzed in

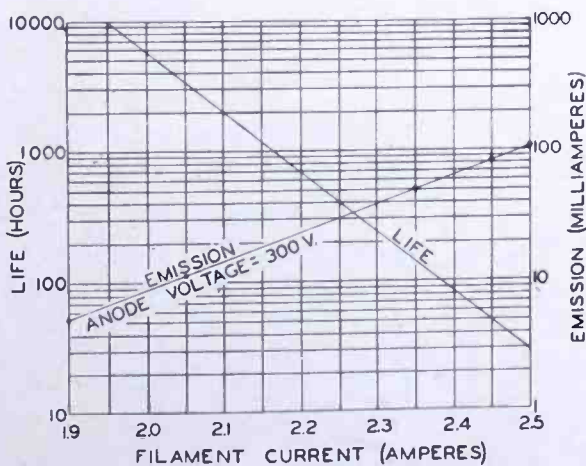


Fig. 6—Minimum life expectancy and measured emission of noise diode.

order to determine the distribution. It is evident that under such conditions the high frequency components will be of reduced amplitude. An analysis for the parallel-plane diode has been given in the literature.³

While the R-6212A coaxial-line noise diode resembles a cylindrical diode there are important differences bearing on the transit time reduction of noise. The tube geometry essential for this discussion is shown in Figure 7. In this construction it is obvious that those electrons leaving the innermost part of the filament experience a different field and hence have a different transit time than those leaving the outermost portion of the filament wire. The transit time correction must, therefore, be an integrated effect accounting for the difference

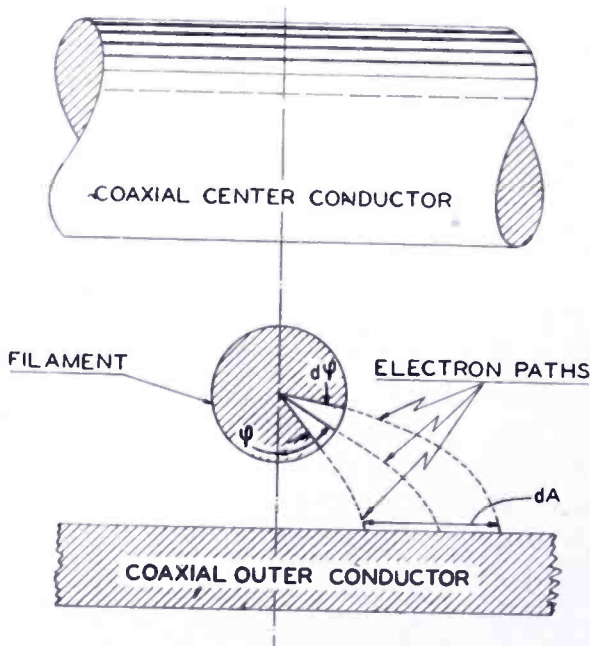


Fig. 7—Geometry of noise diode on an axial plane through one half of diode.

in the electron paths (the shape of the induced current pulse) and the electron transit times (duration of the induced current pulse).

A rigorous computation of the transit time correction would involve the calculation of the shape of the current pulse for each electron path, an adjustment to the proper time scale as determined by the transit time for each path and a summation to find the integrated effect. This is a difficult procedure for the geometry involved; the correction term to be calculated here will be the result of simplifying assumptions in order to obtain at least the approximate correction.

Consider the elementary diode indicated in Figure 7 composed of an emitting surface covering an angle $d\phi$ of the filament wire and the

corresponding active anode surface dA as determined by the connecting electron paths. Let the current pulse induced by the passage of an electron through this elementary diode be

$$i(\phi, t) = e h(\phi, t)$$

where e is the electronic charge and ϕ may be considered a parameter identifying the elementary diode. The shot noise due to this elementary diode is then

$$\overline{di^2} = 2eI_\phi |H^2(\phi, \omega)| df$$

where $H^2(\phi, \omega)$ is the Fourier transform of $h(\phi, t)$ and I_ϕ is the average current through the elementary diode.

The filament wire is assumed to emit uniformly so that

$$I_\phi = \frac{I}{2\pi} d\phi$$

and the total shot noise in a frequency band df being upon integration over the entire emitting surface

$$\overline{di^2} = 2eI df \frac{1}{\pi} \int_0^\pi |H^2(\phi, \omega)| d\phi$$

Now $H^2(\phi, \omega)$ is a slowly varying function over the bandwidth of a receiver so that an integration over df gives

$$\overline{i^2} = 2eI \Delta f \frac{1}{\pi} \int_0^\pi |H^2(\phi, \omega)| d\phi$$

For the purpose of this approximate calculation $H^2(\phi, \omega)$ will be approximated by the form for the parallel plane diode given by Ballantine³ in the form $H^2(\omega\tau)$ where τ is the transit time and in this case is a function of ϕ . Writing θ (the transit angle) for $\omega\tau$, Ballantine gives

$$|H^2(\theta)| = \frac{4}{\theta^4} \{2(1 - \cos \theta) + \theta(\theta - 2 \sin \theta)\} \quad \text{whence}$$

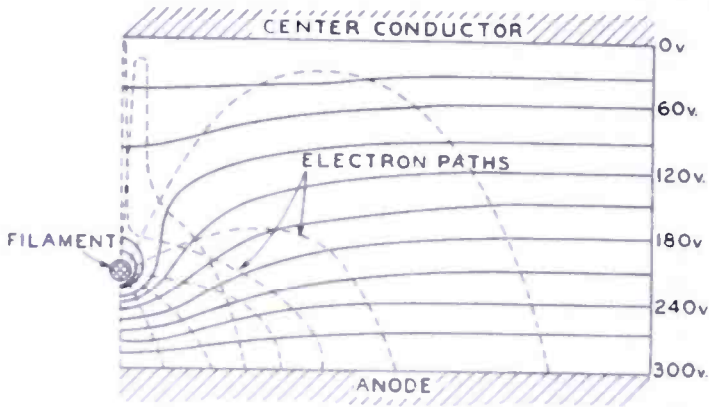


Fig. 8—Approximate field plot and electron paths.

$$\bar{i}^2 = 2el \Delta f \frac{1}{\pi} \int_0^\pi \frac{4}{\theta^4} \{2(1 - \cos \theta) + \theta(\theta - 2 \sin \theta)\} d\phi$$

where θ is a function of ϕ and the frequency.

The integral term is evidently the transit time correction $\Psi(f)$ of equation (2), that is

$$\Psi(f) = \frac{1}{\pi} \int_0^\pi \frac{4}{\theta^4} \{2(1 - \cos \theta) + \theta(\theta - 2 \sin \theta)\} d\phi \quad (6)$$

where $\theta = 2\pi f \tau$ and τ is a function of ϕ .

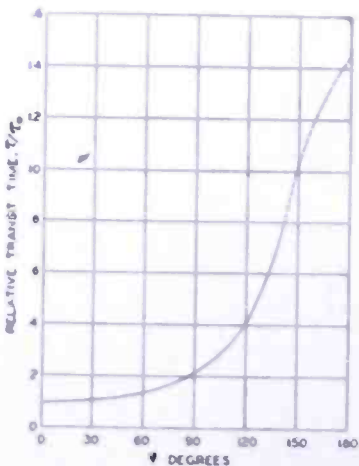


Fig. 9—Variation of transit time with ϕ .

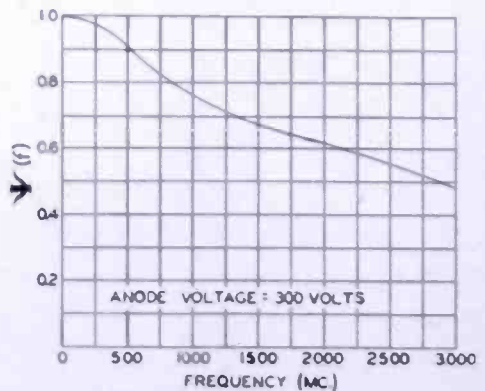


Fig. 10—Calculated approximate transit time reduction of noise in noise diode.

The approximate calculation of $\Psi(f)$ was then made in the following manner. An approximate field plot of the geometry of Figure 7 was obtained in an electrolytic tank with parallel electrodes. From this field plot, together with data from rubber membrane studies, the electron paths were laid out as shown in Figure 8. The transit times for the various paths could then be computed numerically, thus supplying an explicit relation between the transit time (or transit angle for a given frequency) and ϕ as shown in Figure 9. The numerical integration of (6) to determine Ψ could then be performed for a particular frequency.

The resulting transit time correction factor $\Psi(f)$ as a function of frequency is shown in Figure 10. It is seen that the diode noise output drops off to about $\frac{1}{2}$ (3 decibels) at 3000 megacycles.

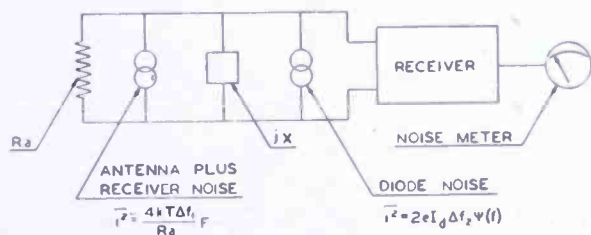


Fig. 11—Equivalent circuit including diode filament capacitance for receiver sensitivity measurements.

EFFECT OF DIODE CAPACITANCE

In the equivalent circuit of Figure 1 it is implied that the diode may be introduced into the antenna circuit without affecting the circuit constants. This is not entirely valid for the R-6212A at ultra-high frequencies because of the impedance discontinuities introduced by the diode. It is of interest to consider the circuit of Figure 11 in which a reactance jX has been added, where this may be considered to be the capacitance added across the line by the diode filament.

In Figure 11, F' is the noise factor of the receiver with an antenna impedance of R_a and jX in parallel. It is evident that a measurement procedure such as that described above will result in the measurement of F' which, however, may differ from F of Figure 1 which is the desired noise factor.

If the receiver is considered to have been adjusted previously for minimum noise factor with respect to changes in the operating parameters, then F' is not sensibly different from F for small changes in the antenna impedance caused by the addition of jX . The extent to which the circuit of Figure 11 may be used to determine the noise

factor of the circuit of Figure 1 depends, under these conditions, on the broadness of the minimum noise factor adjustment with respect to changes in X . This is a characteristic of the receiver and no general statement may be made concerning the limits of its validity.

Lacking specific knowledge of the receiver characteristics it is of interest, in order to gain an insight into the magnitude of the effect of the diode filament capacitance, to consider the variation of the noise power input (i.e. antenna circuit noise or diode noise) into a receiver as the reactance X is varied. It will be assumed that the input impedance of the receiver is matched to a transmission line whose characteristic impedance Z_0 equals R_a . This is very close to the condition of minimum noise factor for ultra-high frequency receivers.

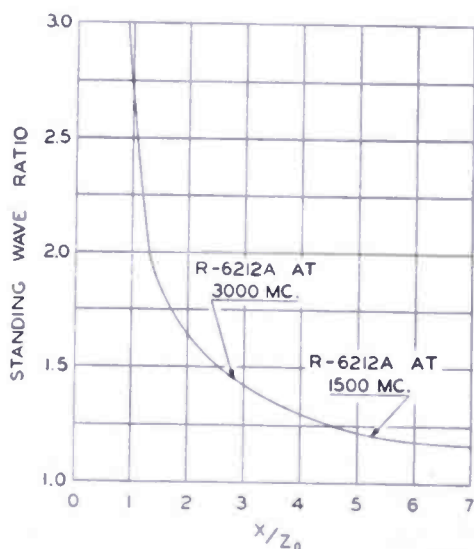


Fig. 12 — Variation of standing wave ratio with filament capacitance.

Since ultra-high-frequency impedance measurements are generally made by means of standing wave measurements on a transmission line, it is desirable to discuss the effect of the diode filament capacitance in terms of the standing wave ratio it introduces in a transmission line which is otherwise terminated in its characteristic impedance. This standing wave ratio, η , is given in Figure 12 as a function of X/Z_0 . The two points indicated for $\eta = 1.2$ and $\eta = 1.4$ indicate the calculated effect of the R-6212A filament capacitance at 1500 and 3000 megacycles respectively.

The variation of the noise power input as a function of the standing wave ratio is shown in Figure 13. It is seen that the change in the noise power input is not large for standing wave ratios less than

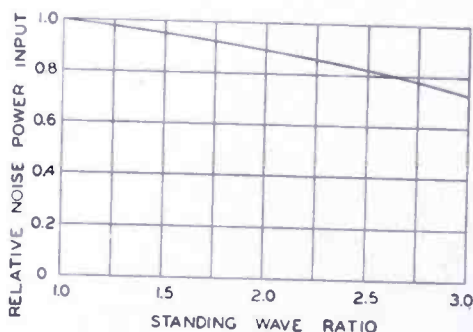


Fig. 13 — Variation of receiver noise power input with standing wave ratio due to filament capacitance.

1.5. In view of the small changes in noise power input (less than 5 per cent) caused by these values of the standing wave ratio, it appears reasonable to expect the presence of the filament capacitance alone would not seriously limit the operation of the tube up to nearly 3000 megacycles. Thus, in an experimental system, if the filament capacitance is so small that the noise input due to the diode is not greatly in error (Figure 13) and, if the noise output of a receiver when connected to the antenna impedance of R_a and jX in parallel differs only a few per cent from that when connected to an antenna impedance R_a , the error in the measured noise factor should be negligible.

The above discussion has been concerned with the effect of the diode filament capacitance alone. In an actual circuit, other sources of reflection are present, for example—the glass beads of the tube, the cable connectors or an improper termination for the diode. A general

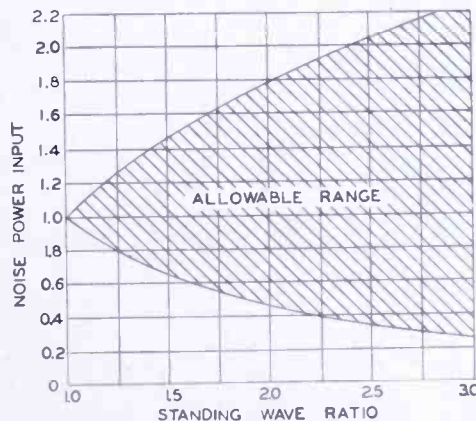


Fig. 14—Ratio of receiver noise power input to that for unity standing wave ratio.

calculation of their effect is not practicable since these sources are disposed along the transmission line and, as mentioned above, one has no knowledge (except in a limited region near the minimum noise factor) of the variation of receiver noise due to these reflections. An insight into the uncertainties of attempting to predict the behavior of a system possessing these distributed sources of reflection may be gained by consideration of the following simple calculation. Let all the sources of reflection lie on the terminated side of the diode filament and assume that the receiver input impedance is that of the characteristic impedance of the connecting transmission line. Then the variation of the noise power input to the receiver from the diode will be in the shaded region of Figure 14 depending on the magnitude and phase of the reflection coefficient associated with the standing wave ratio. It is therefore evident that any usable system must be made as reflectionless as possible.

WIDE BAND TERMINATIONS

One of the principal objectives for the construction of the R-6212A diode in the form of a coaxial line is to make possible its use in wide range (untuned) ultra-high frequency circuits. The circuit techniques to achieve a wide-range circuit equivalent to that of Figure 1, or Figure 11, are more difficult than appears at first sight. This complication arises from the necessity of providing heating power for the diode filament. Although a minimum of work has been done on this aspect of the problem, the development of a suitable termination is essential to the exploitation of the full possibilities of the tube.

Methods of introducing the filament leads through the simpler forms of radio-frequency chokes are generally subject to the criticism of narrow band operation. Possibilities of introducing the filament current through the receiver end of the diode are rejected as undesirable in a generally useful device.

Probably the simplest general method of providing a wide band termination is that of a long "lossy" line. This suggests that the long "lossy" line be constructed of two concentric coaxial pairs as shown in Figure 15 which shows a typical circuit with the R-6212A diode for the noise factor measurement of an ultra-high frequency receiver. In Figure 15, coaxial pair "B" is used for the filament connections and pair "A" having a characteristic impedance of 50 ohms is used for the diode termination. The termination loss may be introduced in the dielectric of pair "A", the outer conductor of pair "A", the inner conductor of pair "A" or a combination of these. If the loss is introduced in the inner conductor of pair "A", this conductor should be a high conductivity tube clad with a high resistivity material. This would provide a low resistance path for the filament current but still introduce loss in pair "A".

Long "lossy" lines are relatively bulky items to handle. To avoid this inconvenience it should be possible to attain relatively wide band operation with a termination in which a high resistivity material is introduced into the interconductor space of pair "A" if the material is introduced in the proper manner. This would make possible a less bulky termination.

Alternatively, the "lossy" line may be made in the form of a two-wire shielded pair; the two inner conductors would be operated in parallel for radio frequencies and serve as the filament connections. The losses are introduced by one of the methods described above. This type of termination, with the loss introduced in the dielectric of the two-wire shielded pair, was used for the experimental checks on the tube performance to be described later. The reasons dictating the use

of this termination were simply those of available materials and facilities. Since the available two-wire line had a 34-ohm characteristic impedance, a tapered section was necessary to transform this impedance to the 50 ohms required for the diode termination. A variant of this type of termination is that of a parallel connection of two coaxial pairs.

EXPERIMENTAL MEASUREMENTS

The noise factor of a receiver was measured both by the conventional signal generator method and by the noise diode using the termination described above. A comparison of the results of several measurements for different receiver adjustments is given in Table II.

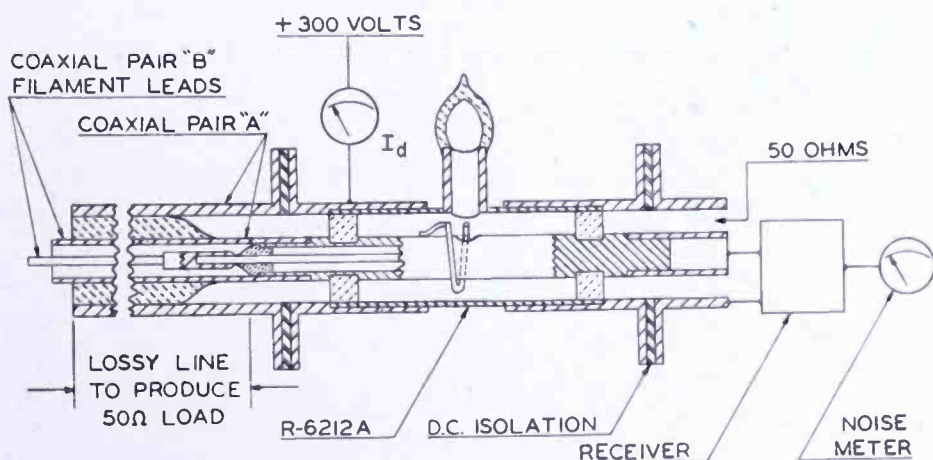


Fig. 15—A typical circuit for measurement of receiver sensitivity with the noise diode.

Table II

Noise Factor Measurement Comparison

(A) Frequency 750 Megacycles

$$\Psi(f) = 0.83$$

$$\Delta f_2 / \Delta f_1 = 1.1$$

$$F = 1.1 \times 0.83 I_d'$$

Signal Generator		Diode		Difference
F	F(db)	F	F(db)	$\Delta F(db)$
12.2	10.9	13.6	11.3	+ 0.4
12.9	11.1	13.6	11.3	+ 0.2
10.2	10.1	10.4	10.2	+ 0.1
38.5	15.9	42.7	16.3	+ 0.4

(B) *Frequency 1500 megacycles*

$$\Psi(f) = 0.67$$

Due to an oversight $\Delta f_2/\Delta f_1$ was not evaluated. It is assumed to be the same as in A.

$$F = 1.1 \times 0.67 I_d'$$

Signal Generator		Diode		Difference
F	$F(db)$	F	$F(db)$	$\Delta F(db)$
40	16.0	42.9	16.3	+ 0.3
45	16.5	44.0	16.4	- 0.1

The termination previously described and used for the above measurements had a standing wave ratio of 1.1 and 1.25 at 750 and 1500 megacycles, respectively, including the cable connectors. With the R-6212A diode inserted, the standing wave ratio was 1.4 and 1.15 at 750 and 1500 megacycles, respectively. At 750 megacycles it was determined that the presence of the filament was the greatest single contributing factor in affecting the standing wave ratio. Since this was the case, the system was expected to satisfy the conditions previously set forth for a usable system, permitting experimental checks to better than 1 decibel. As indicated in Table II such was the case.

* * * *

It is well to point out that general precautionary measures are necessary when making receiver noise measurements by any method. Noise due to hum and interference signals may be attributed to thermal and tube noise in overall receiver output noise measurements unless required steps are observed. It is often necessary to shut down or isolate certain circuits to gain a true evaluation of the effect of thermal and tube noise effects in receiver output noise.

CONCLUSIONS

The convenience of a temperature-limited diode as a noise source in receiver measurement work has been demonstrated, in particular for the determination of the noise factor of a receiver. The development of the R-6212A coaxial-line noise diode has made possible the application of these procedures at ultra-high frequencies. This is due principally to the coaxial form of construction permitting it to be incorporated readily into coaxial-line circuits.

While the R-6212A diode, when used as a standard noise source, must be corrected for transit time effects, experimental measurements of receiver noise factors have shown that the use of the approximate correction calculated above results in agreement on the order of the

experimental accuracy (better than 0.5 decibels) with measurements up to 1500 megacycles using a conventional signal generator. Increased accuracy may be obtained with an experimental calibration.

The usable high-frequency limit of the tube is determined by the reflections arising from imperfections in the tube. Insufficient circuit work was undertaken to establish definitely this upper limit. While the measurement of noise factor has been particularly stressed in this report, the tube may also be used in other applications requiring an ultra-high frequency noise source.

It must be emphasized that the R-6212A coaxial-line noise diode was developed purely as a laboratory and not as a commercial product.

ACKNOWLEDGMENT

Acknowledgment is made of the valuable advice and suggestions so generously contributed by Mr. E. W. Herold during the course of this work.

TECHNICAL EDUCATIONAL REQUIREMENTS OF THE MODERN RADIO INDUSTRY*

BY

PAUL L. GERHART

Chief Instructor, RCA Institutes, Inc., New York, N. Y.

Summary—A primary aim of technical schools is to provide training toward specific existing job objectives. In the field of radio these objectives may be divided into two major classifications according to level.

Within the vocational level, employment is available in the servicing and repair of broadcast, all-wave, communication, frequency-modulation and television receivers. Transmitter operation provides openings in marine, airline, broadcast and special services. Students who have had complete training in receiver and transmitter servicing and operation can be employed as technicians; a wide range of positions is available, including production work, testing and quality check, installation jobs requiring technical skill and maintenance of manufacturing and testing equipment.

Within the higher technological level, courses of training may be given which are of college caliber in the specialized technical phases, even though the absence of prescribed cultural subjects from the curriculum sets the technical school apart from the degree-granting institutions. Such technological training opens the way into more useful employment in the fields mentioned above with the expectation that advancement into more responsible assignments will follow a reasonable period of employment in the less critical tasks available to the beginner in industry. It is possible for the graduate from such a course to become competent in design and research. It is reasonable for him to look forward to further training in institutions of higher learning as his usefulness to his employer increases. Technology courses given in technical schools must pattern their training to conform with the advances made in industry, keeping in sight the available employment and the probable direction of expansion and improvement of the services rendered by the radio industry.

UP TO THE past decade a course in radio servicing was intended to give the student a working knowledge of operation and maintenance of broadcast and short wave receivers. Such courses covered the circuit refinements employed in receivers of that day. The all-electric receiver had such features as single tuning control, automatic volume control or delayed automatic volume control, wide response or, in some cases, variable band width intermediate-frequency amplifiers and band-changing switches. Training courses covered these points by teaching the operation and adjustment of such circuits, giving practice in tracking and alignment of the receiver circuits as well as in checking signal sensitivity and power output. Available

* Decimal Classification: R070.

commercial testing and servicing equipment permitted the trainees to service the receivers using standardized procedure. Receivers having all of the existing refinements were in the numerical minority and the typical servicing task was handled with facility upon completion of such a course of training.

The appearance of commercial frequency modulation and television broadcasting has introduced servicing techniques of more advanced nature. Receivers for these services operate upon principles which in many respects were not formerly employed. Tracking and alignment procedure must be taught in greater detail to prepare students for the more critical adjustments necessary. Sweep frequency oscillators are now used more extensively than before, and their functions and use must be included in a course of training. Square-wave testing devices are now commercially used in servicing procedure. The latter two pieces of equipment provide means for checking rapidly the characteristics of frequency-modulation receivers and especially of television receivers where the wide frequency response is a prerequisite to good receiver performance. The additional theory required for this work should be based upon the performance at higher frequencies of the circuits found in such equipment, with emphasis upon the features which have been introduced as a result of the functional changes in the receiver parts. The associated laboratory practice should provide an opportunity for learning the use of such equipment. The interpretation of the results obtained in the laboratory projects must be correlated with the theory.

The modern course in radio servicing and repair should recognize the value of early opportunity to acquire manipulative skill and familiarity with the tools and equipment of the trade. For this reason beginners in such a course profit by practice work in assembly and wiring while acquiring their basic theory. Laboratory work should continue throughout the course, advancing in level with the theory lessons. As a result of the need for the servicing of the new types of receivers, today's course of training must necessarily be more extensive in total training time than were the earlier courses with the lesser objectives.

Students training for employment as radio operators are now required to pass more comprehensive examinations than formerly in order to become licensed operators. In keeping with this requirement it is necessary that a course of study cover receivers more thoroughly and include more extensive study and practice on transmitters. The highly-refined communication receiver of today with its wide range of useful frequencies and the available crystal-controlled tuned circuits

calls for skill and understanding in its maintenance. Transmitters have become more compact and some of the service frequencies are now much higher. Whether the graduate is employed in marine, airline or broadcast stations he finds today's equipment of more complex design than formerly. The scope of training on basic transmitter principles must now be augmented to include more thorough understanding of power amplifiers at radio frequencies, of neutralization and of the special problems introduced by operating in the higher frequency bands, both with continuous wave and modulated wave transmission. Oscillator theory and performance must be more intensively treated. More time should be allotted to breadboard practice with oscillators and other fundamental circuits which are component parts of transmitters. As in the case of receiver repair courses, students should find early opportunity in the course to acquire manipulative skills. Additional work on the directivity of antenna structures for special service in the higher frequency range becomes a useful part of the training, especially in connection with such equipment as is used by the airlines for guide beams and landing beams. Marine equipment for safety at sea makes use of the circuit refinements of receivers in the design of the automatic alarm receiver, and in direction finders. The maintenance of radio equipment on shipboard today requires a complete course of training as a technician.



In courses which lead toward higher objectives in technology the student is preparing to fill a position in research and development or in production work. His success and prospect for more responsible work are determined by the thoroughness and completeness with which he is trained in fundamental principles and brought upward through the steps of an organized training program.

Courses in mathematics and physics form the foundation. Mathematics courses must now go well beyond introductory levels; advanced studies in analysis of circuits and of radiation problems require the more powerful mathematical methods. The mathematics courses should, from the beginning, be based on the specialized requirements in the field of radio and should regularly be related to the applications in radio. They must provide the tools for solving any of the radio problems which arise. It is necessary that the student acquire facility in identifying the problem and determining the appropriate approach toward its solution, often the most difficult step.

Specialized courses in physics should include work in the subject of mechanics, so that such basic concepts as work, power and energy

can be understood in more advanced applications. Electrical physics will form the foundation for studies in the operation of electrical circuits for radio applications. The physics of heat and sound are directly applicable in the necessary courses of study of vacuum tubes and associated apparatus and in acoustical studies. The student trained in technology must acquire an understanding of the relations between mechanical, acoustical and electrical systems. These analogies require for their analysis a firm background in mathematics and physics. Design and development assignments in industry require a background in the pure sciences.

As an approach toward training in the analysis of radio circuits it is necessary to introduce electrical theory, starting with simple concepts of direct currents. Mesh circuits should be introduced in their simpler forms, and magnetic circuits should be covered thoroughly. Alternating-current courses should be carefully designed for application to steady-state problems, with applications to the radio field shown as the course progresses. Methods of transforming circuits should be introduced, and the simpler network theorems taught. When the student has acquired this understanding of alternating current circuits he should be given the more advanced work in networks and filters. His mathematics courses should by this time have reached a sufficiently advanced stage so that he is able to solve transient problems in connection with these networks. The latter study is becoming more significant as a result of the numerous electronic devices which have become common in the war years and the post-war period. Television and radar equipment depend for their successful operation upon circuits designed to accommodate complex wave shapes and signal impulses whose timing and wave form are critical. At a later point in the course the student should have an opportunity to learn the methods of transient solution with the aid of operational methods. It is important that this work be accompanied by coordinated training in laboratory procedure, so that the student may improve his ability in checking analytical work with experimental procedure. In this manner he becomes competent in measurements and learns the limitations of measuring equipment. The square-wave excitation method commonly used today in determining circuit response, yields more information than the former laborious method. The interpretation of these results calls for more intensive courses in testing procedure and analysis.

The study of the vacuum tube and its associated circuits must today be carried into the field of microwaves. The relation between internal structure and high frequency performance is important in the electronic devices used in television relay equipment, and in other high

frequency apparatus. Communication frequencies today are commercially successful in the microwave bands and the gap between these frequencies and the quasi-optical frequencies is becoming continually narrower. Electron tubes of all types must be treated as a part of the course. Industrial electronic equipment makes use of a wide variety of the newer types of electron tubes. Cathode-ray tubes should be carefully studied, and the analysis of their operation given in considerable detail.

In the courses on transmitters and receivers it becomes necessary to include the higher frequencies and the wider frequency response. Pulse transmission and composite television signal transmission call for apparatus which must be designed with a full understanding of circuit and component performance, and this understanding can come only from the analytical methods mentioned earlier. Recent improvements in both the picture signal and the associated sound of commercial television programs are the result of refinements which are the fruit of experience and engineering skill. It is one of the goals of the modern training course in the field of radio to qualify a student for adaptability to such work. The student well-schooled in the basic principles and whose skill has been developed by laboratory practice should, upon graduation, be able to enter the communications field and handle assignments on modern electronic devices in the field of radio or any of the related subjects such as navigational aids, electronic equipment for diagnosis and treatment in the medical field, industrial heating apparatus, and location and detection equipment. In order that he can be employed in any or all of the above applications his training must be of a broad scope. Navigational aids and detection equipment require training in the high frequencies and in the use of accurately timed pulses of transmission and critically adjusted circuits together with exacting design of antennas. Employment in industrial heating tasks makes demands upon his schooling in the field of high power at radio frequencies and his knowledge of dielectrics. In the medical field his understanding of very low and very high frequency phenomena will be of importance, and his ability to analyze complex wave shapes will depend upon his competence in the mathematical analysis of these shapes. This again emphasizes the need for an adequate level of training in mathematics and its correlation with the electrical theory.

* * *

Today's heavy demand for educational facilities coincides with the need for the expanded scope of courses as indicated above. The expan-

sion of opportunity for employment in all the levels of training mentioned leads to an increased number of opportunities for technically trained personnel to aid in producing the numerous newly-developed electronic devices which will become commonplace parts of modern industry. To bring these requirements together under a coordinated plan of training, the technical school of today must give continuous attention to the modern trends. Course organization must often be revised with a view to pointing always toward specific job objectives and toward employability in as wide a range of positions as is reasonable within the field.

RCA TECHNICAL PAPERS†

Fourth Quarter, 1946

Any requests for copies of papers listed herein should be addressed to the publication to which credited.

- "A Microwave Relay Communication System", G. G. Gerlach, *RCA REVIEW* (December) 1946
- "A Microwave Relay System", L. E. Thompson, *Proc. I.R.E.*, (December) 1946
- "A Unified Approach to the Performance of Photographic Film, Television Pickup Tubes, and the Human Eye", A. Rose, *Jour. Soc. Mot. Pic. Eng.* (October) 1946
- "Absorption of Microwaves by Gases, II", W. D. Hershberger (Coauthor), *Jour. Appl. Phys.* (October) 1946
- "And Now the 'Pylon' Antenna", R. F. Holtz, *Broadcast News* (October) 1946
- "Bikini Observations and Their Significance", A. F. Van Dyck (Coauthor), *Proc. I.R.E.* (December) 1946
- "Consolette Switching Systems", D. Pratt, *Broadcast News* (October) 1946
- "Determining the Population Served by an FM Station", *Broadcast News* (October) 1946
- "Electromagnetic Horns and Parabolic Reflectors", T. Goot e, *Radio News* (November) 1946
- "Electronic Spectroscopy", G. C. Sziklai and A. C. Schroeder, *Jour. Appl. Phys.* (October) 1946
- "Factors Governing the Frequency Response of a Variable-Area Film Recording Channel", M. Rettinger and K. Singer, *Jour. Soc. Mot. Pic. Eng.* (October) 1946
- "Frequency Modulation Distortion Caused by Common- and Adjacent-Channel Interference", M. S. Corrington, *RCA REVIEW* (December) 1946
- "Functional Sound Absorbers", H. F. Olson, *RCA REVIEW* (December) 1946
- "Grounded-Grid Power Amplifiers", E. E. Spitzer, *Broadcast News* (October) 1946
- "Isolation Methods for FM Antennas Mounted on AM Towers", R. F. Holtz, *Broadcast News* (October) 1946
- "Mica Windows as Elements in Microwave Systems", L. Malter, R. L. Jepsen and L. R. Bloom, *RCA REVIEW* (December) .. 1946
- "Microwave Equipment for Television Relay Service", W. J. Poch and J. P. Taylor, *Broadcast News* (October) 1946

† Report all corrections or additions to RCA REVIEW, Radio Corporation of America, RCA Laboratories Division, Princeton, N. J.

- "Panoramic Mass Spectrometer Observation", A. T. Forrester and W. B. Whalley, *Rev. Sci. Instr.* (December) 1946
- "'Plug-In' Amplifiers for Deluxe Studio Installations", H. Duszak, *Broadcast News* (October) 1946
- "Postwar Test Equipment for Theater Servicing", E. Stanko and P. V. Smith, *Jour. Soc. Mot. Pic. Eng.* (December) 1946
- "Pulse Generation", T. Gooteé, *Radio News* (December) 1946
- "Pulse Time Division Radio Relay", B. Trevor, O. E. Dow and W. D. Houghton, *RCA REVIEW* (December) 1946
- "Radio Heating in The Textile Industry", C. N. Batsel, *Radio News* (October) 1946
- "RCA War Research—What It Means to You", L. F. Jones, *Broadcast News* (October) 1946
- "Recording Studio 3A", G. M. Nixon, *RCA REVIEW* (December) 1946
- "'RMS'—Its Meaning and Application", A. N. Goldsmith, *Inter. Project* (November) 1946
- "Simultaneous All Electronic Color Television", *RCA REVIEW* (December) 1946
- "Stability and Frequency Pulling of Loaded Unstabilized Oscillators", J. R. Ford and N. I. Korman, *Proc. I.R.E.* (October) 1946
- "Stem Electrolysis Phenomena in Soft-Glass Rectifier Tubes", J. Gallup, *Jour. Amer. Ceramic Soc.* (October) 1946
- "Teleran", D. H. Ewing and R. W. K. Smith, *RCA REVIEW* (December) 1946
- "TELEVISION—A Bibliography of Technical Papers by RCA Authors (1929-1946), *RCA REVIEW*, RCA Laboratories Division, Princeton, N.J. (November) 1946
- "Television Equipment for Aircraft", M. A. Trainer and W. J. Poch, *RCA REVIEW* (December) 1946
- "The RCA Antennalyzer—An Instrument Useful in the Design of Directional Antenna Systems", G. H. Brown and W. C. Morrison, *Proc. I.R.E.* (December) 1946
- "The TK-30A Camera with the Image Orthicon", N. S. Bean, *Broadcast News* (October) 1946
- "The Universal Electron Microscope as a High Resolution Diffraction Camera", R. G. Picard and J. H. Reisner, *Rev. Sci. Instr.* (November) 1946
- "Twelve-Channel F-M Converter", J. E. Young and W. A. Harris, *Electronics* (December) 1946
- "Type BTF-10B 10 KW FM Transmitter", J. E. Young, *Broadcast News* (October) 1946
- "Type BTF-50A 50 KW FM Transmitter", C. J. Starnier, *Broadcast News* (October) 1946
- "Wide-Range Loudspeaker Developments", H. F. Olson and J. Preston, *Jour. Soc. Mot. Pic. Eng.* (October) 1946
Reprinted from *RCA REVIEW* (June) 1946

NOTE—Omissions or errors in these listings will be corrected in the yearly Index.

CONTRIBUTORS TO THIS ISSUE



ALBERT W. FRIEND received the B.S. (E.E.) degree in 1932 and the M.A. (Physics) degree in 1936 from West Virginia University. He studied Communication Engineering at Cruft Laboratory, Harvard University from 1939 to 1941. Previous to 1934 he operated a radio service business, consulted on communications systems, and was a divisional transmission and distribution engineer for the Ohio Power Company. From 1934 to 1944 he was Instructor and Assistant Professor of Physics (West Virginia University); Research Fellow, Blue Hill Meteorological Observatory; Research Fellow, Cruft Laboratory;

Instructor in Physics and Communication Engineering (Harvard University), Research Associate and Staff Member, Radiation Laboratory; Laboratory Director, Heat Research Laboratory (Massachusetts Institute of Technology) and special consultant to Division 5 of N.D.R.C. Since 1944 he has been an advance development engineer with the RCA Victor Division in Camden, New Jersey. He is working part time on a Navy Research project at Cruft Laboratory, Harvard University. Mr. Friend is a Senior Member of the Institute of Radio Engineers, a Member of the American Institute of Electrical Engineers, The American Meteorological Society, Tau Beta Pi, Sigma Pi Sigma, and Sigma Xi. He is a registered professional engineer.

PAUL L. GERHART received his E.E. degree from Lehigh University in 1924. From 1925 to 1940 he was employed by the Electrical Testing Laboratories as an Inspector of Cables and Technician of Electrical and Physical tests. In 1938 he joined RCA Institutes as a part-time instructor, and advanced to full-time instructor in 1940. He became a Department Head in 1942 and is now Chief instructor. He is now attending the Polytechnic Institute of Brooklyn, studying in the Graduate School of Electrical Engineering. Mr. Gerhart is a former Associate Member of the American Institute of Electrical Engineers.



J. LEWIS HATHAWAY received his B.S. degree in Electrical Engineering from the University of Colorado in 1929. In the same year, he joined the National Broadcasting Company where, as a member of the Development Group, he has since been engaged in all fields of the Company's engineering activities. While on a leave of absence 1941 to 1944, he served as a Special Research Associate at Harvard University performing underwater sound development work. Mr. Hathaway was appointed a Staff Engineer of the National Broadcasting Company in 1945.

DAVID P. HEACOCK received his B.S. degree in Mechanical Engineering from Rutgers University in 1941 and his M.S. degree in Electrical Engineering from Stevens Institute of Technology in 1946. In 1947 he joined the Tube Department of RCA Victor Division at Harrison, N. J. and at the present time is engaged in application work on electron tubes.





JAMES HILLIER received the degree of B.A. in physics in 1937, M.A. in physics in 1938 and Ph.D. in physics in 1941 from the University of Toronto, Canada. From 1939 to 1940 he was a research assistant and demonstrator at the Banting Institute of the University of Toronto Medical School where he and his co-workers developed the first electron microscope on this continent. Since 1940 he has been a research engineer at the RCA Laboratories in Camden and Princeton, New Jersey. Throughout his career, he has been connected with the development of electron microscopes and other types of electronic equipment used in the investigation of the sub-microscopic world. Dr. Hillier is a member of the Society of the Sigma Xi, a fellow of the American Physical Society, a member of the American Association for the Advancement of Science, and past president of the Electron Microscope Society of America.

WILLIAM HOTINE attended Colgate University after which he was employed as a technician by RCA Marine Department in 1923. In 1925 he joined Brunswick-Balke-Collender Co. as a radio engineer, and was engaged in broadcast receiver work until 1930, when he entered the motion picture sound-on-film field with United Research Corporation. From 1935 to 1940 he was chief engineer of Films Inc., engaging in 16-mm sound-on-film projection problems. In 1940 he joined Federal Telephone and Radio Laboratories as a development engineer on U.H.F. radar. In 1942, he became associated with the Raytheon Manufacturing Company as a development engineer on microwave radar. He became a member of the Development Group of the NBC Engineering Department in 1946 where he has been engaged in radio broadcast equipment development.



HARWICK JOHNSON received his B.S. degree in electrical engineering from the Michigan College of Mining and Technology and his M.S. and Ph.D. degrees from the University of Wisconsin. From 1938 to 1942 he was a research fellow and teaching assistant in the Department of Electrical Engineering at the University of Wisconsin. Since 1942 he has been associated with RCA Laboratories Division at Princeton, N. J. Dr. Johnson is a Senior Member of the Institute of Radio Engineers, a Member of Tau Beta Pi, Gamma Alpha and Sigma Xi.

ALBERT P. KAUZMANN received his degree of B.S. at the Massachusetts Institute of Technology in 1927. From 1927 to 1929 he served as radio-tube engineer for the Champion Radio Works at Danvers, Mass., following which he spent a year at the University of Munich. In 1930 he entered the Research and Engineering Department of the RCA Manufacturing Company at Harrison, N. J. At the present time he is associated with the Tube Department, RCA Victor Division, Harrison, N. J. and is working on the design and development of receiving tubes. Mr. Kauzmann is a Senior Member of the Institute of Radio Engineers.





ROBERT S. MAUTNER attended the Polytechnic Institute of Brooklyn from 1928 to 1930 and has studied at New York University, Pratt Institute and RCA Institutes, Inc. He was an instructor in Radio Communications at Nassau Collegiate Center in 1933. During the following two years he worked in the magnetic recording field. In 1937 he joined the Columbia Broadcasting System, transferring in 1941 to become a member of RCA Laboratories Division, Industry Service Laboratory, where he has been engaged in television development. Mr. Mautner is a Member of the Institute of Radio Engineers.

OTTO H. SCHADE graduated from the Reform-Real-Gymnasium, Halle, Germany, in 1922. From 1922 to 1924 he was with the Telephonfabrik A. G. vorm. J. Berliner, Berlin and Dusseldorf; from 1924 to 1925, in charge of the laboratory in the radio manufacturing company "Ratag" in Berlin; and from 1926 to 1931, in the engineering department of the Atwater Kent Manufacturing Company. Since 1931 Mr. Schade has been with RCA and at present is engaged in advance development work in the Tube Department, RCA Victor Division at Harrison, N. J. He received a Modern Pioneer Award from the Radio Manufacturers Association in 1940. Mr. Schade is a Senior Member of the Institute of Radio Engineers.



GILBERT S. WICKIZER received the B.S. degree in electrical engineering from the Pennsylvania State College in 1926. After graduation he was employed by the Radio Corporation of America, Operating Division, at Rocky Point, N. Y. From 1927 to 1929 he was engaged in development work for the Radio Corporation of America at Riverhead, N. Y. From 1929 to 1942 he was in the Research and Advanced Development Group of RCA Communications, Inc., and since 1942 he has been in the Communications Research Section of RCA Laboratories Division, also at Riverhead, N. Y. Mr. Wickizer is a

member of Eta Kappa Nu, a Senior Member of the Institute of Radio Engineers, and a member of the American Meteorological Society.

ANTHONY WRIGHT attended Oxford University. He came to this country in 1923 and joined the Victor Organization in 1929. A year later, he became a member of the RCA Engineering Department in Camden, N. J. He was engaged in Home Receiver Product Design until 1941, and was then assigned to the supervision of Product Design of Airborne Television Equipment used by the Armed Forces. Now, as Section Manager for television receivers in the Home Instrument Department, he is responsible for the Product Design of Home Television Instruments.



